NASA CONTRACTOR REPORT

NASA CR-1207

NASA CR-1207

COMPARATIVE EVALUATION OF ABLATING MATERIALS IN ARC PLASMA JETS

by Nevin K. Hiester and Carroll F. Clark

Prepared by
STANFORD RESEARCH INSTITUTE
Menlo Park, Calif.
for Langley Research Center

NATIONAL AERONAUTICS AND SPACE ADMINISTRATION • WASHINGTON, D. C. • DECEMBER 1968

NASA CR-1207

COMPARATIVE EVALUATION OF ABLATING MATERIALS IN ARC PLASMA JETS

By Nevin K. Hiester and Carroll F. Clark

Prepared under Contract No. NASr-49(15) by
STANFORD RESEARCH INSTITUTE
Menlo Park, Calif.

for

NATIONAL AERONAUTICS AND SPACE ADMINISTRATION

For sale by the Clearinghouse for Federal Scientific and Technical Information
Springfield, Virginia 22151 – CFSTI price $3.00

ABSTRACT

In a round-robin ablation study monitored by Stanford Research Institute in 1964, Teflon and high-density phenolic-nylon models were evaluated at various enthalpies and heating rates under supersonic conditions. The results of that study, published in NASA Contractor Report CR-379, showed that the best description of the test environments for twelve different plasma arc heater facilities was given by the stagnation point heating rate, and pressure. The mass loss rates from all facilities could be correlated in terms of these parameters with a standard deviation of approximately 11 percent for both the Teflon and phenolic-nylon material

The second phase of this study, described in this report, also involved twelve facilities, most of them the same as in the first phase. The same two high-density materials, Teflon and phenolic-nylon, were evaluated at stagnation pressures up to 10 atmospheres for the former and 30 atmospheres for the latter. The effect of model size was also evaluated using both hemispherical and flat-faced Teflon models having effective radii varying from one-quarter to four times the radius used previously. The mass loss rates again correlated with the results from the earlier study, except that high-density phenolic-nylon models showed a rapid increase in ablation above a stagnation pressure of about 2.5 atmospheres. These higher rates were also correlated, and found to agree, with literature data for this same pressure regime.

Five new low-density materials—Langley phenolic-nylon, Hughes phenolic-nylon, Avcoat epoxy-novalac-filled honeycomb, Langley silicone elastomer, and General Electric silicone elastomer—were also studied ~~in the second phase~~ at enthalpies from 2500 to 34,000 Btu/lb and stagnation pressures from 0.004 to 2 atmospheres. Mass loss rates, front surface, and internal temperatures were measured for these materials.

Mass loss rate correlations similar to those developed in the first phase of the study were satisfactory except for the silicone materials, which may suggest that the ablation mechanism varies for these in the range of conditions studied. Dimensional analysis was used to develop new correlations for interrelating front surface, internal temperature rise, and test environment. The resulting relations show that data from the various facilities could be satisfactorily compared.

CONTENTS

CONTENTS

ILLUSTRATIONS

ILLUSTRATIONS

* The units shown on the ordinates or abcissas of these figures are intended to show only the dimensions to be used for the variables involved. To be precisely correct the units should have been raised to the powers indicated.

TABLES

SYMBOLS

a	Constant—differs for each ablation material
a_0	Constant—differs for each ablation material
A	Sensing area—ft^2
A^*	Nozzle throat area—ft^2
b	Constant—differs for each ablation material
b_1	Constant—differs for each ablation material
b_0	Constant—differs for each ablation material
c	Constant—differs for each ablation material
c_0	Constant—differs for each ablation material
C_p	Heat capacity—Btu/lb°F*
C_{pAV}	Temperature averaged heat capacity—Btu/lb°F
d	Constant—varies for each ablation material
D	Model diameter—ft
e	Constant—differs for each ablation material
f	Constant—differs for each ablation material
F_p	Conversion constant—2116 lb force/ft^2 atm
g	Constant—differs for each ablation material
g_0	Constant—differs for each ablation material
g_c	Gravitational constant—32.17 lb ft/lb force sec^2
Δh	Enthalpy potential ($h_t - h_w$)—Btu/lb
h_s	Stagnation enthalpy of gas—Btu/lb
h_t	Total stream enthalpy—Btu/lb
h_w	Wall enthalpy—Btu/lb
H_D	Heat of dissociation—Btu/lb
ΔH_D	Overall heat of decomposition—Btu/lb
H_{eff}	Effective heat of ablation = $\dot{q}_{CW}/\dot{m}_t$—Btu/lb
J_m	Conversion constant—778 ft lb force/Btu

* When the symbol "lb" is used without the modifying word "force", it always means pound mass.

k_w	Catalytic surface activity—cm/sec
K	Conversion constant, see equation (E-3B)
m	Constant—differs for each ablation material
$\dot{m}$	Mass loss rate—lb/ft^2 sec
$\dot{m}_p$	Mass pyrolysis rate, see equation (19)—lb/ft^2 sec
$\dot{m}_t$	Total mass loss rate—lb/ft^2 sec
M	Mass of calorimeter slug—lb
n	Constant—differs for each ablation material
N_{Le}	Lewis Number
N_{Pr}	Prandtl Number
p	Pressure—atm
P_{t_1}	Reservoir, arc chamber, or plenum pressure—atm
P_{t_2}	Model stagnation pressure—atm
$\dot{q}$	Heat transfer rate—Btu/ft^2 sec
$\dot{q}_{k_w \sim \infty}$	Heat transfer rate to fully catalytic surface—Btu/ft^2 sec
r	Constant—differs for each ablation material
R	Model radius—ft
R_{eff}	Effective model radius—ft, see equation (15)
R_{FF}	Radius of flat-face cylinder—ft
R_H	Radius of hemispherical shape—ft
s	Constant—varies for each ablation material
S_R	Proportionality constant in Fay-Riddell relation—$ft^{1.5}$ sec $atm^{0.5}/lb$, see equation (5)
t	Time—sec
Δt	Run time—sec
T_{FS}	Model front surface temperature—°F or °R
ΔT	Temperature rise—°F
$\Delta T/\Delta t$	Slug temperature rise rate—°F/sec
u	Constant—differs for each ablation material
v	Constant—differs for each ablation material
w	Constant—differs for each ablation material

$\dot{w}$	Cooling water flow rate—lb/sec
W	Gas mass flow rate—lb/sec
W_{250}	Weight of ablation material per unit area—lb/ft^2, see equation (40)
x	Linear distance from original model surface—in.
X	Linear measurement along the model axis—ft
y	Constant—differs for each ablation material
z	Constant—differs for each ablation material
α	Constant—heat necessary to raise the material to the ablation temperature and to decompose it—Btu/lb
β	Transpiration shielding factor
ϵ	Total surface emissivity
μ	Viscosity—lb/ft sec
π_A	Dimensionless group, involvimg char failure stress, see equation (12)
π_D	Dimensionless group, involving density, see equation (49)
π_f	Dimensionless group based on Fay-Riddell relation, see equation (E-7)
π_h	Dimensionless group, involving enthalpy potential, see equation (29)
π_m	Dimensionless group, involving mass loss rate, see equation (E-4)
π_p	Dimensionless group, involving stagnation pressure see equation (E-5)
π_q	Dimensionless group, involving heat transfer rate, see equation (E-6)
π_s	Dimensionless group, involving front surface temperature, see equation (41)
π_t	Dimensionless group, involving exposure time, see equation (48)
π_T	Dimensionless group, involving internal temperature rise, see equation (47)
π_X	Dimensionless group, involving position in model, see equation (46)
ρ	Density—lb/ft^3
ρ_{VR}	Density of virgin ablation material—lb/ft^3

σ	Stefan-Boltzmann constant = 4.76×10^{-13} Btu/ft^2 sec °R^4
τ	Mechanical stress on char—lb force/ft^2
$\psi(N_{Le})$	Function of the Lewis Number for the gas, see equation (E-2)

SUBSCRIPTS

AV	Average value
c	Char surface location
CALC	Calculated value
CR	Char thickness
CW	Cold wall condition
FAC	Instrument supplied by facility
meas	Measured value
P	High-density phenolic-nylon material
R	Char recession
RR	Phase I round robin
s	Stagnation condition
SRI	Instrument supplied by SRI
T	Teflon material
1.25FF	Refers to 1.25-in.-diameter, flat-faced models tested during Phases I and II round robins
250	Internal temperature rise of 250°F
∞	Free stream condition

I INTRODUCTION

The Office of Research Grants and Contracts, National Aeronautics and Space Administration, (NASA), in 1963 asked Stanford Research Institute to act as a program manager on a round-robin test study to determine whether ablation tests of representative materials at different plasma arc heater facilities would yield self-consistent results.

This work involved definition of the extent to which realistic environmental conditions are simulated by such devices; conduction of comparative ablation tests on standardized materials at selected organizations possessing suitable equipment; provision of the specialized instrumentation and test models required; and correlation of test results with analyses to determine the feasibility of developing a standardized method.

The twelve participating organizations, five government and seven industrial, tested over 170 models and, in addition, performed numerous calibration experiments. The resulting data, published in NASA Contractor Report CR-379,[1] showed that

1. A procedure for comparing ablation test results (on a given material) at each supersonic plasma arc heater facility is feasible through use of a standard mass loss rate, heating rate (or calculated enthalpy), and stagnation pressure correlation.
2. The applicability of the procedure outside the range of materials, model sizes, and arc heater operating conditions studied in the program needed further investigation.

The program was subsequently extended to assess the validity of the findings of the Phase I study and to determine their generality by providing a more detailed comparison of results over a wider range of ablation variables. This involved the study of more severe test conditions, changes in model geometry, new low-density materials, and more extensive measurements on the ablating models. Thus, the Phase II research, which was also to involve a round robin, fell naturally into four major categories—facility parameters, model parameters, measurements, and analysis of results. More specifically, the following studies were to be considered:

1. Facility Parameters

   a. Higher stagnation pressures
   b. Uniformity of plasma stream

2. Model Parameters

   a. Geometry
   b. New materials

3. Measurements

   a. Front surface temperature
   b. Internal temperature rise
   c. Mass and length changes
   d. Char behavior

4. Analysis of Results

   a. Comparison of measurement techniques
   b. Correlation of data

II SUMMARY

The ablation conditions studied in Phase I with the high-density Teflon (T)* and phenolic-nylon (P) materials were extended to higher stagnation pressures and to models of different shapes and dimensions. In addition, five new low-density materials were evaluated during Phase II of the round robin, and more extensive front surface and internal temperature measurements were made with the models. The new materials were

- Langley phenolic nylon (PLL), density = 35.5 lb/ft^3
- Hughes phenolic- nylon (PLH), density = 35.7 lb/ft^3
- Avcoat epoxy-novalac-filled honeycomb (A), density = 31 lb/ft^3
- Langley silicone elastomer (SP), density = 33.5 lb/ft^3
- General Electric silicone elastomer (SG), density = 36.8 lb/ft^3

Insofar as possible the same test facilities were used in the new program. Several new organizations were added to replace those which could not be used and to provide capabilities at higher test pressures or larger model dimensions. The twelve participants, six government and six industrial, finally chosen were

1. Gas Dynamics Branch, Ames Research Center—NASA†
2. Magneto Plasma Dynamics Branch, Ames Research Center—NASA
3. Applied Materials and Physics Division, Langley Research Center—NASA†
4. Entry Structures Branch, Langley Research Center—NASA†
5. Manned Spacecraft Center, Subsonic Facility—NASA†
6. Manned Spacecraft Center, Supersonic Facility—NASA
7. Aerotherm Corporation
8. AVCO Corporation†
9. Giannini Scientific Corporation†
10. Martin Company†

* SRI designated code for these materials.

† Participant in Phase I round robin

11. Space General Corporation

12. Cornell Aeronautical Laboratory, Inc.

Calorimeters and ablation models, some instrumented with internal thermocouples, were supplied to each participant for use in the round-robin test program. Radiometers were also supplied for determining front surface temperature. In addition to model and calibration runs, each facility was asked to make a heating rate and stagnation pressure traverse of the plasma stream. The results showed that all the test facilities exhibited some nonuniformity of the stream, with "coring" occurring in several cases. However, the degree of uniformity in the region of the model was satisfactory in most cases.

The SRI and facility calorimeters when compared in the test environment had a standard deviation of 12 percent, which is slightly better than that found in the Phase I round robin. As in the earlier study, it was observed that when the plasma flow through the supersonic nozzle is far removed from equilibrium, such as with high expansion ratios or very low test pressures, surface catalytic effects on the calorimeter will influence the measured heating rate.

Comparison of the measured enthalpy to that calculated from the heating rate and stagnation pressure, through the Fay-Riddell relation, was not satisfactory. As in the Phase I study, those facilities having quite uniform stream traverses showed good agreement between the two values, indicating that in those cases the center-line enthalpy is probably close to the average enthalpy by the energy balance method. Stream enthalpy is a most important variable in material ablation studies, yet it is the most difficult to measure accurately.

The primary measurements made on the models were weight loss, recession, char depth, char density, front surface temperature, and internal temperature. These data, along with heating rate, stagnation pressure, and enthalpy, were the inputs for correlation of the data.

Initial interpretation involved further evaluation of the data from the Phase I round robin. Dimensional analysis suggested the following dimensionless relation, involving groups proportional to mass loss rate, $\dot{m}_t$, heating rate, $\dot{q}_{CW}$, and stagnation pressure, P_{t_2}, and also containing the effective radius of the model, R_{eff}, and the overall heat of decomposition, ΔH_D, for each material:

$$\pi_m = a_0 \pi_q^n \pi_P^m$$

In the absence of a means to determine ΔH_D independently, the dimensionless correlation was expanded into a dimensional form similar to those described in the Phase I report (NASA Report No. CR-379), namely,

$$\dot{m}_t = b(R_{eff})^{n+m-1}(\dot{q}_{CW})^n(P_{t_2})^m$$

A considerable amount of supersonic arc-jet test data on Teflon and high-density phenolic-nylon materials is available in the literature. Inclusion of these data for Teflon, along with the Phase I round-robin results, leads, by regression analysis, to the following values of b, n, and m:

$$(\dot{m}_t)_T = 0.0046(R_{eff})^{-0.21}(\dot{q}_{CW})^{0.55}(P_{t_2})^{0.24}$$

with a standard deviation of 10 percent. For high-density phenolic-nylon, the relation is

$$(\dot{m}_t)_P = 0.0010(R_{eff})^{-0.32}(\dot{q}_{CW})^{0.55}(P_{t_2})^{0.13}$$

with a standard deviation of 10 percent.

The results of the Phase II, high stagnation pressure experiments were interpreted in terms of the above dimensional correlations. The Teflon data were found to fit the relation up to the highest pressure used, 33 atm. On the other hand, at stagnation pressures above 2.7 atm, the high-density phenolic-nylon data showed higher mass loss rates than predicted by the above relation. These phenolic-nylon data, plus literature data obtained under similar conditions, fit a second correlation:

$$(\dot{m}_t)_P = 0.0010(\tau/2116)^{-0.75}(R_{eff})^{-0.32}(\dot{q}_{CW})^{0.55}(P_{t_2})^{0.13+0.75}$$

where τ is the mechanical stress, in pounds force per square foot, at which failure of the char occurs. This relation, derived by dimensional analysis, permits determination of τ from the intercept of the new correlation line.

The stress of the char at failure was found to be 5610 lb force/ft.^{2} This assumption of char failure appears valid since the high-density phenolic-nylon models showed almost no char after exposure to the high stagnation pressure environments and thus had reduced thermal protection.

A limited number of studies were performed using variable radii models and calorimeters. The heat transfer data showed the proper inverse relationship with square root of calorimeter shroud radii. The mass loss data also showed the proper effect of radius but exhibited greater scatter than for the standard models. Plasma coring and stream blockage may be partially responsible.

The low-density materials ablated somewhat differently in terms of char appearance. With the low-density phenolic-nylon materials the char was cracked with a columnar structure oriented parallel to the direction of ablation. The silicone chars had two types of appearance. At low heat fluxes, they were black, but at higher heating rates the surface showed a grey, fused, inorganic coating, apparently due to the formation of SiO_2. The Avcoat chars usually had a depression in the honeycomb filler material, with the web being slightly raised and with fused droplets of inorganic material at the model periphery.

The properties and composition of these chars are less reproducible than those of the high-density materials. This is also true of the appearance and dimensions of the charred core, the latter being difficult to measure.

The mass loss rate data for the five low-density materials all showed the same form of correlation as for the high-density materials, namely,

$$\dot{m}_t = a\left(\dot{q}_{\substack{CW \\ SRI}}\right)^n (P_{t_2})^m$$

The effective radius term has been combined with b in this case and replaced by "a" since no planned studies of these materials were made with varying radii models. The values of the constants are

MATERIAL	a	n	m	PERCENT STANDARD DEVIATION
PLL	0.0047	0.36	0.26	15
PLH	0.0039	0.36	0.19	14
A	0.0036	0.47	0.33	16
SP	0.00032	0.81	0.19	24
SG	0.00019	1.03	0.28	36

Note that the standard deviation is higher than that found for the high-density materials in the Phase I round robin owing to the more difficult char measurements. The correlations for the silicone materials are particularly poor, suggesting that the mechanisms of ablation may vary in the range of conditions studied. Therefore, less credence should be given to the correlation constants found for these latter materials. Attempts to correlate mass loss rates with other variables were no more successful.

Front surface temperature, as measured with facility optical pyrometers, correlated well with pyrolysis rate and stagnation pressure, thus

$$T_{FS} = a(P_{t_2})^v(\dot{m}_p)^w$$

The values of the constants are

MATERIAL	a	v	w	PERCENT STANDARD DEVIATION
PLL	10,980	0.031	0.21	5
PLH	10,710	0.044	0.20	6
A	10,040	0.039	0.18	6
SP	7,660	0.012	0.16	4
SG	5,210	0.028	0.072	5

This relation was derived by dimensional analysis and then expanded into the above form.

The internal temperature profiles were correlated in terms of heating rate and stagnation pressure by adding the position and time at which a given temperature rise occurs. The correlation is

$$x = a(P_{t_2})^b(\dot{q}_{\substack{SRI \\ CW}})^c(t)^d(\Delta T)^e$$

The values of the constants are

MATERIAL	a	b	c	d	e	PERCENT STANDARD DEVIATION
PLL	0.034	0.053	0.30	0.63	-0.28	13
PLH	0.056	0.035	0.15	0.58	-0.24	9
A	0.037	0.018	0.27	0.60	-0.26	14
SP	0.072	0.022	0.18	0.52	-0.30	12
SG	0.12	0.031	0.098	0.54	-0.28	8

This relation compares with analogous relations and with the results in the literature. A markedly improved correlation is obtained when only the 250°F temperature rise isotherm is considered. The relation in this case is

$$x_{250} = a(P_{t_2})^b(\dot{q}_{\substack{SRI \\ CW}})^c(t_{250})^d$$

and the constants are

MATERIAL	a	b	c	d	PERCENT STANDARD DEVIATION
PLL	0.014	0.083	0.18	0.61	8
PLH	0.017	0.079	0.14	0.60	5
A	0.023	0.105	0.15	0.62	6
SP	0.0082	0.016	0.26	0.54	9
SG	0.033	0.065	0.046	0.55	2

Both of the temperature rise correlations were derived by dimensional analysis.

The data obtained for the low-density materials can be used to compare their ablation performance. For environments leading to low front surface temperatures, the silicone materials show the lowest mass loss rates. However, at high front surface temperatures, the silicones perform much more poorly than the low-density phenolic-nylon materials. This marked difference undoubtedly relates to the chemical reactions involving silicon, oxygen, and carbon. Below the melting point of silica, the surface is protected by this material and some silicon carbide. Above the melting point, however, the silica reacts with carbon to form carbon monoxide and silicon monoxide which are rapidly lost as vapors. This change in ablation mechanism undoubtedly causes the difficulties in correlating the silicone mass loss data. The internal temperature rises show that the best insulator, on both a volume and a weight basis, is the Langley low-density phenolic-nylon.

III EXPERIMENTAL PROGRAM

The Phase II round-robin study was organized and undertaken in a very similar manner to the Phase I program. The following sections describe the study in more detail.

A. Scope and Participants

The test environments, model responses, and ablation materials to be studied are outlined in the scope. Choice of the organizations to participate in the round robin were based on somewhat similar criteria to those used in the earlier study.

1. Scope of Program

Representatives of the Ames Research Center, Langley Research Center, Manned Spacecraft Center, Jet Propulsion Laboratory, Advanced Research Programs Office of NASA, and Stanford Research Institute met early in the Phase II program to determine the test conditions, model dimensions, and materials to be evaluated. It was agreed that three separate areas should be studied in the new program, as follows:

1. Extension of previous test conditions
2. Variation from previous model dimensions
3. Addition of new low-density materials

In the first area, the major interest was in increased stagnation pressures. In order to minimize changes in other variables, model dimensions were kept the same as in Phase I, and the same materials were used for the study, namely,

- Teflon, type TFE 7, white variety, density = 135.6 lb/ft^3
- Phenolic-nylon (50-50%), density = 74.3 lb/ft^3

The second area involved changes in effective diameter, and both larger and smaller models than used previously were considered. Test conditions were kept the same as in Phase I, and Teflon was used as one of the materials. However, because of an insufficient quantity of

high-density phenolic-nylon polymer from the previous program, a low-density version was used instead, namely,

- Low-density phenolic-nylon (Hughes 5), density = 35.7 lb/ft^3

The major purpose of the third area of the program was to compare certain low-density, charring ablators. For this reason, test conditions and model dimensions were kept the same as in Phase I, but more extensive measurements were taken on the models. In addition to the Hughes low-density phenolic-nylon (noted above), the new materials involved were

- Low-density phenolic-nylon (Langley Scout R/4B) density = 35.5 lb/ft^3
- Epoxy-novalac-filled honeycomb (Avcoat 5026-39 HC/G) density = 31 lb/ft^3
- Silicone elastomer (Langley Modified Purple Blend E4A1) density = 33.5 lb/ft^3
- Silicone elastomer (G.E. ESM 1004AP), density = 36.8 lb/ft^3.

Phase II of the round robin thus consisted of the exposure of the above models under the appropriate conditions at various arc-heated plasma jet facilities. The participants supplied information about test conditions and the Institute measured the physical and chemical changes in the models.

2. Selection of Participating Organizations

Several factors governed the selection of supersonic testing facilities to participate in the new round-robin program. These were: (1) that the test models could be accomodated in the plasma stream, (2) that the facility operate in the range of test conditions desired, and (3) that insofar as possible the facilities used were either participants in the Phase I round robin or would bring a new capability to the study.

All twelve of the organizations used in the Phase I round robin were contacted and asked to indicate their interest in further work. Lack of facility time or high preliminary cost estimates eliminated five of the twelve. Other organizations were then contacted and their facilities assessed, using the criteria mentioned in the Phase I report. Inspection trips were made to the new facilities.

Of particular interest was the ability of supersonic plasma arc jets to test models as large as 5 inches in diameter or at stagnation pressures up to 30 atm. These facilities would be used to extend the Phase I studies on Teflon and high-density phenolic-nylon materials.

As in the Phase I round robin, availability of funds determined the number of commercial participants. Two of these had high stagnation pressure capabilities (AVCO Corporation and Cornell Aeronautical Laboratory), and one had a capability for testing large models (Martin Company). After including these organizations in the program, the remaining funds permitted the selection of four participants for the studies on the ablation of low-density materials, namely

- Aerotherm Corporation
- Giannini Scientific Corporation
- Martin Company
- Space General Corporation

Three of the commercial organizations had participated in the Phase I round robin: Giannini, Martin, and AVCO.

Five government organizations also agreed to participate in the studies on the ablation of low-density materials, namely,

- Gas Dynamics Branch, Ames Research Center—NASA
- Magneto Plasma Dynamics Branch, Ames Research Center—NASA
- Applied Materials and Physics Division, Langley Research Center—NASA
- Entry Structures Branch, Langley Research Center—NASA
- Manned Spacecraft Center— -NASA

The last of these, Manned Spacecraft Center, has a subsonic facility which was included to provide a comparison with supersonic facility results.

The Entry Structures Branch had a higher enthalpy facility under construction and had planned to use it as well as the low enthalpy arc jet used in the Phase I round robin. Delay in completing the new facility prevented the performance of any tests on it. The Applied Materials and Physics Division also had a capability for testing large models and therefore participated in that portion of the program.

B. Models and Instrumentation

Approximately thirty ablation models, one calorimeter, and one total radiation pyrometer were furnished by SRI to each participant. Each facility also provided instrumentation to monitor the test environments.

1. Models

In general, the models had the same configuration as in the earlier study. The new materials introduced additional fabrication problems and the need for thermocouple instrumentation.

a. Fabrication

The ablation models used in the second NASA round robin were machined from the materials listed in Table I.

The Langley low-density phenolic-nylon was supplied as two 12-in.-diameter × 4-in.-thick billets, and the Hughes phenolic-nylon was furnished in the form of five 12-in.-diameter × 1.5-in.-thick pieces. One-quarter inch of material was discarded from the periphery of all low-density phenolic-nylon billets to ensure uniform models.

The Avcoat material was supplied as two 12 × 12 × 2-in. sheets, and model cores of this material were cut with a single honeycomb centered in the core face. The Avcoat and low-density phenolic-nylon materials were fabricated with high-speed cutting techniques.

The Modified Purple Blend models were machined approximately ten percent oversize from a 16-in.-diameter × 4-in. billet, and then cured at 100°C for four hours. The heat-up rate before the start of cure was 150°C per hour, and the cool-down rate after cure was 75°C per hour. After cure, the models were machined to size by high-speed cutting and grinding.

The General Electric silicone material was supplied in the form of two 24 × 24 × 1-in. sheets. Models of this material were fabricated by rough, high-speed cutting followed by high-speed grinding.

The 1.25-in.-diameter Teflon and high-density phenolic-nylon models were fabricated from the same material used in the Phase I round-robin tests, as described in the report on that study.[1] The large-diameter Teflon models were prepared from the identical grade of material provided by the same supplier used in the first round robin.

Table I

ABLATION MATERIALS EVALUATED

MATERIAL	ORGANIZATION		IDENTIFICATION CODE	SRI MODEL PREFIX DESIGNATION*	DENSITY (lb/ft^3)	APPROXIMATE COMPOSITION
	Manufacturer	Supplier				
Low-Density Phenolic-Nylon	Langley	Langley	Scout R/4B FB/30 AM/30 Scout R/4B FB/31 AM/31	PLL PLL	35.5 35.5 35.5	Phenolic resin, 25%; phenolic Microballoons, 25%; nylon powder, 50%
Low-Density Phenolic-Nylon	Hughes Aircraft	Ames	Hughes 5 - No. 3 Hughes 5 - No. 4 Hughes 5 - No. 5 Hughes 5 - No. 6 Hughes 5 - No. 7	PLH PLH PLH PLH PLH	36.7 35.7 35.6 35.8 35.6 35.7	Hexa-cured phenolic-novalac, phenolic Microballoons, 23%; nylon powder, 40%
Avcoat 5026-39 HC/G	AVCO	Manned Spacecraft Center	K5-13002-7 N5-80070	A A	30.8 31.2 31	Proprietary filler; epoxy-novalac resin, chopped Fiberglass, phenolic Microballoons; in Fiberglass honeycomb
Modified Purple Blend Silicone	Langley	Langley	E4A1 Elastomer, RDY 150, H3365	SP	33.5	Sylgard 182 silicone, 75%; Eccospheres, 15%; phenolic Microballoons, 10%
General Electric Silicone	General Electric	Jet Propulsion Laboratory	ESM 1004AP	SG	36.8	Methylphenyl silicone elastomer; aluminum silicate fibers, 12%; small amount of iron oxide
Teflon	Du Pont	R. S. Hughes	TFE 7, Teflon	T	135.6	Polytetrafluoroethylene
High-Density Phenolic-Nylon	Ames	Ames	P11, P12	P	74.3	Phenolic resin, 50%; nylon powder, 50%

* These letter symbols will be used hereafter in text, tables, figures, and appendices to denote the materials investigated.

All models were constructed with removable cores to simulate one-dimensional heat flow to the model stagnation region. Since the low-density materials being evaluated were porous in structure, the back face of the core and the inside surface of the shroud were coated with a thin layer of RTV silicon to prevent hot gas from passing through the material. This simulates having the material bonded to a substrate. The core diameter was one half of the total model diameter for all sizes.

b. Thermocouple Instrumentation

The cores of approximately sixty models were instrumented with four 36-gauge Chromel-Alumel thermocouples spaced at 0.1-in. intervals back from the model front surface. The thermocouples were formed with a Dynatec thermocouple welder.

In the case of the two elastomeric materials, the thermocouples were inserted into the model cores with a hypodermic needle using a positioning jig. The low-density phenolic-nylon and Avcoat cores were instrumented by drilling 0.007-in.-diameter longitudinal holes and drawing in the thermocouples. After assembly, the instrumented models were X-rayed at 90° planes, and the thermocouple positions measured on the X-ray films with a Telereadex viewer.

Sketches of the instrumented and uninstrumented models are shown in Fig. 1. The assembled 1.25-in.-diameter models, with their plastic shipping containers, are shown in Fig. 2. The uninstrumented Teflon and low-density phenolic-nylon models with diameters ranging from a 1-in. hemisphere to 5 inches flat face are shown in Fig. 3.

2. Instrumentation

Two instruments, a calorimeter and a radiometer, were supplied by SRI for use in the experiments. All other instrumentation at the test facility was made available by the participating organization.

a. SRI Calorimeter

The SRI calorimeter supplied to each facility was identical in dimensions and shape to the calorimeter used during the Phase I round robin. The calorimeter was a transient, slug type based on a design developed at Ames Research Center, NASA. The slug was oxygen-free copper with a 0.5 mil-thick nickel plating on the front face. The slug was isolated from the copper shroud by three sapphire bearings, as shown in Fig. 4. The slug diameter was 0.625 in., which was equal to the sample

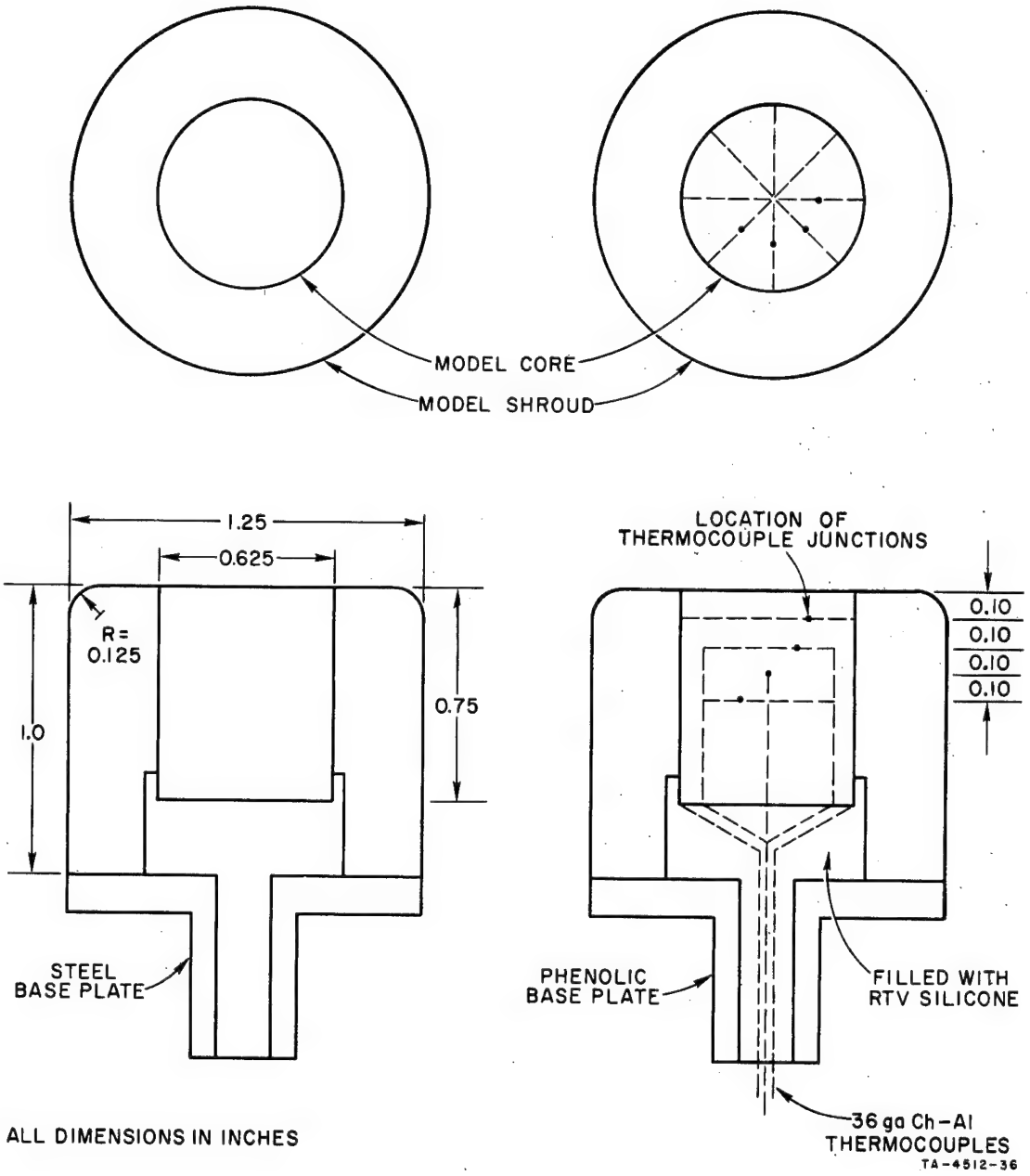

FIG. 1 DIMENSIONS OF MODELS

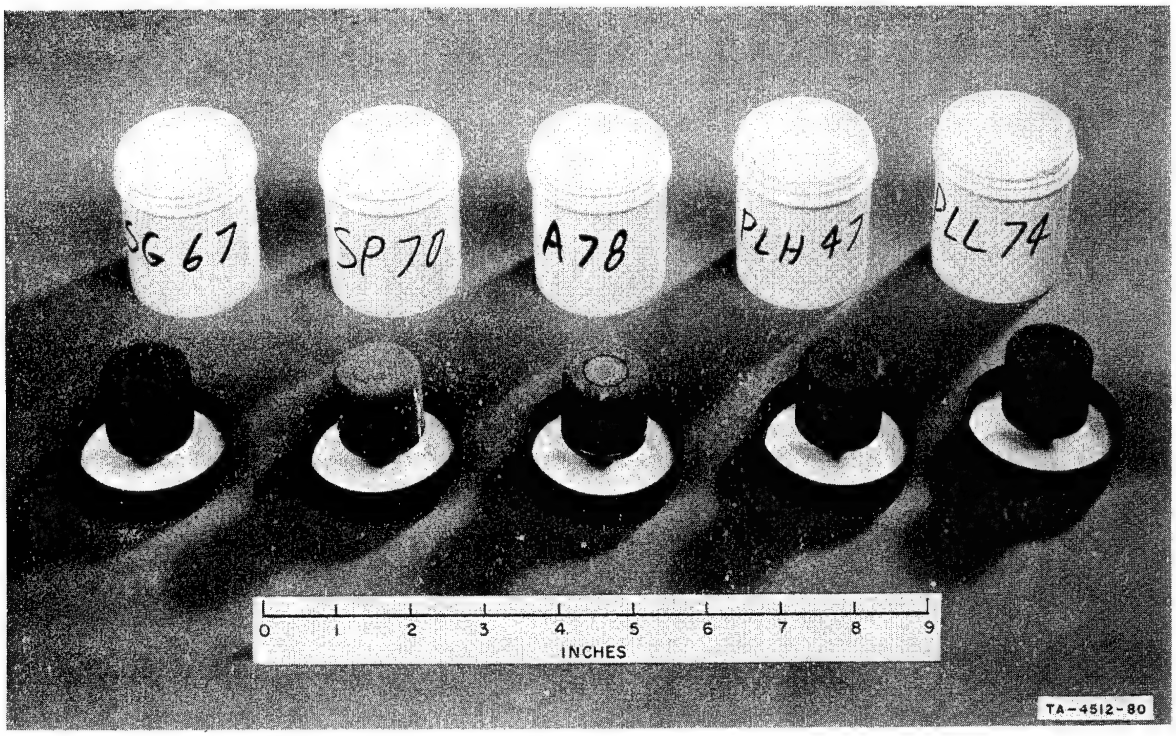

FIG. 2 MODELS FABRICATED FROM LOW-DENSITY MATERIALS

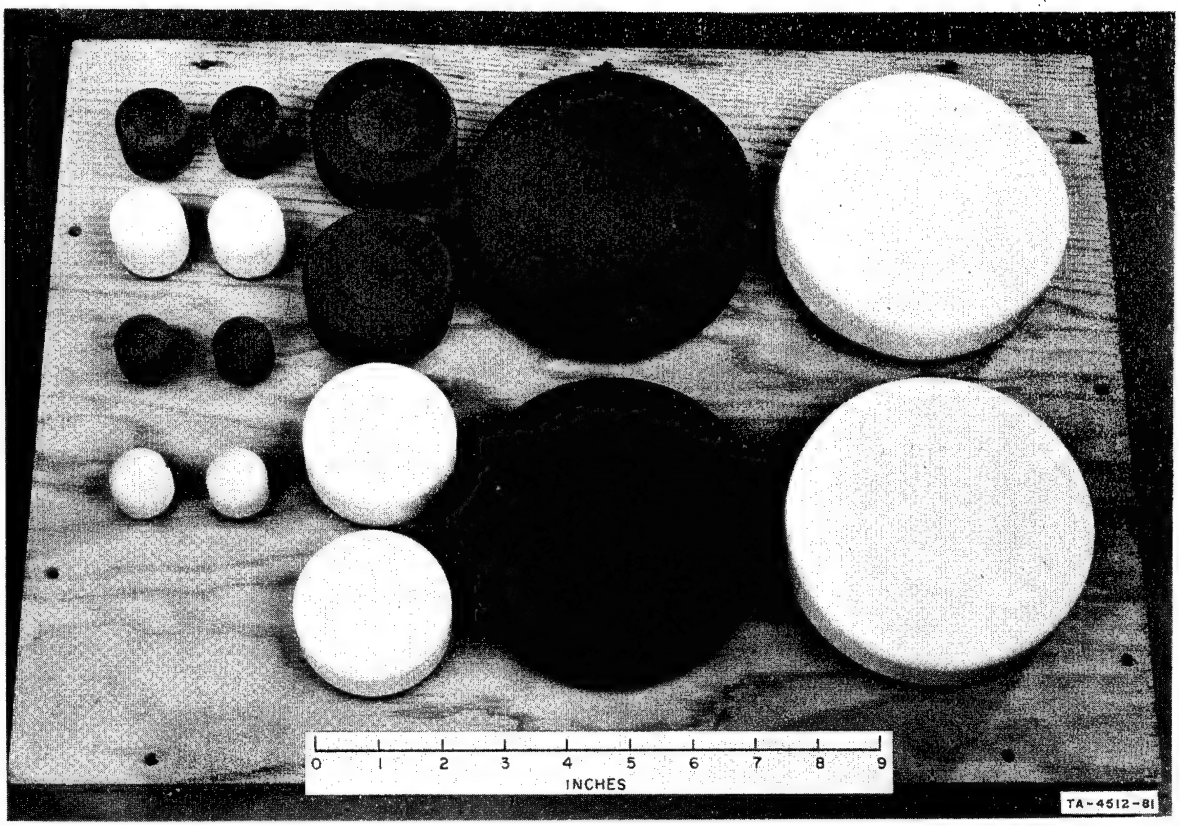

FIG. 3 MODELS OF VARIABLE RADIUS

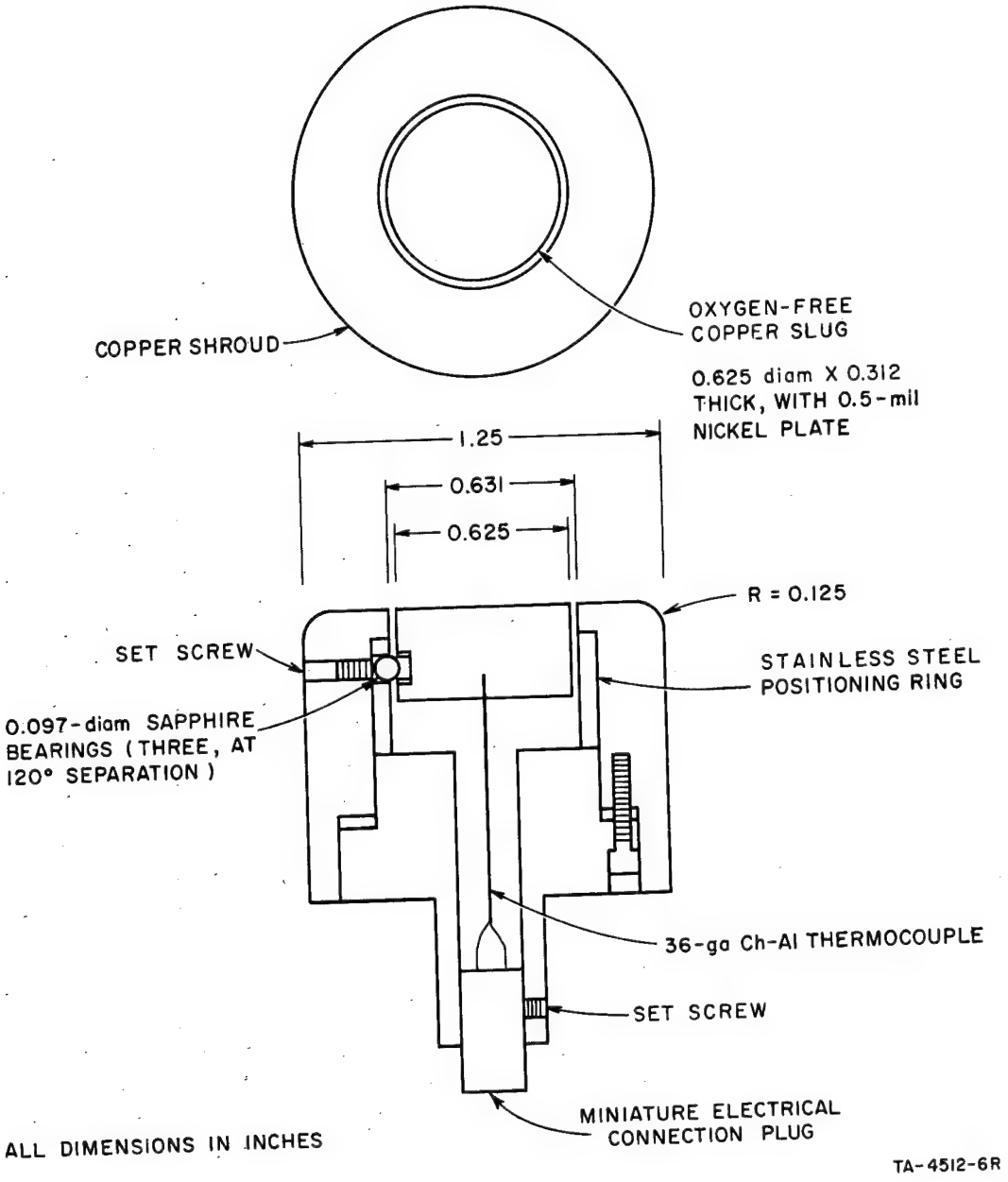

FIG. 4 DESIGN AND DIMENSIONS OF SRI CALORIMETER

core diameter in the 1.25-in.-diameter models. The average slug temperature was sensed by two parallel, 36-gauge Chromel-Alumel thermocouples peened into holes in the slug base.

The weight of each slug in pounds was stamped on the calorimeter base, and each facility was provided with a graph of the slug specific heat versus temperature. The heat flux was calculated by the facility, using the following relationship:

$$\dot{q}_{\substack{SRI \\ CW}} = \frac{MC_{pAV}}{A} \frac{\Delta T}{\Delta t} \qquad (1)$$

where

$\dot{q}_{\substack{SRI \\ CW}}$ = heat transfer rate, (cold wall), SRI calorimeter—Btu/ft^2 sec

M = mass of the calorimeter slug—lb

A = calorimeter sensing area—0.00213 ft^2

C_{pAV} = temperature averaged heat capacity of copper—Btu/lb°F

$\frac{\Delta T}{\Delta t}$ = slug temperature rise rate—°F/sec

b. SRI Radiometer

In an effort to minimize the scatter in front surface temperature data that was observed in the Phase I round robin when each facility had its own special pyrometer, each facility was provided with an identical reference pyrometer for measuring the front surface temperature of the model. The selection of this pyrometer was governed by the necessity for a moderate cost, durable instrument; and a radiometer, or total radiation-type pyrometer, was chosen as best satisfying these requirements. The instrument selected, which will later be referred to as the SRI radiometer, was a Honeywell Radiamatic Detector, Model R12-354546-7. This instrument had a fused silica lens and viewed the total radiation over the range of wavelengths from 0.3 to 3.9 microns. The instrument required a 0.5-in.-diameter target with a 24-in. sighting distance to the target; it required a larger size target for greater sighting distances.

The millivolt output of the SRI radiometers was calibrated over a range of temperatures from 2000 to 4600°F by viewing an inductively heated graphite black body. The black body cavity was 1.5 in. internal

diameter × 2.0 in. height, with an 0.75-in-diameter top viewing port. The viewed bottom of the cavity was covered with a layer of lamp black. The entire graphite block was surrounded by two molybdenum radiation shields and an argon-filled chamber with the glass viewing port removed. The cavity temperature was monitored with a Micro Optical Pyrometer No. 95 and a Leeds-Northrup optical pyrometer. Each facility was provided with plots of the radiometer output versus temperature plus instructions for mounting the radiometer.

c. Facility Instruments

The equipment and instruments that were used by each facility for the Phase II round-robin ablation tests are summarized in Appendix A. This information was based on data collected at the time the model tests were witnessed. A detailed description of each facility is beyond the scope of this report, and the information contained in Appendix A is intended only as a brief summary of this equipment.

C. Experimental Procedures

Each participating facility received a run plan, specifying three tunnel test conditions and the test run times. Tunnel test conditions were selected that would be within the capability envelope for each facility and at the same time provide testing of the ablation materials over the widest range of conditions. The tunnel conditions specified were enthalpy, heating rate, and stagnation pressure. The range of test parameters and the number of models involved in the Phase II round robin are given in Table II.

Three models were tested at varying run times at the tunnel condition giving the lowest heating rate. The run times were set to give total heat loads ($\dot{q}_{cw}\Delta t$) of 1500, 3000, and 5000 Btu/ft^2. Two of the three models were uninstrumented, and the remaining model was instrumented with four thermocouples. The instrumented model was usually run at the highest heat load condition.

The two uninstrumented models were tested at varying run times for each of the other two tunnel conditions. The total heat loads for these conditions were 2000 and 5000 Btu/ft^2.

Table II

TEST PARAMETERS FOR NASA ROUND-ROBIN ABLATION PROGRAM

	DENSITY lb/Ft^3	PHASE I - ROUND ROBIN	PHASE II - ROUND ROBIN		
			TASK A HIGH PRESSURE	TASK B VARYING R_{eff}	TASK C NEW MATERIALS
TUNNEL CONDITIONS					
Enthalpy Range (Btu/lb)		1500-16,000	1700-7000	9500-12,000	3000-34,000
Heating Rate Range (Btu/ft^2 sec)		40-700	500-3300	75-450	50-1100
Model Stagnation Pressure Range (atm)		0.006-1.0	0.3-30	0.02	0.004-1.0
Model R_{eff} (ft)		0.172	0.172	0.0416-0.688	0.172
NUMBER TESTED					
Langley P-N Scout R/4B	35.5				65
Hughes P-N H-5	35.7			16	73
Avcoat 5026-39 HC/G	31				70
Modified Purple Blend E4A1	33.5				56
G.E. Silicone ESM1004AP	36.8				55
Teflon	135.6	76	7	16	5
High-Density Phenolic-Nylon	74.3	97	8		5

PARTICIPANTS

GDB, Ames - I, II C
MPDB, Ames - II C
AMPD, Langley - I, II B, II C
ESB, Langley - I, II C
MSC, Houston (supersonic) - II C
MSC, Houston (subsonic) - I, II C
FMD, Wright-Patterson AFB - I
Aerotherm - II C
AVCO - I, II A, II C
Boeing - I
General Dynamics - I
General Electric - I
Giannini - I, II C
Martin - I, II B, II C
North American - I
Space General - II C
Cornell - II A

I = Phase I, II A = Phase II - Task A

The participating organization then provided information on the test environment and the model response. Each facility was also requested to make a heating rate and pressure profile survey of the jet stream for each of the three test conditions.

1. Measurement of Test Environment

The tunnel operating conditions that were used for each ablation test are tabulated in Appendix B. The tables contain all data reported by the facilities in their original form; that is, if the facility reported the tunnel calibration data separately, they are listed separately in Appendix B. Some facilities with limited insertion capability combined calibration and run data, although these were obtained at different times. The tables contain pertinent footnotes on the facility measurement techniques.

Although the tunnel conditions and run times were specified by SRI, an effort was made not to influence the measurement techniques and methods used by each facility. The only instructions issued by the Institute covered the use of the SRI calorimeter and radiometer.

a. Enthalpy

Eight of the twelve participating facilities measured the average total enthalpy of the plasma stream with a single technique; three organizations used two methods; and one group used three methods.

Ten of the facilities measured the mean enthalpy of the plasma stream by the energy balance method; three groups used the sonic flow method; and two groups calculated a local enthalpy from the heat transfer data. Cornell calculated the enthalpy of the test gas in the Wave Superheater from the temperature and pressure of the helium driver gas.

None of the groups used an enthalpy probe to determine localized enthalpy, and while interest in this type of instrument is continuing, the results to date have been somewhat discouraging. The local enthalpy in the vicinity of the model can be inferred from the Fay-Riddell relation when flow is supersonic, and it was calculated from the heating rate and stagnation pressure traverses that were made at each facility. These traverses are reported in Section IV-A.

Some of the problems and difficulties encountered when measuring enthalpy by various methods are detailed below.

(1) Energy Balance Enthalpy. The majority of participants preferred the energy balance method of measuring enthalpy. The average enthalpy of the plasma stream was calculated by subtracting the heat losses in the arc generator and nozzle from the total input power and dividing the resulting net power by the mass gas flow. The power losses were determined by measuring the cooling water flow rates and the small temperature rise of the water as it passes through the apparatus. Some facilities used a thermopile arrangement of the thermocouples to increase the accuracy of the water temperature rise measurements. The energy balance method is simple in concept but may require from five to ten separate readings, each with its attendant error, and the accumulated errors can be considerable.

(2) Sonic Flow Enthalpy. The mean total enthalpy, h_t, of the jet can be calculated from the gas mass flow rate, W, the reservoir pressure, P_{t_1}, and nozzle throat area, A^*, according to the following relationship:[2]

$$h_t = (280 P_{t_1} A^*/W)^{2.5} \qquad (2)$$

One problem encountered with this method is the difficulty of measuring a true static chamber pressure, since most arc heaters are vortex or magnetically stabilized, which can result in a dynamic pressure component. Any measurement error is magnified when raised to the power indicated in equation (2). Another difficulty arises when the stream is not in chemical and thermodynamic equilibrium. A correction for frozen flow that increases with increasing enthalpy must then be added to the above relationship.

A modification of the sonic flow method was developed by R. Pope[3] of the Gas Dynamics Branch at Ames Research Center whereby the temperature of the gas in the reservoir prior to expansion in the nozzle is calculated. The calculation then permits the enthalpy of the plasma stream in the center-line area of the model to be determined.[4-6]

(3) Heat Flux Enthalpy. A local enthalpy of the plasma stream can be calculated from the cold wall heat flux using the relationships of Fay-Riddell[7] or Lees.[8] This method has the advantage of indicating an enthalpy in the same area of the stream as the ablating samples are

exposed to and will be described in Sec. IV-A. Its disadvantages are variations in the heat flux measurement resulting from geometry and recombination effects; these will be discussed later.

b. Heat Flux

The calorimeters that were used by the various facilities are described in Appendix A and in the footnotes to Appendix B. The details of these calorimeters are summarized in Table III. Five of the calorimeters were commercially available designs, primarily of the Gardon type, and seven were "in-house" designs. Five of the calorimeters were hemispherically shaped and seven were flat faced. A wide range of total diameter and sensing area diameters was present in the facility calorimeters. The calorimeter sensing areas were constructed of four different metals.

Table III

FACILITY CALORIMETER DESCRIPTION

FACILITY	CALORIMETER TYPE	CALORIMETER SHAPE	SURFACE MATERIAL	TOTAL DIAMETER (in.)	SENSING DIAMETER (in.)
SRI	Transient slug	Flat face	Nickel plate on copper	1.25	0.625
Ames Research Center-GDB	Transient slug	Hemisphere	Teflon coating on copper	0.75	0.313
Ames Research Center-MPDB	Transient slug	Hemisphere	Gold plate on copper	1.25	0.375
Langley Research Center-AMPD	Transient, thin-shell multiple TC's	Hemisphere	Stainless steel	2.0	2.0
Langley Research Center-ESB	Transient, thin-shell multiple TC's	Hemisphere	Stainless steel	1.5	1.5
Manned Spacecraft Center	Hy-Cal, asymptotic	Flat face	Constantan	1.25	0.15
Aerotherm Corp.	Hy-Cal, asymptotic	Flat face	Constantan	1.5	0.20
AVCO Corp.	Transient, long slug	Flat face	Copper	1.25	0.375
Giannini Scientific Corp.	Steady state	Hemisphere	Copper	0.625	0.625
Martin Co.	Thermogage, asymptotic	Flat face	Constantan	1.25	0.10
Space General Corp.	Hy-Cal, asymptotic	Flat face	Constantan	1.25	0.10
Cornell Aeronautical Lab.	Transient slug	Hemisphere with conical skirt	Copper	0.6	0.090

As pointed out earlier, each facility conducted heat flux traverses for each tunnel condition; the results are reported in Sec. IV-A.

(1) Transient Calorimeters. The majority of the transient calorimeters used during this study could be categorized as "medium-length" slug calorimeters, i.e., slug length of one-half to one times the slug diameter. These calorimeters were exposed to the plasma stream for a few seconds; the heat flux was determined from the slug temperature rise rate by a relation analogous to equation (1).

The two Langley facilities used a thin-walled, slug-type calorimeter containing a thin, stainless steel hemisphere instrumented with a number of thermocouples. This arrangement permitted determination of the heat flux distribution not only at the stagnation point but also over the hemisphere. The AVCO calorimeter was a specially designed, long-slug calorimeter, in which the thermocouple was mounted in a 1.5-in.-long copper slug, 0.020 in. from the front sensing surface. The temperature rise rate was evaluated with a computer program to calculate the cold wall heat flux.

(2) Steady-State Calorimeters. The steady-state calorimeter used by Giannini was a water-cooled, temperature-rise type. The heat flux was calculated with the relation:

$$\dot{q}_{CW} = (\dot{w}C_p\Delta T)/A \qquad (3)$$

where

$\dot{w}$ = cooling water flow rate—lb/sec

C_p = heat capacity of water—Btu/lb°F

ΔT = temperature rise of the cooling water—°F

A = sensing area—Ft^2

Since the sensing area covered the entire hemisphere, they corrected the average heat flux to center-line stagnation conditions with the special relation $\dot{q}_{CW} = 2.1\dot{q}_{\substack{AV \\ CW}}$.

The majority of the steady-state calorimeters used during this study were of the Gardon or asymptotic types manufactured by either Hy-Cal or Thermogage. The heat flux was determined by measuring the temperature difference between the center and the cooled periphery of a thin constantan disc. A small-diameter copper wire was connected to the center of the disc and the disc periphery was welded to the cooled copper shroud, forming the hot and cold thermocouple junctions. The radial temperature difference on the disc is a function of heat flux, disc thickness, diameter, and thermal properties. Since the last three factors are constant for a given instrument, the heat flux can be calculated from the millivolt difference between the two thermocouple junctions.

c. Pressure

Because the Phase I study revealed a good correlation between the SRI uncooled pitot probe and the various facility probes, it was decided not to include an SRI pressure probe in this study. Therefore, all model stagnation values listed in Appendix A were measured with the facility pitot probes and pressure gauges or transducers. The majority of the pitot probes were water-cooled, flat-faced cylinders ranging in size from 0.375 to 0.75 in. in diameter. The stagnation pressure P_{t_2}, was measured with a wide variety of gauges and transducers, as described in Appendix A. Stagnation pressure traverses of the plasma jet were made at each facility for each tunnel condition; the results are reported in Section IV-A.

The expansion of the jet through the nozzle was controlled at most facilities by bleeding air into the test section or by throttling the vacuum line. Some facilities monitored the jet expansion by matching the test chamber pressure to the nozzle exit pressure, and the remainder of the groups monitored the stream visually.

2. Measurement of Model Response

Measurements of model response were made both during the run and after its completion. These include model temperatures as well as physical changes in the model.

a. Front Surface and Internal Temperature

To reduce the scatter of front surface temperature data that was experienced during the first round robin, eleven facilities were supplied with identical, calibrated total radiation pyrometers. They were also sent suggestions for mounting the pyrometer in the tunnel and instructions for the use of the instrument.

In most cases, a facility pyrometer was used in addition to the SRI radiometer; however, Ames-GDB also used a total radiation pyrometer. Most facility instruments were either manual or automatic monochromatic optical pyrometers. All the instruments measured the brightness temperature of the model surface, and the results were reported assuming an emissivity of unity.

The Langley-AMPD group used a photographic pyrometer that viewed the entire model surface and made exposures at frequent intervals. The surface temperatures were then measured from densitometer traces of the developed film. Internal temperatures were measured at eight facilities which had the capability of connecting the model thermocouples to instrument leads in the insertion probe. The output of the thermocouples was then fed into a continuous multichannel recorder.

These model temperatures were received from the facilities in the form of graphs of temperature versus time. Since reproduction of these graphs in their entirety was impractical, sufficient data were taken from them to allow redrawing of the original curves. These data are tabulated in Appendix C.

b. Mass and Length Changes

A preliminary check indicated that the model core weights of the low-density materials were not constant under varying ambient conditions. Consequently, a study was made of the equilibrium water content of the five low-density materials at various relative humidities; the results are shown in Fig. 5. As a result of the study, it was decided to equilibrate the model cores to 50 percent relative humidity before and after testing. The length and diameter of all model cores were measured and the cores conditioned for 24 hours at 50 percent relative humidity and 70-75°F before weighing on an analytical balance. The model was then assembled, reweighed, and its total length determined with a dial micrometer.

The facility determined the model recession and the total model weight loss after completion of the test. The models were returned to the Institute, and the total model weight loss and front surface recession were again measured. Model base plates were removed and the recession of the front surface of the core rechecked. The model core was pressed out of the shroud, reconditioned as described above, and the weight loss of the core determined. The core char cap was removed and the substrate scraped back to the start of the pyrolysis zone. The cores were reweighed and measured so that char weight, thickness, and density could be calculated.

The measurements made at SRI on the models are listed in the last five columns of the tables in Appendix B. The weights listed in the tables are for the 0.625-in.-diameter (0.00213 ft^2 cross-sectioned area) cores, except where noted. Mass loss rates were determined for each material and each tunnel condition and are listed in Appendix D with other derived information. For cases when two models with varying run times were tested, the mass loss rate was calculated as the slope between the two data points. When three or more samples were run, the mass loss rate was determined from the slope of the best straight line through the data. In a very few instances the mass loss rate was determined from a single run, and for these cases the slope was assumed to pass through zero.

c. Char Density

The variation in char density from the front surface to the virgin-material interface was measured on a few samples using an X-ray measurement technique that was developed at SRI. A 0.5-in.-wide × 0.1-in.-thick sample including the char was cut along the center line from the front to the back of the ablated model core. The char layer was then scanned from the front surface to the virgin material with a 0.250 × 0.003-in.-thick X-ray beam normal to the original model core axis. Attenuation of the X-ray beam indicated the char density profile.

3. Test Procedure

The tunnel operating variables such as power and gas flow rate were established by trial and error at each facility to meet the tunnel condition requested by the Institute. The facility was allowed to match either the requested enthalpy and stagnation pressure or a specified heat flux and pressure.

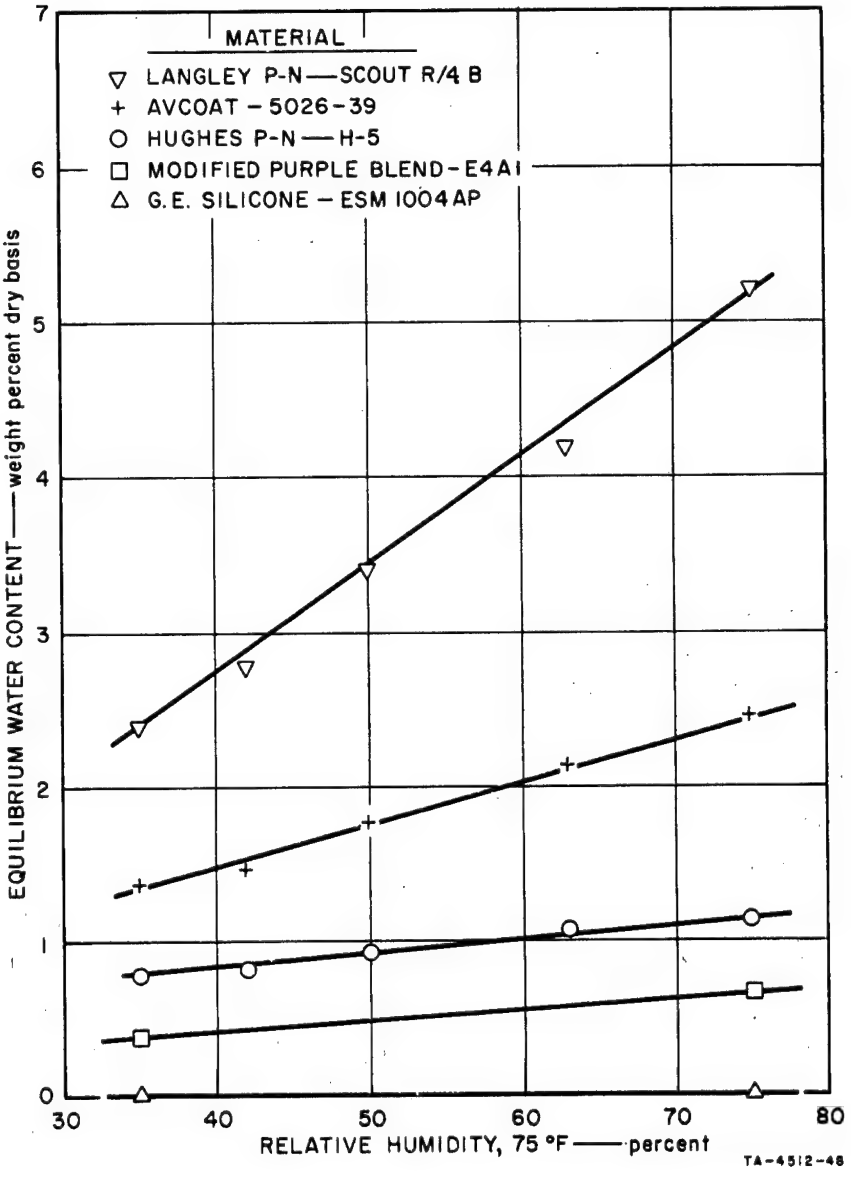

FIG. 5 EFFECT OF HUMIDITY ON WEIGHT OF MATERIALS

The sequence followed by the facility in measuring the requested tunnel variables was largely dictated by the number of instruments that could be sequentially inserted into the plasma stream during a single run. We have termed this the "tunnel insertion capability," and it refers to the number of model supports in the test chamber. Tunnels with four supports could make all requested measurements during a single start-up;facilities with fewer supports required progressively more runs to obtain the required information. The relative reproducibility of a facility's results is, of course, dependent on the run-to-run variation in tunnel conditions compared to the variations during a single-run.

Table IV is a summary of the operating sequence followed at each facility for calibrating the tunnel conditions and testing the ablation models.

Table IV

SEQUENTIAL ORDER OF TEST MEASUREMENTS

FACILITY	REFERENCE (APPENDIX TABLE NUMBER)	NUMBER OF INSERTIONS	DATA DETERMINED DURING SAME RUN			
			$\dot{m}_t$ $\dot{q}_{SRI}$ $\dot{q}_{FAC}$ P_{t_2}	$\dot{m}_t$ $\dot{q}_{SRI}$ P_{t_2}	$\dot{m}_t$ $\dot{q}_{FAC}$ P_{t_2}	$\dot{q}_{SRI}$ $\dot{q}_{FAC}$ P_{t_2}
Ames-GDB	B-1	8	M			C
Ames-MPDB	B-2	5	M			C
Langley-AMPD	B-3	2		M		
Langley-ESB	B-4	2	I			
Manned Spacecraft Center	B-5	2			M	C
Aerotherm Corp.	B-7	5	M			C
AVCO Corp.	B-8	1	II			
Giannini Scientific Corp.	B-9	3			M	C
Martin Co.	B-10	5	M			
Space General Corp.	B-11	4			M	C
Cornell Aeronautical Lab.	B-12	1	II			

M - Model runs.

C - Calibration runs.

I - $\dot{q}_{SRI}$, P_{t_2} estimated and reported from calibration runs.

II - $\dot{q}_{FAC}$, $\dot{q}_{SRI}$, P_{t_2} estimated and reported from calibration runs.

IV EXPERIMENTAL RESULTS

The results of the experimental program covered three broad areas: test environment, high-density materials, and low-density materials, these are covered in the following sections. The test environment is not only measured, but the various techniques and instruments for determining its parameters are cross-compared. The ablation behavior of the high-density materials is described and correlated with the results from the Phase I program. The ablation behavior of the low-density materials is described in more detail, and correlations for these results are suggested.

A. Evaluation of Test Conditions

The matrix of test conditions for the second round robin was designed by selecting three test conditions for each participating group that would utilize the full range capability of the facility and at the same time provided the widest distribution of test conditions for all facilities. The distribution of test conditions used in the Phase II round robin is shown in Fig. 6. Also shown in the figure is the envelope of the conditions for the Phase I round robin.

Since the ablation of Teflon and high-density phenolic-nylon had been investigated during the first round robin in the low and medium pressure range, testing of these materials was restricted primarily to the 0.3 to 30 atm stagnation pressure range. The five new low-density materials had been designed for low pressure applications and were therefore tested primarily in the 0.004 to 0.7 atm pressure range.

During the first round robin, the model stagnation pressure measured with an SRI pitot probe of the same geometry as the ablation models was compared to the stagnation pressure measured with the facility pitot probe. The results were in excellent agreement and therefore this comparison was not in the Phase II round robin. Instead a stagnation pressure and heating rate traverse of the plasma streams was substituted.

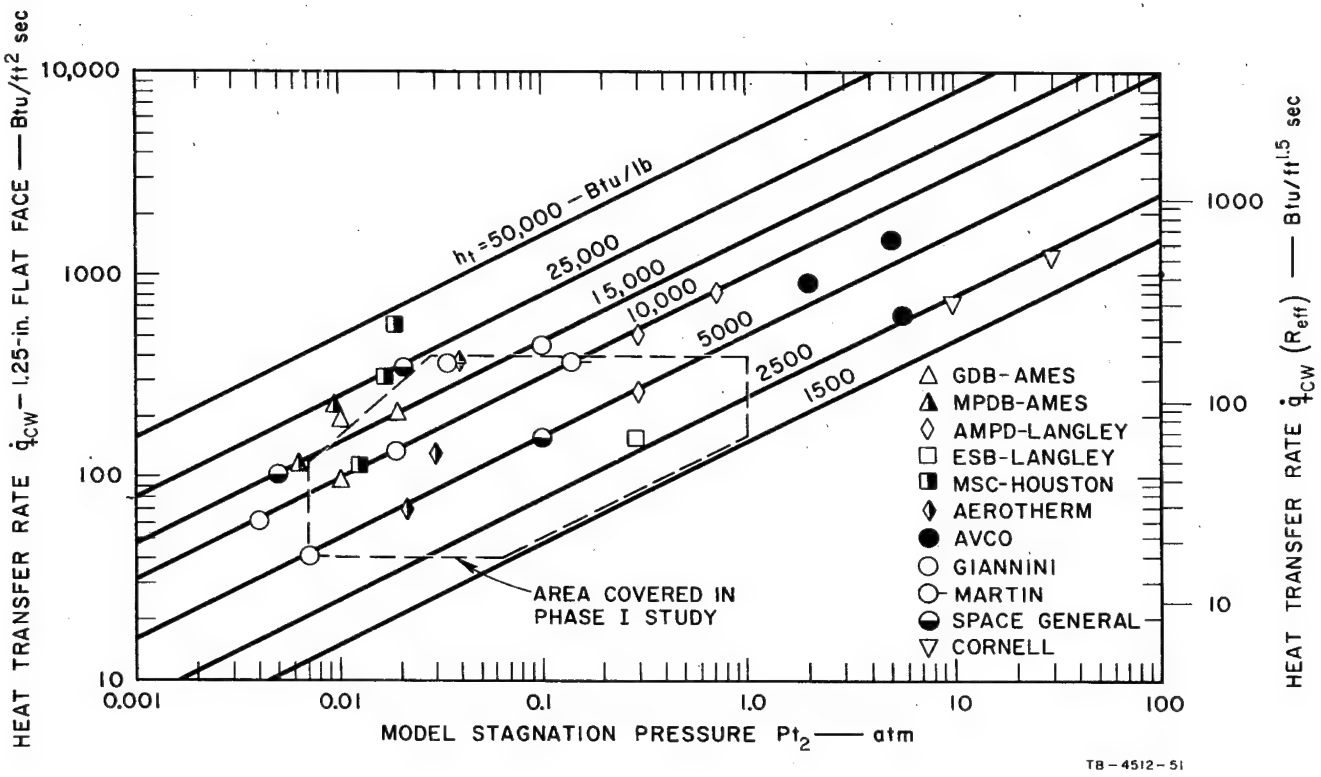

FIG. 6 TEST CONDITIONS FOR PHASE II ROUND ROBIN

1. Plasma Stream Uniformity

The results of the plasma stream traverse of heating rate and model stagnation pressure at each facility are shown in Figs. 7 through 16. These plots were prepared by normalizing the local measured heating rates at various distances from the nozzle center line in terms of the measured heating rate at the center-line position. The same procedure was followed for the model stagnation pressures.

A 1.25-in.-diameter ablation model, drawn to the same scale as the nozzle exit diameter, is shown at the top of each plot to indicate the stream uniformity in the area of the model and core. A scale sketch of the calorimeter, showing its shape, total diameter, and sensing diameter, is also included at the top of each plot.

The nonuniformity of the plasma stream can result from a variety of causes such as heat losses to the nozzle wall, nozzle expansion characteristics, pressure mismatch between the nozzle exit and the test chamber, method used to stabilize the arc, and the position of the measuring instrument. It is impossible to generalize on the causes for the stream nonuniformities shown in Figs. 7-16. One may only state that these were the measured heating rates and pressures for a particular apparatus, tunnel operating condition, and model geometry.

Actually, for this particular series of tests, the plasma streams were apparently quite uniform in the center-line area where the model cores were located. An average of all the participating groups indicated that the heat flux at the model core outer diameter (0.625 in.) was 99 percent of the center-line heat flux. The stagnation pressure at the same point was 97 percent of the center-line value. At the model outer, or shroud diameter (1.25 in.), location the average heat fluxes were 89 percent of center-line values and average pressures were 85 percent of those at the center. The dropoff in heating rate when moving out of the center of the plasma stream is somewhat compensated for with the flat-faced shape which gives a higher heat flux at its periphery. This is indicated in Fig. 17 (Graph A) which shows the heat flux at various positions on the hemispherical and flat-face calorimeters used by the Martin Company in the study of varying model diameter. This plot is in reasonable agreement with the results of Marvin and Sinclair.[9] Graph B of Fig. 17 shows the plasma stream uniformity at the same facility.

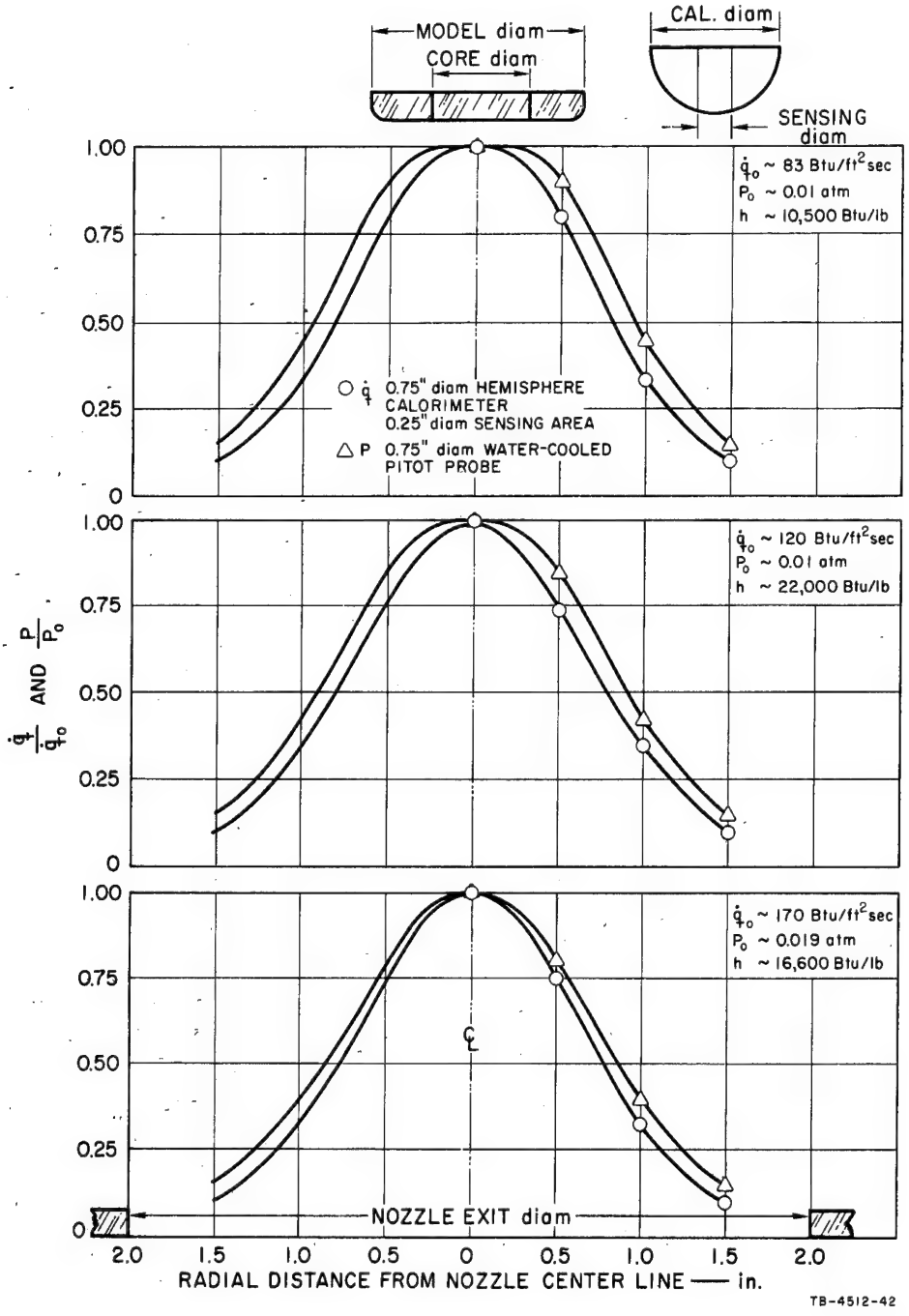

FIG. 7 PLASMA STREAM UNIFORMITY AT GAS DYNAMICS BRANCH, AMES RESEARCH CENTER

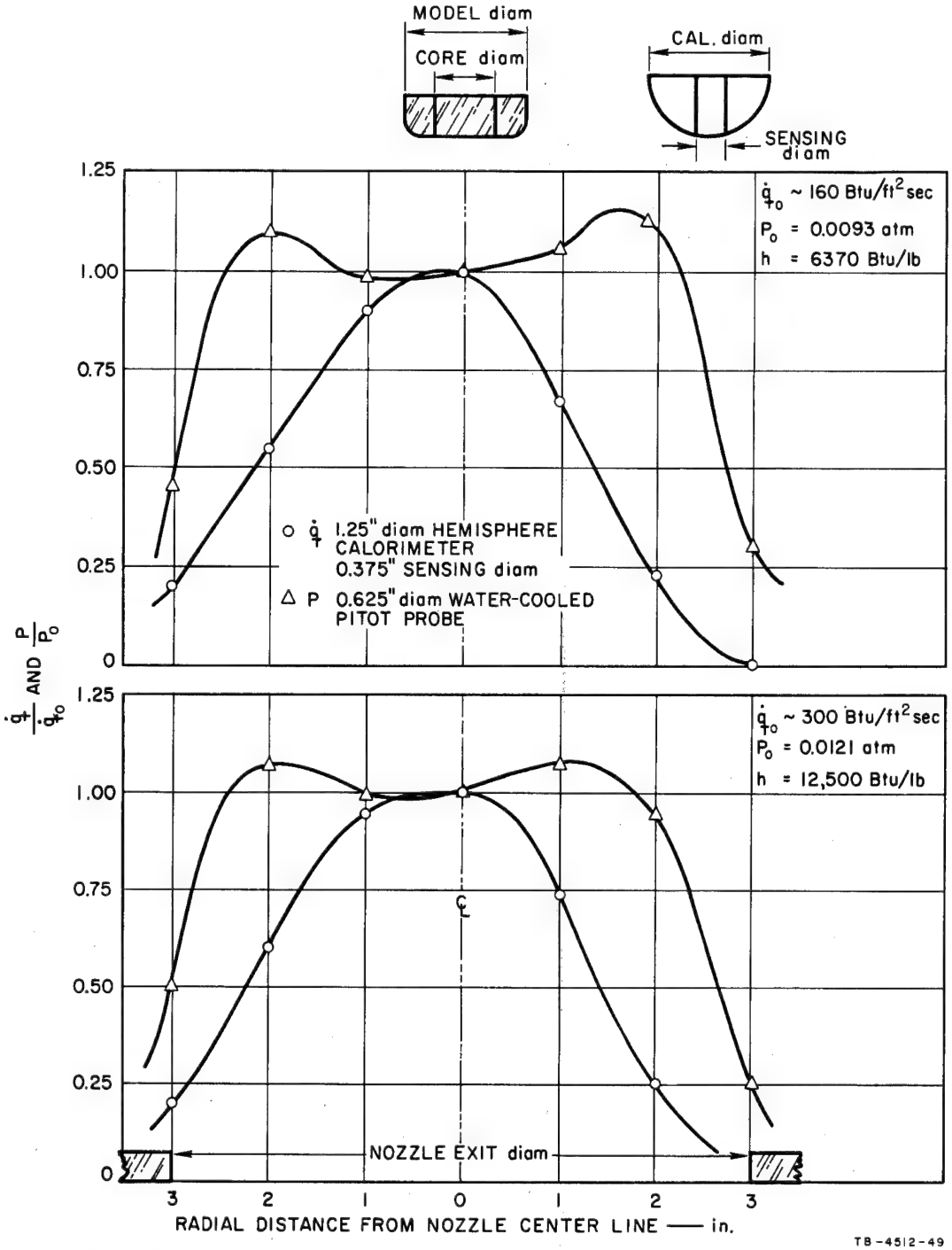

FIG. 8 PLASMA STREAM UNIFORMITY AT MAGNETO PLASMA DYNAMICS BRANCH, AMES RESEARCH CENTER

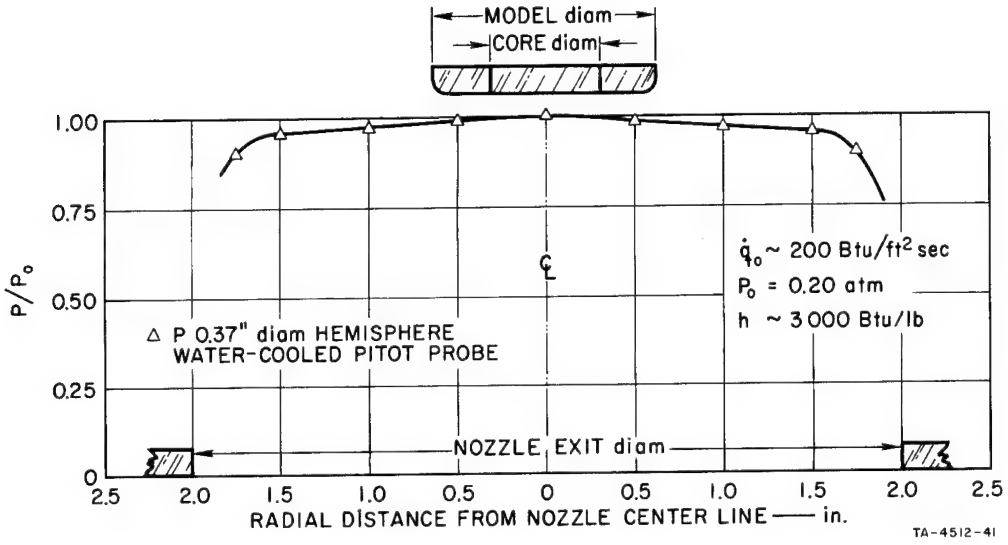

FIG. 9 PLASMA STREAM UNIFORMITY AT ENTRY STRUCTURES BRANCH, LANGLEY RESEARCH CENTER

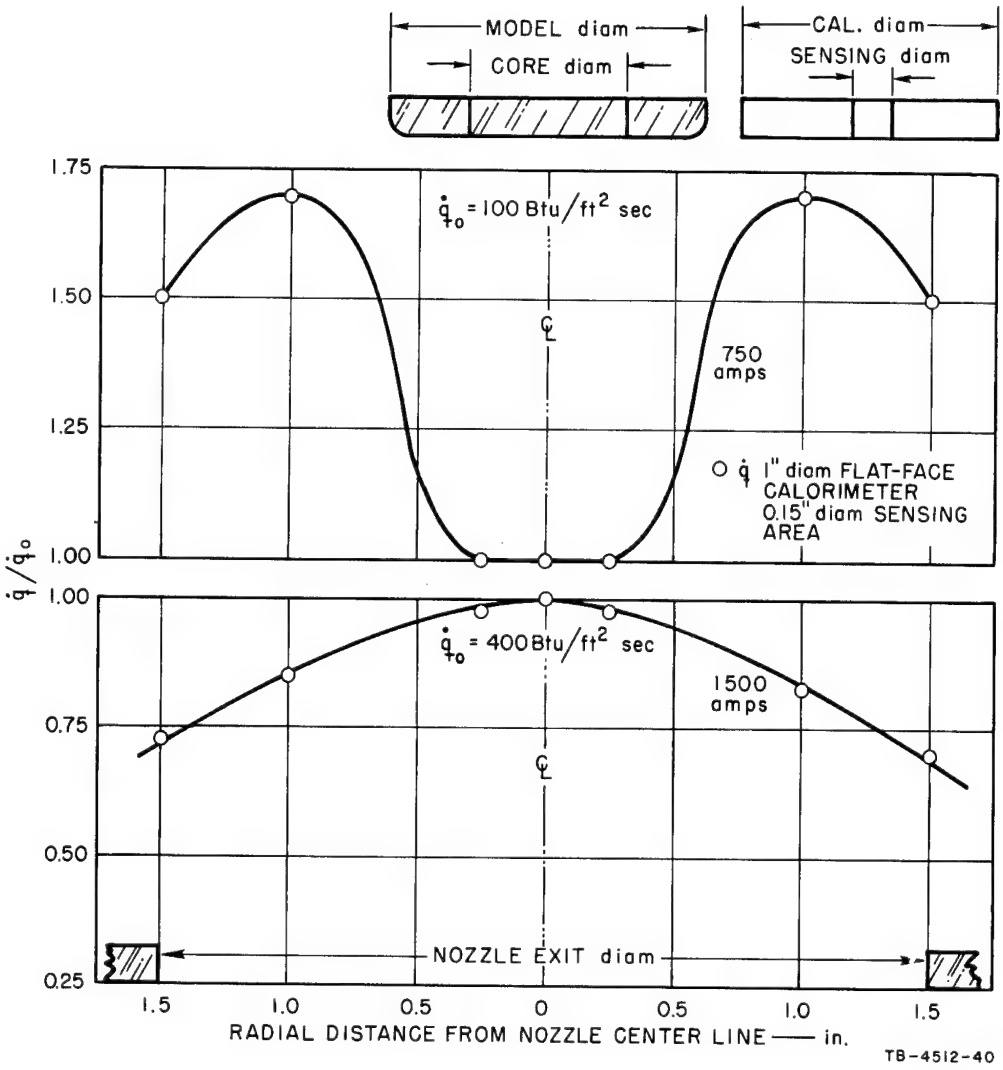

FIG. 10 PLASMA STREAM UNIFORMITY AT MANNED SPACECRAFT CENTER (Subsonic Facility)

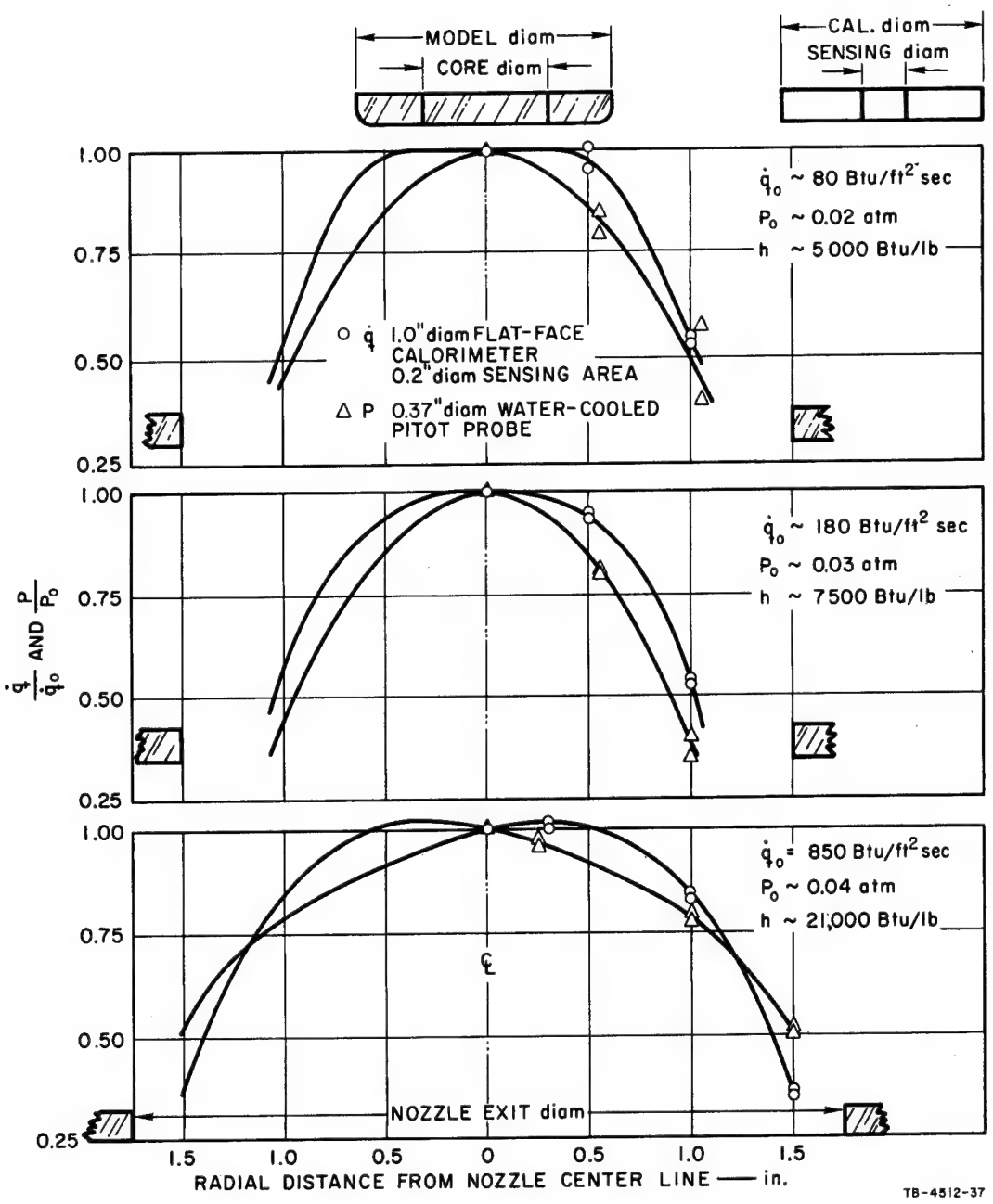

FIG. 11 PLASMA STREAM UNIFORMITY AT AEROTHERM CORPORATION

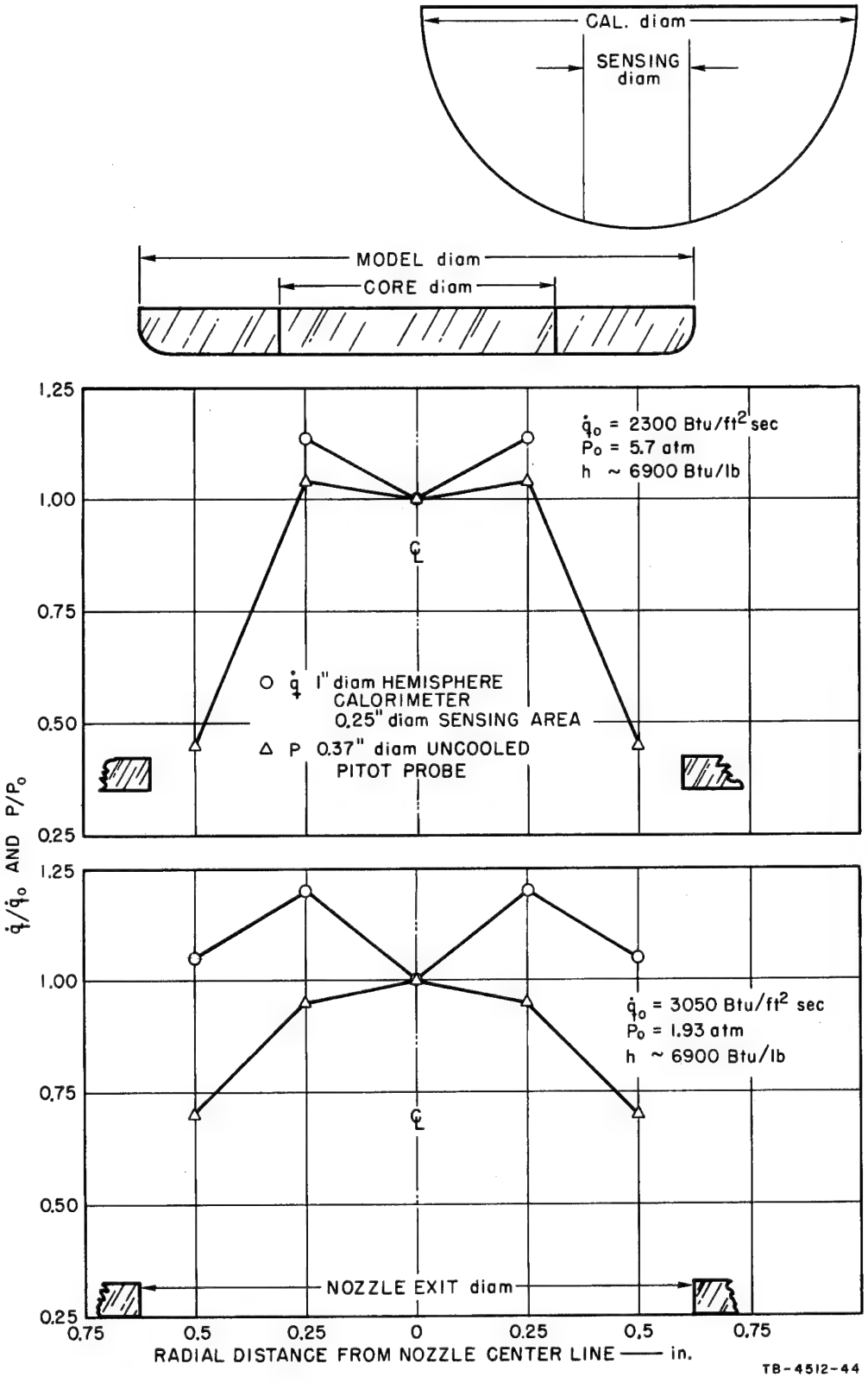

FIG. 12 PLASMA STREAM UNIFORMITY AT AVCO (10-Mw Facility)

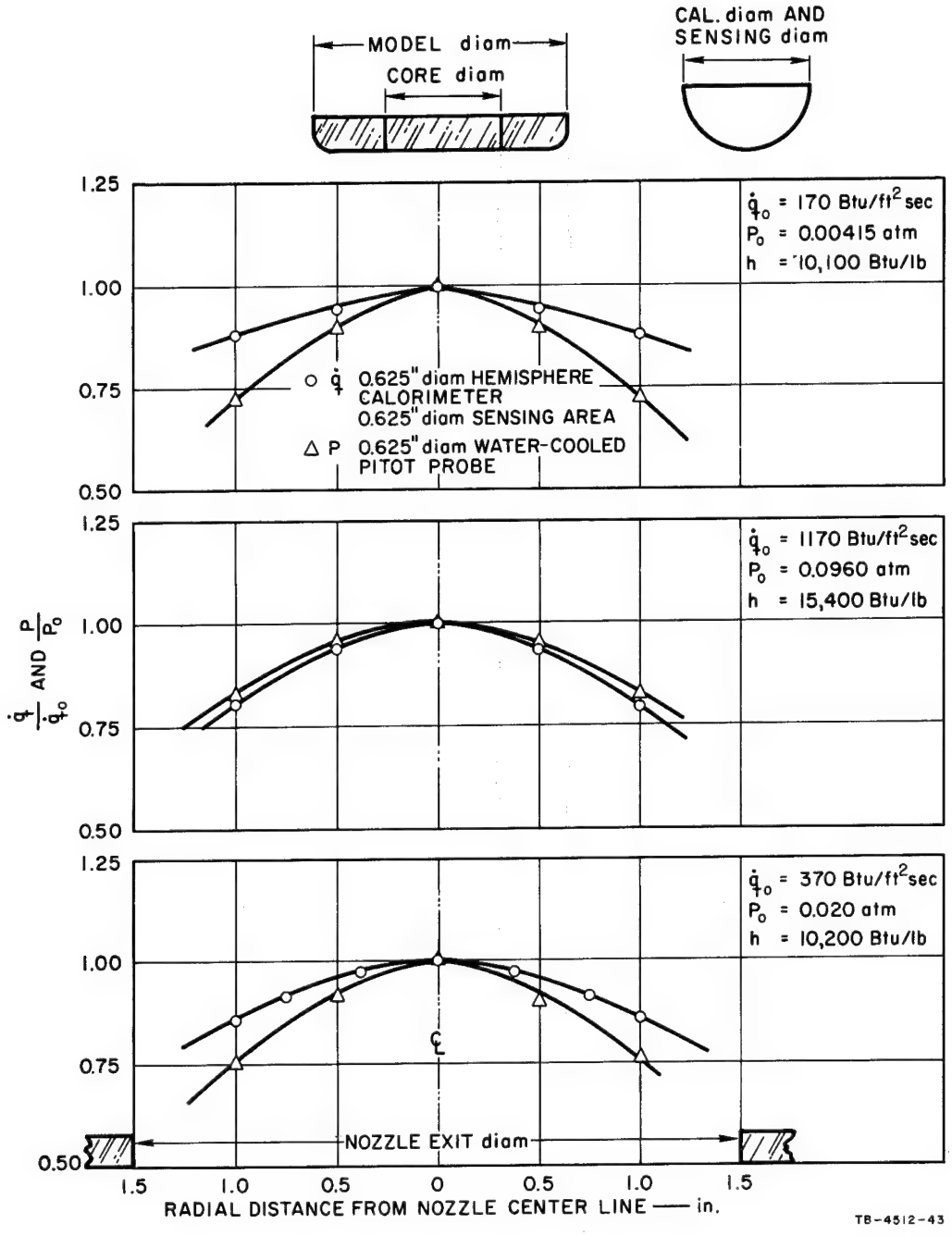

FIG. 13 PLASMA STREAM UNIFORMITY AT GIANNINI SCIENTIFIC CORPORATION

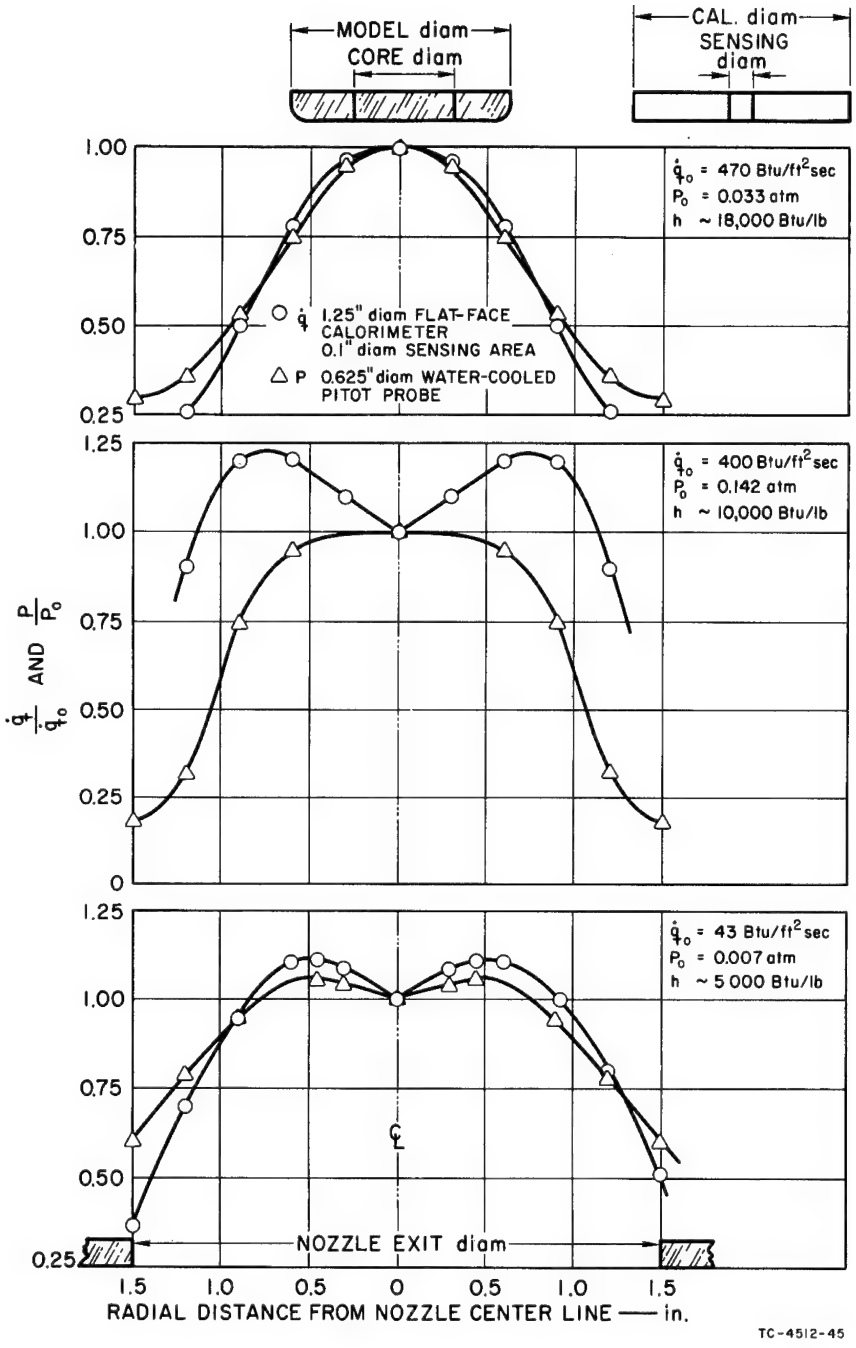

FIG. 14 PLASMA STREAM UNIFORMITY AT MARTIN COMPANY

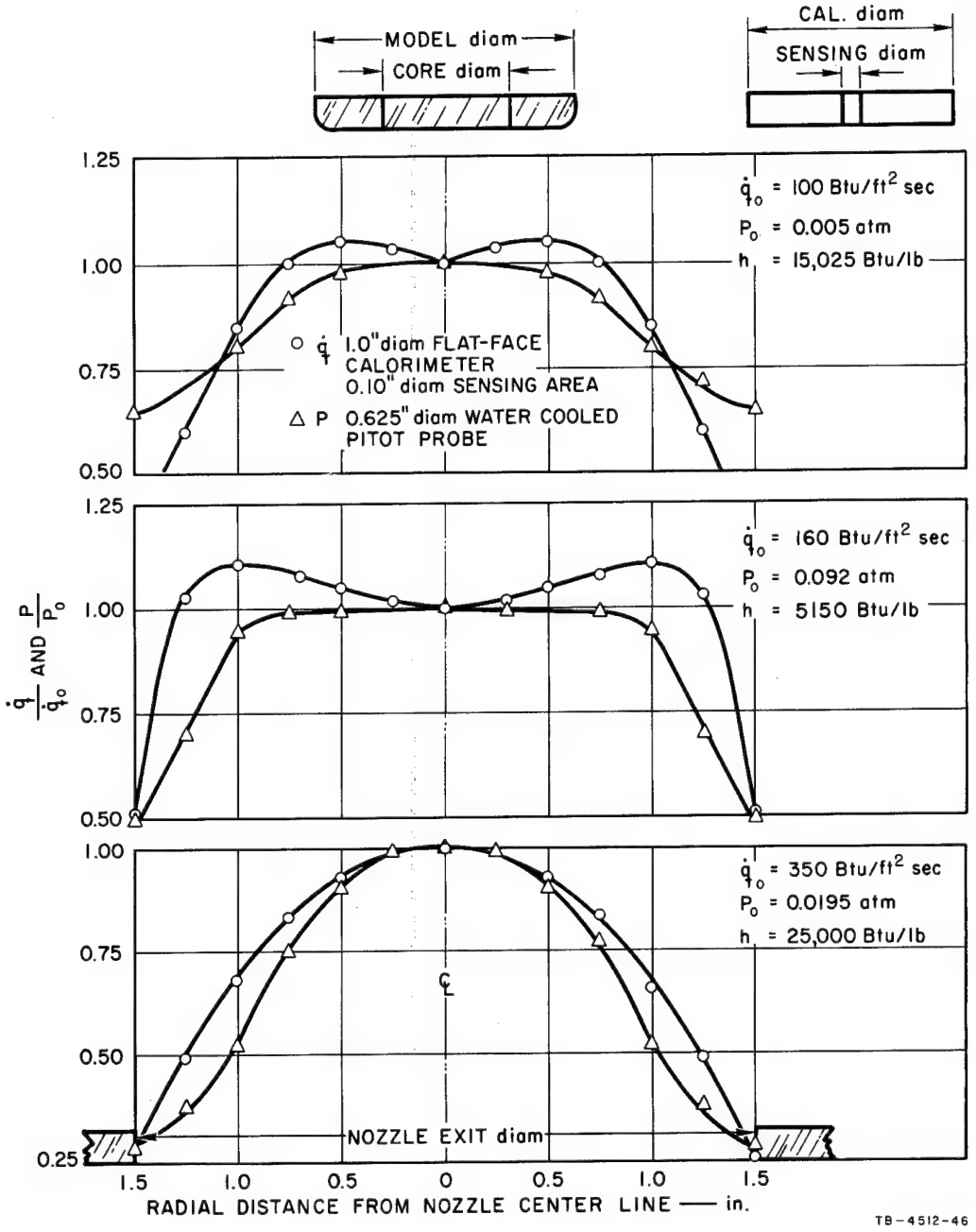

FIG. 15 PLASMA STREAM UNIFORMITY AT SPACE GENERAL CORPORATION

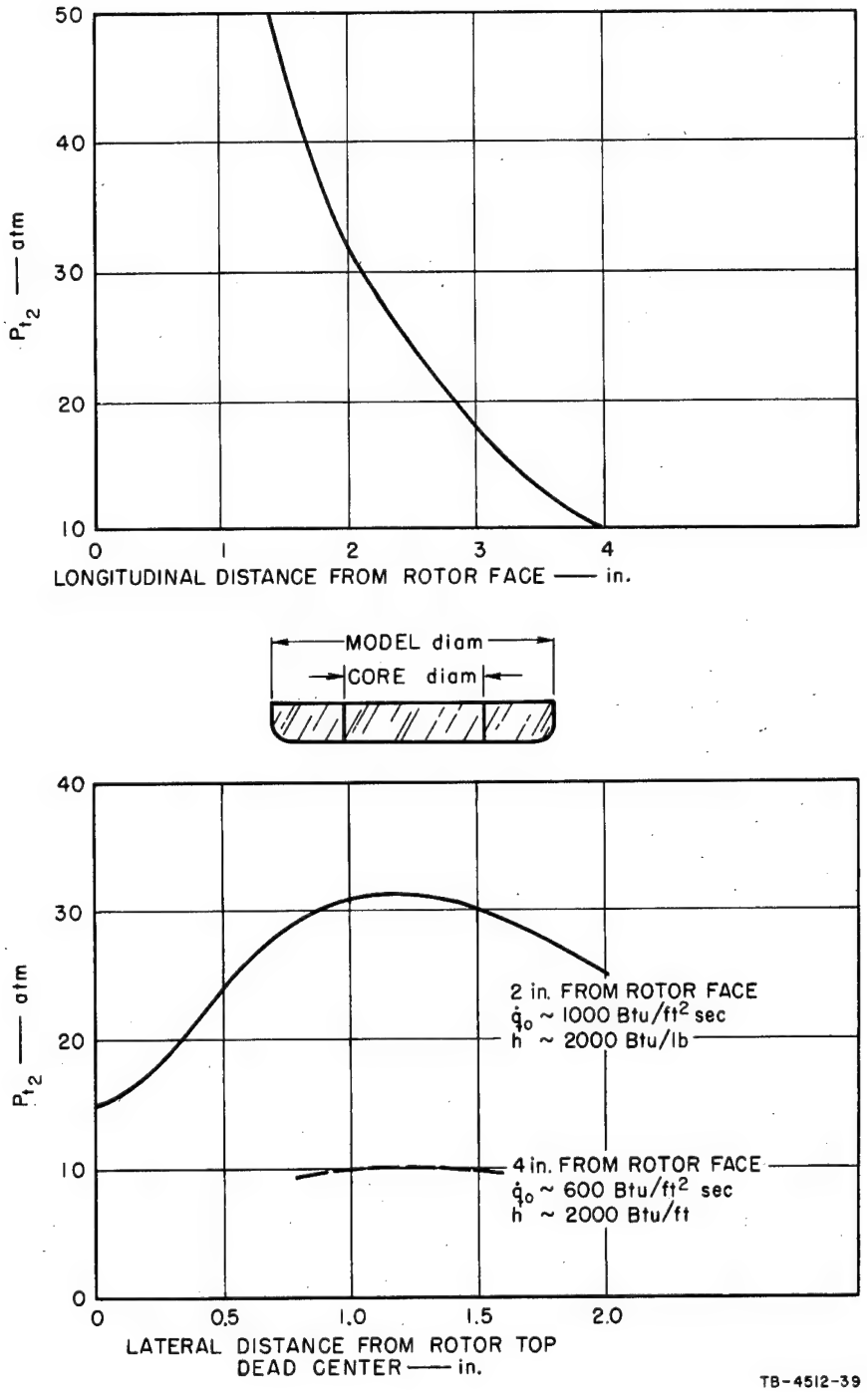

FIG. 16 PLASMA STREAM UNIFORMITY AT CORNELL AERONAUTICAL LABORATORY

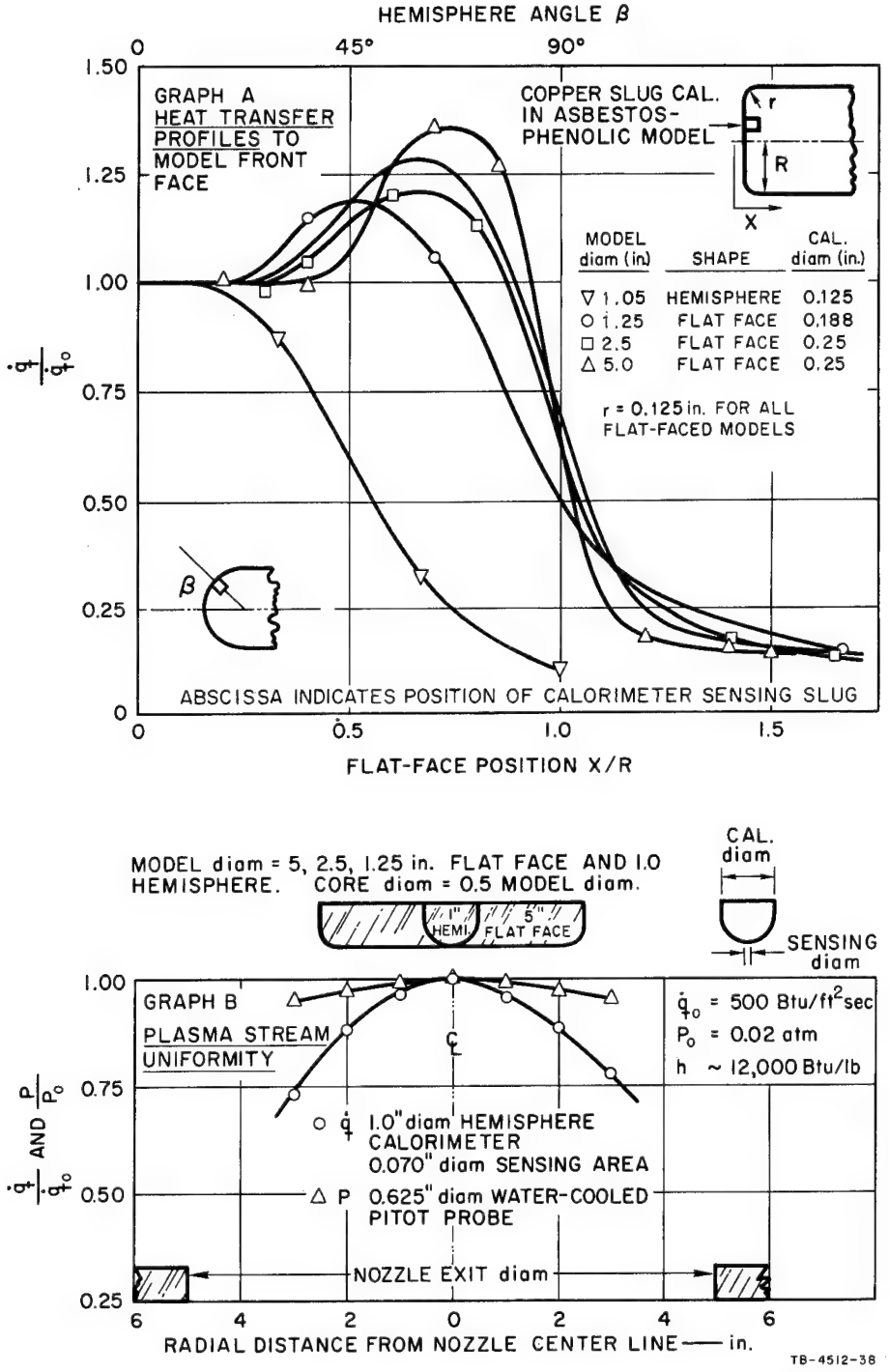

FIG. 17 HEAT TRANSFER PROFILE ACROSS MODEL, AND PLASMA STREAM UNIFORMITY AT THE MARTIN COMPANY

The chemical nonuniformity of the plasma streams was not studied during this work, but the Giannini group, which has conducted such studies, reported that a varying oxygen-to-nitrogen ratio can exist across the stream depending on where and how the oxygen enters the stream. The oxygen level of the test stream will of course have a marked effect on the material ablation rate.

Probably the greatest significance of the plasma stream traverse is that the average stream enthalpy measured by an energy balance does not represent the center-line enthalpy where the model is being tested.

2. Stagnation Point Heating Rate

As stated previously, the cold wall heat flux was measured at most facilities with both a facility calorimeter and the SRI calorimeter. The calorimeter designs differed both from facility to facility and from the SRI design. The main differences in calorimeter designs were shape, total diameter, sensing diameter, and the surface material of the sensing area.

a. Effect of Calorimeter Design

Ideally, the calorimeter used to measure cold wall heat flux should have the same shape and dimensions as the ablation models being tested. Unfortunately each set of ablation models may differ, and the usual practice is to recalculate the measured calorimeter heat flux to conform to the model shape and size. Selection of a calorimeter is further complicated because for a task such as a stream traverse it might be desirable to have a small diameter hemispherical shape, whereas for model testing, and to reduce the surface catalytic effect, it would be desirable to have a larger diameter calorimeter.

(1) Shape and Diameter Corrections. The shape and diameter of a calorimeter determine the velocity gradients over its surface and thus the heat flux to the surface. It is generally accepted that under supersonic conditions the heat flux to different sized calorimeters with the same shape will vary inversely with the square root of the calorimeter radius, R, or diameter, D, according to the following relation:

$$\dot{q}_1/\dot{q}_2 = (R_2/R_1)^{0.5} = (D_2/D_1)^{0.5} \qquad (4)$$

where the subscripts designate two different calorimeters.

The above relationship was used to correct the facility heat flux data when the facility calorimeter was flat faced and had a different diameter than the SRI model.

Heat transfer relationships such as the one proposed by Fay-Riddell[7] are based on the heat flux to a hemispherical shape. Thus, the effective radius, R_{eff}, equals the hemispherical radius. Heat transfer to other shapes may be expressed as some fraction of the heat flux to an equal radius but hemispherical body. Equivalently a correction may be made to the actual radius to give the R_{eff}.

At the completion of the first round robin, the facility heat flux data for hemispherical calorimeters were compared to the SRI flat-faced calorimeter and were found to effectively follow the relations:

$$\dot{q}_{FF} = 0.55\ \dot{q}_{H}$$

$$R_{eff} = 3.3\ R_{FF}$$

These results agreed well with the data of Stoney and Markly[10] and were used to adjust facility hemispherical calorimeter results to the SRI shape.

In the Phase II round robin most facility calorimeters were flat faced and required only diameter corrections. In addition, the two Ames facilities corrected their hemispherical calorimeter results with factors that they had previously established experimentally. The few remaining facility hemispherical calorimeters were corrected using the same factors that were used in the Phase I round robin.

(2) Surface Catalytic Effects. In the area of materials evaluation, the plasma arc has been the most versatile test device developed for reproducing free flight heating conditions. There are, however, obvious differences between ground test conditions and free flight conditions. In free flight the air preceding the vehicles shock wave is at rest and at chemical equilibrium, except at extreme altitudes. In arc plasma testing, the model is stationary, and the test gas preceding the model shock wave has been preheated to a very high temperature level and then expanded to low pressure to simulate free flight conditions. The high gas temperature, together with this expansion through a supersonic nozzle to obtain high velocity, can give a plasma stream that is not in chemical

equilibrium. This is particularly true with large expansion ratios. Recombination of the dissociated gas molecules behind the model shock wave thereby influences the heat flux to the calorimeter or model. The recombination mechanism has not been fully quantified but is known to be a function of the atomic concentration and gas density in the boundary layer, the wall temperature, model geometry, and wall catalytic activity.[11]

The amount of heat released by catalytic recombination becomes important when the heat flux measurements are used to calculate the enthalpy in the center of the nonequilibrium plasma stream at the model location. Heat transfer relationships such as Fay-Riddell assume an infinitely catalytic surface and complete recovery of all energy. Metal calorimeter surfaces have varying finite catalytic reaction rate constants, and the measured heat flux will be less than that for infinitely catalytic surfaces. Further, for a given surface material, the ratio of measured heat flux to the heat flux at a fully catalytic surface will increase with increasing stream density and calorimeter diameter, and the ratio will decrease with increasing enthalpy and wall temperature.

The Gas Dynamics Branch of Ames Research Center conducted a study of the effect, on the measured heat flux, of calorimeter surface catalytic activity and some of the other variables noted above. During the study, the Ames copper-surface calorimeter and the SRI nickel-surface calorimeter were exposed to a range of enthalpies (8000 Btu/lb and greater) at two stagnation pressures. Identical calorimeters that had been sprayed with a thin coating of Teflon were also exposed to the same conditions. These tests were performed at a relatively high expansion ratio.

The results of the study are shown in Fig. 18, in which the ratio of measured heat flux, $\dot{q}_{meas}$, to the heat flux for an infinitely catalytic surface, $\dot{q}_{k_w \sim \infty}$, is plotted versus the total stream enthalpy as determined by the modified sonic flow method (see footnote 2, Appendix B-1). The value of $\dot{q}_{k_w \sim \infty}$ was calculated using the Fay-Riddell relation and the total stream enthalpy reported by Ames with their experimental relation of $R_{eff} = 2.91\ R_{FF}$. It should be noted that the higher pressure runs shown in the figure were made by entering part of the gas at the plenum location, thereby changing the equilibrium condition and giving an accentuated effect of stagnation pressure on the heat flux ratio, $\dot{q}_{meas}/\dot{q}_{k_w \sim \infty}$.

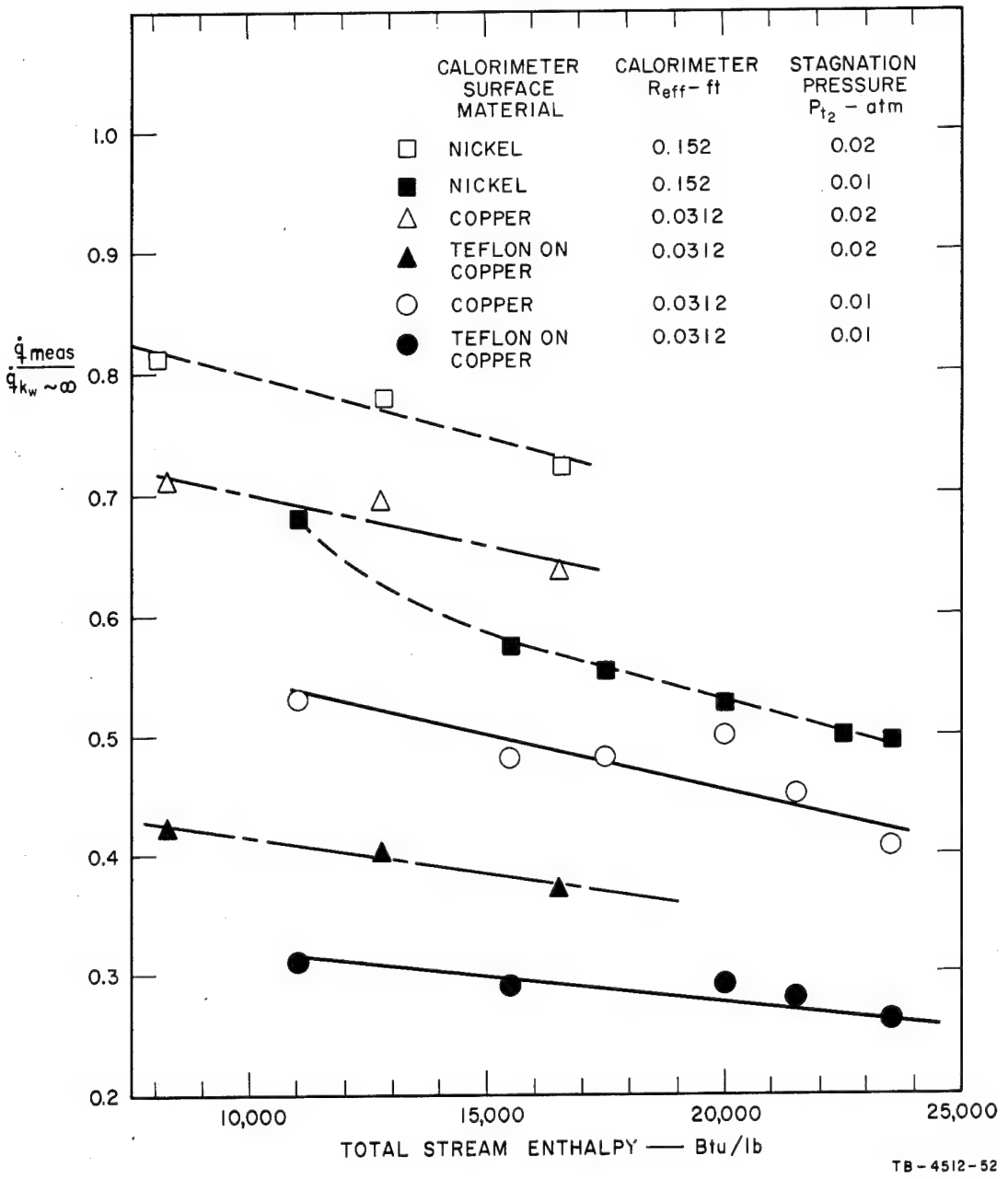

FIG. 18 EFFECT OF CALORIMETER DESIGN ON HEAT FLUX MEASUREMENTS IN A NONEQUILIBRIUM STREAM

The data were also used by Ames to estimate the catalytic reaction rate constant, k_w, for each surface. The k_w was found to be 500 to 700 cm/sec for copper, 300 cm/sec for nickle, and to be much lower for Teflon; the values for the metals agree with those of Goulard.[11]

The results indicate the importance of calorimeter surface catalytic activity, calorimeter geometry, and stream conditions on the measured heat flux. No simple correlation of all variables has been developed to date; however, studies in this field are now under way. The general conclusions at this time are that, when the arc generator-nozzle system tends to lead to a nonequilibrium plasma, the calorimeter surface should be a clean metal having high catalytic activity such as silver, copper, or nickel. Further, the calorimeter diameter should be as large as is practicable. Finally, an indication of the stream nonequilibrium condition can be obtained by comparing the measured flux to a catalytic metal surface to the heat flux measured with an identical calorimeter that has been sprayed with a thin coating of Teflon to give a noncatalytic surface. This, of course, is not possible at high heat fluxes where the Teflon would sublime rapidly.

b. Comparison of Results

Using the correction techniques discussed above, the measured facility heat flux data were adjusted to the 1.25-in.-diameter SRI model shape. The facility and SRI calorimeter results are compared in Fig. 19, the standard deviation was found to be 13 percent. These results are a slight improvement over the first round-robin data, which showed a standard deviation of 16 percent.

The Cornell data gave the greatest deviation, with the SRI calorimeter reading about 1.6 times the Cornell value. Cornell reported that they have previously experienced even higher readings at high pressure conditions with calorimeters which are similar to the SRI design but which have an air gap surrounding the slug. Apparently the high pressure gases flow through this air gap and can preferentially heat the thermocouple junction, thereby giving a high temperature rise rate. The problem may be further accentuated by the nonsymmetry of the stream at this facility. Cornell solves this problem by filling a short section of the air gap with a refractory cement. However, this solution is not completely satisfactory, since increased contact between the slug and the shroud

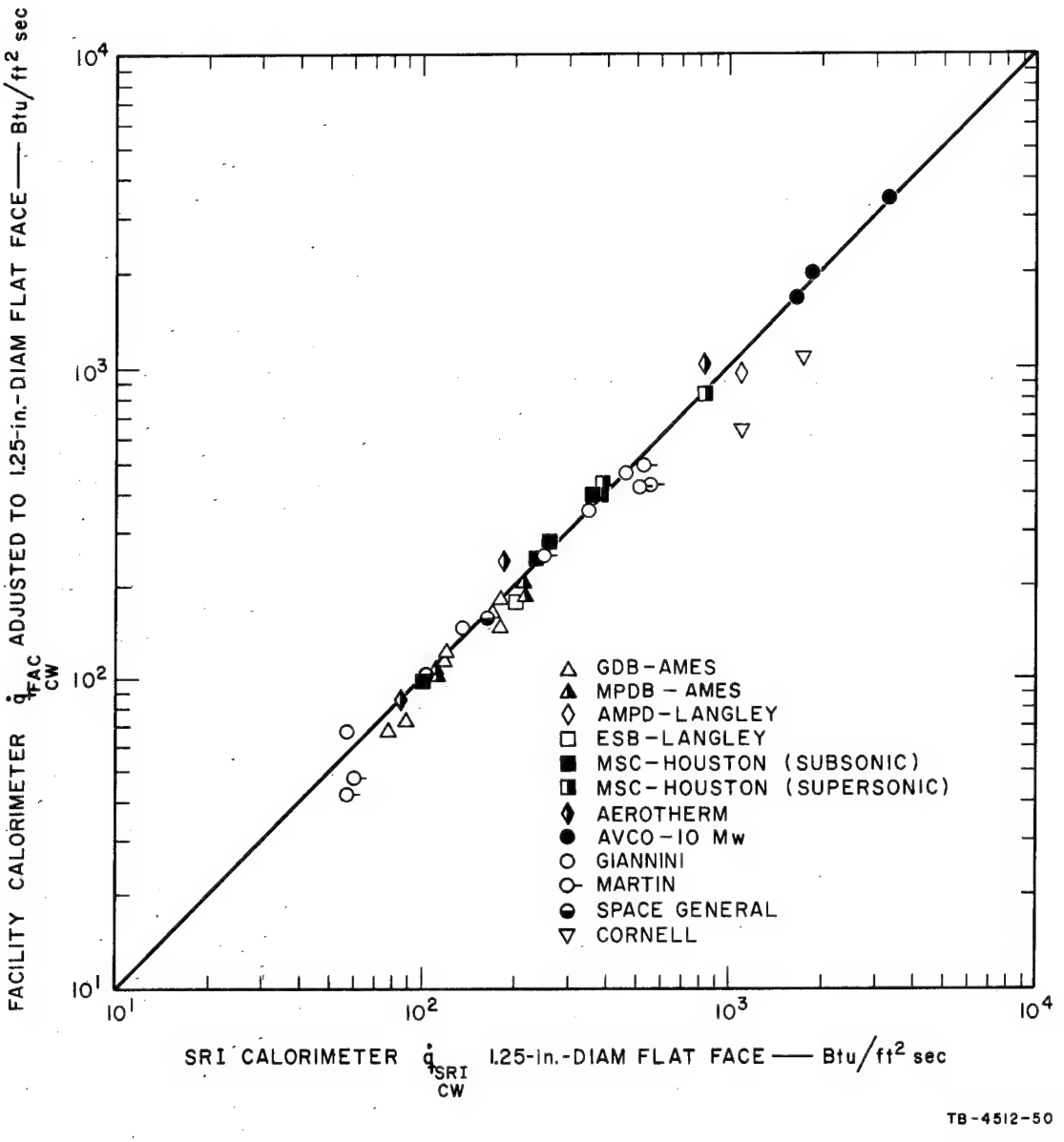

FIG. 19 COMPARISON OF FACILITY AND SRI CALORIMETERS

can lower the measured heat flux. Perhaps the best solution is to seal the calorimeter for pressure conditions considerably above 1.0 atm and to isolate the slug with an air gap for lower pressures.

3. Prediction of Stagnation Point Enthalpy

The stagnation point enthalpy in the vicinity of the model can be calculated from the model stagnation pressure and the cold wall heat flux values. The following form of the Fay-Riddell equation was used to calculate the stagnation enthalpy potential, Δh, for each facility from the $\dot{q}_{\substack{SRI \\ CW}}$ and P_{t_2} data:

$$\Delta h_{\substack{calc \\ CW}} = S_R \dot{q} (R_{eff})^{0.5} / (P_{t_2})^{0.5} \qquad (5)$$

where S_R is 24 as shown in Appendix E, Sec. A.

The above relation assumes air at chemical and thermodynamic equilibrium as the test gas with an invariant Lewis number equal to 1 and a Prandtl number equal to 0.72. The value of R_{eff} was taken as 0.172 ft based on the 1.25-in.-diameter flat-faced shape and $R_{eff} = 3.3\ R_{FF}$. The resulting values of enthalpy have been tabulated in Appendix D and are compared in Fig. 20 to the reported enthalpy as measured by the technique preferred by the facility.

Figure 20 shows a prepondence of data above the correlation line indicating that the center-line enthalpy in the area of the model was probably higher than the average measured enthalpy reported by some of the facilities. Facilities such as AMPD-Langley and ESB-Langley that prefer the heat flux method for measuring enthalpy gave a good correlation as would be expected. The differences for these two facilities result from different calorimeters and calculation methods. Giannini's and Space General's measured enthalpies agreed well with the calculated values. These two facilities also reported quite uniform stream traverses, indicating that the center-line enthalpy is probably close to the average enthalpy by the energy balance method.

Personnel at GBD-Ames feel that for moderate to high pressure nonuniform streams the heat flux enthalpy is preferable to other methods of measuring average enthalpy, but they also believe that this enthalpy can

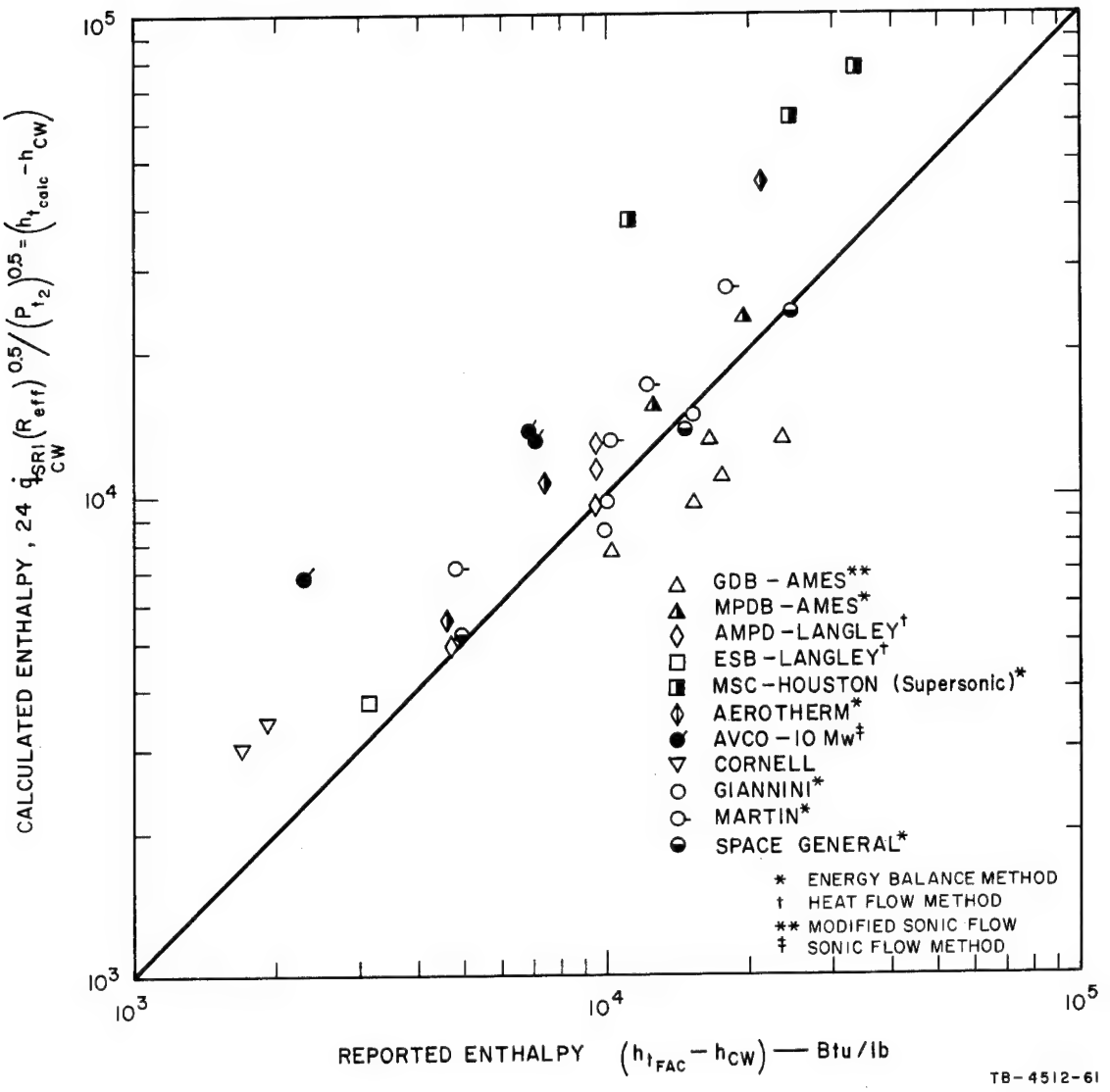

FIG. 20 COMPARISON OF CALCULATED AND REPORTED ENTHALPIES

be severely in error on the low side, as shown by their data in Fig. 20, when used for low pressure, nonequilibrium streams. The problem results from the necessity of using calorimetric surfaces with less than infinite catalytic activity, as discussed in the previous section. The group at GDB-Ames has therefore developed a modified sonic flow method which allows them to calculate the stream temperature and resulting enthalpy in the model area. The enthalpies calculated by the modified sonic flow method can be 1.5 times higher than the heat flux method as seen in Fig. 20.

It appears that although the stream enthalpy is undoubtedly the most important variable in material ablation studies, it is also the most difficult to measure accurately.

B. Performance of High-Density Ablation Materials

In order that the effects of extended test conditions, and especially of varying dimensions, could be evaluated, a dimensional analysis of ablation variables was undertaken. This analysis and its use to correlate ablation data for the high-density Teflon and phenolic-nylon materials used in the Phase I study is covered in Appendix E.

In the present round-robin program (Phase II), two groups of experiments were performed to extend the variables studied in Phase I. The first was the use of high-density Teflon and phenolic-nylon models of the standard size (same as in Phase I) but exposed to considerably higher stagnation pressures. The second group involved Teflon and low-density phenolic-nylon models having effective radii varying from four times as large to about four times as small as the standard models. The results of these experiments and how they fit the correlations are discussed below.

1. High Stagnation Pressure Environments

The lack of fit of the data obtained by Walberg at high stagnation pressures, as shown in Fig. E-2 of Appendix E, suggests that the correlation does not properly take into account such environmental conditions. This was confirmed, at least for the high-density phenolic-nylon models, when the data from the Phase II round robin experiments at high stagnation pressures were checked against that figure and were shown to have the same displacement. Reconsideration of these relations was therefore in order, and, at this point, it was decided to use the separate correlations

represented by Equations (E-18A) and (E-18B) in Appendix E since there appeared to be a difference in the behavior of Teflon and phenolic-nylon at high stagnation pressures.

a. Behavior of Teflon

The approach tried was to separate the pressure term from the rest of the relation. Rearrangement of Equation (E-18A) in this manner leads to

$$\dot{m}_t(R_{eff})^{0.18}/(\dot{q}_{CW})^{0.57}_{SRI} = 0.0044(P_{t_2})^{0.25} \qquad (6)$$

A plot of the left-hand side of this relation against stagnation pressure, P_{t_2}, on logarithmic coordinates should show the indicated slope of 0.25 and intercept of 0.0044 for the right-hand term. It should be remembered that Equation (6) is based on the Phase I round-robin results. When such a plot was made with the Teflon literature data given in Table E-1 (Appendix E), the best correlation line showed a slightly different slope and intercept. These data were therefore correlated by the regression program in terms of relation (E-16B), namely,

$$\dot{m}_t(R_{eff}) = b(\dot{q}_{CW}R_{eff})^n(P_{t_2}R_{eff})^m \qquad (7)$$

The computer gave the following values for the constants using the Teflon literature data:

$$b = 0.0048, \quad n = 0.52, \quad m = 0.22$$

Multiple correlation coefficient = 0.99

Standard deviation = 11 percent

The multiple correlation coefficient is maximized by the regression analysis. The closer this coefficient is to unity, the more significant is the correlation.

Averaging these constants with the Phase I round-robin constants of 0.0044, 0.57, and 0.25 and giving the latter ones slightly more credence, since they represent more data points, the corrected form of Equation (6) would be

$$\dot{m}_t(R_{eff})^{0.21}/(\dot{q}_{CW})^{0.55} = 0.0046(P_{t_2})^{0.24} \qquad (8)$$

This corrected form is plotted in Fig. 21 and is based not only on the Phase I round-robin results and literature data, but also on the Phase II round-robin high stagnation pressure runs performed at AVCO and Cornell. As can be seen in the figure there appears to be no effect of the stagnation pressure on the correlation, at least to pressures of 33 atm. This is not unexpected since Teflon ablates by sublimation and thus should be little affected by mechanical forces.

b. Behavior of High-Density Phenolic-Nylon

A similar approach was used in evaluating the phenolic-nylon data. The rearranged Equation (E-18B) gave

$$\dot{m}_t(R_{eff})^{0.32}/(\dot{q}_{CW})^{0.55} = 0.0010(P_{t_2})^{0.13} \qquad (9)$$

The effect of the literature data on the constants was not checked, since there was insufficient information for use in a regression analysis. A plot of Equation (9) is shown in Fig. 22 and is based on the Phase I round-robin results and literature data, as well as on the Phase II round-robin, high stagnation pressure runs at Cornell and AVCO.

This plot shows that at high stagnation pressure the phenolic-nylon models exhibit higher mass loss rates than would be predicted by the Phase I round-robin correlation. However, these higher rate data do fit a correlation line of steeper slope, with a transition between the two correlations occurring at a stagnation pressure of about 2.7 atm. Thus, the correlations for high-density phenolic-nylon might be expressed for $P_{t_2} \leq 2.7$ atm as

$$\dot{m}_t = 0.0010(R_{eff})^{-0.32}(\dot{q}_{CW})^{0.55}(P_{t_2})^{0.13} \qquad (10)$$

and for $P_{t_2} \geq 2.7$ atm (and at least up to 29 atm) as

$$\dot{m}_t = 0.00048(R_{eff})^{-0.32}(\dot{q}_{CW}^{SRI})^{0.55}(P_{t_2})^{0.13+0.75} \qquad (11)$$

This variation in behavior might have been predicted because phenolic-nylon ablates by a charring mechanism which is particularly sensitive to the mechanical stresses brought on by high stagnation pressures.

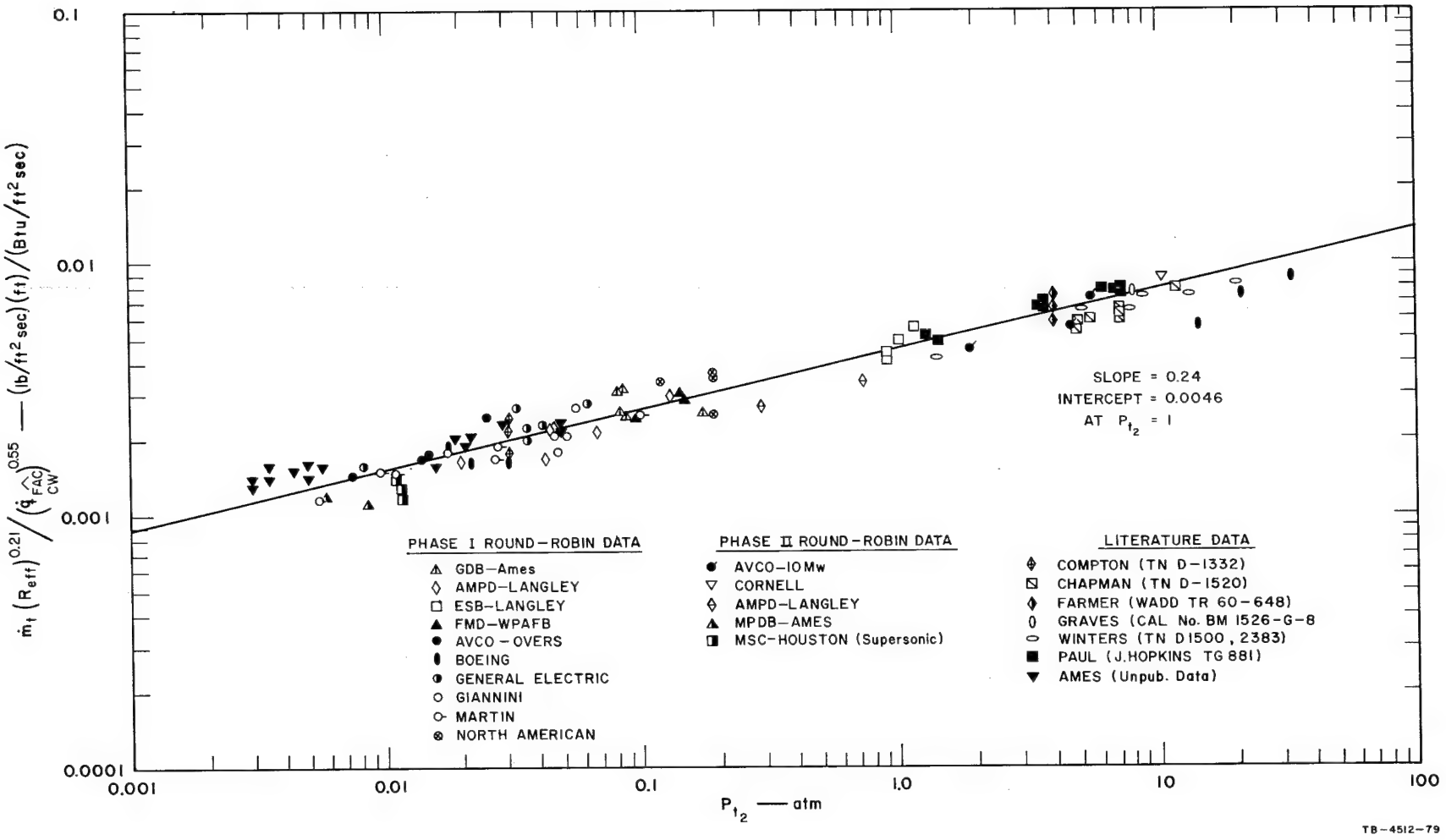

FIG. 21 CORRELATION OF TEFLON DATA

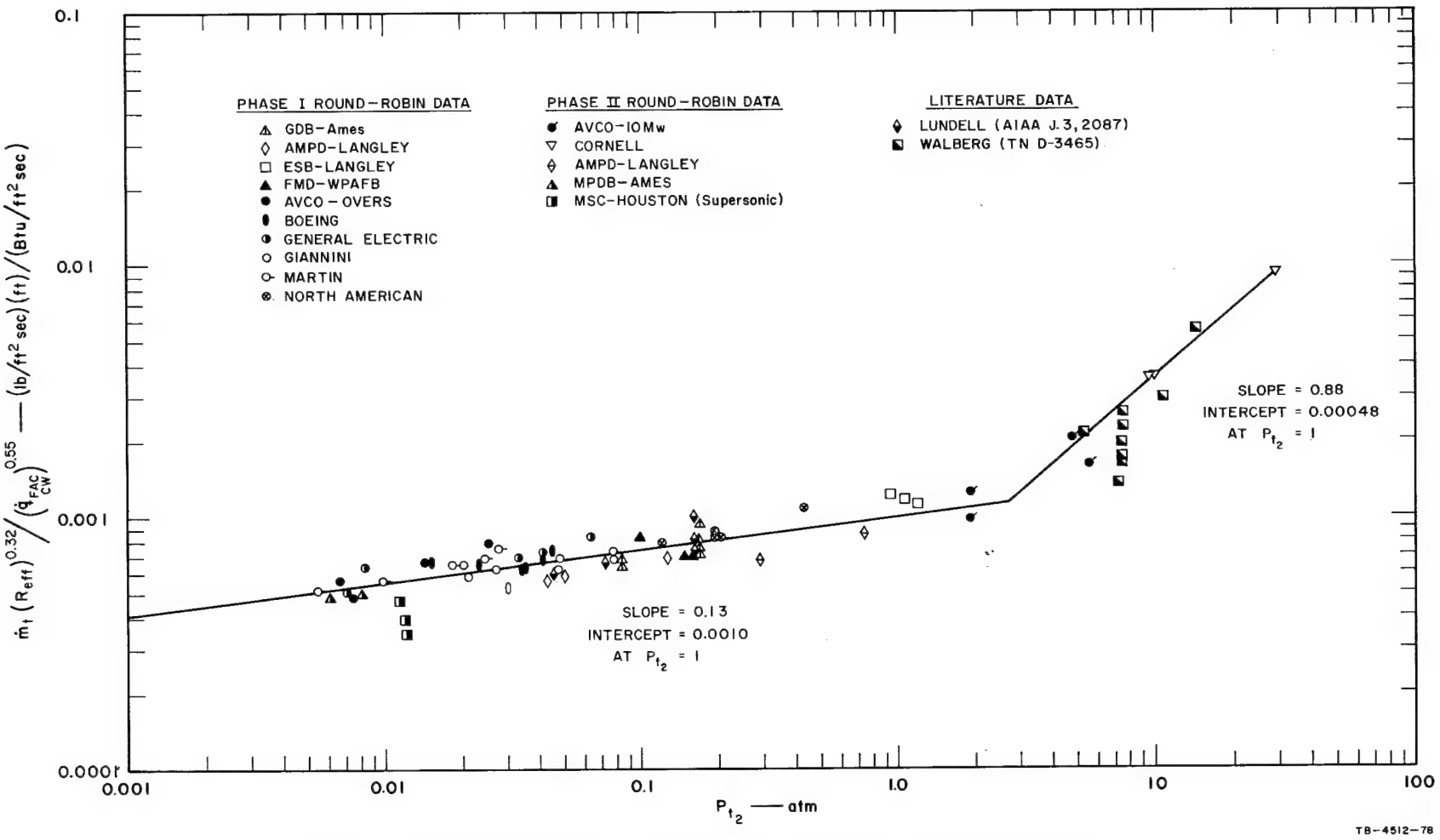

FIG. 22 CORRELATION OF HIGH-DENSITY PHENOLIC-NYLON DATA

This is verified by the fact that the phenolic-nylon models from these tests showed almost no char after exposure to the high stagnation pressure environments, and thus had reduced thermal protection.

The use of the double exponent on the pressure term in Equation (11) is based on this fact of char failure. The dimensionless form of Equation (9) is given in expanded form by Equation (E-10) of Appendix E. This form would imply that the exponent on the effective radius would have to increase to a positive number with this large an exponent on the stagnation pressure. There is no evidence for this behavior and it appears more logical that one additional dimensionless group should be added to Equation (E-9) based on a new variable , τ, the failure stress of the char. Normal units for this variable are pound force per square foot. Converted to the pound-foot-second system, it becomes τg_c with converted units of lb/ft sec^2. This has the same converted units as stagnation pressure, P_{t_2}. Section A of Appendix E shows the converted form of this as $P_{t_2} F_p g_c$ Thus, the simplest form of the new dimensionless group would be

$$\pi_A = P_{t_2} F_p / \tau \tag{12}$$

Equation (E-9) then becomes

$$\pi_m = a_0 \pi_q^n \pi_p^m \pi_A^r \tag{13}$$

Expanded into dimensional form, this equation becomes

$$\dot{m}_t = b(F_p/\tau)^r (R_{eff})^{n+m-1} (\dot{q}_{CW})^n (P_{t_2})^{m+r} \tag{14}$$

where b is as defined in Equation (E-17) and is equal to 0.0010 as shown in Equation (10).

This is identical to Equation (11) with r equal to 0.75 and the value of the constant there can be compared with b from Equation (10) to determine the value of τ from Equation (14). Hence, τ is found to be 5610 lb force/ft^2 or 2.65 atm.

2. Models with Variable Radii

a. Phase II Round-Robin Data

The Phase II studies with models of varying radii involved both heat transfer and mass loss measurements, thus permitting a check of the

radius effect in both cases. It should be remembered, however, that only a limited amount of effort was put into these studies.

(1) Heat Transfer Rate. It is generally accepted that under supersonic conditions the heat flux to different sized calorimeters with the same shape will vary inversely with the square root of the calorimeter radius. Further, the dimensions of different shaped models can be expressed in terms of their effective radii, and, as pointed out in Equation (13) of the Phase I report,[1] this is

$$R_{eff} = R_H = 3.3\,R_{FF} \tag{15}$$

Thus, the heat flux will decrease with increasing calorimeter size according to the relation

$$\dot{q}_{CW}/(\dot{q}_{CW})_{1.25FF} = [(R_{eff})_{1.25FF}/R_{eff}]^{0.5} \tag{16}$$

A logarithmic plot of the heat flux ratio versus the effective radius is shown in Fig. 23.

The calorimeters used by AMPD-Langley and Martin were those that best matched the SRI calorimeters. The AMPD facility used a four-inch shroud for the flat-face model and calorimeter rather than a five-inch shroud; this was done to minimize stream blockage at the diffuser.*

As can be seen from the plot, a slope of -0.5 fits the data well, and the intercept at an effective radius of unity is equal to the square root of the effective radius of a 1.25-inch, flat-face calorimeter, namely, 0.415. Except for the Martin high point at the five-inch, flat-face effective radius, where stream blockage may be occurring, and a low point for the one-inch hemispherical calorimeter, the data confirm the inverse square root relation.

(2) Mass Loss Rate. The predicted effect of model radius on Teflon mass loss rate is shown by Equation (E-18A). Rearrangement of this equation in terms of effective radius gives

$$\dot{m}_t/(\dot{q}_{CW})^{0.57}_{SRI}(P_{t_2})^{0.25} = 0.0044(R_{eff})^{-0.18} \tag{17}$$

* The core diameter, however, remained at 2.5 inches. Also the corner radius on the AMPD models was made one-fifth of the shroud radius to reduce stream blockage. The corner radius on the Martin models was constant at one-eighth inch regardless of shroud radius so that the ratio varied, as shown in Graph A of Fig. 17.

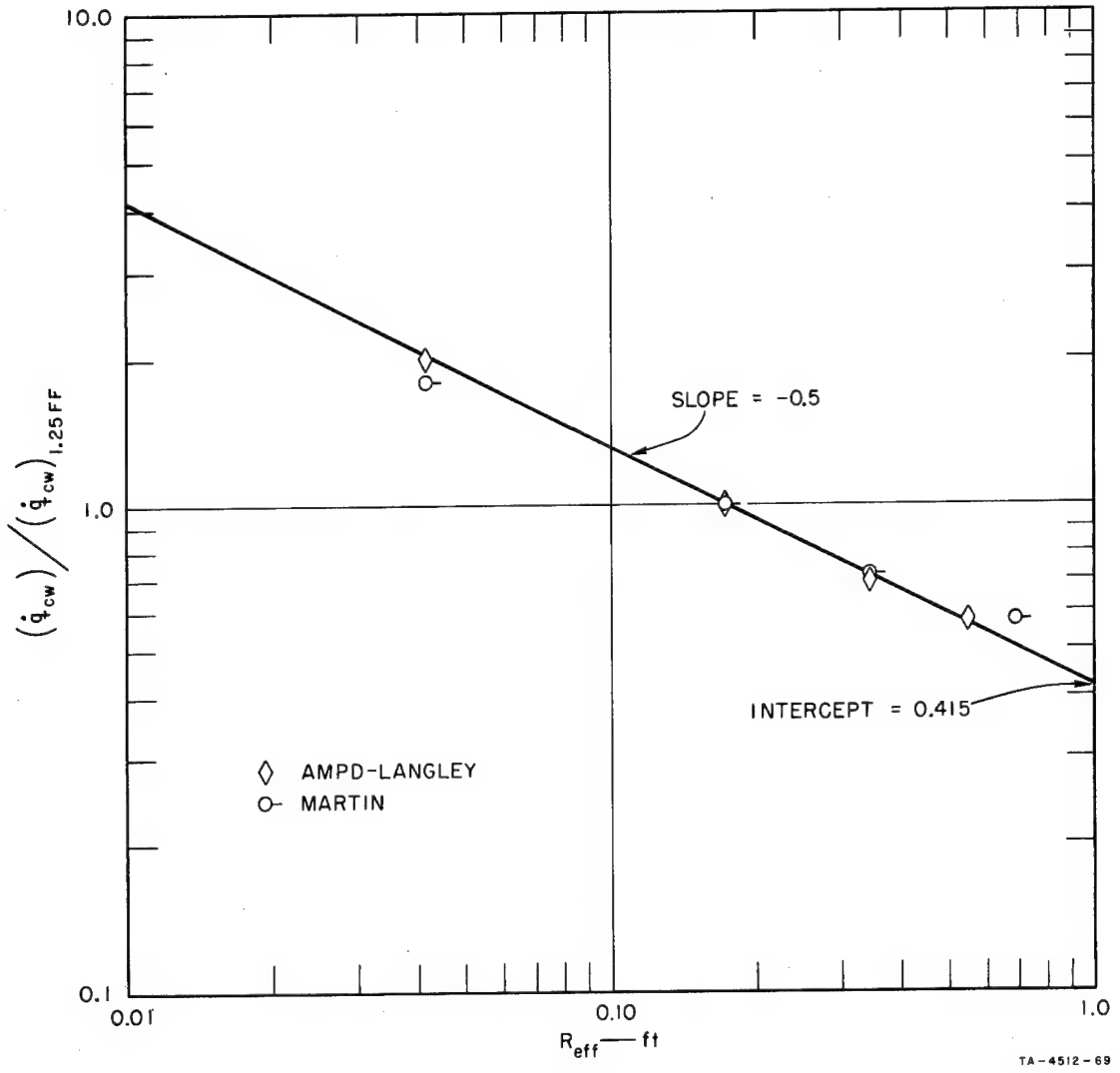

FIG. 23 VARIATION OF HEAT TRANSFER RATE WITH EFFECTIVE RADIUS

Using the data from the Phase II experiments of variable radii Teflon models, the left-hand side of this relation was calculated and plotted against effective radius in the top half of Fig. 24. The slope of the line is -0.18 and the intercept is 0.0044 at R_{eff} = 1 ft. It appears that the data could be fitted with a line of this slope but at a lower intercept. The reason for this is unknown but must relate to the way in which the experiment was performed and in which the measurements were made, since data obtained at this facility using other standard 1.25-inch flat-face models fit the general correlation well, yet the data obtained with a standard model in this series of experiments are also displaced downward.

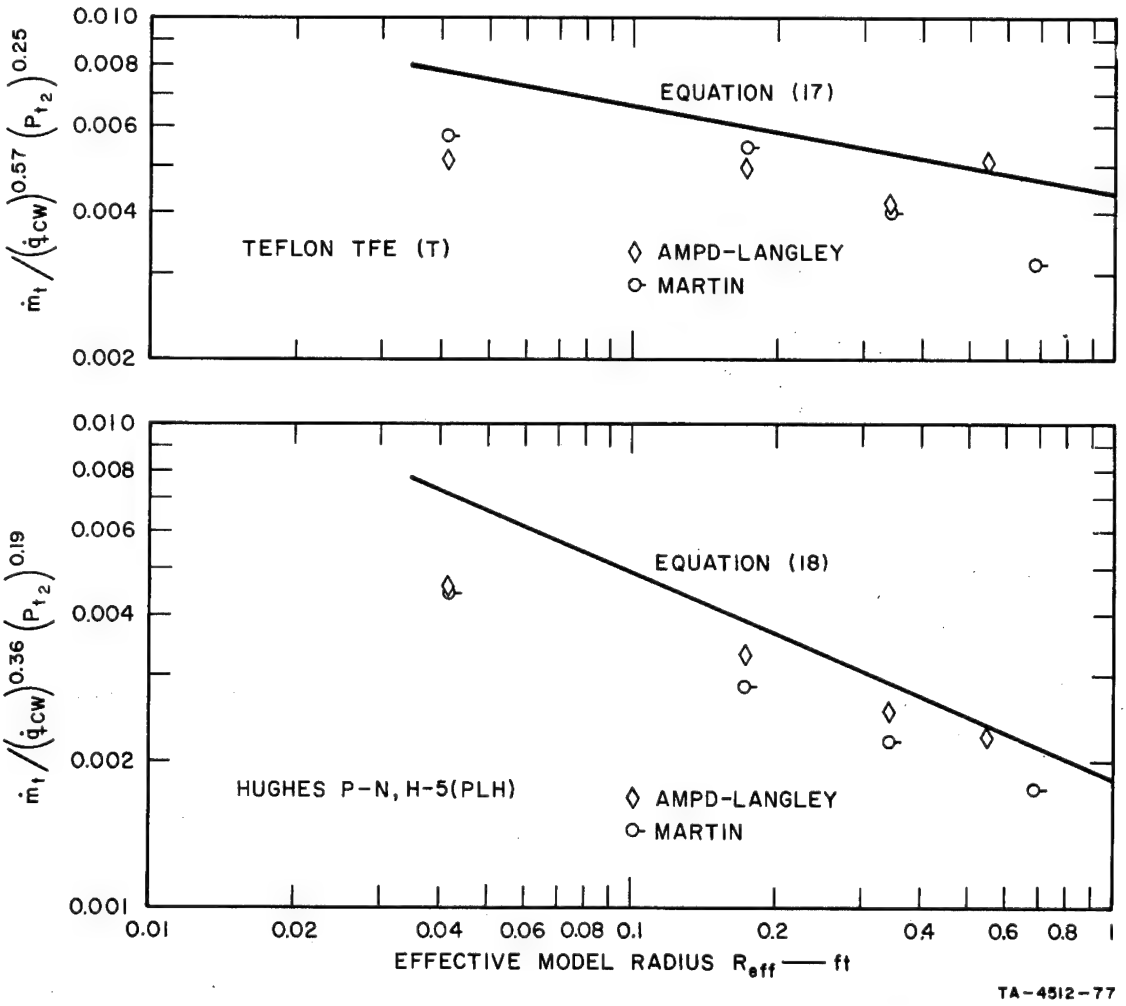

FIG. 24 VARIATION OF MASS LOSS RATE WITH EFFECTIVE RADIUS

One possible explanation relates to the fact that as the model diameters were increased, the core diameters were increased in the same proportions. However, the calorimeters kept the same sensing area and merely increased the shroud diameter. With the plasma coring exhibited by the facilities involved this could provide misleading information about the thermal environment to which the core was exposed.

The same pattern was found with Phase II variable radii data for the Hughes low-density phenolic-nylon models. As will be seen in Sec. IV-C, the mass loss rate correlation, cast into the same form as Equation (17), is

$$\dot{m}_t/(\dot{q}_{\substack{CW \\ SRI}})^{0.36}(P_{t_2})^{0.19} = 0.0018(R_{eff})^{-0.45} \qquad (18)$$

This is plotted in the bottom half of Fig. 24.

b. Literature Data

The correlation of the literature data from supersonic facilities in Appendix E, Sec. C, covered radii varying from 0.0156 to 0.55 ft and had a very low standard deviation. The effect of radius on mass loss rate, predicted by the dimensionless correlation (see Equation (E-10), or its revised form (E-16A)), has therefore been well verified.

C. Performance of Low-Density Ablation Materials

More extensive measurements were made on the low-density materials during the ablation experiments. These permitted a more detailed determination of the response of these materials to the test environment. As a result, additional correlations were considered for interpreting these data.

1. Ablation Behavior

This section contains information on temperature measurements and physical changes in the low-density materials evaluated during the Phase II round-robin.

a. Front Surface Temperature

The front surface temperature data from the first round robin showed considerable scatter. To avoid this, the facilities were supplied with identical, calibrated total radiation pyrometers. A description of

the pyrometers and calibration technique is given in Sec. III-B. The facilities also received suggestions for mounting the pyrometer in the tunnel and instructions for the use of the instrument.

A comparison of reported front surface temperatures as measured with the SRI-supplied radiation pyrometer and the facility optical pyrometer is presented in Fig. 25. The data shown in this figure are from Appendix B and are the surface temperatures measured on the Langley phenolic-nylon (PLL) material. The same pattern of data was also evident on the other materials that were evaluated.

The measured surface temperatures given in Fig. 25 are "brightness" temperatures, assuming a surface emissivity of unity. Since the actual emissivity is less than one, the true-surface temperatures are higher than those indicated. If an emissivity of 0.8 is assumed for the (PLL) material, the following corrections must be added to the measured values to give the true temperatures:

MEASURED TEMPERATURE (°F)	RADIATION PYROMETER CORRECTION (°F)	OPTICAL PYROMETER CORRECTION AT 0.655μ (°F)
2000	+100	+35
3000	+160	+70
4000	+220	+130

The effect of these corrections is shown by the correlation line labeled $\epsilon = 0.8$ in the figure.

Examination of Fig. 25 indicates that some facilities such as GDB-Ames, MSC-Houston (subsonic), Giannini, and Martin had good agreement between the facility and SRI pyrometers when an emissivity of 0.8 - 0.9 was assumed. AMPD-Langley, Aerotherm, and Space General did not display as good an agreement in surface temperature. Part of the lack of agreement seemed to have resulted from the radiometer mounting location and optical path to the radiation pyrometer, as described briefly in Appendix A. When the radiometer was located outside the tunnel, with narrow grazing angles off intervening windows, the attenuation of the optical signal resulted in low surface temperatures of the model. In a few cases the radiometer was mounted with a narrow viewing angle to the model front surface and the model rapidly ablated out of focus.

The group at GDB-Ames has used radiation pyrometers extensively and is aware of the precautions that must be followed in their use. It

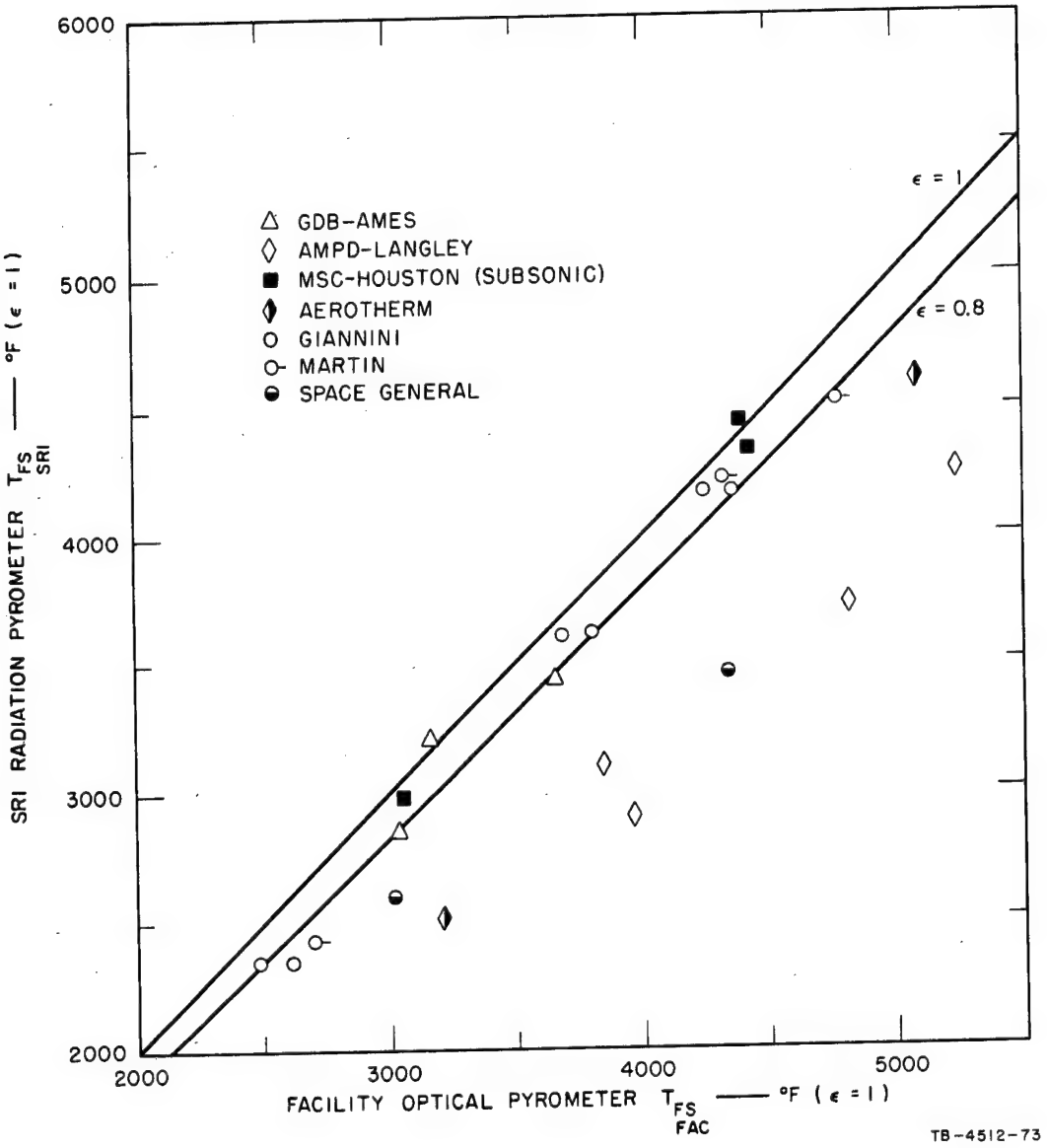

FIG. 25 COMPARISON OF SRI RADIOMETER AND FACILITY OPTICAL PYROMETERS

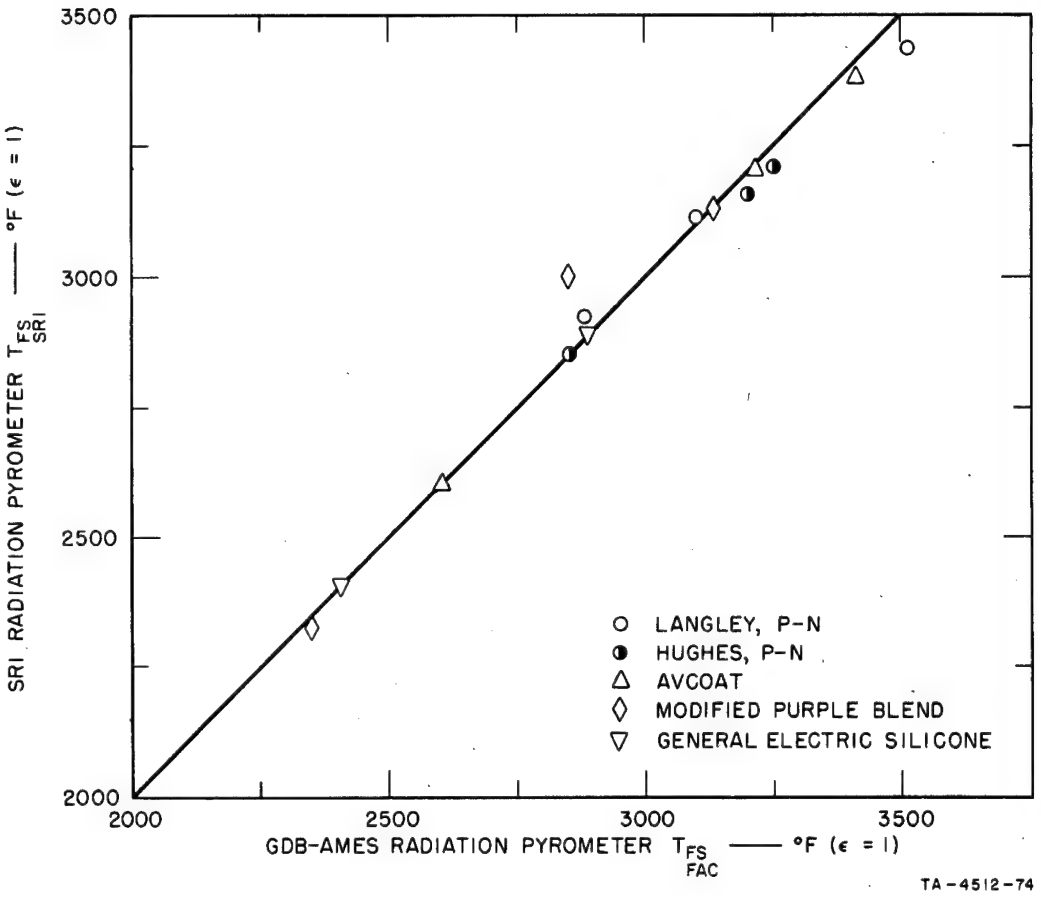

FIG. 26 COMPARISON OF SRI AND GDB-AMES RADIOMETERS

is probably for this reason that they obtained a good correlation between their radiation pyrometer and the SRI radiometer, as indicated in Fig. 26.

Since the radiometers were not calibrated in position on the tunnels, it was decided that the facility pyrometer temperatures were more reliable and were therefore used in all front surface temperature correlations. This points up the general problem of using identical calibrated instruments to cross-correlate facilities. Either their use must be rigidly specified and followed, or they must be further calibrated in position on the tunnel.

b. Internal Temperature Rise

A plot of the temperature data for the run on model PLL 96 performed at GDB-Ames is given in Fig. 27. This figure shows the temperature rise of the four internal thermocouples and the model front surface

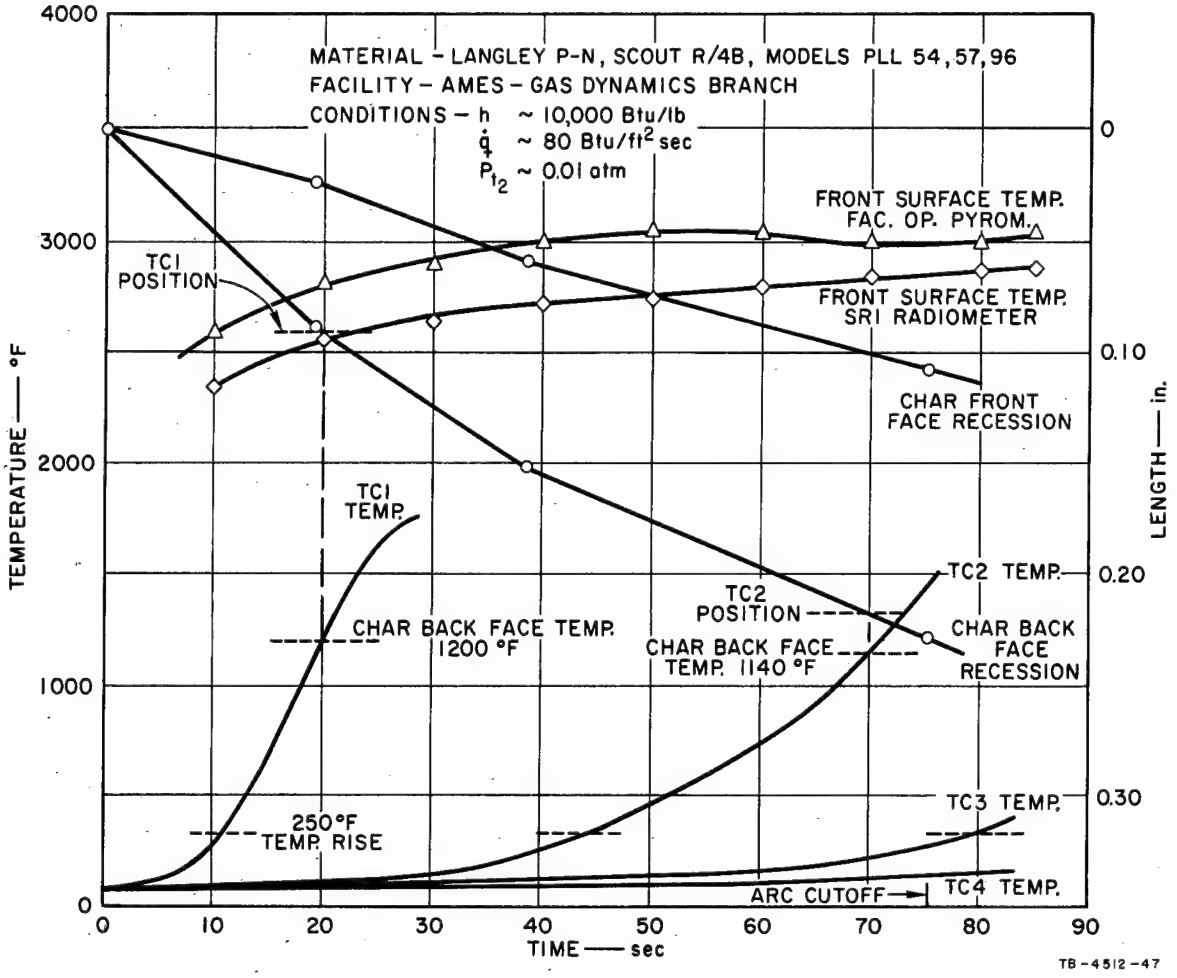

FIG. 27 MODEL TEMPERATURES AND RECESSION DURING ABLATION RUN

temperature as measured with a facility optical pyrometer and the SRI radiometer and is based on the data in Appendix C. A length scale was added to the right-hand ordinate of each temperature graph, and the model recession and char thickness data from Appendix B were plotted for the three varying run times used on models PLL 54, 57, and 96. The initial thermocouple distances were added to the graphs and the time noted when the char-virgin material interface passed each thermocouple position. The temperature of the thermocouple at the above noted time was designated as the char-virgin material interface temperature and is recorded in Appendix C.

Although the data showed considerable scatter, they also followed a particular pattern indicating that the char-virgin material interface temperature increases with increasing mass pyrolysis rates. The scatter probably resulted from the difficulty of measuring the position and temperature of a receding boundary layer and the fact that the temperature gradient in the material is very steep at the char in the decomposition zone. The temperature gradients at the interface ranged upwards to 35°F/0.001 in. for the high pyrolysis rate condition, indicating the importance of small thermocouple wire diameter and of position measurement.

The instantaneous mass pyrolysis rate was calculated at the time the char interface passed each thermocouple position. It was assumed that all material back to the interface had been pyrolized and consumed. Comparison of the data for the mass pyrolysis rate versus char interface temperature for the Avcoat and the two low-density phenolic-nylon materials indicated that above a minimum temperature of about 800°F the pyrolysis rate was approximately a function of the fourth power of the interface temperature.

c. Mass Loss Rates

The model core weight losses were determined on all models returned to SRI. The methods are outlined in Sec. III-C. The equivalent mass loss per area, in pounds per square feet, was calculated and plotted against time for each material. Examples of these plots are given in Figs. 28 and 29 for Langley low-density phenolic-nylon and Avcoat material.

The plots show a typical higher initial mass loss rate of charring ablation as the char is established and the front surface temperature increases. This is followed by a period of slightly lower mass loss and the

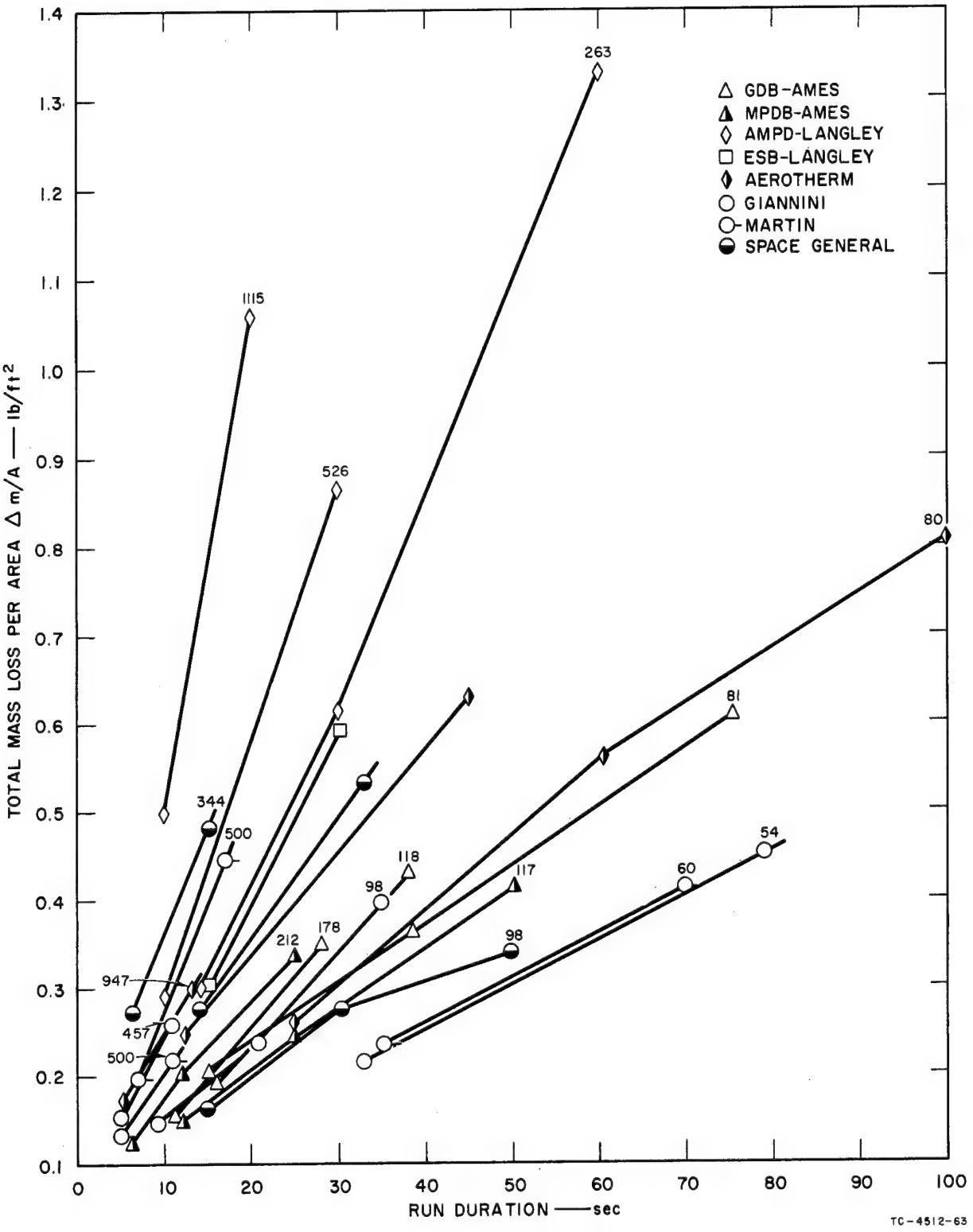

FIG. 28 MASS LOSS OF LANGLEY LOW-DENSITY PHENOLIC-NYLON AS A FUNCTION OF RUN DURATION (Heat Transfer Rate Indicated for Each Facility)

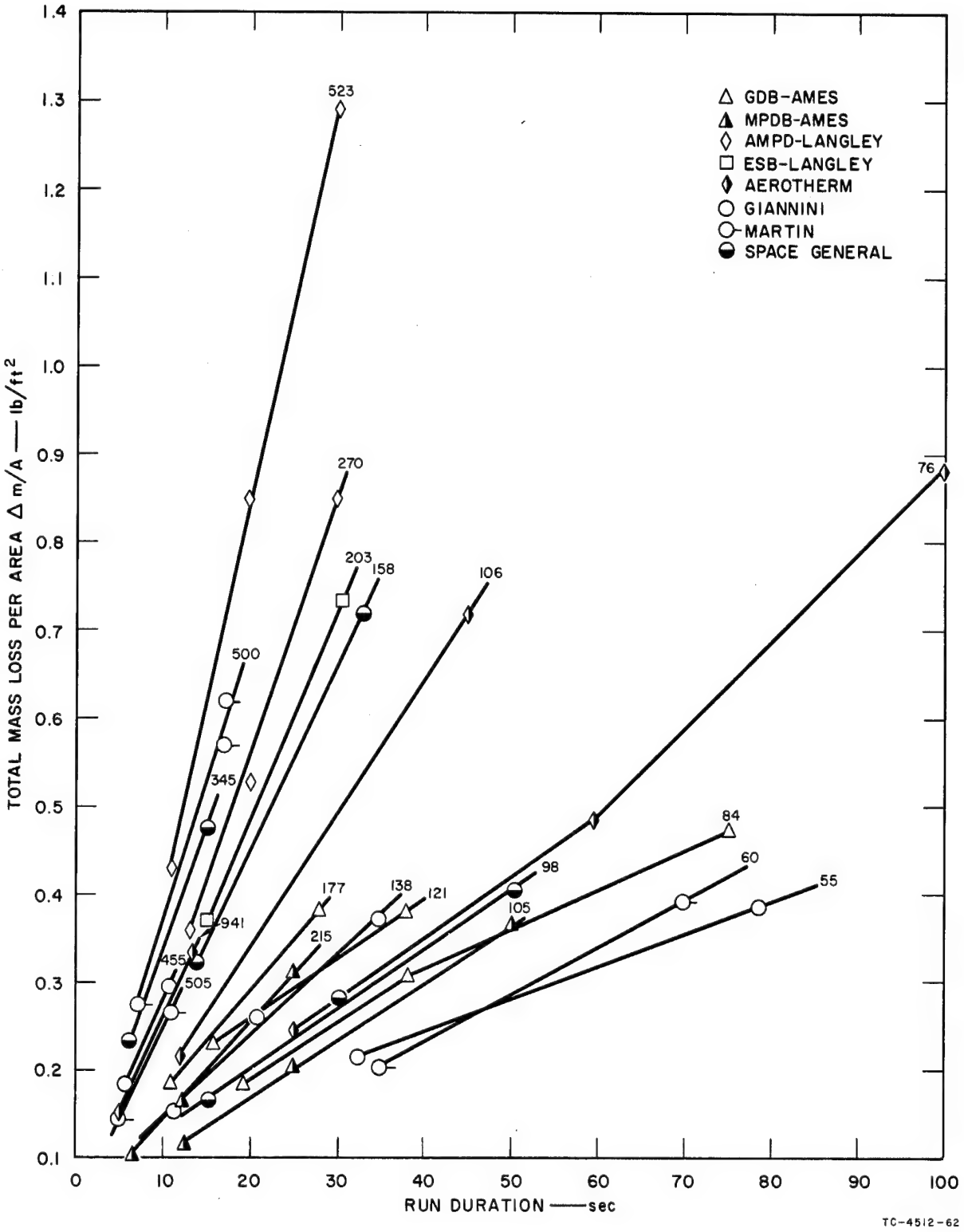

FIG. 29 MASS LOSS OF AVCOAT MATERIAL AS A FUNCTION OF RUN DURATION
(Heat Transfer Rate Indicated for Each Facility)

establishment of a quasi steady-state mass loss rate. The induction period ranged from a fraction of a second at the very high fluxes to approximately eight seconds for the lowest fluxes.

As stated in Sec. III-C, when more than two models were tested, the mass loss rate, $\dot{m}_t$, was determined from the slope of the best straight line through the data. When two models were tested the mass loss rate was determined from the slope between the two data points, and for the occasional runs involving one model, the slope was assumed to intersect zero. The calculated mass loss rates have been tabulated in Appendix D.

The mass pyrolysis rate, $\dot{m}_p$, was also calculated, as follows, for all tests involving two or more models:

$$\dot{m}_p = \rho_{VR}[(X_R + X_{CR})_2 - (X_R + X_{CR})_1]/(t_2 - t_1) \qquad (19)$$

Here, X_R and X_{CR} are the recession of the front surface of the char and char thickness, respectively; ρ_{VR} is the virgin material density; and the subscripts 2 and 1 denote long and short duration runs, respectively. The mass pyrolysis rate thus represents the rate at which the char-virgin material interface is moving into the model. These results are also tabulated in Appendix D.

The mass pyrolysis rate described above is defined slightly differently than the mass pyrolysis rate reported in the Phase I report, but it is consistent with Lundell's definition.[12] The Phase I data can be corrected to equal the Phase II data by adding the $\dot{m}_{CR}$ listed in Appendix C of the Phase I report[1] to the listed values of $\dot{m}_p$.

Although the char removal rate, $\dot{m}_{CR}$, is not tabulated in Appendix D for the Phase II data, it was used to determine how closely the ablation of the low-density materials correlates with Scala's predicted regimes for the combustion of graphite.[13] This involved calculation of $\dot{m}_{CR}/(P_{t_2}/R_{eff})^{0.5}$ and the plotting of this against front surface temperature, T_{FS}, in degrees Rankine.

The high-density phenolic-nylon data from Phase I agree well with theory in showing a diffusion-rate-controlled plateau above 3000°R. On the other hand, the high stagnation pressure data from Phase II for this same material show considerably higher rates. The five low-density materials showed no plateau above 3000°R, in fact, varied as much as sixfold without any discernible pattern.

d. Char Properties

Chars on the low-density phenolic-nylon materials had a cracked appearance on the surface and a columnar structure oriented parallel to the direction of ablation. This could indicate that the pyrolysis gases take preferential paths to the surface. The pyrolysis zone, as indicated by the slight change in color of the virgin material, was very narrow (approximately 0.025 in.) in most models. The char caps had adequate adhesion to remain on the cores during model disassembly but were easily cleaved from the core, with part of the char remaining on the model core. The char remaining on the core was scraped off before making length and weight measurements.

Chars on the Modified Purple Blend and the G.E. silicones generally had two types of appearance, depending on the exposure history of the model. At low heat fluxes they were black, carbonized chars that swelled during short exposure times, followed by slow recession at longer run times. Higher heating rates resulted in a grey, fused inorganic-appearing surface with the indication that the material was removed from the model by melting and flowing down the sides. The pyrolysis zone on these materials was very narrow (0.020 in.) and the chars could be completely removed from the cores without scraping.

The Avcoat chars usually had a depression in the honeycomb filler material, with the honeycomb web being slightly raised. There were fused droplets of inorganic material at the model periphery. The char had excellent adhesion to the substrate and required moderate scraping to remove. The pyrolysis zone seemed wider in the Avcoat materials than in the other materials, and there was evidence that the honeycomb web preferentially conducted heat to the substrate.

The char densities were calculated for each model and are tabulated in the last column of each table in Appendix D. Analysis of these data indicates that the ablation process and its effect on char properties and char dimensions is a continually changing balance of many competing processes. External variables affecting char properties and thickness are heat flux, stagnation pressure, and run time ($\dot{q}$, P_{t_2}, t); gas test composition is also an external variable, but since all NASA round-robin tests were conducted in air, no statements can be made on its effects. Internal or material factors affecting the charring process are the pyrolysis kinetics of the polymer and the thermal and physical properties of the char.

For a given charring material, the char thickness appears to be largely a function of $\dot{q}$, P_{t_2}, and t. At low $\dot{q}$'s and P_{t_2}'s, the char will continue to increase in thickness as a function of time. At high $\dot{q}$'s and P_{t_2}'s, a constant char thickness is rapidly established, and the front surface recedes as rapidly as the char-virgin material interface. Progressively higher $\dot{q}$'s and P_{t_2}'s result in increasingly thinner char layers (AVCO tests) until the char thickness is effectively zero (Cornell tests).

The char densities were found to increase with increasing $\dot{q}$, P_{t_2}, and t. This probably results from the kinetics of the polymer pyrolysis process and the kinetics of coke deposition within the char. The char density was found to increase with front surface temperature and mass loss rate, since both are dependent on $\dot{q}$ and P_{t_2}. At a low $\dot{q}$ and P_{t_2}, the char density was approximately four tenths of the virgin density, and at extremely high $\dot{q}$ and P_{t_2}, the char density approached the virgin material density. Char yield can be calculated from char density in two ways, depending on whether char recession is allowed for. If it is, and if the virgin polymer interface does not recede at the same rate, then char yield will be a function of run time with yield decreasing as more and more recession occurs. On the other hand, if char yield is based on the amount of virgin polymer represented by the char cap, then yield is directly proportional to char density, and the above remarks on effects of the different variables on density refer also to char yield.

A density traverse of the char layer was made using the X-ray techniques described in Sec. III-C, and the results of four of these tests are given in Fig. 30. These curves show a sharp drop in density close to the char-virgin material interface which is at the left side of the plot. This is followed by an additional drop in density, possibly resulting from the volatilization of ablation products. The density then increases, probably resulting from cracking of the gases and redeposition of carbon.

2. Mass Loss Rate Correlations

In view of the success in relating the mass loss rate to a power function of the environmental parameters for Teflon and high-density phenolic-nylon, it was decided to use the same approach for the low-density materials. Stagnation pressure was one of these parameters in almost every case. The other parameters considered are discussed in the following sections.

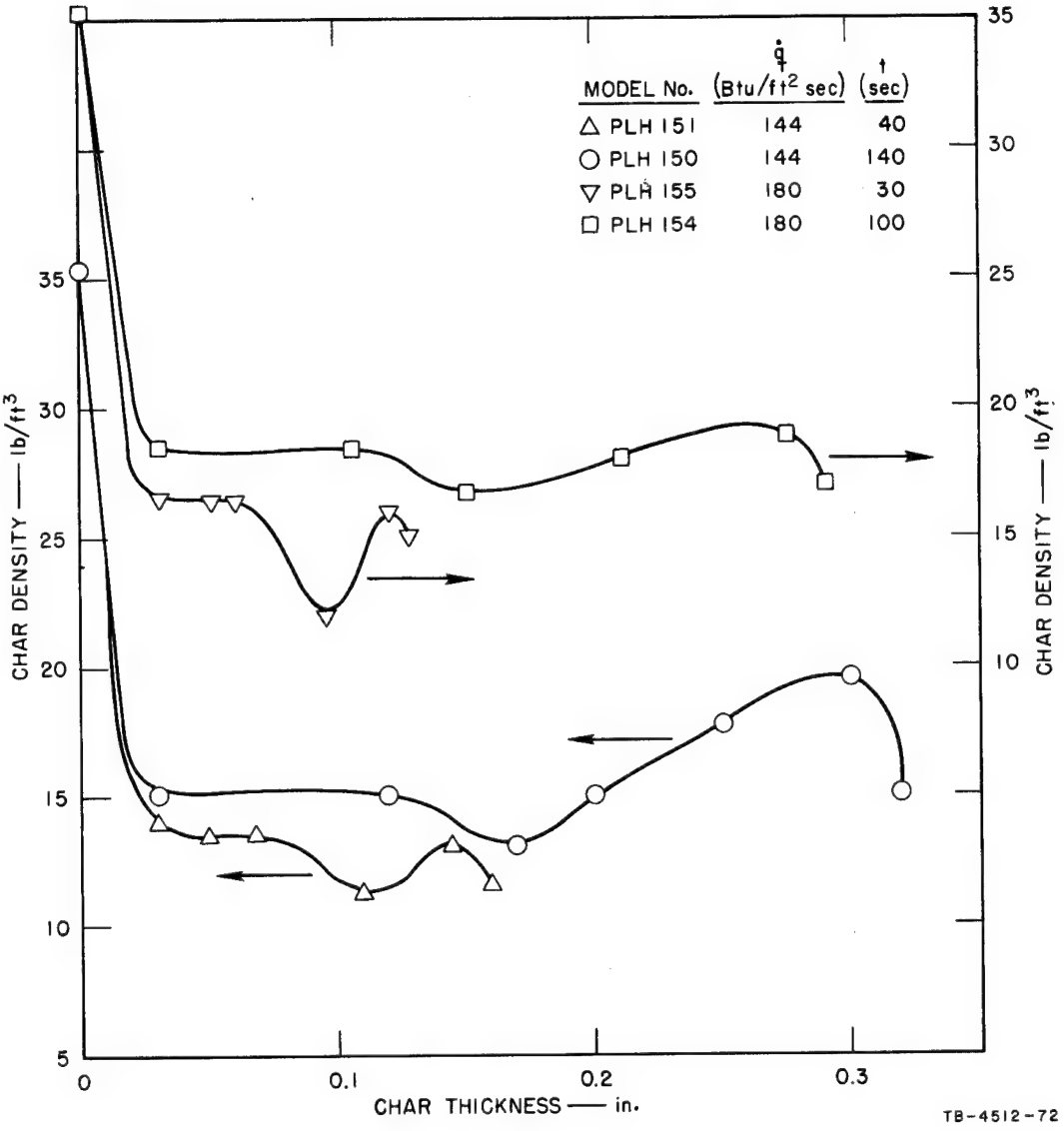

FIG. 30 DENSITY PROFILES OF HUGHES LOW-DENSITY PHENOLIC-NYLON CHARS

a. SRI Calorimeter Cold Wall Heating Rate

The general form of the relation evaluated was

$$\dot{m}_t = a(\dot{q}_{\substack{SRI \\ CW}})^n (P_{t_2})^m \qquad (20)$$

using the correlation data from Appendix D for the five low-density materials. The values of the constants found, the degree of correlation, and the percent standard deviation are tabulated below.

MATERIAL	a	n	m	MULTIPLE CORRELATION COEFFICIENT	PERCENT STANDARD DEVIATION
PLL	0.00465	0.36	0.26	0.96	15
PLH	0.00388	0.36	0.19	0.94	14
A	0.00357	0.47	0.33	0.97	16
SP	0.000317	0.81	0.19	0.94	24
SG	0.000188	1.03	0.28	0.92	36
T*	0.0060	0.57	0.25	0.97	10
P*	0.0018	0.55	0.13	0.96	10

* Data from Phase I round robin.

The increased standard deviation for the low-density materials, as compared to the higher density materials, is not surprising. Their composition and ablated appearance is less reproducible and it is more difficult to measure linear dimensions on the charred core. In fact, attempts to correlate the pyrolysis rate, $\dot{m}_p$, as a power function of heating rate and stagnation pressure showed a poorer fit of 18, 20, and 24 percent for PLL, PLH, and A, respectively.

Plots of the correlations for the five low-density materials are shown in Figs. 31 through 35. The MSC-Houston subsonic data also shown on each graph so that they can be compared to the supersonic results. The subsonic data were not considered in calculating the intercept, exponents, and standard deviation for the correlations.

It is visually apparent that the correlations are poorest for the silicone materials. Also, the exponents on heating rate and stagnation pressure vary from material to material. This tends to reinforce the suggestion that the Teflon and high-density phenolic-nylon material should not be combined into a single correlation.

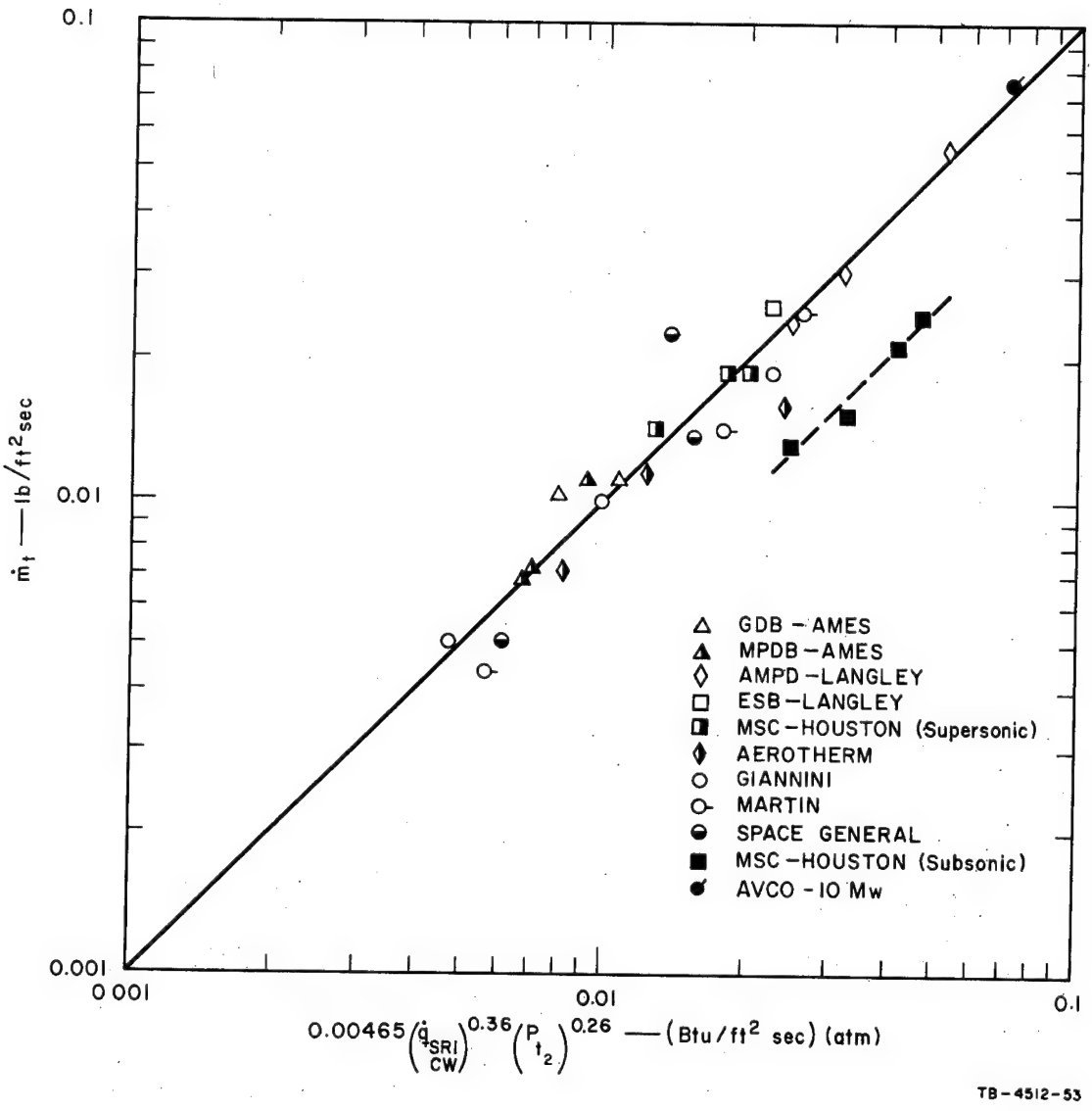

FIG. 31 MASS LOSS RATE CORRELATION FOR LANGLEY LOW-DENSITY PHENOLIC-NYLON

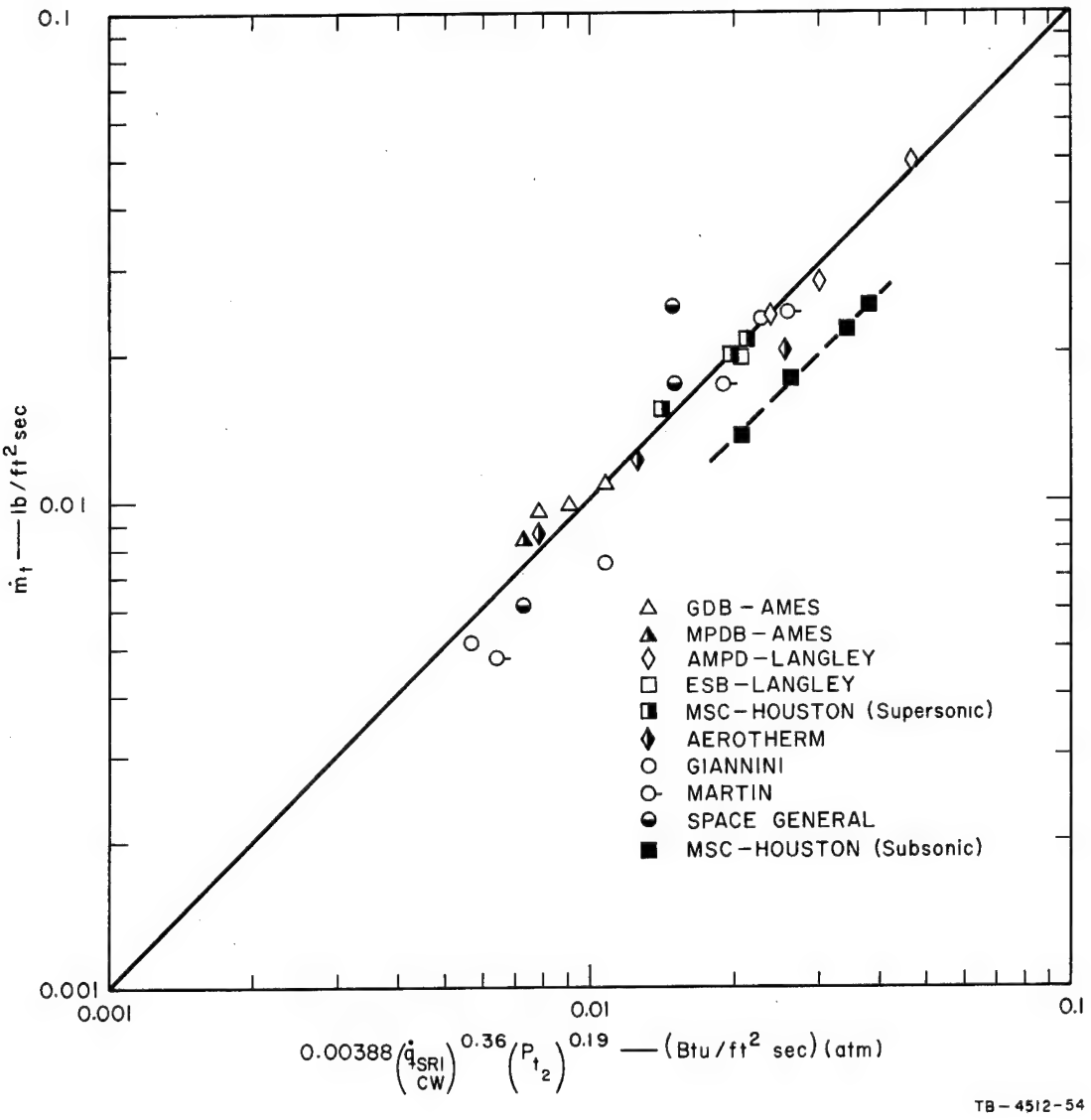

FIG. 32 MASS LOSS RATE CORRELATION FOR HUGHES LOW-DENSITY PHENOLIC-NYLON

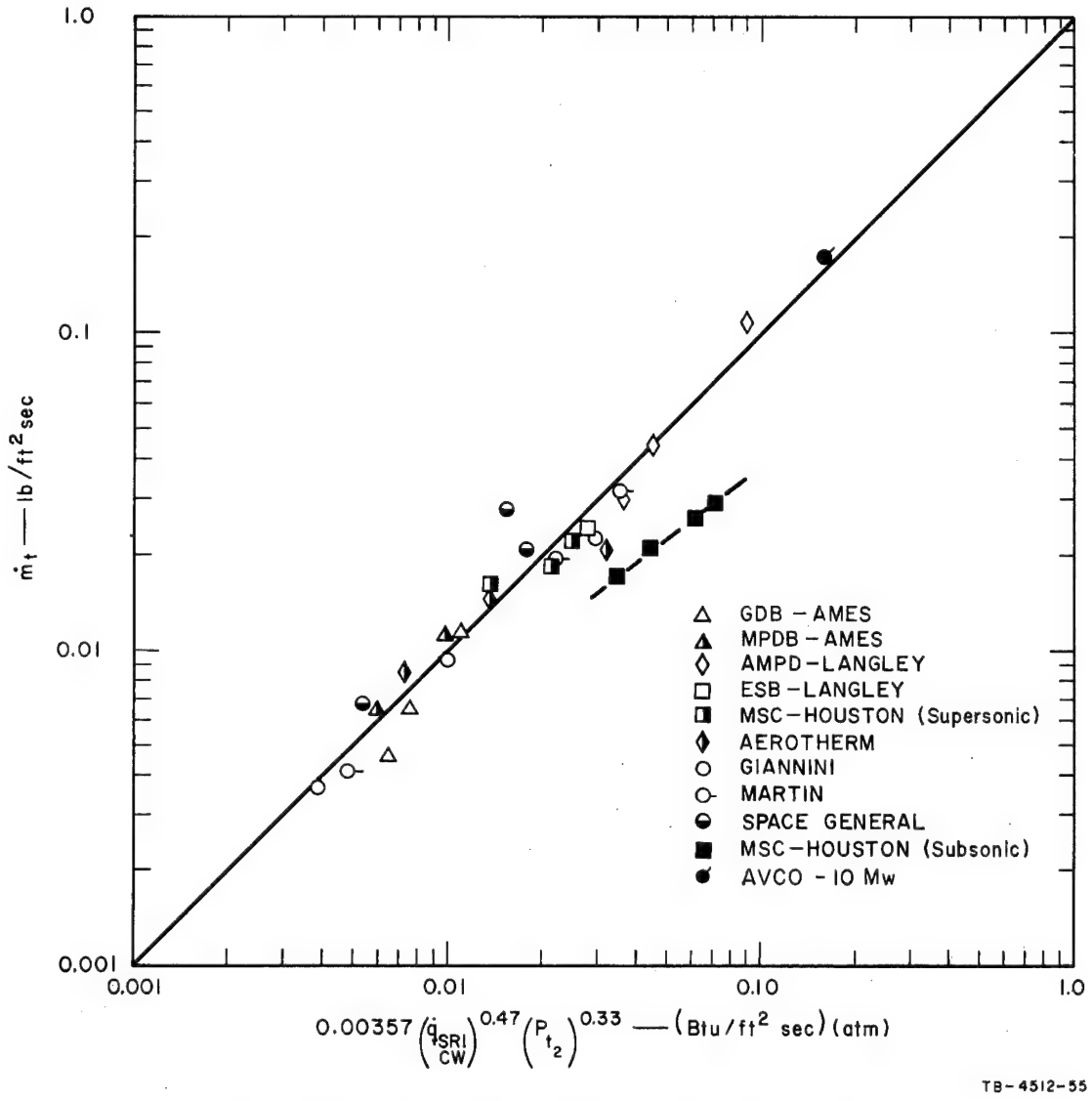

FIG. 33 MASS LOSS RATE CORRELATION FOR AVCOAT

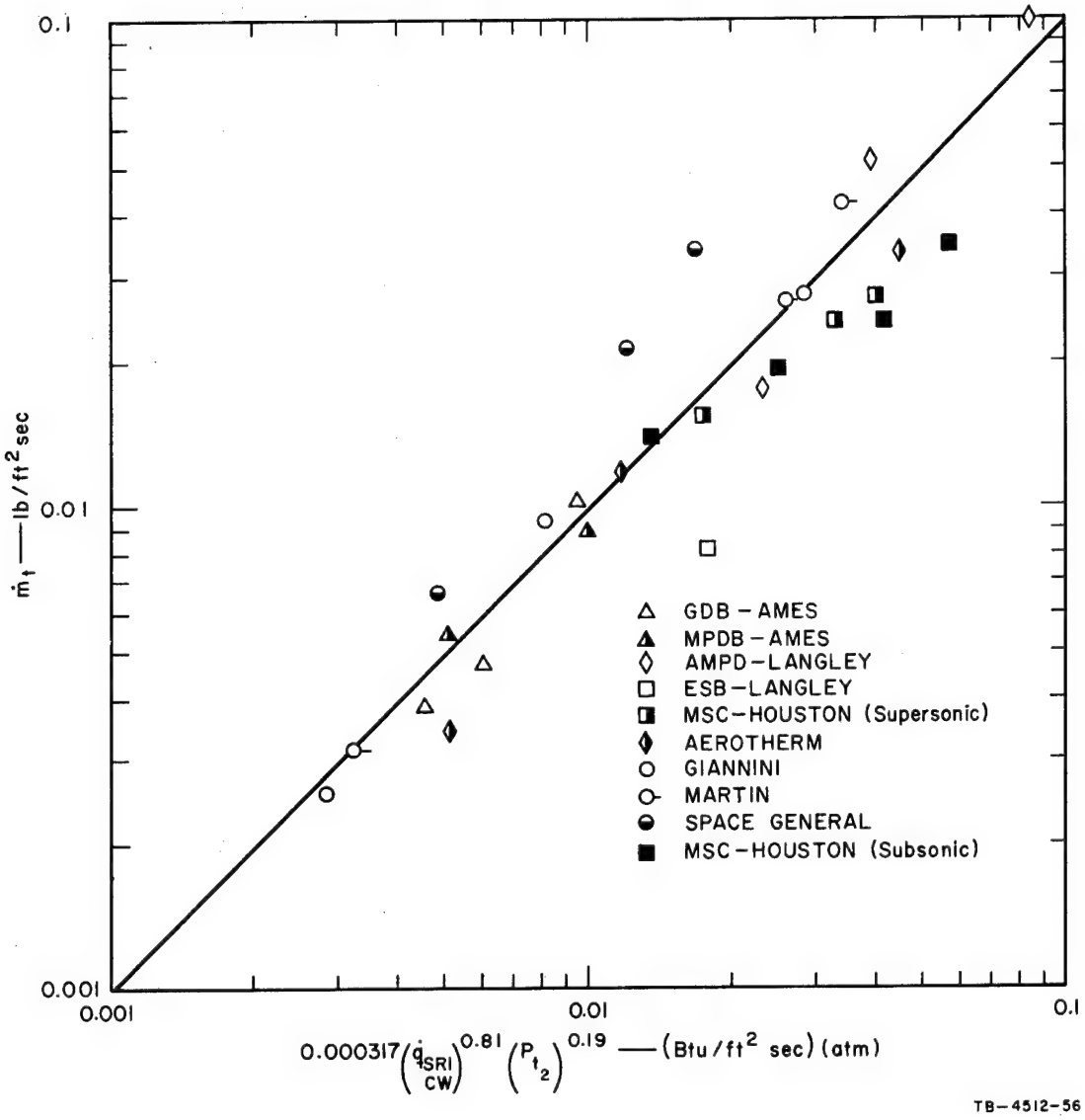

FIG. 34 MASS LOSS RATE CORRELATION FOR MODIFIED PURPLE BLEND SILICONE

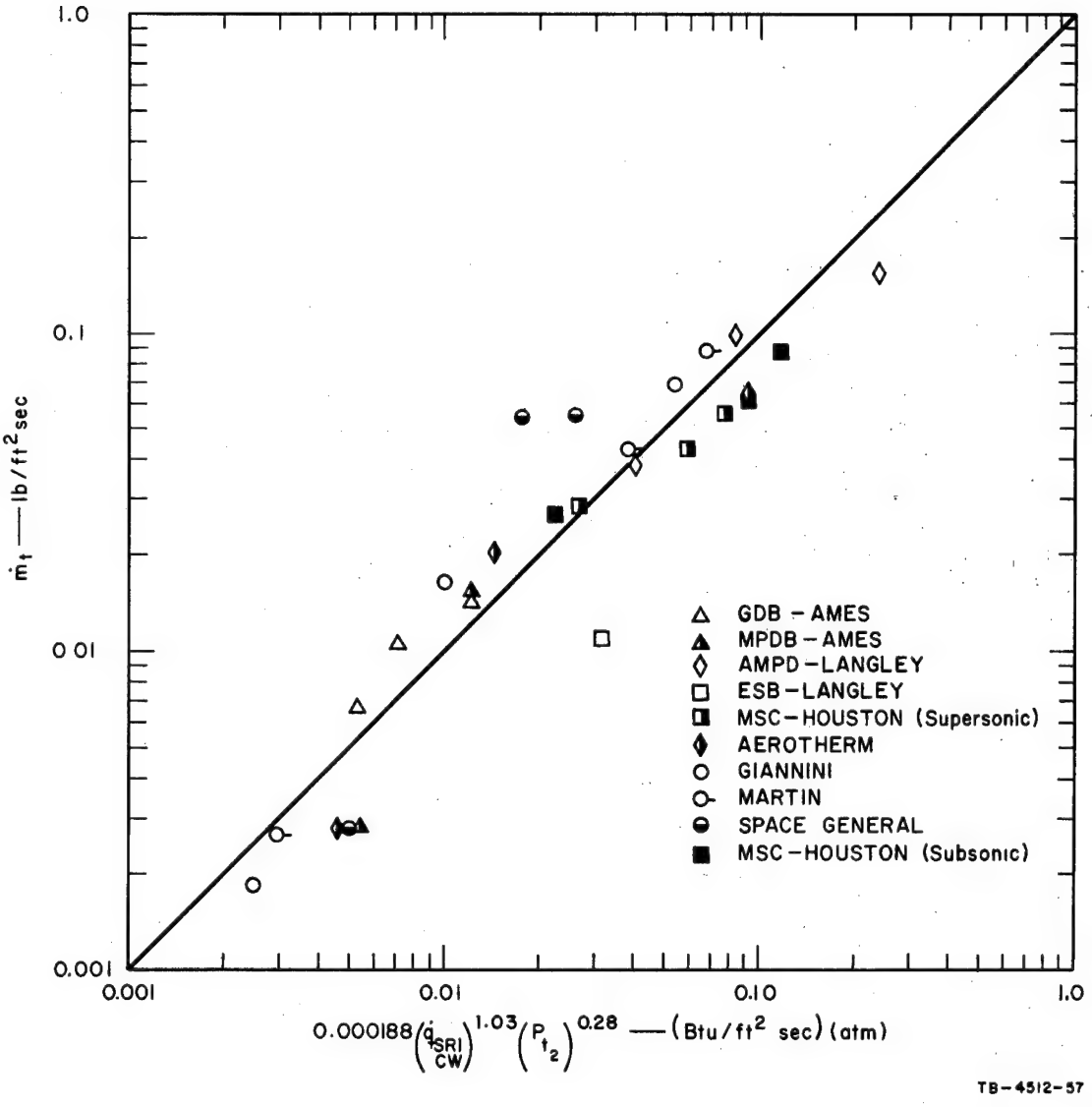

FIG. 35 MASS LOSS RATE CORRELATION FOR GENERAL ELECTRIC SILICONE

b. Facility Calorimeter Cold Wall Heating Rate

The form of the relation is essentially similar to that used for the SRI calorimeter heating rate correlation:

$$\dot{m}_t = a(\dot{q}_{\substack{FAC \\ CW}})^n (P_{t_2})^m \qquad (21)$$

This was evaluated using the regression program available on the SRI computer and the data from Appendix D. The results are:

MATERIAL	a	n	m	MULTIPLE CORRELATION COEFFICIENT	PERCENT STANDARD DEVIATION
PLL	0.00538	0.32	0.25	0.95	15
PLH	0.00430	0.35	0.20	0.91	16
A	0.00414	0.44	0.33	0.97	16
SP	0.000420	0.75	0.18	0.91	26
SG	0.000299	1.00	0.34	0.91	39
T*	0.011	0.48	0.29	0.98	11
P*	0.0034	0.46	0.18	0.97	8

*Data from Phase I round robin.

The data scatter for the low-density materials is nearly the same as when the SRI calorimeter is used, except that the silicone materials show a slightly poorer correlation. As would be expected, the constants are roughly the same for the two correlations.

c. Measured Enthalpy Potential

The correlation evaluated for this environmental parameter was

$$\dot{m}_t = a(\Delta h_{meas})^u (P_{t_2})^v \qquad (22)$$

The data from Appendix D were used in the regression program with the following results:

MATERIAL	a	u	v	MULTIPLE CORRELATION COEFFICIENT	PERCENT STANDARD DEVIATION
PLL	0.000980	0.46	0.47	0.96	16
PLH	0.000650	0.48	0.41	0.94	15
A	0.000966	0.52	0.60	0.90	21
SP	0.0000133	0.98	0.64	0.92	28
SG	0.00000189	1.32	0.86	0.91	40
T*	0.0017	0.59	0.57	0.92	21
P*	0.0010	0.49	0.41	0.78	30

* Data from Phase I round robin

The data for the two low-density phenolic-nylon materials show nearly as good a correlation as when the cold wall heating rate is used. Greater standard deviations are found for most of the other materials.

d. Heat of Ablation

A common method of interpreting mass loss data is in terms of the effective heat of ablation, H_{eff}. This is determined and related to the measured enthalpy potential as shown below:

$$\dot{q}_{\substack{SRI \\ CW}}/\dot{m}_t = H_{eff} = \alpha + \beta(\Delta h_{\substack{meas \\ CW}}) \qquad (23)$$

The coefficient α is derived to be the heat necessary to raise the material to the ablation temperature and to decompose it, and thus is identical to the term defined earlier as ΔH_D, whereas β is a dimensionless number defined as the transpiration shielding factor. A regression analysis of the data from Appendix D, on this basis, leads to the following values for the constants:

MATERIAL	α	β	MULTIPLE CORRELATION COEFFICIENT
PLL	5,654	1.16	0.67
PLH	5,428	1.03	0.68
A	4,248	1.03	0.78
SP	12,580	0.476	0.52
SG	14,130	0.040	0.03

It is apparent that this is not a suitable correlation for the data for a number of reasons. The multiple correlation coefficient is so low as to suggest that a number of sets of α and β could be used equally well. A plot of the best correlation, that for Avcoat, is shown in Fig. 36.

Equation (23) for Avcoat can also be arranged for logarithmic plotting as

$$H_{eff} - 4248 = 1.03(\Delta h_{\substack{meas \\ CW}}) \qquad (24)$$

This has been graphed in Fig. 37 and the relation shows a standard deviation of 34 percent. This is over twice the standard deviation of 16 percent for the power function correlation graphed in Fig. 33 and shows the superiority of Equation (20) over Equation (23) or (24).

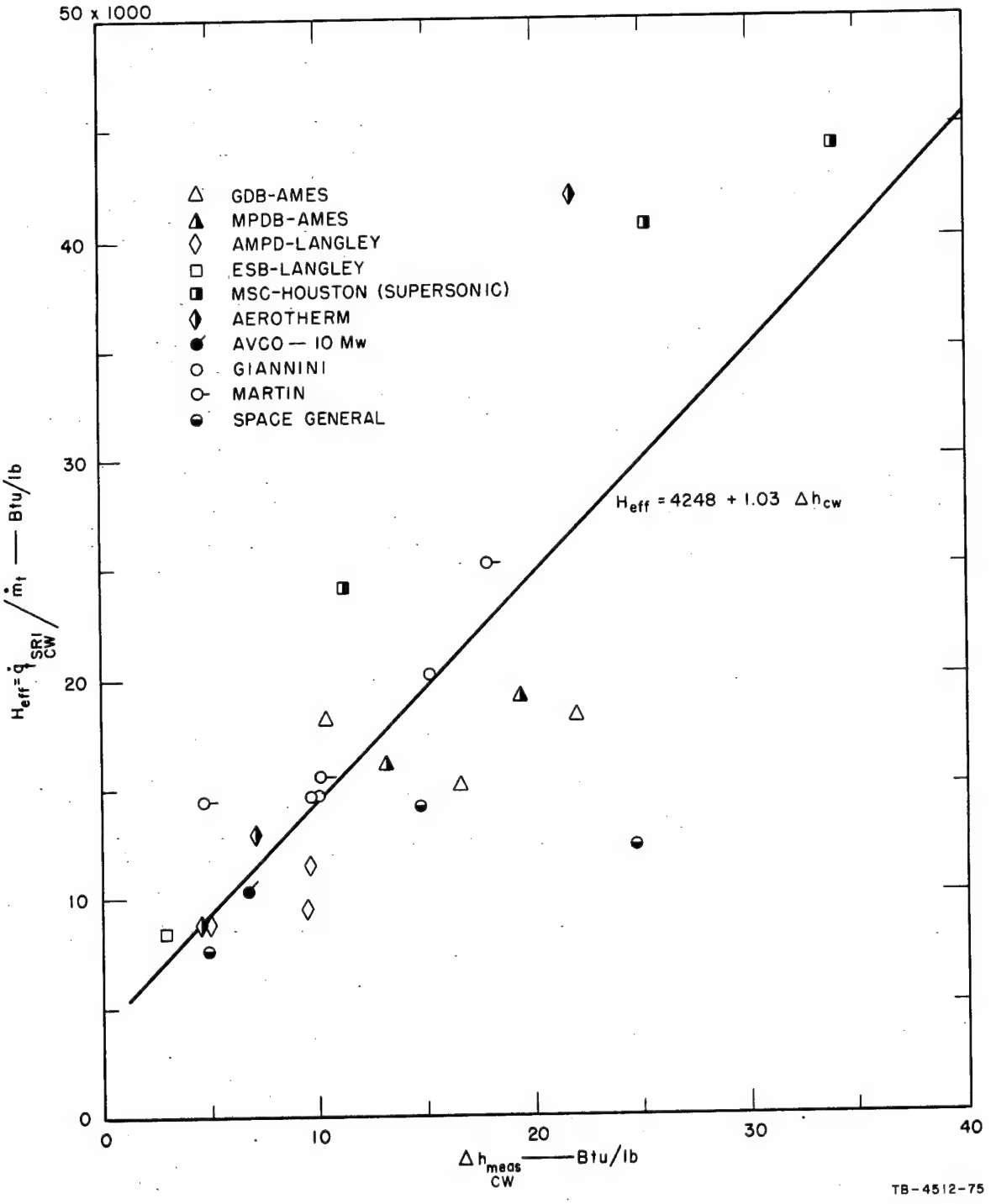

FIG. 36 EFFECTIVE HEAT OF ABLATION CORRELATION FOR AVCOAT

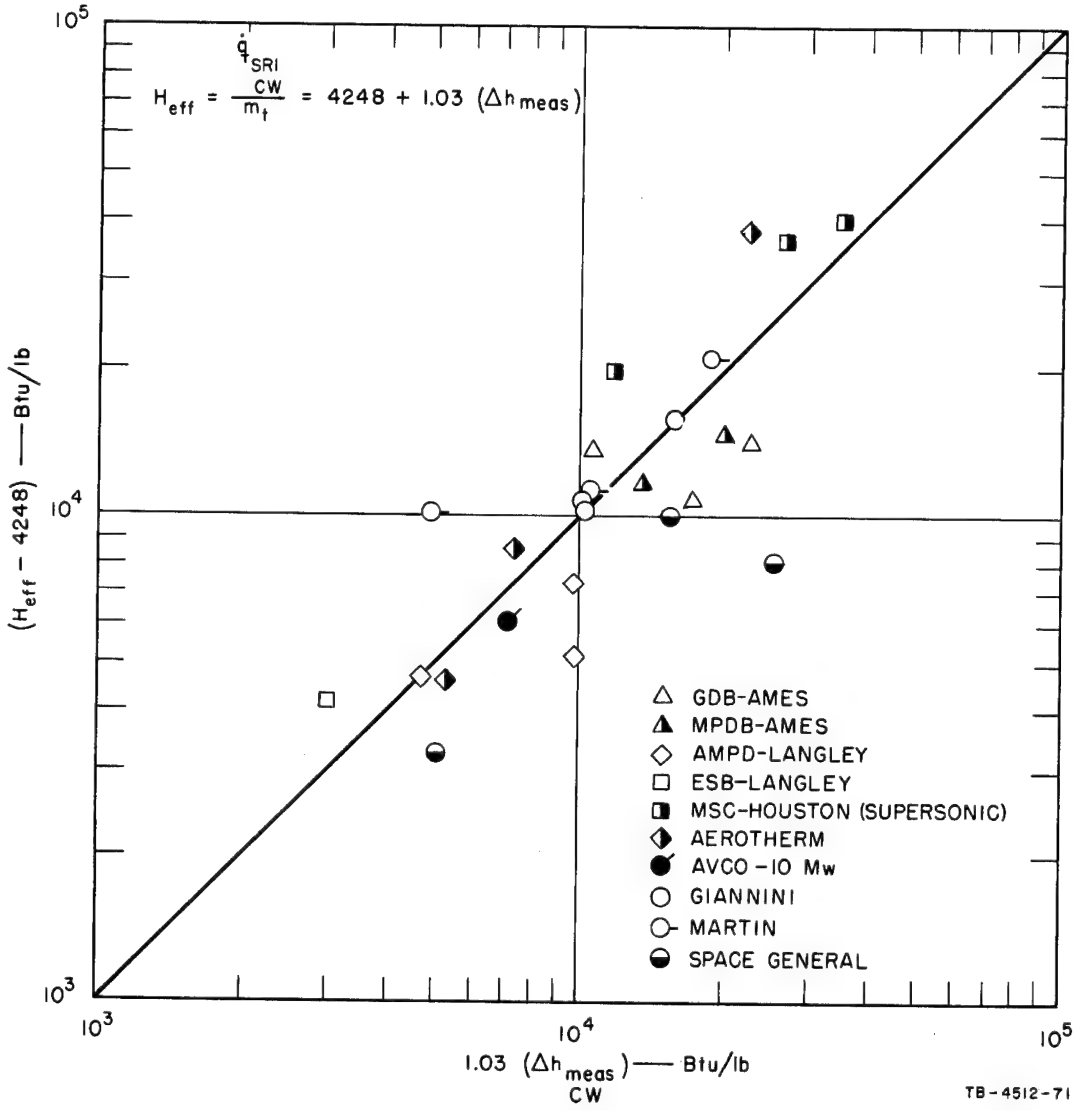

FIG. 37 EFFECTIVE HEAT OF ABLATION CORRELATION FOR AVCOAT (Logarithmic Form)

e. Dimensionless Forms of Correlations

As with the Phase I round-robin data, the power function correlations can be expressed in dimensionless form. Thus Equations (20) and (21) can be expressed in the same form as Equation (E-9), namely,

$$\pi_m = a_0 \pi_q^n \pi_p^m \qquad (25)$$

with the π-groups defined as in Equations (E-4) to (E-6). However, since the values of a_0 and ΔH_D are not known for these materials, Equation (25) must be reduced to the dimensional form shown in Equation (E-16A), namely,

$$\dot{m}_t = b(R_{eff})^{n+m-1} \dot{q}_{CW}^{n} P_{t_2}^{m} \tag{26}$$

where

$$b = a(R_{eff})_{RR}^{1-n-m} \qquad \text{with} \qquad (R_{eff})_{RR} = 0.172 \text{ ft} \tag{27}$$

In the case of the measured enthalpy potential correlation, Equation (22) can be expressed as

$$\pi_m = a_0 \pi_h^u \pi_p^v \tag{28}$$

where

$$\pi_h = (\Delta h)_{CW}^{meas} / \Delta H_D \tag{29}$$

and the other π-groups are as previously defined in Appendix E. Expansion of this in dimensional form leads to

$$\dot{m}_t = a(\Delta h_{CW}^{meas})^u (P_{t_2})^v \tag{30}$$

where

$$a = a_0 (S_R^2 R_{eff})^{v-1} (\Delta H_D)^{(1/2)-u-v} (K)^{1-2v} \tag{31}$$

Since ΔH_D is not known, this can be converted to

$$\dot{m}_t = b_1 (R_{eff})^{v-1} (\Delta h_{CW}^{meas})^u (P_{t_2})^v \tag{32}$$

where

$$b_1 = a(R_{eff})_{RR}^{1-v} \qquad \text{with} \qquad (R_{eff})_{RR} = 0.172 \text{ ft} \tag{33}$$

Equation (32) has the same form as Equation (27) in the Phase I report[1] except that the b given there equals $b_1(R_{eff})^{v-1}$ here.

3. Temperature Correlations

Two distinct sets of temperature measurements were made during the Phase II round robin. These were front surface temperature during exposure and internal temperature of the ablation model during a run. The results of these measurements have been tabulated in Appendix C. A discussion of these data and of correlations based on them follow.

a. Front Surface Temperature

As pointed out earlier, several optical techniques were used for determining front surface temperature, and in most cases the results were not directly comparable. However, the facility pyrometers were previously calibrated in place and the data from these instruments were used for correlation purposes. Relations involving such factors as mass loss rate, pyrolysis rate, heating rate, and stagnation pressure were evaluated, but the simplest was

$$T_{FS} = a(\dot{m}_p)^w \tag{34}$$

where T_{FS} is the front surface temperature in degrees Rankine. The regression analysis led to

MATERIAL	a	w	MULTIPLE CORRELATION COEFFICIENT	PERCENT STANDARD DEVIATION
PLL	12,150	0.26	0.94	5
PLH	12,440	0.27	0.90	7
A	10,780	0.23	0.88	6
SP	7,820	0.17	0.94	4
SG	5,370	0.11	0.84	5
P*	7,510	0.18	0.84	5

* Data from Phase I round robin.

Plots of the correlations for these six materials are given in Figs. 38 through 40. The correlation and percent standard deviation for the high-density phenolic-nylon were determined with the General Electric data excluded. Their pyrometer differed from the other optical parameters supplied by the various facilities during the Phase I round robin in that it was a special, in-house, two-color design. These correlations were quite satisfactory.

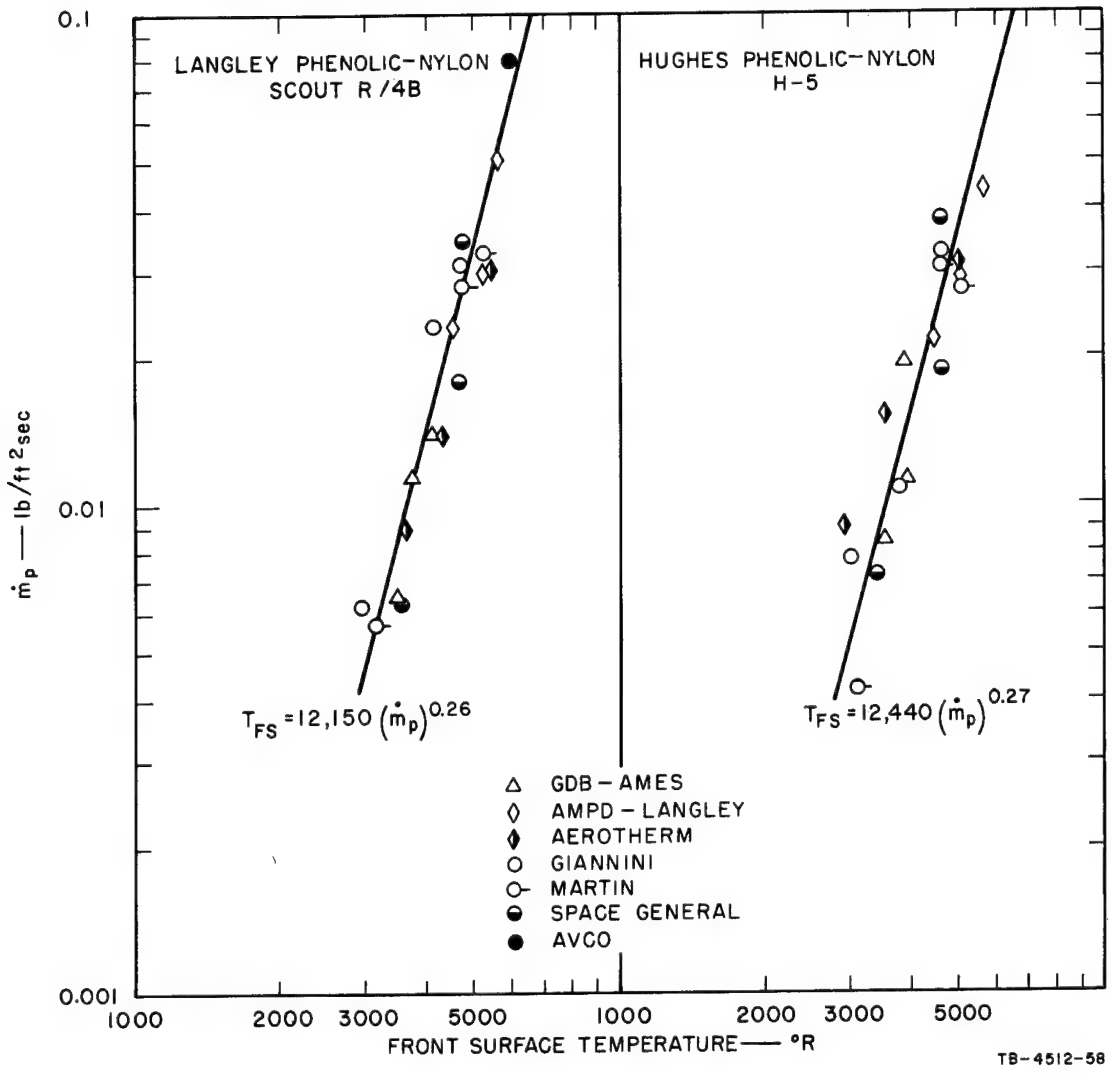

FIG. 38 FRONT SURFACE TEMPERATURE CORRELATION FOR LANGLEY AND HUGHES LOW-DENSITY PHENOLIC-NYLONS

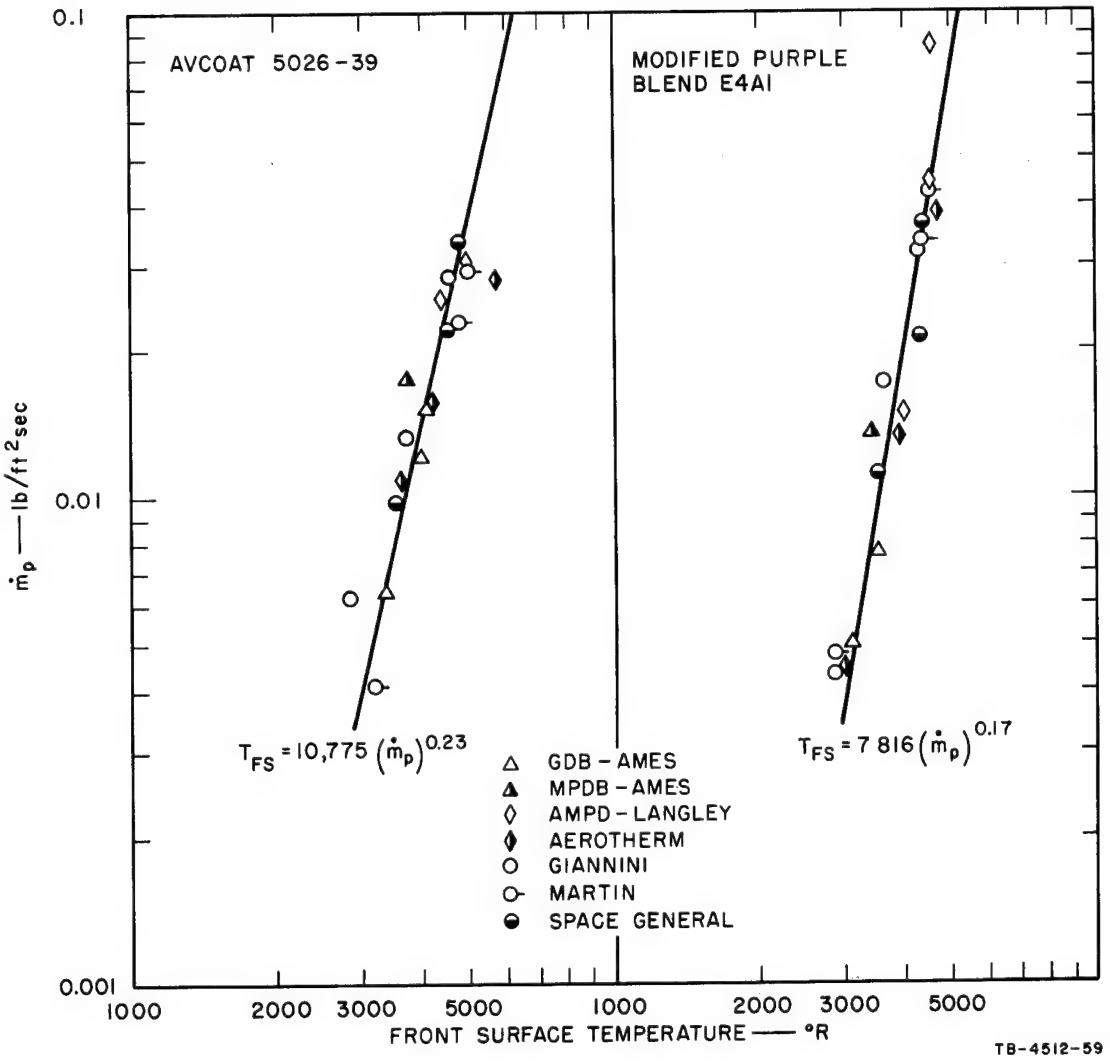

FIG. 39 FRONT SURFACE TEMPERATURE CORRELATION FOR AVCOAT AND MODIFIED PURPLE BLEND SILICONE

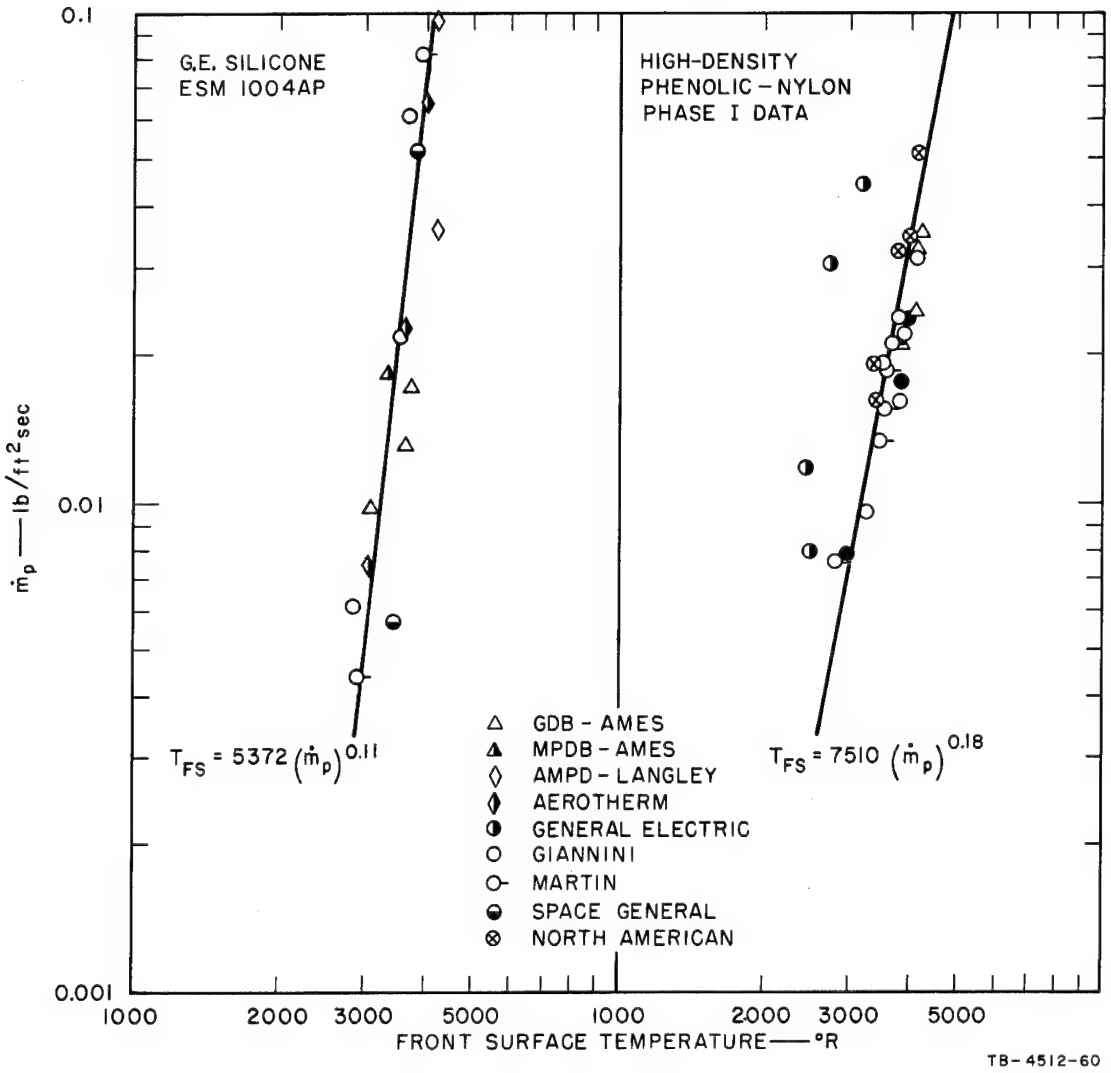

FIG. 40 FRONT SURFACE TEMPERATURE CORRELATION FOR GENERAL ELECTRIC SILICONE AND HIGH-DENSITY PHENOLIC-NYLON

As good a correlation was obtained by replacing $\dot{m}_p$ with $\dot{m}_t$. Other equally good correlations were

$$T_{FS} = a(P_{t_2})^v(\dot{m}_p)^w \tag{35}$$

and

$$T_{FS} = a(\dot{q}_{\substack{SRI \\ CW}})^n(P_{t_2})^m \tag{36}$$

This was expected since T_{FS} correlates with $\dot{m}_p$ (see Equation (21) or $\dot{m}_t$, and they correlate with heating rate and stagnation pressure (see Equation (20)). For Equation (35), with the pyrolysis rate, $\dot{m}_p$, used, the regression analysis gave

MATERIAL	a	v	w	MULTIPLE CORRELATION COEFFICIENT	PERCENT STANDARD DEVIATION
PLL	10,980	0.031	0.21	0.95	5
PLH	10,710	0.044	0.20	0.92	6
A	10,040	0.039	0.18	0.90	6
SP	7,660	0.012	0.16	0.95	4
SG	5,210	0.028	0.072	0.86	5
P*	7,260	0.0076	0.17	0.84	4

* Data from Phase I round robin.

b. Internal Temperature Rise

A number of the models for all five of the low-density materials were internally instrumented with thermocouples. The method of preparing these models and the information obtained have been described earlier.

(1) Any Temperature Rise. Of considerable interest in ablation design is the thickness of a given material required to prevent the bond line from reaching a given temperature before a given time. It was therefore decided to try correlating thermocouple position, x (in inches), with the time to reach a given temperature, t (seconds for a temperature rise of (ΔT), and the environmental parameters of heating rate and stagnation pressure. The form of the relation evaluated was

$$x = a(P_{t_2})^b(\dot{q}_{\substack{SRI \\ CW}})^c(t)^d(\Delta T)^e \tag{37}$$

Approximately six points from each temperature profile given in Appendix C, covering the range from low temperature rises to values of approximately 1200°F, were used in the regression analysis. The results were

MATERIAL	a	b	c	d	e	MULTIPLE CORRELATION COEFFICIENT	PERCENT STANDARD DEVIATION
PLL	0.034	0.053	0.30	0.63	-0.28	0.93	13
PLH	0.056	0.035	0.15	0.58	-0.24	0.97	9
A	0.037	0.018	0.27	0.60	-0.26	0.92	14
SP	0.072	0.022	0.18	0.52	-0.30	0.95	12
SG	0.12	0.031	0.098	0.54	-0.28	0.97	8

A. J. Chapman[14] interpreted model temperature data in a similar way. For a low-density phenolic-nylon prepared at Langley (ρ = 39 lb/ft^3), his relation, converted to be comparable to Equation (37), was $x = 0.013\ \dot{q}^{0.39} t^{0.89} \Delta T^{-0.39}$. This is not far different from the values for phenolic-nylon (PLL) when one considers that the experiments were performed in a subsonic facility with an invariant stagnation pressure of one atmosphere. Therefore, P_{t_2} could not be included in the relation.

Recently, postlaunch reports have become available for several of the unmanned Apollo spacecrafts which used Avcoat (A) for the ablating material on the heat shield. Data from these manned Spacecraft Center Reports[15,16] were used in Equation (37) along with the above constants for Avcoat (A) to predict the positions of the 600 and 1000°F isotherms. These predictions are listed with the NASA predictions and measured depths in Table V. They compare very favorably.

(2) Temperature Rise of 250°F. A more limited correlation was tried in which the temperature rise, ΔT, was 250°F; for this, the time was designated t_{250}. The form of this relation was

$$x = a(P_{t_2})^b (\dot{q}_{\substack{SRI \\ CW}})^c (t_{250})^d \qquad (38)$$

The regression analysis, using the time to a 250°F temperature rise at each thermocouple position, as tabulated in Appendix C, led to

MATERIAL	a	b	c	d	MULTIPLE CORRELATION COEFFICIENT	PERCENT STANDARD DEVIATION
PLL	0.014	0.083	0.18	0.61	0.97	8
PHL	0.017	0.079	0.14	0.60	0.99	5
A	0.023	0.105	0.15	0.62	0.99	6
SP	0.0082	0.016	0.26	0.54	0.97	9
SG	0.033	0.065	0.046	0.55	0.99	2

Table V

PREDICTED AND MEASURED ISOTHERMS FOR AVCOAT MATERIAL ON APOLLO MISSIONS

	TOTAL HEAT $Q = \dot{q}t$ (Btu/ft^2) (1)	FLIGHT TIME t (sec) (2)	HEAT TRANSFER RATE $\dot{q}_{AV}$ (Btu/ft^{2}sec) (3)	STAGNATION PRESSURE $P_{t_{2AV}}$ (atm) (4)	INITIAL TEMPERATURE $T_{i_{oF}}$ (5)	SRI PREDICTED 1000°F Isotherm (in.) $\Delta T = 900°F$	SRI PREDICTED 600°F Isotherm (in.) $\Delta T = 500°F$	HEAT SHIELD LOCATION (6) Z (in.)	HEAT SHIELD LOCATION (6) Y (in.)	NASA PREDICTED 1000°F Isotherm (in.)	NASA PREDICTED 600°F Isotherm (in.)	NASA MEASURED 1000°F Isotherm (in.)	NASA MEASURED 600°F Isotherm (in.)
Misson AS 201	6,100	85	71.8	0.408	100	0.28	0.35	71	0	0.25	0.39	0.32	0.47
								0	0	0.29	0.42	0.21	0.35
								-71	0	0.26	0.38	0.21	0.35
								0	39	0.32	0.45	0.22	0.37
	8,800	85	104	0.408	100	0.31	0.38	0	71	0.32	0.45	0.25	0.38
	(7)	(8)		(8)	(9)			(10)		Extrapolated Isotherms 1000°F	Extrapolated Isotherms 600°F	Char Depth	Discoloration Depth
Misson AS 202	20,000	750	27	0.061	100	0.74	0.91	70	0	0.73	1.07	0.68	1.08
								64	0	0.63	0.95	0.66	1.00
								34.5	0	0.47	0.68	0.61	0.94
								0	1.5	0.50	0.80	0.59	0.91
								-67.5	0	0.52	0.75	0.46	0.80
								0	+38	0.40	0.57	0.58	0.84
								0	+69.5	0.63	0.87	0.75	0.96

(1) From Fig. 7.4-9, pp. 7-83, MSC-A-R-66-4.
(2) From Fig. 6.2-1, pp. 6-19, MSC-A-R-66-4.
(3) $Q/t = \dot{q}_{AV}$.
(4) From Fig. 6.2-1, pp. 6-19, MSC-A-R-66-4.
(5) From Fig. 7.4-7, pp. 7-77, MSC-A-R-66-4.
(6) From Table 7.4-I, pp. 7-69, MSC-A-R-66-4.
(7) From Fig. 7.3-1, pp. 7-58 and pp. 1-2, MSC-A-R-66-5.
(8) From Fig. 7.3-2, pp. 7-64, MSC-A-R-66-5.
(9) From Fig. 7.4.2-4, pp. 7-104, MSC-A-R-66-5.
(10) From Table 7.4.2-I, pp. 7-100, MSC-A-R-66-5.

As expected, the multiple correlation coefficient rises and the percent standard deviation drops, as compared to the correlation given in Equation (37), since one would predict from one-dimensional heat transfer theory that ΔT would enter into the relation in a more complex way than a simple power function.

A plot of this correlation was difficult to make with these data because the various thermocouple positions were essentially the same in all models, causing the points to bunch up at these values of x. For this reason, the relation was inverted to make t_{250} the dependent variable, as follows:

$$t_{250} = a(P_{t_2})^b(\dot{q}_{\substack{SRI \\ CW}})^c(x_{250})^d \qquad (39)$$

Results of the regression analysis were

MATERIAL	a	b	c	d	MULTIPLE CORRELATION COEFFICIENT	PERCENT STANDARD DEVIATION
PLL	1110	-0.26	-0.33	1.54	0.98	13
PLH	930	-0.13	-0.25	1.62	0.99	8
A	470	-0.166	-0.25	1.58	0.99	9
SP	7250	+0.0074	-0.53	1.70	0.97	16
SG	370	-0.12	-0.087	1.81	0.99	5

The constants and exponents are not directly convertible between Equations (38) and (39) because the regression analysis maximizes the multiple correlation coefficient for the dependent variable. The closer this coefficient is to unity, however, the better is the conversion between the constants and the exponents. The difference in percent standard deviation also arises from the fact that it is calculated for the dependent variable, and t_{250} is more sensitive to x_{250} (because the coefficient d in Equation (39) is greater than unity) than vice versa.

The correlation given in Equation (39) is graphed in Figs. 41 through 45 for the various materials. It should be remembered that in all cases the thickness represented by x_{250} can be converted to weight per unit area, W_{250} (in pounds per square foot), by use of the polymer density, ρ_{VR} (in pounds per cubic foot).* Thus,

$$W_{250} = x_{250}(\rho_{VR}/12)^{VR} \qquad (40)$$

* Polymer densities are given in Table I.

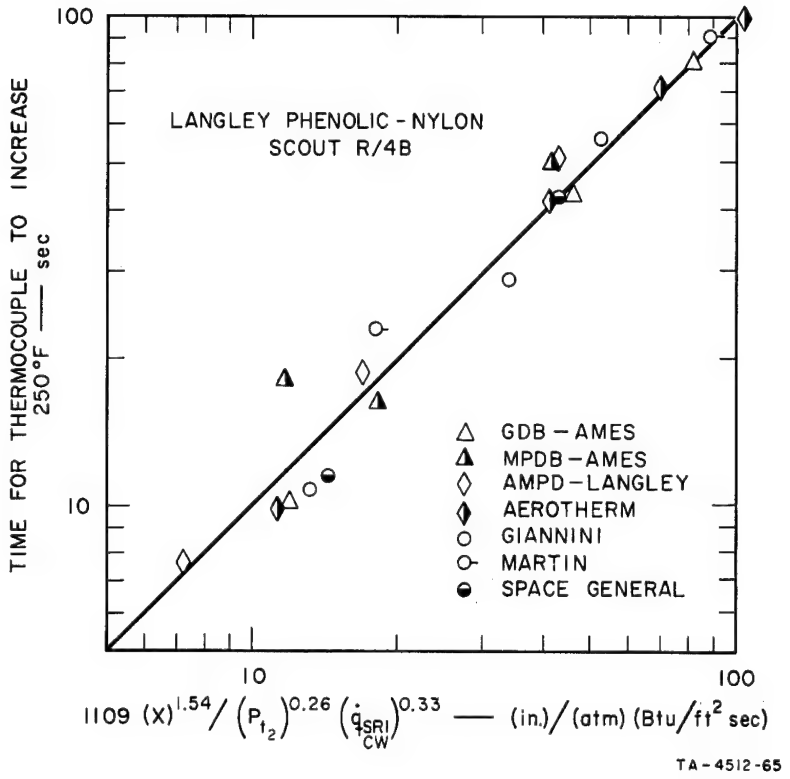

FIG. 41 INTERNAL TEMPERATURE CORRELATION FOR LANGLEY LOW-DENSITY PHENOLIC-NYLON

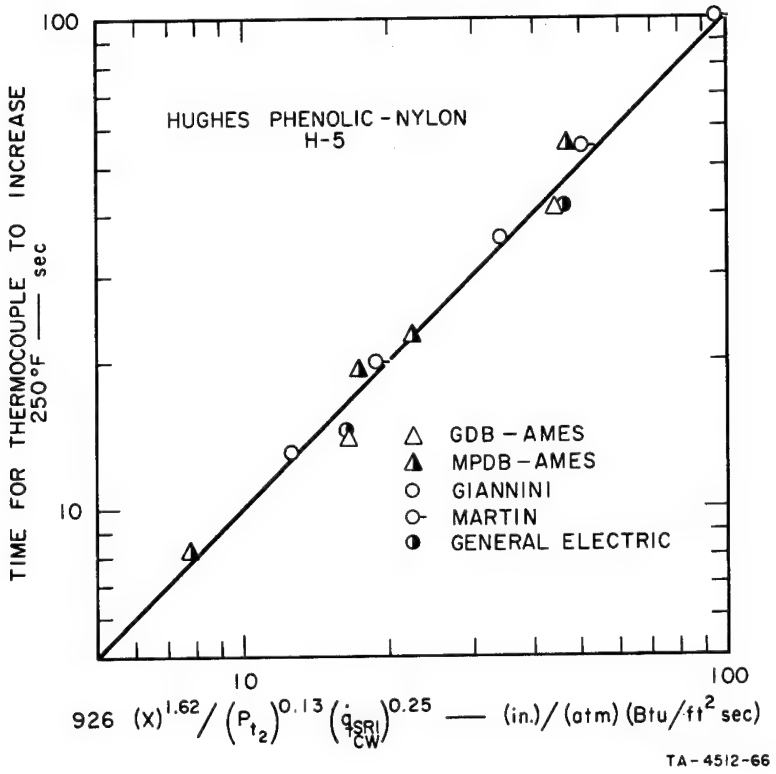

FIG. 42 INTERNAL TEMPERATURE CORRELATION FOR HUGHES LOW-DENSITY PHENOLIC-NYLON

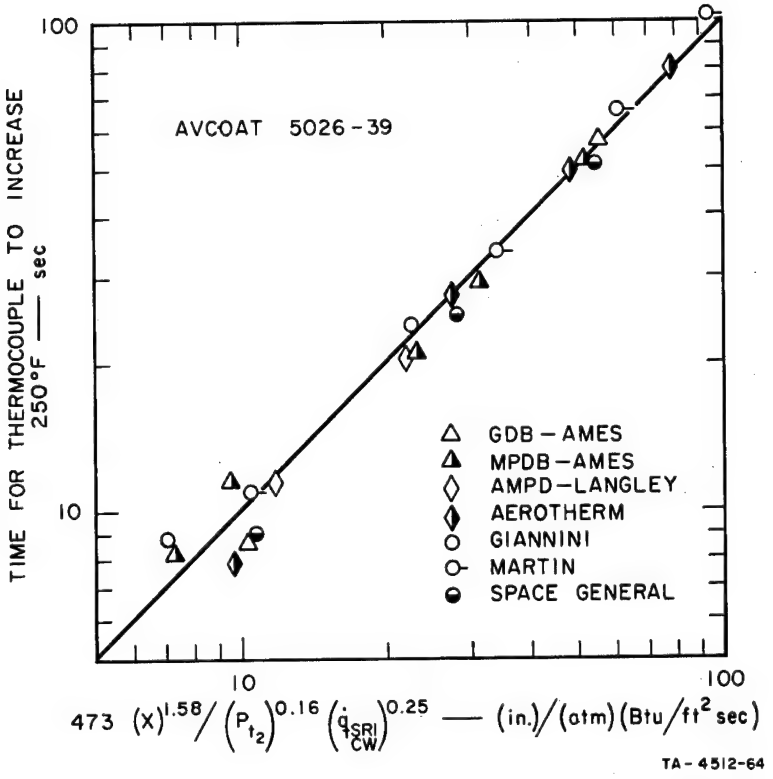

FIG. 43 INTERNAL TEMPERATURE CORRELATION FOR AVCOAT

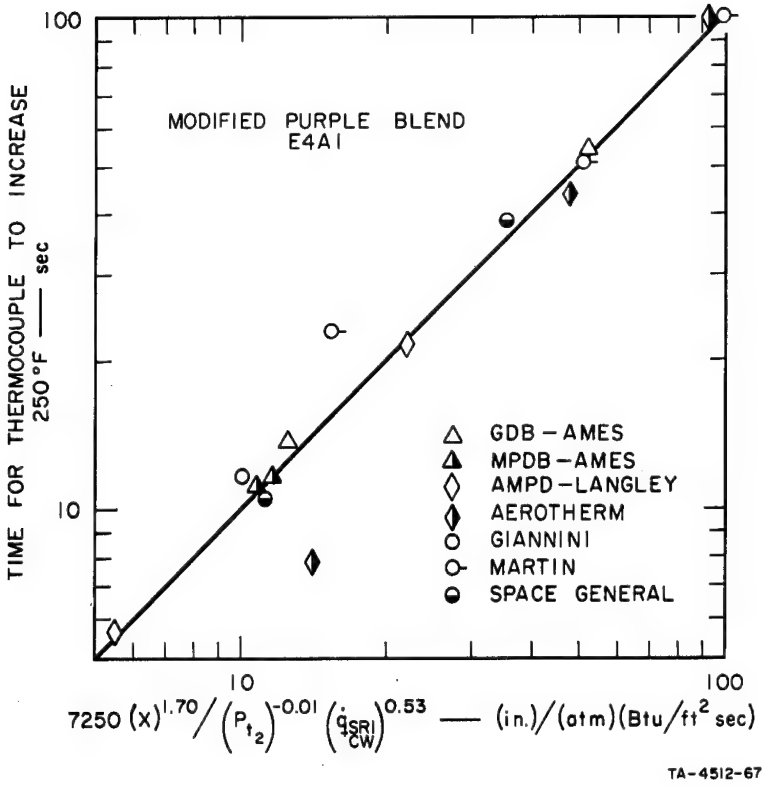

FIG. 44 INTERNAL TEMPERATURE CORRELATION FOR MODIFIED PURPLE BLEND SILICONE

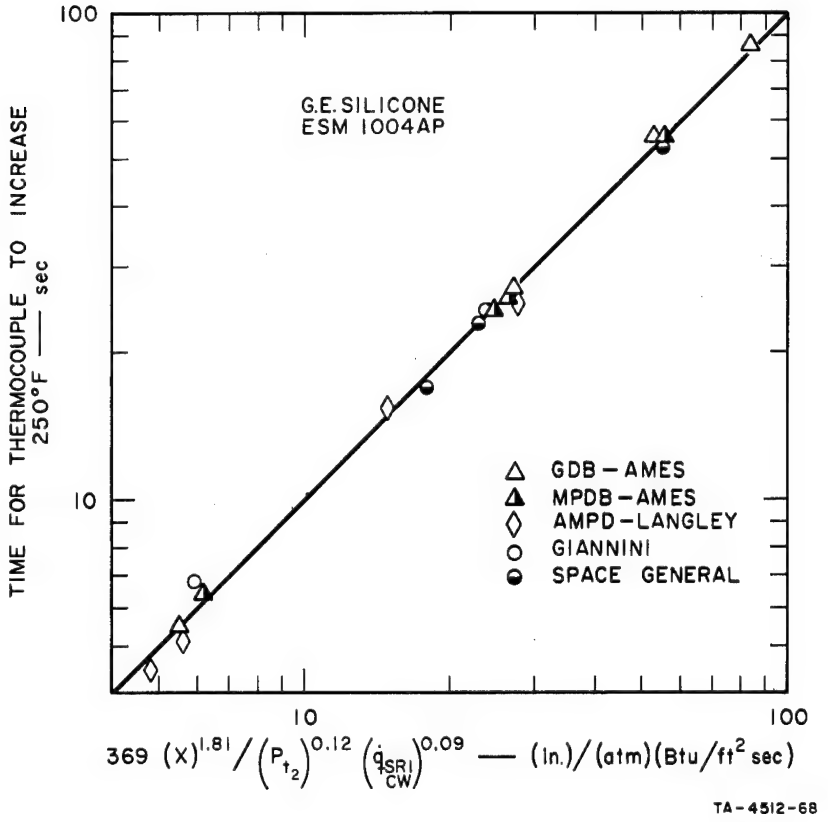

FIG. 45 INTERNAL TEMPERATURE CORRELATION FOR GENERAL ELECTRIC SILICONE

c. Dimensionless Forms of Correlations

The development of dimensionless forms for the temperature correlations involve additional variables over those considered in the mass loss cases. These additional variables differ for the two cases of concern: front surface and internal temperature.

(1) Front Surface Temperature. The variables considered in the dimensional analysis are similar to those listed in Appendix E, except for the elimination of the mass loss rate, $\dot{m}_t$, and its dimensionless group, π_m, since it is a function of π_q and π_p. In addition, new variables to be added are the front surface temperature, T_{FS}, and the emissivity of the ablating surface, ϵ. The units for these variables are:

VARIABLES	UNITS	CONVERTED VARIABLES	CONVERTED UNITS
T_{FS}	^{o}R	T_{FS}	^{o}R
ϵ	None	ϵ	None

These involve one additional dimension, temperature, and so one additional dimensionless group is required (=2 - 1). This group is

$$\pi_s = (\epsilon \sigma T_{FS}^4 S_R^2 R_{eff})/(\Delta H_D^{1.5} K) \qquad (41)^*$$

The Stefan-Boltzmann constant, σ, is a conversion factor having the following value

$$\sigma = 4.76 \times 10^{-13} \text{ Btu/ft}^2 \text{ sec } ^{\circ}R^4$$

In its converted variable form, it becomes $\sigma J_m g_c$ with units of $\text{lb/sec}^3\ ^{\circ}R^4$ Definitions of J_m and g_c are given in Equation (E-3A) of Appendix E.

Neglecting the Fay-Riddell group, π_f, for the experiments performed under supersonic flow conditions, the correlation relation might be

$$\pi_s = b_0 \pi_q^u \pi_p^v \qquad (42)$$

* See Equation (E-3B) of Appendix E for the definition of the conversion factor K.

However, there is already a power function relation between the last two π-groups and π_m (see Equation (20)), and so one of them, π_q, can be eliminated to give

$$\pi_s = c_0 \pi_p^z \pi_m^y \tag{43}$$

Since ΔH_D is still not known for these materials, expansion of this relation into a dimensional form leads to

$$T_{FS} = a(P_{t_2})^{z/4}(\dot{m}_p)^{y/4} \tag{44}$$

where

$$a = \left(\frac{c_0}{\epsilon\sigma}\right)^{0.25} (S_R^2 R_{eff})^{(z+y-1)/4} \Delta H_D^{(3-2z-y)/8} K^{(1-2z-y)/4} \tag{45A}$$

and

$$z = 4v, \qquad y = 4w \tag{45B}$$

in Equation (35). If z/4, or v, is quite small, the pressure term will approach unity and Equation (44) reduces to

$$T_{FS} \simeq a(\dot{m}_p)^{y/4} \tag{46}$$

where y = 4w in Equation (34) and "a" is the same as in Equation (45A) except that z is set to zero. The exponents given for these cases and their converted values are given below, where it is seen that v is indeed relatively small.

	Equations (35 and (44) $T_{FS} = a(P_{t_2})^v(\dot{m}_p)^w$				Equations (34) and (46) $T_{FS} = a(\dot{m}_p)^w$	
Material	v	w	z = 4v	y = 4w	w	y = 4w
PLL	0.031	0.21	0.13	0.84	0.26	1.04
PLH	0.044	0.20	0.18	0.80	0.27	1.08
A	0.039	0.18	0.16	0.72	0.23	0.92
SP	0.012	0.16	0.048	0.64	0.17	0.68
SG	0.028	0.072	0.12	0.29	0.11	0.44

The values of a, v, and w in Equations (34) and (35) when the mass loss rate, $\dot{m}_t$, is used in the correlations are given in Table VI. This table also gives the values of a, n, and m for Equation (36). It should be remembered that these are directly interconvertible with Equation (11) because of the emphasis the regression program puts on the dependent variable in determining the best correlation.

Table VI

CONSTANTS FOR ADDITIONAL FRONT SURFACE TEMPERATURE CORRELATIONS

A. Equation (34) $T_{FS} = a(\dot{m}_t)^w$

MATERIAL	a	w	MULTIPLE CORRELATION COEFFICIENT	PERCENT STANDARD DEVIATION
PLL	11,260	0.23	0.90	6
PLH	13,480	0.28	0.91	6
A	7,990	0.16	0.86	6
SP	7,410	0.15	0.96	3
SG	5,000	0.082	0.89	4

B. Equation (35) $T_{FS} = a(P_{t_2})^v(\dot{m}_t)^w$

MATERIAL	a	v	w	MULTIPLE CORRELATION COEFFICIENT	PERCENT STANDARD DEVIATION
PLL	10,260	0.019	0.19	0.91	6
PLH	12,530	0.017	0.25	0.91	6
A	8,620	0.026	0.20	0.87	6
SP	7,530	-0.016	0.17	0.96	3
SG	5,010	0.0067	0.076	0.90	4

C. Equation (36) $T_{FS} = a(\dot{q}_{\substack{SRI \\ CW}})^n(P_{t_2})^m$

MATERIAL	a	n	m	MULTIPLE CORRELATION COEFFICIENT	PERCENT STANDARD DEVIATION
PLL	2,870	0.10	0.052	0.94	5
PLH	2,600	0.12	0.055	0.93	5
A	2,280	0.13	0.025	0.90	6
SP	2,110	0.13	0.028	0.93	5
SG	2,680	0.077	0.032	0.88	4
P*	2,530	0.096	0.032	0.80	5

* Data from Phase I round-robin.

(2) Internal Temperature Rise. In this dimensional analysis, two variables—the front surface temperature, T_{FS}, and its related term, ϵ,—can be dropped since their dimensionless group, π_s, is a function of π_q and π_p and can be eliminated. The five new variables to be considered are the position, x, at which a given temperature rise, ΔT, has taken place at a given time, t, the heat capacity, C_p, and the density of the virgin polymer, ρ_{VR}. The units of these variables are

Variables	Units	Converted Variables	Converted Units
x	ft	x	ft
ΔT	°F	ΔT	°F
t	sec	t	sec
C_p	Btu/lb °F	$C_p J_m g_c$	ft^2/sec^2 °F
ρ_{VR}	lb/ft^3	ρ_{VR}	lb/ft^3

A net of three new variables has been added without any change in the number of dimensions, and there is one dimensionless group to be replaced, π_s; thus four (3 + 1) new dimensionless groups are required. In their simplest form, these are

$$\pi_x = x/R_{eff} \tag{47}$$

$$\pi_T = C_p\Delta T/\Delta H_D \tag{48}$$

$$\pi_t = t(\Delta H_D J_m g_c)^{0.5}/R_{eff} \tag{49}*$$

$$\pi_D = \rho_{VR} S_R^2 R_{eff} F_p g_c \tag{50}*$$

The numerator of the second of these (48) represents the heat stored in the virgin polymer per unit mass and is the cause of the temperature rise. Other variables might be considered, such as those to allow for conductive heat flow, but this would require definition of another temperature difference and does not add new information.

The correlation proposed is

$$\pi_x = b_0 \pi_p^b \pi_q^c \pi_t^d \pi_T^e \pi_D^f \tag{51}$$

* See Equation (E-3A) of Appendix E for definitions of conversion factors g_c, J_m, and F_p.

Again, ΔH_D is not known for these materials, and so the expanded dimensional form is

$$x = a(P_{t_2})^b(\dot{q}_{\substack{SRI \\ CW}})^c(t)^d(\Delta T)^e \qquad (52)$$

where

$$a = b_0(R_{eff})^{1+b+c-d+f}(S_R^2)^{b+c+f}(\Delta H_D)^{(d-2b-3c-2e)/2}(C_p)^e(\rho_{VR})^f \cdot J_m^{(d-2b-c)/2}F_p^{2b+c+f}g_c^{(2f+d+2b+c)/2} \quad . \qquad (53)$$

In the case of the 250°F isotherm, the π_T term becomes a constant so that Equation (51) becomes

$$\pi_x = g_0\pi_p^b\pi_q^c\pi_t^d\pi_D^f \quad . \qquad (54)$$

The expanded dimensional form is then

$$x_{250} = a(P_{t_2})^b(\dot{q}_{\substack{SRI \\ CW}})^c(t_{250})^d \qquad (55)$$

where

$$a = g_0(R_{eff})^{1+b+c-d+f}(S_R^2)^{b+c+f}(\Delta H_D)^{(d-2b-3c)/2}(\rho_{VR})^f \cdot J_m^{(d-2b-c)/2}F_p^{2b+c+f}g_c^{(2f+d+2b+c)/2} \quad . \qquad (56)$$

Also,

$$g_0 = b_0(C_p\Delta T/\Delta H_D)^e \quad \text{and} \quad \Delta T = 250°F \quad . \qquad (57)$$

The value of the exponent f is almost impossible to determine since density cannot be changed enough to determine its effect without also affecting other properties of the material. However, the success in using Equation (40) to predict isotherms in the Apollo, which has a very much larger effective radius than the models tested in this program, would suggest that the exponent on R_{eff} is very small. If it is assumed to be zero, then f is approximately equal to d - 1 - b - c.

4. Comparative Ablation

The correlations reported in the previous sections permit comparison of the ablation behavior of the materials studied as a function of environment.

a. Mass Loss Rate

Equation (20) relates the mass loss rate to the stagnation point heating rate and pressure,

$$\dot{m}_t = a(\dot{q}_{\underset{CW}{SRI}})^n (P_{t_2})^m \tag{20}$$

or by use of the Fay-Riddell relation, $\pi_f = 1$, in terms of the enthalpy potential,

$$\dot{m}_t = b(\Delta h_{\underset{CW}{calc}})^n (P_{t_2})^{(2m+n)/2} \tag{58}$$

where

$$b = a(S_R)^{-n}(R_{eff})^{-n/2} \tag{59}$$

Figure 46 is a logarithmic plot of Equation (58) based on the values of constants in Equation (20) for the five low-density materials. Stagnation pressure values of 0.03 and 0.3 atm were assumed, and R_{eff} was taken to be the same as the 1.25-in. flat-face model, i.e., 0.172 ft.

At the lower pressures (i.e., higher altitudes) the silicone materials, SP and SG, show much lower mass loss rates at low enthalpies (i.e., low flight velocities). At higher enthalpies, however, the low-density phenolic-nylons, PLL and PLH, have the lowest rates, followed closely by Avcoat (A). With higher stagnation pressures, representing lower altitudes, the low-density phenolic-nylons are best, across almost the entire range of enthalpies.

The behavior of high-density phenolic-nylon (P) and Teflon (T) is also shown at the higher stagnation pressure. The Teflon shows very poor performance, but the high-density phenolic-nylon is better than the silicones at high enthalpies. One factor not considered here is the threshold stagnation pressures at which mechanical forces markedly increase the mass loss rate. This appears to occur at lower pressures for the low-density materials so that high-density phenolic-nylon may behave better at higher pressures.

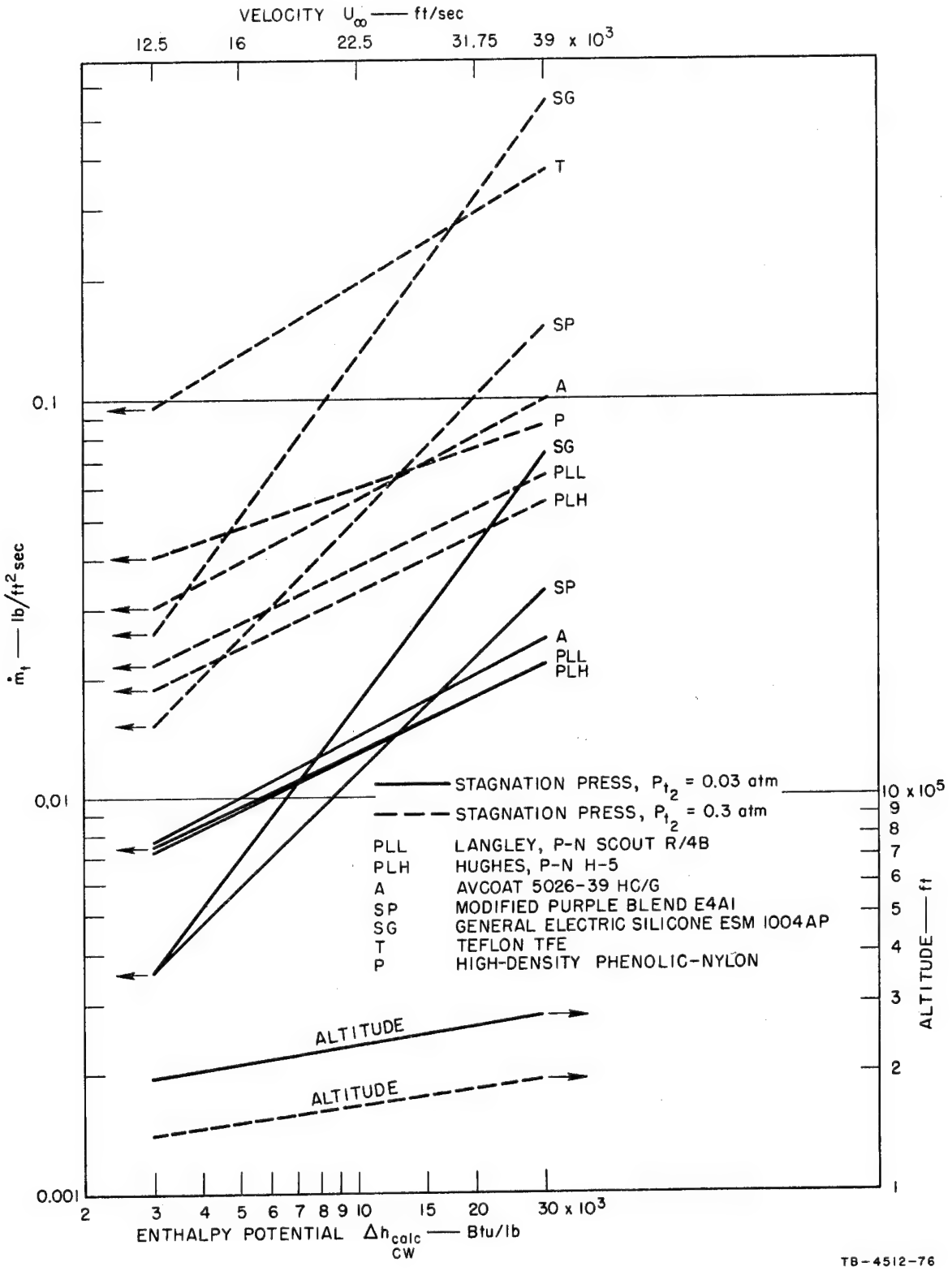

FIG. 46 COMPARATIVE ABLATION OF LOW-DENSITY MATERIALS

b. Front Surface Temperature

Relation of pyrolysis rate to front surface temperature is given by Equation (34):

$$T_{FS} = a(\dot{m}_p)^w \quad . \tag{34}$$

The constants for the various materials can be used to calculate the pyrolysis rate at several values of T_{FS}. The results are tabulated below.

	$\dot{m}_p$ (lb/ft^2 sec)	
MATERIAL	T_{FS} = 2000°F	T_{FS} = 4000°F
PLL	0.0021	0.021
PLH	0.0025	0.022
A	0.0016	0.022
SP	0.0011	0.037
SG	0.00085	0.19
P	0.0021	0.055

This again shows that at the lower thermal environments the silicone materials, SP and SG, perform best; i.e., they have the lowest pyrolysis rates by a factor of two or three. At the higher front surface temperature, 4000°F, their behavior is reversed, and they show the highest pyrolysis rates.

The marked change in pyrolysis rate with temperature is undoubtedly related to the chemical reactions involving silicon, oxygen, and carbon.[17] Below the melting point of silica, and this is intermediate to the two temperatures selected for the above tabulation, the surface is protected by silica and some silicon carbide. The latter is formed with the evolution of carbon monoxide. Above the melting point, however, the silica reacts with carbon to form, in addition, liquid silicon and gaseous silicon monoxide which are rapidly removed from the surface.

c. Internal Temperature Rise

The heat rejection and insulating power of the various materials is best represented by the internal temperature correlation Equation (39), as follows:

$$t_{250} = a(P_{t_2})^b \left(q_{\substack{SRI \\ CW}}\right)^c (x_{250})^d \tag{39}$$

Again using the Fay-Riddell relation, $\pi_f = 1$, to express this in terms of enthalpy potential, this becomes

$$t_{250} = g(P_{t_2})^{b+(c/2)}(\Delta h_{\underset{CW}{calc}})^{c}(x_{250})^{d} \qquad (60)$$

where

$$g = a(S_R)^{-c}(R_{eff})^{-c/2} \quad . \qquad (61)$$

The time for the 250°F isotherm to reach a position of 0.4 in. back of the front surface has been calculated at a stagnation pressure of 0.03 atm and an R_{eff} of 0.172 ft for two different enthalpies. The results based on the constants found for Equation (39) are tabulated below.

MATERIAL	W_{250} (lb/ft^2)	t_{250} (sec)	
	x_{250} = 0.4 in.	$\Delta h_{\underset{CW}{calc}}$ = 3000	$\Delta h_{\underset{CW}{calc}}$ = 30,000
PLL	1.19	180	86
PLH	1.18	120	69
A	1.03	72	41
SP	1.11	190	58
SG	1.22	74	60

The best insulator over the range of enthalpies is the Langley low-density phenolic-nylon (PLL); the poorest is Avcoat (A), probably because of conduction along the web.

The lower density of the Avcoat material can be taken into account by selecting material depths that give the same weight loading. When this is done, the tabulation becomes

MATERIAL	x_{250} (in.)	t_{250} (sec)	
	W_{250} = 1.03 lb/ft^2	$\Delta h_{\underset{CW}{calc}}$ = 3000	$\Delta h_{\underset{CW}{calc}}$ = 30,000
PLL	0.35	140	69
PLH	0.35	97	56
A	0.40	72	41
SP	0.37	167	51
SG	0.34	54	44

The comparative performance of Avcoat improves in this case, but not sufficiently to outrate the other materials at high enthalpies.

V CONCLUSIONS AND RECOMMENDATIONS

The results of the Phase II round robin confirm the earlier findings that the mass loss rates of a given material can be correlated in terms of heating rate and stagnation pressure. This is based on more extensive measurements over a wider range of variables. It was also again confirmed that determination of enthalpy by the energy balance method is not satisfactory. This is particularly true when the plasma stream exhibits heating rate and stagnation pressure gradients as was found for many of the facilities used in this study.

The use of a standard calorimeter helped in the interrelating of results, but the use of a standard, calibrated, total radiation pyrometer to measure front surface temperature was successful only when calibrated properly to account for the actual paths and viewing angles. Dimensional analysis shows that the Phase I round-robin data, for both Teflon and high-density phenolic-nylon, can be correlated by a single dimensionless relation in which the values for certain constants vary for each material. One of these, namely, the overall heat of decomposition of the material, cannot easily be determined separately, and for this reason the dimensionless form is converted to a dimensional relation by including this constant in another constant term. The latter relation permits proper allowance for the effective radius of the model in interpreting the data. The success of the dimensional relation in correlating literature data, which cover a thirty-five-fold range of effective radii, confirms this allowance.

The high stagnation pressure runs in Phase II fit the Phase I correlation, in the case of Teflon, up to pressures of 33 atm. The high-density phenolic-nylon data, on the other hand, showed rapidly increasing mass loss rates at pressures above 2.7 atm. The latter data can be correlated successfully, however, in terms of a mechanical stress at which failure of the char occurs. This is confirmed by the fact that these models showed essentially no char layer after testing.

The mass loss rate correlations for the low-density materials show the same form but different exponents than exhibited by the correlations for the high-density materials. The silicone materials do not correlate

as well as the low-density phenolic-nylon or Avcoat because there is evidence of an ablation mechanism change over the range of test environments.

Analogous correlations were obtained for front surface temperature and internal temperature rise for the low-density materials, and these can be derived, except for the values of the constants, by dimensional analysis. These three types of correlations can be used for predicting the performance of these materials and also for comparing their ablation behavior under different environments.

Attempts to include subsonic data in these correlations were unsuccessful because only one facility was involved and a broader range of fractional Mach numbers could not be studied.

Based on the results of the Phase II round robin; it is recommended that the following areas be studied further:

1. Determination of the critical stagnation pressure at which char failure begins for the low-density materials
2. Evaluation of other means than the use of energy balance to obtain accurate enthalpy measurement
3. Further correlation of available data and interpretation of the dimensionless correlations in terms of fundamental mechanisms
4. Evaluation of techniques for independently obtaining overall heat of decomposition for materials

Perhaps the most important recommendation of all is the following one suggested by success of the present program in showing that ablation results from different hyperthermal, convective test facilities can be interrelated.

5. Establishment of a round-robin program to determine whether ablation results from facilities having combined radiative and convective test devices can be interrelated.

APPENDICES

APPENDICES

The appendices contain detailed information about the test facilities and the data gathered at each, plus new correlations for the data from the Phase I round-robin study. The specific appendices are as follows:

Appendix A - Facility Information and Instrumentation Used for Phase II NASA Round-Robin Ablation Tests

Appendix B - Phase II Tunnel Calibration and Test Data

Appendix C - Model Temperature Data

Appendix D - Summary of Phase II Correlation Data

Appendix E - Dimensionless Correlation of Previous Data

The first two appendices are organized primarily by facility, listed in the following order:

1. Gas Dynamic Branch, Ames Research Center-NASA (GDB-Ames)
2. Magneto Plasma Dynamics Branch, Ames Research Center-NASA (MPDB-Ames)
3. Applied Materials and Physics Division, Langley Research Center-NASA (AMPD-Langley)
4. Entry Structures Branch, Langley Research Center-NASA (ESB-Langley)
5. Manned Spacecraft Center-NASA (MSC-Subsonic)
6. Manned Spacecraft Center-NASA (MSC-Supersonic)
7. Aerotherm Corporation (Aerotherm)
8. Avco Corporation (AVCO)
9. Giannini Scientific Corporation (Giannini)
10. Martin Company (Martin)
11. Space General Corporation (Space General)
12. Cornell Aeronautical Laboratory (Cornell)

The abbreviation used to designate the facility in tables and graphs is given in the parentheses following each listing.

The next two appendices are organized primarily by test material. Specifically these are:

a. Langley Phenolic-Nylon, Scout R/4B (PLL)

b. Hughes Phenolic-Nylon, H-5 (PLH)

c. Avcoat 5036-39, HC/G (A)

d. Modified Purple Blend Silicone, E4A1 (SP)

e. G. E. Silicone, ESM 1004AP (SG)

f. Teflon, TFE (T)

g. High-Density Phenolic-Nylon (P)

The symbols in the parentheses are those used to designate these materials and are part of the model number used in the tables.

APPENDIX A

FACILITY INFORMATION AND INSTRUMENTATION USED FOR PHASE II NASA ROUND-ROBIN ABLATION TESTS

Appendix A tabulates, by facility, a description of each plasma arc jet heater. The tables first describe the arc heater and power supply, then nozzle and test chamber dimensions, as well as the vacuum system and insertion capability. The section of the table on instrumentation describes the instruments or procedures used to measure the parameters indicated.

Appendix A

FACILITY INFORMATION AND INSTRUMENTATION USED FOR PHASE II NASA ROUND-ROBIN ABLATION TESTS

	A-1	A-2	A-3	A-4
Facility	NASA—Ames Research Center Gas Dynamics Branch	NASA—Ames Research Center Magneto Plasma Dynamics Branch	NASA—Langley Research Center Applied Materials and Physics Division	NASA—Langley Research Center Entry Structures Branch
Location	Moffett Field, California	Moffett Field, California	Langley Station, Hampton, Virginia	Langley Station, Hampton, Virginia
Tunnel Designation	Planetary Entry Ablation Facility	Low Density Constricted—Arc Supersonic Jet	20-in. Hypersonic Arc Heated Tunnel	Structures 5-Mw Arc Powered Tunnel
Facility Personnel	B. H. Wick R. B. Pope N. S. Vojvodich	H. A. Stine A. F. Okuno	B. Cocke G. D. Walberg R. E. Middan	W. A. Brooks G. M. Stokes R. D. Brown
Arc Heater				
- Design	Giannini MK-4	NASA, Ames design	NASA, Langley design	NASA, Langley design, 3 phase AC
- Electrode Material	Tungsten cathode, copper anode	Thoriated tungsten cathode, Multiple (24) Copper rod anodes	Copper cathode and anode	Water-cooled copper cathode and anode
- Stabilization	Gas vortex stabilized	Constrictor wall stabilizer	Magnetic stabilization	Magnetic, 1500 gauss
- Input Power	44-130 kw DC	100-750 kw DC	500-2000 kw DC	250-4800 kw AC
- Plenum Pressure	0.20-0.50 atm	0.5-3.3 atm	6.8-34.0 atm	0.1-7.0 atm
- Gas Flow Rate	0.0025 lb/sec through heater 0-0.00125 lb/sec, diluent to plenum	0.004-0.025 lb/sec	0.05-0.80 lb/sec	0.05-1.0 lb/sec air
Power Supply				
- Design	40 kw AC to DC selenium rectifiers	Silicon rectifiers, saturable core reactor control, 3 Mw	DC batteries, 1440 at 2.2 v each	AC, 3 phase, 1380 v
- Make	Miller	Temescal	Exide	--
- Maximum Current	2000 amp	4800 amp	3000 amp	4800 amp
Nozzle				
- Throat Diameter, D_t	0.467 in.	0.50 in.	0.538 in.	1.5 in.
- Exit Diameter, D_e	4.0 in.	6.125 in.	2.0 and 3.3 in.	4.0 in.
- Nozzle Expansion Section	Contoured, free jet	Conical, free jet	Conical, free jet	Conical, free jet
- D_t to D_e	--	10.5 in.	7.06 and 11.7 in.	6.75 in.
- D_e to Model Face	1.625 in.	4.25 in.	--	0.50 in.
- Mach No. of jet	4.1	4.5	3.2 and 3.7	2.8
Test Chamber				
- Diameter	48 in.	36 x 36 in. square	24 x 24 in. square	60 in.
- Length	54 in.	35 in.	38 in.	60 in.
- Cooling	None	Water heat exchanger	None	None
Vacuum System	19,700 ft^3 spheres pumped down to 40 microns Hg with Kinney and Stokes vacuum pumps	5-stage steam ejector, 4500 cfm, 20 microns at no flow	77,000 ft^3 sphere, 3 vacuum pumps, 50 microns at no flow	113,000 ft^3 Vacuum sphere
Multiple Model Insertion Capability, Maximum per Run	8	6	2	2

		A-2		A-4
Tunnel Instrumentation				
Input Power				
- Voltage	Voltage divider to C.E.C. recorder	Voltage divider to C.E.C. recorder and G.E. voltmeter	Voltage divider to C.E.C. recorder	Westinghouse wattmeter, Hall effect transducer to Beckman magnetic tape recorder
- Current	Hall effect device to C.E.C. recorder	Shunt to transductor to C.E.C. and Simpson Ammeter	Shunts to C.E.C. recorder	Current transducers to Esterline Angus, indicate only
Power Losses				
- Water Flow	Fisher-Porter rotometers	Differential pressure across "Rinco" Venturi	Turbine type flow meter	Airtronics turbine meter, Potter frequency converter to Beckman recorder
- Temperature Rise	Delta-T-Co differential temperature transducers to C.E.C. recorder	Differential temperature transducer to C.E.C.	Thermocouples to C.E.C. recorder	Ch-Al thermocouples to Beckman recorder
Test Gas				
- Composition	23% oxygen - 77% nitrogen by weight	Air	Air	Air
- Gas Flow Rate	Sonic flow orifices	Rotometer and pressure gage	Orifice plates	Laminar flow tube, Boonshaft and Fuchs system to Beckman recorder
- Gas Temperature	Thermometers ahead of orifices	Bimetallic well thermometer	--	Ch-Al thermocouple to Beckman tape recorder
Pressures				
- Reservoir	Statham ±5 psid transducer to C.E.C.	Statham transducer to C.E.C.	Strain gage type pressure	Statham transducers to Brown and Beckman recorder
- Nozzle Exit	--	--	Transducers to C.E. recorder	Not measured
- Test Chamber	0 to 1 in. water Dwyer Magnehellic gage	McLeod gage	--	Statham transducers to Beckman recorders
- Model Stagnation	0.75 in. diameter hemisphere to Statham 0 to 1 psia transducer to C.E.C.	Statham transducer to C.E.C.	--	Alnico transducers, M.B. Electronics, to Beckman, 3/8-in. water cooled hemisphere pitot probe
Model Temperatures				
- Facility Pyrometer Model Front Surface Temperature	1. Honeywell total radiation radiometer, 0.37 in. aperture, 0.3-3.8 microns, to C.E.C. recorder 2. Inst. Dev. Lab., Pyro 650 to C.E.C., 0.653 microns	--	Temperature camera (NASA TN D-2660)	Not measured
- SRI Radiometer	Located inside test chamber, model viewed with front surface mirror recorded on C.E.C.	Located inside test chamber viewed model with front surface mirror recorded on C.E.C.	--	Not measured
- Internal Temperatures	Ch-Al to C.E.C.	Ch-Al to C.E.C.	Ch-Al to C.E.C. recorder	Not measured
SRI Calorimeter	SRI Calorimeter No. 13 to C.E.C. recorder	SRI calorimeter to C.E.C.	SRI calorimeter to C.E.C. recorder	SRI calorimeter to Beckman recorder
Facility Calorimeter				
- Type	Transient slug type, similar to SRI design	Transient slug type, similar to SRI design	Langley design—thin wall, transient	Transient—thin wall, 0.030 wall thickness Langley design
- Shape	Hemisphere cylinder	Hemisphere cylinder	Flat face cylinder	Hemisphere
- Surface Material	Copper and Teflon coating	1 mil gold plate on copper	Stainless steel	Stainless steel
- Shroud Diameter	0.75 in.	1.25 in.	1.0 in.	1.5 in.
- Sensing Diameter	0.3125 in.	0.375 in.	1.0 in. - Multiple thermocouples inside shell	1.5 in. - Multiple thermocouples inside hemisphere
Run Time	Exposure time automatically controlled, models protected with water cooled shield, time on C.E.C.	Automatically controlled water cooled rotary sting mounts	From C.E.C. recorder	Automatic model withdrawal, limit switches on model holder to Honeywell Visicorder
Camera	Giannini Scientific, 32 mm movie and pulse framing camera	Kodak Cine Special 16 mm	--	Kodak Cine, 16 mm, 48 fps

Appendix A (Continued)

	A-5	A6	A-7	A-8
Facility	NASA Manned Spacecraft Center	NASA Manned Spacecraft Center	Aerotherm Corporation	Avco Corporation
Location	Houston, Texas	Houston, Texas	Palo Alto, California	Wilmington, Massachusetts
Tunnel Designation	MSC 1-Mw Arc Jet Subsonic	MSC 1.5-Mw Arc Tunnel	Aerotherm Arc Plasma Facility	10-Mw Arc Facility
Facility Personnel	D. H. Greenshields D. J. Tillian	J. E. Grimaud D. J. Tillian	D. T. Flood J. J. Reese	H. E. Hoercher R. W. Freeman J. Duggan
Arc Heater				
– Design	Modified Giannini	Segmented Constricted Arc, Electro-Optical Systems Design	Aerotherm design	AVCO design
– Electrode Material	Copper	Thoriated tungsten cathode silver-plated copper pin anodes	Thoriated tungsten cathode, copper anode	Carbon cathode, copper anode
– Stabilization	Magnetic field and gas vortex	Vortex stabilized	Gas vortex stabilized	Magnetic field and gas vortex
– Input Power	1000 kw DC	250-1000 kw DC	60-1000 kw DC	250-10,000 kw DC
– Plenum Pressure	1-3 atm	(Cathode) 0.1 to 2.0 atm	0.06-8.0 atm	0.5-28.0 atm
– Gas Flow Rate	0.02-0.05 lb/sec	0.0022-0.044 lb/sec	0.002-0.05 lb/sec	0.08-1.0 lb/sec
Power Supply				
– Design	1500 kw DC silicon rectifiers, saturable core reactor control	Silicon rectifiers, saturable core reactor control	2 diesel-electric generators: 1-1000 hp, 1-600 hp	2080 – 12 v, 200 amp hr truck batteries
– Make	---	A. O. Smith	---	Willard
– Maximum Current	2000 amp	3000 at 500 v, 1500 at 1000 v, 750 at 2000 v	3000 amp	6000 amp
Nozzle				
– Throat Diameter, D_t	Subsonic	0.7813 in.	1.05 and 1.00 in.	0.765 and 1.25 in.
– Exit Diameter, D_e	3.0 in.	5.8 in.	2.98 and 3.50 in.	1.178 and 1.25 in.
– Nozzle Expansion Section	Subsonic	Conical	Contoured, freejet and conical, free jet	Conical
– D_t to D_e	1.5 in.	5.2 in.	12.0 8.5 in.	1.0 in.
– D_e to Model Face	1.5 and 2.0 in.	4.0 in.	1.5 in.	3.0 in.
– Mach No. of Jet	Subsonic	3.8	3.0 and 3.2	2.2
Test Chamber	None			
– Diameter	---	72 in.	42 in.	Free jet, no test chamber used for this program
– Length	---	96 in.	180 in	Approximately 48 in.
– Cooling	---	Chamber cooling – circulated air	Cooled diffuser and heat exchanger	Water-cooled
Vacuum System	None	4-stage steam ejector, 0.01 lb/sec at 0.001 atm, 0.035 lb/sec at 0.01 atm, and 0.5 mm Hg at no flow	5-stage steam ejector, 0.036 lb/sec at 200 microns, 0.004 lb/sec at 50 microns, 30 microns Hg at no flow	None used
Multiple Model Insertion Capability, Maximum per Run	2	2	5	1

	A-5	A-6	A-7	A-8
Tunnel Instrumentation				
Input Power	Nobotrol transducers to Bristol recorder and to Systems Engineering Lab. digital system	Nobotrol transducers to Bristol recorder and Systems Engineering Lab. analog to digital system	Vidar voltage to frequency converter 260	Voltage divider to C.E.C. recorder
– Voltage				
– Current	Mv shunt to Bristol recorder	Mv shunt to Bristol and S.E.L. reorder	Vidar voltage to frequency converter 260	Shunt to C.E.C. recorder
Power Losses	Hydropoise flow transducer to frequency converter and recorder. Analog to digital magnetic tape record of most test variables			
– Water Flow		Turbine flow meters and frequency converters to S.E.L.	ASME orifice and manometer, plus Statham ΔP transducer to Vidar 260	Not measured
– Temperature Rise		Thermocouples and ΔT meter Ch-Al thermocouple	Delta T differential temperature transducer to Vidar 260	Not measured
Test Gas				
– Composition	Nitrogen plus oxygen to equal air	Nitrogen plus oxygen to equal air	Nitrogen plus oxygen to equal air	Air
– Gas Flow Rate	Choked orifices, electrical pressure transducers	Choked orifices, Statham transducers to S.E.L.	Fisher Porter rotometers plus orifice and Statham transducers	Fisher Porter flow meters and sonic flow orifices
– Gas Temperature	Thermocouple	Ch-Al thermocouple	I-C Thermocouple to M-H indicating pot.	
Pressures				
– Reservoir	Not measured	Statham transducer (0-15 psia) to S.E.L.	Statham abs. pressure transducer to C.E.C. 5-119 recorder	Electrical pressure transducer to C.E.C. recorder
– Nozzle Exit	Not measured	Statham transducer (0-1 psia) to S.E.L.	Wallace Tiernan gages	Not measured
– Test Chamber	Not measured	Statham transducer to S.E.L.	Wallace Tiernan gages	
– Model Stagnation	Not measured	Statham transducer (0-5 psia) to S.E.L. Wallace-Tiernan gages for checks	Statham diff. pressure transducer to C E.C. 5-119 recorder, 0.375 in diameter flat face water cooled pitot probe	Uncooled 1.25 in. diameter pitot probe, to C.E.C. pressure transducer, to C.E.C. recorder
Model Temperatures				
– Facility Pyrometer, Model Front Surface Temperature	Pyro-optical pyrometer Barnes R4D radiometer	Optical pyrometer—0.65 microns	Infrared Industries-TD9CH 0.8 ± 0.015 microns	Instrument Development Lab. recording pyrometer, 0.653 microns
– SRI Radiometer	SRI radiometer to S.E.L.	Not measured	SRI radiometer to C. P. Inst. 850 m.v. recorder	Not measured
– Internal Temperatures	Ch-Al to tape recorder	Not measured	Ch-Al to C.E.C. 5-119 recorder	Not measured
SRI Calorimeter	Recorded on S.E.L.	Recorded on Bristol and S.E.L.		
Facility Calorimeter		Hy-Cal Engineering (120-1000 Btu/ft^{2}sec)		
– Type	Hy-Cal Engineering	High Temperature Lab. (120-1000 Btu/ft^{2}sec)	Hy-Cal Engineering	AVCO null point transient calorimeters
– Shape	Flat face	Flat face	Flat faced cylinder	1. Flat faced cylinder 2. Hemispherical cone
– Surface Material	Constantan plus carbon coating	Constantan disc plus carbon coating	Constantan plus carbon black	Copper Copper
– Shroud Diameter	1.0 in. calorimeter in 1.25 in. shroud	1.0 in. copper body in 1.25 in. graphite shroud	1.0 in.	1.25 in. 1.0 in.
– Sensing Diameter	0.15 in.	0.060 in.	0.18 in.	0.375 in. 0.25 in.
Run Time	Microswitch on sting to S.E.L.	Microswitches on sting to S.E.L	C.E.C. recorder and stopwatch	From C.E.C. recorder and pressure and current traces
Camera	Milliken	Milliken	Triad Photosonics, 1B, 16 mm	Bolex Reflex, 300 mm lens 32 fps

	A-9	A-10	A-11	A-12
Facility	Giannini Scientific Corporation	Martin Company	Space General Corporation	Cornell Aeronautical Laboratory
Location	Santa Ana, California	Baltimore, Maryland	El Monte, California	Buffalo, New York
Tunnel Designation	1-Mw Hyperthermal Test Facility	Plasma Arc Laboratory, Facility B	Electro-Thermal Facility	Wave Superheater Hypersonic Tunnel
Facility Personnel	J. P. Todd E. Muehlberger	A. Guido G. J. Schmidt G. Guenterberg R. A. Woodward	S. L. Grindle M. W. Searcy	J. Carpenter R. Clements K. W. Graves
Arc Heater				Device consists of 288 (0.6 x 1.5-in.) shock tubes mounted on periphery of a rotating drum. Hot helium driver gas is supplied to the shock tubes from pebble bed heater. Energy is transferred to high pressure air, and forms steady supersonic jet.
- Design	Giannini design	Thermal Dynamics F 5000	Space General design	
- Electrode Material	Tungsten cathode, copper anode	Tungsten cathode, copper anode	Tungsten cathode, copper anode	
- Stabilization	Gas vortex stabilized	Gas vortex and magnetic field at anode	Gas vortex and magnetic field	
- Input Power	35-1000 kw DC	40-1500 kw DC	25-1500 kw DC	
- Plenum Pressure	0.02-0.36 atm	0.03-68 atm	0.01-40 atm	
- Gas Flow Rate	0.0005-0.01 lb/sec	0.0015-0.6 lb/sec	0.0001-0.2 lb/sec	5 lb/sec
Power Supply				
- Design	Six 150 kw, silicon rectifiers	3 phase full ware rectifier, saturable reactor control	Two 750 kw AC to DC silicon rectifiers, moving coil control	Does not apply
- Make	A. O. Smith	A. O. Smith	Glenn Pacific	
- Maximum Current	3000 amp	4000 amp at 500 v, 2000 amp at 1000 v	3500 amp	
Nozzle				
- Throat Diameter, D_t	1.0 in.	1.245 in.	1.0 in.	Free jet has dimensions of 1.5 in. height x 0.6 in. width at jet exit (rotor face).
- Exit Diameter, D_e	3.0 in.	3.0 in.	3.0 in.	
- Nozzle Expansion Section	Contoured, free jet	Conical, free jet	Contoured nozzle, free jet	
- D_t to D_e	6.18 in.	6.625 in.		
- D_e to Model Face	5.0 in.	--	2.25 in.	2.25 and 4.0 in.
- Mach No. of jet	3.0	2.7	3.0	2.7 and 3.6
Test Chamber				
- Diameter	30 in.	48 in.	36 in.	None used for these tests
- Length	72 in.	96 in.	84 in.	
- Cooling	Water-cooled chamber and vacuum line	Water-cooled test chamber, models and instruments held in separate chamber before insertion in stream	Chamber water-cooled and diffuser heat exchanger	
Vacuum System	Kinney vacuum pumps, 9000 cfm, 0.2 mm Hg at no flow.	5-stage steam ejector, 95,000 scfm, 2×10^{-5} atm at no flow.	2 Roots blowers followed by Stokes vacuum pump, 14,000 cfm, 0.1 mm Hg at no flow	None used
Multiple Model Insertion Capability, Maximum per Run	3	5	4	1

	A-9			A-12
Tunnel Instrumentation				A computation is made for the shock process as it occurs inside the rotor using the driver helium and charge air input temperatures and pressures.
Input Power				
- Voltage	Westinghouse PX 161	Greibach Instrument Mo 700	Westinghouse PX 161	
- Current	Westinghouse PX 161	Greibach Instrument Mo 700	Westinghouse PX 161	
Power Losses				
- Water Flow	Hydropoise turbine meter to Erie electronic counter	Cox and Potter turbine meters to Cox counter	Potter turbine meters to electronic counter	
- Temperature Rise	I-C thermocouples to Brown multipoint recorder	Bosemont Engineering platinum resistance thermometer	C-C thermocouples to DeVar recorders	
Test Gas				
- Composition	Nitrogen plus oxygen to equal air	Nitrogen plus oxygen to equal air	79% Nitrogen, 21% oxygen by volume	Air
- Gas Flow Rate	Standard orifice plates to Heise gage	Cox Instruments turbine meter and counter	Critical flow orifices to Heise gages	Not measured
- Gas Temperature	I-C thermocouples to Brown recorder	Tri-R thermister	--	Thermocouple monitors
Pressures				
- Reservoir	Wallace and Tiernan gages	Hg manometer, Heise gage	Wallace and Tiernan gages	100 atm maximum C.E.C. transducer and recorder
- Nozzle Exit	Wallace and Tiernan gages	Transsonic differential pressure	Wallace and Tiernan gages	Not measured
- Test Chamber	Wallace and Tiernan gages	MKS Instruments - 77MXRP-3	Wallace and Tiernan gages	Not measured
- Model Stagnation	Wallace and Tiernan differential pressure gage. Statham pressure transducer to Texas Instruments recorder	MKS differential pressure, 0.625 in. diameter water cooled pitot probe	Statham Transducer to DeVar recorder, 0.625 in. diameter water cooled pitot probe	10-85 atm, C.E.C. transducer and recorder
Model Temperatures				
- Facility Pyrometer, Model Front Surface Temperature	1. Infrared Industries, Thermodot TD6RT Recording Pyrometer (1 6-2.3 microns) to Texas Instruments F4W recorder 2. LN optical Pyrometer 8622C (0.655 microns)	Instrument Development Lab., Pyro 650	1. Leeds Northrup optical Pyrometer 8632F	Infrared Industries, Thermodot TDA-6
- SRI Radiometer	SRI radiometer to Midwest 1500B oscillograph	SRI radiometer to Offner oscillograph	SRI radiometer to LN Speedomax H recorder	Not measured
- Internal Temperatures	Ch-Al thermocouples to Midwest 1500B oscillograph	Ch-Al thermocouples to Systrac 160E2	Ch-Al to Texas Instruments F4W recorder	Not measured
SRI Calorimeter	SRI calorimeter to Midwest oscillograph			SRI calorimeter to C.E.C. recorder
Facility Calorimeter	1. Giannini steady state water temperature rise / 2. Giannini transient slug	1. Thermogage, Gardon / 2. Martin, transient		
- Type			HyCal Engineering asymptotic calorimeter	Cornell design
- Shape	Hemispherical / Flat face	Flat face cylinder / Flat face	Flat face cylinder	Hemispherical
- Surface Material	Copper / Copper	Constantan / Copper	Constantan	Copper
- Shroud Diameter	0.625 in. / 1.25 (graphite)	1.25 in. / 1.25 in.	1.25 in.	0.50 in.
- Sensing Diameter	0.625 in. / 0.25 in.	0.125 in. / 0.25 and 0.625	0.10 in.	0.125 in.
Run Time	Stop watch plus electric timer with switch on sting	Automatic run time record and arc shut off	Stop watch plus electronic timer activated by microswitch on sting	Test is started with model in place, run termination is automatically controlled
Camera	Bolex H16 movie camera	None used	Bolex H16 reflex movie camera	Two Photosonics

APPENDIX B

PHASE II TUNNEL CALIBRATION AND TEST DATA

This appendix contains separate tables of the data reported by each participating facility, plus the measurement data on all models that were determined at the Institute. The latter data constitute the last five columns of the tables.

The calibration runs were assigned numbers by the Institute so that they could be identified in the text. Pertinent remarks applicable to specific columns of data are indicated in the footnotes.

Table B-1

TUNNEL CALIBRATION AND TEST DATA REPORTED BY GAS DYNAMICS BRANCH, AMES RESEARCH CENTER—NASA

Ref: Letter Report by C. A. Syvertson, Ames Research Center, December 2, 1966

	MODEL NO.	AVERAGE ENTHALPY h_t (Btu/lb)			HEAT TRANSFER RATE $\dot{q}_{CW}$ (Btu/ft^2 sec) Calorimeter				MODEL STAGNATION PRESSURE P_{t_2} (atm)	PLENUM PRESSURE P_{t_1} (atm)
					Facility			SRI		
		(1)	(2)	(3)	(4)	(5)	(6)			
Langley Phenolic-Nylon Scout R/4B	PLL54	10,430	10,170		143	67.6	84	77	0.0106	0.235
	PLL57	10,430	10,170		143	67.6	84	77	0.0106	0.235
	PLL96	10,670	10,670		145	68.5	89	85	0.0109	0.248
	PLL58	25,700	22,830		240	113.5	128	118	0.0106	0.300
	PLL59	25,700	22,830		240	113.5	128	118	0.0106	0.300
	PLL60	15,360	16,590		300	141.9	190	178	0.0182	0.435
	PLL61	15,360	16,590		300	141.9	190	178	0.0182	0.435
Avcoat 5026-39	A53	9,984	10,170		147	69.5	78	80	0.0108	0.234
	A54	9,984	10,170		147	69.5	78	80	0.0108	0.234
	A61	10,707	10,670		140	66.2	85	81	0.0109	0.248
	A93	10,449	10,750		132	62.4	86	89	0.0108	0.250
	A55	23,920	22,120		259	122.5	143	121	0.0102	0.314
	A56	23,920	22,120		259	122.5	143	121	0.0102	0.314
	A57	15,330	16,670		349	165.	183	177	0.0185	0.438
	A60	15,330	16,670		349	165.	183	177	0.0185	0.438
Modified Purple Blend Silicone E4A1	SP48	10,134	10,170		148	70.	80	73	0.0105	0.234
	SP49	10,134	10,170		148	70.	80	73	0.0105	0.234
	SP96	10,678	10,670		133	62.9	85	87	0.0109	0.248
	SP51	23,340	21,850		--	--	146	114	0.0097	0.312
	SP52	23,340	21,850				146	114	0.0097	0.312
	SP50	15,970	16,480		338	159.8	196	172	0.0185	0.431
G. E. Silicone ESM 1004AP	SG35	10,153	10,069		152	71.9	81	89	0.0106	0.231
	SG39	10,749	10,670		146	69.	86	87	0.0106	0.248
	SG36	24,010	22,120		259	122.5	138	120	0.0098	0.314
	SG37	24,010	22,120		259	122.5	138	120	0.0098	0.314
	SG38	15,510	16,590		358	169.3	183	170	0.0183	0.435
	SG44	15,510	16,590		358	169.3	183	170	0.0183	0.435
Hughes Phenolic-Nylon H-5	PLH6	10,216	10,170		144	68.1	78	78	0.0106	0.234
	PLH98	10,322	10,730		142	67.1	89	85	0.0111	0.248
	PLH42	24,970	22,750		273	129.	147	125	0.0102	0.316
	PLH43	24,970	22,750		273	129.	147	125	0.0102	0.316
	PLH24	15,870	16,620		345	163.1	188	166	0.0185	0.436
	PLH50	15,870	16,620		345	163.1	188	166	0.0185	0.436
Calibration Runs	C1	11,254	11,030	6,915	143	67.7	82	82	0.0105	0.235
	C2	15,571	15,400	9,210	173	81.5	103	96	0.0098	0.260
	C3	18,025	17,500	9,770	196	92.8	120	108	0.0097	0.275
	C4	22,120	20,220	11,760	211	99.9	134	117	0.0097	0.290
	C5	24,023	21,580	11,410	225	106.5	142	124	0.0094	0.301
	C6	25,580	23,490	11,740	224	115.5	148	134	0.0101	0.312
	C7	8,194	8,100	5,800	160	75.8	94	89	0.0140	0.326
	C8	12,770	12,690	8,070	265	125.5	154	150	0.0162	0.329
	C9	16,530	17,090	9,720	352	166.7	208	183	0.0189	0.428
	C10	10,594	10,390	6,340	135	63.9	84	80	0.0106	0.240
	C11	25,154	22,640	11,180	263	124.6	154	126	0.0099	0.309

(1) Enthalpy measured by energy balance method, average enthalpy at reservoir entrance, i.e., arc heater exit.

(2) Enthalpy of free jet at test position by frozen sonic flow method and using Z. Ref: NASA TN D2233 and NASA TR R-50. Also see Column (7).

(3) Enthalpy by energy balance method, average enthalpy at nozzle exit.

(4) Ames transient calorimeter, 0.75-in. diameter hemisphere cylinder, copper slug 0.3125-in. diameter supported in shroud with sapphire microspheres.

(5) Calorimeter described under (4), calculated to 1.25-in. diameter flat face stagnation value: $\dot{q}_{FAC_{COR}} = 1.112\ \dot{q}_{FAC}[0.75/(3.3 \times 1.25)]^{0.5}$. The term 1.112 corrects the average $\dot{q}$ over sensing area to the stagnation point value.

(6) Calorimeter described under (4), sprayed with Teflon coating to give noncatalytic surface.

Z (7)	GAS FLOW RATE (lb/sec)	MAXIMUM FRONT SURFACE TEMPERATURE T_{FS} $\epsilon = 1$ (°F)			RUN TIME (sec)	CORE WEIGHT LOSS (g)	CORE CHAR WEIGHT (g)	CORE RECESSION (in.)	CHAR THICKNESS (in.)	CHAR DENSITY (lb/ft^3)
		Facility (8)	(9)	SRI						
1.56	0.0025	2,850	2,580	2,559	19.3	0.202	0.076	0.023	0.065	14.5
1.56	0.0025	2,990	2,710	2,785	38.6	0.349	0.107	0.058	0.093	14.3
1.57	0.0025	3,030	2,810	2,846	75.4	0.587	0.160	0.107	0.122	16.3
2.22	0.0025	3,260	2,960	2,918	15.6	0.215	0.079	0.026	0.069	14.2
2.22	0.0025	3,150	3,200	3,226	38.2	0.414	0.134	0.064	0.018	14.1
1.86	0.00375	3,660	3,280	3,247	11.2	0.153	0.084	0.019	0.074	14.1
1.86	0.00375	3,650	3,510	3,432	28.2	0.335	0.150	0.052	0.122	15.3
1.55	0.0025	2,870	2,560	2,600	19.4	0.174	0.110	0.024	0.079	17.3
1.55	0.0025	2,860	2,600	2,590	19.4	0.203	0.118	0.028	0.087	16.8
1.57	0.0025	2,890	2,680	2,682	38.2	0.294	0.181	0.052	0.121	18.5
1.56	0.0025	2,920	2,650	2,692	75.5	0.445	0.264	0.101	0.167	19.6
2.15	0.0025	3,360	3,080	3,000	15.5	0.220	0.110	0.027	0.081	16.9
2.15	0.0025	3,550	3,230	3,196	38.4	0.366	0.188	0.078	0.138	16.9
1.86	0.00375	3,520	3,270	3,226	11.2	0.177	0.120	0.027	0.077	19.3
1.86	0.00375	3,660	3,420	3,350	28.2	0.369	0.157	0.085	0.120	16.2
1.55	0.0025	2,620	2,360	2,446	19.5	0.153	0.110	+0.023	0.093	14.7
1.55	0.0025	2,680	2,480	2,446	38.4	0.249	0.145	+0.065	0.155	11.6
1.57	0.0025	2,550	2,350	2,323	75.5	0.375	0.200	+0.052	0.205	12.1
2.14	0.0025	2,910	2,760	2,764	15.4	0.146	0.126	+0.031	0.102	15.3
2.14	0.0025	3,080	3,070	2,826	40.6	0.263	0.198	+0.038	0.166	14.8
1.87	0.00375	3,330	3,130	3,144	28.1	0.287	0.160	0.019	0.116	17.1
1.55	0.0025	2,640	2,390	2,477	38.5	0.147	0.345	+0.007	0.134	31.6
1.57	0.0025	2,610	2,390	2,405	75.5	0.387	0.458	+0.005	0.199	28.6
2.15	0.0025	2,990	2,770	2,785	15.5	0.097	0.207	+0.001	0.086	29.9
2.15	0.0025	3,210	2,880	2,846	38.2	0.330	0.257	0.069	0.112	28.5
1.87	0.00375	3,290	2,910	2,898	11.3	0.187	0.142	0.035	0.055	32.0
1.87	0.00375	3,270	2,880	2,846	28.3	0.422	0.184	0.118	0.060	38.1
1.55	0.0025	2,890	2,690	2,723	38.4	0.318	0.117	0.044	0.097	15.0
1.56	0.0025	3,090	2,850	2,857	75.3	0.653	0.165	0.115	0.132	15.5
2.18	0.0025	3,260	3,020	2,949	15.6	0.198	0.081	0.017	0.071	14.2
2.18	0.0025	3,500	3,250	3,206	38.5	0.414	0.135	0.056	0.120	14.0
1.87	0.00375	3,470	3,200	3,165	11.4	0.177	0.071	0.011	0.067	13.2
1.87	0.00375	3,470	3,200	3,165	11.7	0.201	0.070	0.012	0.066	13.2
1.62	0.0025									
1.87	0.0025									
1.98	0.0025									
2.10	0.0025									
2.15	0.0025									
2.23	0.0025									
1.45	0.00375									
1.67	0.00375									
1.92	0.00375									
1.56	0.0025									
2.19	0.0025									

(7) $Z = 1 + \alpha$, $\gamma = (4 + 3Z)/(4 + Z)$, $\dot{w}/P_{t_1}A^* = c\{\gamma[2/(\gamma + 1)]^{(\gamma+1)/(\gamma-1)}\}^{0.5}(ZT_t)^{-0.5}$; T_t is calculated from the preceding equation and is used to get enthalpy under (2). Ref: JANAF Interim Thermochemical Tables, Dow Chemical Co., Dec. 31, 1960.

(8) Instrument Development Lab, Pyro 650 recording pyrometer, $\epsilon = 1$, $T_T = [(1/T_B) + 2.52 \times 10^{-5} \ln \epsilon_\lambda]^{-1}$.

(9) SRI radiometer, 0.375-in. aperture, $\epsilon = 1$, $T_T = T_B/\epsilon^{0.25}$. T_T is true temperature and T_B is brightness temperature.

Table B-2

TUNNEL CALIBRATION AND TEST DATA REPORTED BY MAGNETO PLASMA DYNAMICS BRANCH, AMES RESEARCH CENTER—NASA

Ref: Data Reported by A. Okuno, MPDB, Ames Research Center

	MODEL NO.	AVERAGE ENTHALPY h_t (Btu/lb)		HEAT TRANSFER RATE $\dot{q}_{CW}$ (Btu/ft^2 sec) Calorimeter				MODEL STAGNATION PRESSURE P_{t_2} (atm)	PLENUM PRESSURE P_{t_1} (atm)
				Facility		SRI			
		(1)	(2)	(3)	(4)	(5)	(6)		
Langley Phenolic-Nylon Scout R/4B	PLL70	6,736	12,664	160.3	103.8	117.1		0.00572	1.035
	PLL69	6,736	12,664					0.00572	1.035
	PLL87	6,736	12,664					0.00572	1.035
	PLL72	12,508	19,638	281.5	182.4	212.2		--	0.986
	PLL71	12,508	19,638						0.986
	PLL89	12,508	19,638						0.986
Avcoat 5026-39	A72	6,973	13,109	162.5	105.3	105.3		0.00582	0.990
	A71	6,973	13,109					0.00582	0.990
	A84	6,973	13,109					0.00582	0.990
	A76	12,320	19,342	313.	202.8	215.2		0.00947	0.997
	A75	12,320	19,342					0.00947	0.997
	A85	12,320	19,342					0.00947	0.997
Modified Purple Blend Silicone E4A1	SP66	6,451	12,128	150.6	97.6	103.5		--	0.990
	SP65	6,451	12,128						0.990
	SP85	6,451	12,128						0.990
	SP68	12,561	19,721	286.9	185.9	221.0		0.00847	1.014
	SP67	12,561	19,721						1.014
	SP89	12,561	19,721						1.014
G. E. Silicone ESM 1004AP	SG56	6,903	12,978	150.6	97.6	104.4		--	0.993
	SG55	6,903	12,978						0.993
	SG51	6,903	12,978						0.993
	SG58	12,253	19,232	280.5	181.8	210.8		0.00827	1.007
	SG57	12,253	19,232					0.00827	1.007
	SG53	12,253	19,232					0.00827	1.007
Hughes Phenolic-Nylon H-5	PLH62	6,442	12,111	142.8	92.5	92.2		--	1.049
	PLH61	6,442	12,111						1.049
	PLH97	6,442	12,111						1.049
	PLH65	12,162	19,094	293.2	190.	223.9		0.00787	1.017
	PLH64	12,162	19,094					0.00787	1.017
	PLH63	12,162	19,094					0.00787	1.017
Teflon	T117	6,177	11,613	147.9	95.9			0.00597	0.983
	T116	6,177	11,613					0.00597	0.983
	T115	12,052	18,922	294.	190.5	221.1		--	0.968
	T112	12,052	18,922						0.968
Phenolic-Nylon (75 lb/ft^3)	P11A6	7,025	13,207	170.6	110.5	116.1		--	1.028
	P11A5	7,025	13,207						1.028
	P12B3	11,927	18,725	289.6	187.7	223.2		0.00812	0.990
	P12A7	11,927	18,725					0.00812	0.990
Calibration Runs	C1	12,214	19,176			224.9	231.3	--	
	C2	12,289	19,294			229.2	140.7 (5)	--	
	C3	6,919	13,007			109.1	64.6 (6)	--	

(1) Enthalpy measured by energy balance method.

(2) Enthalpy calculated by facility from facility heat flux data: $h = 24\ \dot{q}_{FAC}(R_{eff}/P_{t_2})^{0.5}$.

(3) Ames transient slug calorimeter, 1.25-in. diameter hemisphere cylinder, gold-plated copper slug 0.375-in. diameter supported with sapphire microspheres.

(4) Facility calorimeter results under (3) corrected by facility to 1.25-in. flat face stagnation condition with relation: $\dot{q}_{\substack{FAC \\ COR}} = \dot{q}_{FAC}[(0.84 \times 1.25)/(2 \times 1.25)]^{0.5}$.

(5) SRI calorimeter as received by facility.

(6) SRI calorimeter sprayed with Teflon coating to give noncatalytic surface.

TEST CHAMBER PRESSURE (atm)	POWER TO ARC (Mw)	AIR FLOW RATE (lb/sec)	ARGON CATHODE SHIELD FLOW RATE (lb/sec)	MAXIMUM FRONT SURFACE TEMPERATURE T_{FS} $\epsilon = 1$ (^{o}F)	RUN TIME (sec)	CORE WEIGHT LOSS (g)	CORE CHAR WEIGHT (g)	CORE RECESSION (in.)	CHAR THICKNESS (in.)	CHAR DENSITY (lb/ft^3)
0.00072	0.0924	0.01018	0.000403		12.4	0.144	0.063	0.008	0.054	14.5
0.00072	0.0924	0.01018	0.000403		24.6	0.231	0.089	0.019	0.079	14.0
0.00072	0.0924	0.01018	0.000403		50.6	0.400	0.143	0.064	0.117	15.2
0.00072	0.1462	0.0079	0.000494		6.2	0.122	0.051	0.012	0.047	13.5
0.00072	0.1462	0.0079	0.000494		12.0	0.193	0.078	0.020	0.071	13.6
0.00072	0.1462	0.0079	0.000494		24.8	0.321	0.129	0.038	0.109	14.7
0.00072	0.0958	0.01015	0.000403		12.2	0.112	0.087	0.005	0.067	16.1
0.00072	0.0958	0.01015	0.000403		25.1	0.196	0.129	0.017	0.098	16.3
0.00072	0.0958	0.01015	0.000403		50.2	0.352	0.207	0.069	0.143	18.0
0.00072	0.147	0.00806	0.000494	2,900	6.1	0.098	0.073	0.004	0.051	17.8
0.00072	0.147	0.00806	0.000494	3,100	12.0	0.158	0.112	0.011	0.070	19.8
0.00072	0.147	0.00806	0.000494	3,330	24.8	0.301	0.164	0.045	0.125	16.3
0.00072	0.0908	0.01021	0.000403		12.7	0.102	0.080	+0.018	0.069	14.4
0.00072	0.0908	0.01021	0.000403		24.7	0.192	0.142	+0.027	0.163	10.8
0.00072	0.0908	0.01021	0.000403		50.5	0.307	0.232	+0.018	0.170	16.9
0.00072	0.1487	0.00809	0.000494	2,700	6.2	0.115	0.057	+0.043	0.079	9.0
0.00072	0.1487	0.00809	0.000494	2,900	12.1	0.161	0.111	+0.029	0.093	14.8
0.00072	0.1487	0.00809	0.000494	2,980	25.0	0.278	0.163	0.004	0.121	16.7
0.00072	0.0964	0.01037	0.000403		12.0	0.082	0.158	+0.005	0.072	27.2
0.00072	0.0964	0.01037	0.000403		24.8	0.106	0.238	+0.019	0.121	24.4
0.00072	0.0964	0.01037	0.000403		50.0	0.187	0.392	+0.005	0.171	28.4
0.00072	0.148	0.00821	0.000494	2,700	6.2	0.071	0.121	0.005	0.049	30.6
0.00072	0.148	0.00821	0.000494	2,800	12.1	0.161	0.144	0.020	0.071	25.2
0.00072	0.148	0.00821	0.000494	2,870	24.9	0.352	0.174	0.067	0.081	26.7
	0.0914	0.01048	0.000403		12.0	0.140	0.049	0.008	0.053	11.5
	0.0914	0.01048	0.000403		24.9	0.255	0.096	0.022	0.087	13.7
	0.0914	0.01048	0.000403		50.2	0.451	0.129	0.042	0.125	12.8
	0.1416	0.00806	0.000494		6.1	0.107	0.049	0.004	0.044	13.8
	0.1416	0.00806	0.000494		12.1	0.178	0.067	0.010	0.069	12.1
	0.1416	0.00806	0.000494		24.9	0.303	0.115	0.027	0.111	12.9
0.00072	0.0875	0.01045	0.000358		11.9	0.214		0.017		
0.00072	0.0875	0.01045	0.000358		50.2	1.037		0.087		
0.00072	0.1447	0.00806	0.000474		6.1	0.169		0.013		
0.00072	0.1447	0.00806	0.000474		24.9	0.736		0.061		
0.00072	0.0964	0.01012	0.000358		12.3	0.165	0.031	0.001	0.019	20.2
0.00072	0.0964	0.01012	0.000358		50.5	0.570	0.121	0.023	0.070	21.5
0.00072	0.142	0.00802	0.000494		6.2	0.127	0.021	0.001	0.014	18.6
0.00072	0.142	0.00802	0.000494		24.9	0.411	0.087	0.015	0.053	20.4
0.00072	0.1462	0.00805								
0.00072	0.1481	0.00806								
0.00072	0.0968	0.01045								

Table B-3

TUNNEL CALIBRATION AND TEST DATA REPORTED BY APPLIED MATERIALS AND PHYSICS DIVISION, LANGLEY RESEARCH CENTER—NASA

Ref: Letter Report by P. F. Korycinski, Langley Research Center, January 9, 1967

	MODEL NO.	TOTAL ENTHALPY h_t (Btu/lb) (1)	HEAT TRANSFER RATE $\dot{q}_{CW}$ (Btu/ft^{2}sec) Calorimeter		MODEL STAGNATION PRESSURE P_{t_2} (atm)
			Facility	SRI	
Langley Phenolic-Nylon Scout R/4B	PLL30	4,900		267	0.284
	PLL32	4,900		261	0.284
	PLL93	4,900		256	0.284
	PLL33	4,900		271	0.284
	PLL29	9,700		460	0.293
	PLL31	9,700		592	0.293
	PLL34	9,700		1,150	0.735
	PLL35	9,700		1,080	0.735
Avcoat 5026-39	A30	4,900		260	0.284
	A90	4,900		280	0.284
	A34	4,900		269	0.284
	A29	9,700		479	0.293
	A33	9,700		541	0.293
	A31	9,700		531	0.293
	A32	9,700		541	0.293
	A45	9,700		1,090	0.735
Modified Purple Blend Silicone E4A1	SP30	4,900		260	0.284
	SP93	4,900		273	0.284
	SP32	4,900		275	0.284
	SP29	9,700		481	0.293
	SP31	9,700		539	0.293
	SP34	9,700		--	0.735
	SP35	9,700		1,065	0.735
	SP33	9,700		--	0.735
G. E. Silicone ESM 1004AP	SG22	4,900		259	0.284
	SG49	4,900		263	0.284
	SG24	4,900		249	0.284
	SG21	9,700		478	0.293
	SG23	9,700		551	0.293
	SG25	9,700		1,110	0.735
Hughes Phenolic-Nylon H-5	PLH26	4,900		260	0.284
	PLH93	4,900		250	0.284
	PLH28	4,900		293	0.284
	PLH25	9,700		492	0.293
	PLH27	9,700		607	0.293
	PLH29	9,700		1,134	0.735
	PLH30	9,700		1,145	0.735
Teflon	T124	9,700		516	0.293
	T126	9,700		1,055	0.735
Phenolic-Nylon (75lb/ft^3)	P11A2	9,700		524	0.293
	P11A3	9,700		--	0.735
	P11A4	9,700		996	0.735
			(5)		
			940	1,120	

(1) Enthalpy calculated by facility from $\dot{q}_{SRI}$ and P_{t_2} using Fay-Riddell relation.

(2) Model front surface temperature measured with facility photographic pyrometer. Ref: NASA TN D-2660.

(3) SRI radiometer located outside tunnel; viewed model through 1 in. thick glass window; radiation from model redirected inside tunnel with mirror, 30° to mirror surface. Data not corrected for window or mirror losses.

MAXIMUM FRONT SURFACE TEMPERATURE T_{FS} $\epsilon = 1$ ($^{\circ}F$)			RUN TIME (sec)	CORE WEIGHT LOSS (g)	CORE CHAR WEIGHT (g)	CORE RECESSION (in.)	CHAR THICKNESS (in.)	CHAR DENSITY (lb/ft^3)
Facility (2)		SRI (3)						
4,100		2,930	14	0.288	0.115	0.042	0.091	15.7
4,010		2,950	30	0.592(4)	0.131	0.126	0.111	14.6
3,940		2,900	30	0.510(4)	0.115	0.137	0.099	14.4
3,960		2,915	60	1,287	0.115	0.381	0.097	14.7
--		3,620	11	0.280	0.141	0.036	0.103	17.0
4,810		3,730	30	0.835	0.164	0.181	0.151	13.5
5,170		3,540	10	0.484	0.127	0.111	0.098	16.1
5,230		4,245	20	1,021	0.103	0.300	0.080	16.0
--		2,880	14	0.350	0.112	0.089	0.077	18.1
3,920		1,845	20	0.510	0.085	0.177	0.061	17.3
3,900		2,840	30	0.823	0.105	0.276	0.062	21.0
--		3,520	11	0.417	0.075	0.106	0.059	15.8
4,600		3,455	20	0.822	0.077	0.281	0.049	19.5
4,500		3,430	30	1.243	0.087	0.377	0.070	15.4
--		--	30	1.542	0.055	0.453	0.062	11.0
4,680		3,400	5	0.566	0.028	0.242	0.006	
3,580		2,560	14	0.212	0.151	+ 0.004	0.097	19.3
3,600		2,505	30	0.548	0.150	0.070	0.117	16.0
--		2,510	60	1.012	0.135	0.214	0.097	17.3
4,070		3,075	11	0.424	0.056	0.082	0.049	14.2
4,140		2,910	30	1.386	0.032	0.412	0.022	18.1
3,940		--	5	0.870	0.005	0.253	0.004	15.5
3,980		2,580	5	0.727	0.011	0.190	0.022	
4,170		2,970	10	1.228	0.008	0.382	0.003	
--		2,660	14	0.205	0.278	0.032	0.081	42.6
3,830		2,570	30	0.830	0.154	0.201	0.070	27.3
3,740		2,540	40	1.168	0.159	0.309	0.037	53.3
--		2,600	11	0.726	0.066	0.181	0.018	45.5
3,720		2,580	20	1.588	0.053	0.448	0.013	50.6
3,780		2,855	5	0.760	0.033	0.218	0.010	41.0
4,040		2,835	14	0.295(4)	0.103	0.036	0.085	15.0
3,940		2,800	30	0.582(4)	0.139	0.119	0.115	
3,960		2,940	60	1.308	0.114	0.355	0.101	14.0
4,730		3,590	11	0.301	0.139	0.032	0.103	16.7
4,680		3,610	30	0.813	0.183	0.168	0.147	15.4
5,320		4,330	10	0.496	0.127	0.108	0.098	16.1
5,120		3,980	20	0.970	0.116	0.260	0.094	15.3
--		--	21	2.460		0.201		
--		--	10	2,165		0.180		
4,530		3,350	21	0.750	0.267	0.040	0.099	33.5
5,050		4,030	10	0.701	0.238	0.039	0.098	30.2
5,280		4,180	20	1.298	0.280	0.135	0.109	31.8

(4) Mass loss estimated from linear recession data.

(5) Facility thin wall transient flat face calorimeter, 1 in. total diameter, instrumented with multiple thermocouples. Corrected to 1.25 in. flat face with relation $\dot{q}_{1.25\ FF} = (1.0/1.25)^{0.5} \cdot \dot{q}_{FAC.\ meas}$

Table B-3 (Continued)

TUNNEL CALIBRATION AND TEST DATA FOR VARIOUS DIAMETER MODELS
REPORTED BY APPLIED MATERIALS AND PHYSICS DIVISION,
LANGLEY RESEARCH CENTER— NASA
Ref: Data sheets on AMPD runs 1108 to 1138

	MODEL NO.	TOTAL ENTHALPY h_t (Btu/lb) (1)	MODEL STAGNATION PRESSURE P_{t_2} (atm)	MODEL DIAMETER AND SHAPE (in.) (2)	CALORIMETER DIAMETER AND SHAPE (in.)
Teflon	T164	8200	0.0192	1.0 Hemi.	1.25 FF
	T165	9100	0.0192	1.0 Hemi.	1.25 FF
	T160	9700	0.0192	1.25 FF	1.25 FF
	T161	9100	0.0192	1.25 FF	1.25 FF
	T156	9100	0.0192	2.5 FF	2.5 FF
	T157	9800	0.0192	2.5 FF	2.5 FF
	T153	8700	0.0192	4.0 FF	4.0 FF
	T154	9800	0.0192	4.0 FF	4.0 FF
Hughes Phenolic-Nylon H-5	PLH164	8500	0.0192	1.0 Hemi.	1.25 FF
	PLH165	10300	0.0192	1.0 Hemi	1.25 FF
	PLH160	8700	0.0192	1.25 FF	1.25 FF
	PLH161	9100	0.0192	1.25 FF	1.25 FF
	PLH156	9000		2.50 FF	2.50 FF
	PLH157	8800	0.0192	2.50 FF	2.50 FF
	PLH153	9100	0.0192	4.0 FF	4.0 FF
	PLH154	9900	0.0192	4.0 FF	4.0 FF

HEAT TRANSFER RATE (Btu/ft^{2}sec)(2) $\dot{q}_{CW}$			
No. 9 Calorimeter (2)	No. 10 Calorimeter		
1.25 FF	1.25 FF	2.5 FF	4.0 FF
115.7		94.6	
132			76.7
125			76.0
130		95.0	
112	107		
164	156		
136	137		
136	128		
130	134		

HEAT TRANSFER RATE $\dot{q}_{CW}$ (Btu/ft^{2}sec) (3)	(4)	RUN TIME (sec)	CORE DIAMETER (in.)	CORE WEIGHT LOSS (g)	CORE CHAR WEIGHT (g)	CORE RECESSION (in.)	CHAR THICKNESS (in.)	CHAR DENSITY (lb/ft^3)
116	236	49	0.5	1.461		0.207		
130	264	49	0.5	1.510		0.217		
137		97	0.625	2.764		0.242		
130		97	0.625	2.846		0.247		
91.6		140	1.25	10.667		0.236		
93.2		140	1.25	11.378		0.247		
70		~57	2.5	19.422		0.100		(5)
78		63	2.5	33.739		0.184		(6)
120	244	49	0.5	0.491	0.106	0.154	0.171	12.1(7)
147	298	49	0.5	0.535	0.119	0.162	0.168	13.7
124		97	0.625	0.799	0.227	0.118	0.207	13.6
129		97	0.625	0.908	0.227	0.160	0.197	14.3
90.5		140	1.25	3.377	1.037	0.110	0.223	14.4
88.6		140	1.25	3.175	1.032	0.104	0.225	14.2(8)
129		168	2.5					(9)
78.5		180	2.5	13.939	5.209	0.100	0.270	14.9

(1) Enthalpy calculated from measured heating rates and pressures.

(2) All flat-faced models had peripheral shoulder radius equal to one-tenth model radius.

(3) All heating rates measured with SRI 1.25-in. calorimeters. A shroud was added to the SRI calorimeter to equal the 2.5-in. and 4.0-in.-diameter models.

(4) Heating rate calculated from (3) with the relation: $\dot{q}_{CW} = q_{meas}\,(3.3 \times 1.25/1.0)^{0.5}$

(5) Tunnel unstarted after ~55 sec, pressure and heating rate increased.

(6) Tunnel unstarted after 60 sec.

(7) Calorimeter may be in error.

(8) Electrode burn out—model was wet.

(9) Tunnel unstarted when model entered stream—model destroyed.

Table B-4

TUNNEL CALIBRATION AND TEST DATA REPORTED BY ENTRY STRUCTURES BRANCH, 5Mw FACILITY, LANGLEY RESEARCH CENTER—NASA

Ref: Letter Report by P. F. Korycinski, Langley Research Center, December 23, 1966

	MODEL NO.	TOTAL ENTHALPY h_t (Btu/lb) (1)	(2)	HEAT TRANSFER RATE $\dot{q}_{CW}$ (Btu/ft^{2}sec) SRI CALORIMETER (3)	MODEL STAGNATION PRESSURE P_{t_2} (atm) (4)	CHAMBER PRESSURE P_{t_1} (atm)
Langley Phenolic-Nylon	PLL54	3160	3250	203	0.281	1.389
Scout R/4B	PLL52	2970	3250	203	0.281	1.389
Avcoat 5026-39	A7	3050	3250	203	0.278	1.376
	A48	3100	3250	203	0.279	1.381
Modified Purple Blend	SP45	3100	3250	203	0.280	1.385
Silicone E4A1	SP46	3090	3250	203	0.281	1.392
G.E. Silicone	SG34	3120	3250	203	0.281	1.389
ESM 1004AP	SG33	3060	3250	203	0.281	1.389
Hughes Phenolic-Nylon	PLH41	3070	3250	203	0.281	1.389
H-5	PLH40	3140	3250	203	0.281	1.389

(1) Enthalpy measured by energy balance method.

(2) Enthalpy calculated from pressure and heat transfer to 1.5-in. diameter hemispherical facility calorimeter, and from theory of Fay and Riddell. This method of calculating enthalpy is considered standard and is preferred by the Entry Structures Branch.

(3) Heat transfer to SRI calorimeter determined during separate run.

(4) Model stagnation pressure calculated from chamber pressure $P_{t_2}/P_{t_1} = 0.202$.

GAS FLOW RATE (lb/sec)	POWER TO ARC (Mw)	RUN TIME (sec)	CORE WEIGHT LOSS (g)	CORE CHAR WEIGHT (g)	CORE RECESSION (in.)	CHAR THICKNESS (in.)	CHAR DENSITY (lb/ft^3)
0.2	2.15	15.3	0.202	0.076	0.023	0.065	14.5
0.2	2.13	30.4	0.578	0.131	0.131	0.108	15.0
0.2	2.14	15.3	0.357	0.104	0.102	0.075	17.2
0.2	2.15	30.4	0.710	0.103	0.243	0.067	19.0
0.2	2.15	15.3	0.162	0.190	+0.020	0.106	22.2
0.2	2.13	30.4	0.282	0.276	0.006	0.147	23.2
0.2	2.15	15.3	0.149	0.275	0.009	0.101	33.7
0.2	2.12	30.4	0.310	0.300	0.018	0.151	24.6
0.2	2.15	15.3	0.318	0.116	0.037	0.098	14.6
0.2	2.14	30.4	0.604	0.109	0.125	0.108	13.1

Table B-5

CALIBRATION AND TEST DATA REPORTED BY MANNED SPACECRAFT CENTER, SUBSONIC FACILITY—NASA

Ref: MSC Letter Report ES5/10-17/81L, October 19, 1966

	MODEL NO.	TOTAL ENTHALPY h_t (Btu/lb) (1)	HEAT TRANSFER RATE $\dot{q}_{CW}$ (Btu/ft^{2}sec) Calorimeter		DISTANCE NOZZLE EXIT TO MODEL FACE (in.)	MODEL STAGNATION PRESSURE P_{t_2} (atm)	GAS FLOW RATE (lb/sec)
			Facility (2)	SRI			
Langley Phenolic-Nylon Scout R/4B	PLL38	8223	404		2.0	1.0	0.04
	PLL39	8280	401		2.0	1.0	0.04
	PLL40	9975	590		1.5	1.0	0.04
	PLL41	8930	600		1.5	1.0	0.04
	PLL36	4500	100		2.0	1.0	0.04
	PLL37	4622	100		2.0	1.0	0.04
	PLL95	3888	101		2.0	1.0	0.04
	PLL42	5475	205		2.0	1.0	0.04
Avcoat 5026-39	A38	8440	406		2.0	1.0	0.04
	A39	8198	399		2.0	1.0	0.04
	A40	9078	590		1.5	1.0	0.04
	A41	9483	590		1.5	1.0	0.04
	A36	4822	106		2.0	1.0	0.04
	A37	4375	103		2.0	1.0	0.04
	A91	4275	104		2.0	1.0	0.04
	A42	4853	210		2.0	1.0	0.04
	A92	4950	207		2.0	1.0	0.04
Modified Purple Blend Silicone E4A1	SP42	8440	405		2.0	1.0	0.04
	SP39	8218	396		2.0	1.0	0.04
	SP40	9595	600		1.5	1.0	0.04
	SP41	9792	590		1.5	1.0	0.04
	SP36	4400	104		2.0	1.0	0.04
	SP37	4445	104		2.0	1.0	0.04
	SP95	4113	105		2.0	1.0	0.04
	SP38	4850	205		2.0	1.0	0.04
G. E. Silicone ESM 1004AP	SG28	8050	400		2.0	1.0	0.04
	SG29	9300	613		1.5	1.0	0.04
	SG30	9050	599		1.5	1.0	0.04
	SG26	4674	105		2.0	1.0	0.04
	SG27	4625	105		2.0	1.0	0.04
	SG50	4609	106		2.0	1.0	0.04
Hughes Phenolic-Nylon H-5	PLH32	8130	410		2.0	1.0	0.04
	PLH33	8040	406		2.0	1.0	0.04
	PLH34	9250	590		1.5	1.0	0.04
	PLH35	9300	608		1.5	1.0	0.04
	PLH31	4493	101		2.0	1.0	0.04
	PLH36	4980	205		2.0	1.0	0.04
Calibration Runs	C1	8640	396	388	2.0	1.0	0.04
	C2	6838	314	297	2.0	1.0	0.04
	C3	5205	251	226	2.0	1.0	0.04
	C4	3565	93	101	2.0	1.0	0.04
	C5	4050	94	103	2.0	1.0	0.04
	C6	5300	276	251	2.0	1.0	0.04
	C7	8700	400	366	2.0	1.0	0.04
	C8	4100	108	100	2.0	1.0	0.04
	C9	5350	276	261	2.0	1.0	0.04
	C10	8650	398	360	2.0	1.0	0.04

(1) Enthalpy measured by heat balance method.

(2) Facility Hy-Cal asymptotic calorimeter.

(3) Measured with an optical pyrometer.

POWER TO ARC (Btu/sec)	MAXIMUM FRONT SURFACE TEMPERATURE T_{FS} $\epsilon = 1$ ($^{\circ}F$)		RUN TIME (sec)	CORE WEIGHT LOSS (g)	CORE-CHAR WEIGHT (g)	CORE RECESSION (in.)	CHAR THICKNESS (in.)	CHAR DENSITY (lb/ft^3)
	Facility (3)	SRI						
687.5		4350	8.0	0.226	0.155	0.017	0.109	17.6
688.0	4380	4450	20.4	0.479	0.260	0.065	0.175	18.4
744.1	4155	4280	10.7	0.325	0.196	0.043	0.132	18.0
767.5	4420	4330	20.5	0.557	0.260	0.081	0.181	17.8
330.0	3000		15.5	0.191	0.165	0.008	0.114	17.9
332.4	2935	2750	30.5	0.374	0.238	0.034	0.160	18.4
327.4	3050	2980	60.8	0.762	0.373	0.070	0.267	17.3
373.1	3105	3250	31.0	0.453	0.262	0.063	0.185	11.4
671.3		4210	8.6	0.269	0.142	0.051	0.097	18.2
647.4		4310	20.4	0.572	0.186	0.146	0.114	20.2
752.4	4175	4100	10.7	0.394	0.133	0.108	0.096	17.2
768.2	4005	4040	20.3	0.656	0.147	0.202	0.100	18.2
314.1	3085	3300	16.7	0.201	0.237	0.023	0.145	20.3
315.5	3105	3280	30.4	0.382	0.333	0.051	0.212	19.5
320.	3105	3400	60.4	0.913	0.975	0.137	0.276	22.8
385.5	3295	3160	30.2	0.519	0.255	0.121	0.164	19.3
385.0	3430	3240	60.5	1.169	0.243	0.378	0.150	20.1
690.6		4200	7.8	0.267	0.154	0.004	0.099	19.3
685.8		4150	20.5	0.572	0.286	0.101	0.110	32.2
764.6	3790	3940	11.5	0.489	0.152	0.111	0.071	26.5
752.4	3850	3820	20.1	0.783	0.314	0.218	0.086	45.3
316.0	3105	3320	15.5	0.190	0.271	+0.037	0.153	22.0
315.9	3105	3300	30.6	0.424	0.394	+0.035	0.228	21.4
315.1	3160	3400	60.1	1.078	0.528	0.038	0.320	20.5
384.0	3260	3220	30.4	0.575	0.273	0.005	0.205	16.5
658.6	3320	3480	20.5	1.213	0.183	0.355	0.043	52.8
765.0	3140	3210	10.5	0.931	0.127	0.273	0.026	60.6
740.0	3390	3070	20.4	1.752	0.159	0.521	0.036	54.8
319.5	3000	3240	20.6	0.182	0.419	+0.005	0.168	30.9
320.0	3105	3350	50.9	0.732	0.810	0.085	0.234	42.9
318.4	3105	3300	60.8	1.210	0.626	0.225	0.204	38.1
662.2		4300	9.0	0.249	0.159	0.023	0.113	17.4
665.2		4420	20.3	0.489	0.265	0.072	0.171	19.2
765.0	4030		10.6	0.343	0.199	0.045	0.137	18.0
765.0	4135	4330	20.4	0.574	0.282	0.094	0.189	18.5
326.3	2980	2800	20.3	0.267	0.169	0.016	0.117	17.9
384.7	3295	3200	30.8	0.516	0.280	0.069	0.178	19.5

Table B-6

TUNNEL CALIBRATION AND TEST DATA REPORTED BY MANNED SPACECRAFT CENTER, SUPERSONIC FACILITY—NASA

Ref: MSC Letter Report ES5/2-27/35L , March 1, 1967

	MODEL NO.	AVERAGE ENTHALPY (Btu/lb) (1)	HEAT TRANSFER RATE $\dot{q}_{CW}$ (Btu/ft^{2}sec) Calorimeter		CATHODE PRESSURE (atm) (3)(4)
			Facility (2)	SRI	
Langley Phenolic-Nylon Scout R/4B	PLL65	11,500	436		0.625
	PLL66	24,500	800		0.700
	PLL67	34,000	988		0.976
Avcoat 5026-39	A62	11,500	431		0.625
	A63	25,466	780		0.710
	A64	34,000	954		0.976
Modified Purple Blend Silicone E4A1	SP59	11,500	426		0.625
	SP60	24,500	794		0.704
	SP61	34,000	958		0.976
G. E. Silicone ESM1004AP	SG59	11,500	436		0.625
	SG60	11,500	433		0.625
	SG61	23,500	780		0.682
	SG62	34,150	954		0.976
Hughes Phenolic-Nylon H-5	PLH54	11,500	431		0.625
	PLH55	24,600	797		--
	PLH56	34,150	1000		0.976
Teflon	T129	11,500	438		0.625
	T130	11,500	433		0.625
	T131	24,500	780		0.678
	T133	34,500	928		0.976
Phenolic-Nylon (75 lb/ft^3)	P11B1	11,500	431		0.625
	P11B2	11,500	433		0.625
	P11B3	26,500	818		0.720
	P11B5	34,300	954		0.976
	C1	11,000	424	394	
	C2	22,500	824	839	

(1) Enthalpy measured by energy balance method.

(2) Facility Hy-cal Engineering asymptotic flat-face calorimeter, 0.060-in. sensing diameter, 1.25-in. total diameter.

(3) Models run at h = 11,000 had model stagnation pressures ranging from 0.011 to 0.0125 atm; at h = 25,000, P_{t_2} = 0.0163 to 0.0178 atm; at h = 34,000, P_{t_2} = 0.0192 atm. Model stagnation pressures were measured with a Grey-Rad enthalpy probe.

(4) Nozzle exit pressures ranged from 0.00065 to 0.0012 atm for the above tests and chamber test section pressures were controlled within the same range of values.

GAS FLOW RATE (lb/sec)	MODEL FRONT SURFACE TEMPERATURE T_{FS} $\epsilon = 1$ (°F)	RUN TIME (sec)	CORE WEIGHT LOSS (g)	CORE CHAR WEIGHT (g)	CORE RECESSION (in.)	CHAR THICKNESS (in.)	CHAR DENSITY (lb/ft^3)
	Facility (5)						
0.013	3890	31.0	0.430	0.256	0.039	0.184	17.3
0.013	3950	30.0	0.555	0.346	0.051	0.243	17.7
0.013	3810	30.0	0.540	0.351	0.047	0.246	17.7
0.013	3880	29.5	0.474	0.229	0.073	0.169	16.8
0.013	--	30.0	0.563	0.254	0.110	0.200	15.8
0.013	3880	20.0	0.430	0.208	0.068	0.171	15.1
0.013	3525	30.5	0.462	0.141	0.029	0.131	13.4
0.013	3900	30.0	0.719	0.081	0.187	0.063	15.9
0.013	3890	20.4	0.546	0.085	0.102	0.082	12.9
0.013	2975	31.0	0.819	0.093	0.252	0.041	28.1
0.013	3160	30.0	0.830	0.098	0.251	0.044	27.6
0.013	3380	30.0	1.259	0.076	0.408	0.036	26.2
0.013	3575	20.0	1.042	0.097	0.329	0.034	35.4
0.013	3870	30.0	0.448	0.240	0.044	0.171	17.4
0.013	3805	30.0	0.581	0.344	0.055	0.232	18.4
0.013	3840	20.0	0.409	0.207	0.027	0.151	17.0
0.013	--	30.0	1.724		0.151		
0.013	--	29.5	1.409		0.123		
0.013	--	30.0	1.903		0.168		
0.013	--	20.0	1.528		0.136		
0.013	2975	31.0	0.656	0.211	0.021	0.102	25.7
0.013	2920	29.5	0.626	0.205	0.018	0.100	25.4
0.013	2950	30.0	0.818	0.396	0.030	0.148	33.2
0.013	3840	20.2	0.522	0.163	0.006	0.081	24.9
0.013							
0.013							

(5) Facility optical pyrometer, 0.65 microns.

Table B-7

TUNNEL CALIBRATION AND TEST DATA REPORTED BY AEROTHERM CORPORATION

Ref: Aerotherm Report No. 66-6

	MODEL NO.	TOTAL ENTHALPY h_t (Btu/lb)			HEAT TRANSFER RATE $\dot{q}_{CW}$ (Btu/ft^{2}sec) Calorimeter		MODEL STAGNATION PRESSURE P_{t_2} (atm)	PLENUM PRESSURE P_{t_1} (atm)
		(1)	(2)	(3)	Facility (4)	SRI		
Langley Phenolic-Nylon Scout R/4B	PLL43	4,748		5,583	92.1	80.1	0.0204	0.0693
	PLL46	4,085		4,146	82.3	57.4	0.0190	0.0704
	PLL97	4,748		5,583	92.1	80.1	0.0204	0.0693
	PLL45	7,612		10,783	270.0	188.0	0.0301	0.1034
	PLL48	7,612		11,304	270.0	188.0	0.0301	0.1034
	PLL15	21,206		46,535		973.0	0.0433	0.3547
	PLL18	21,598		44,625		921.0	0.0422	0.3547
Avcoat 5026-39	A74	4,783		5,644	86.2	76.5	0.0182	0.0682
	A44	4,085		4,608	82.3	57.4	0.0190	0.0704
	A98	4,783		5,644	86.2	76.5	0.0182	0.0682
	A58	7,227		11,304	267.0	196.0	0.0298	0.1034
	A59	7,227		11,530	267.0	196.0	0.0298	0.1034
	A15	21,973		45,224		941.0	0.0429	0.3536
	A17	21,925		45,007		941.0	0.0433	0.3558
Modified Purple Blend Silicone E4A1	SP56	4,566		5 469	83.2	77.7	0.0200	0.0704
	SP53	4,242		10,783	77.4	63.8	0.0190	0.0716
	SP97	4,566		5,469	83.2	77.7	0.0200	0.0704
	SP55	7,158		11,530	263.0	200.0	0.0298	0.1046
	SP57	7,158		10,111	263.0	200.0	0.0298	0.1046
	SP15	21,871		45,751		952.0	0.0429	0.3570
	SP18	21,650		46,197		958.0	0.0426	0.3536
G. E. Silicone ESM 1004AP	SG41	4,158		4,839	80.3	69.1	0.0202	0.0682
	SG42	4,158		4,839	80.3	69.1	0.0202	0.0682
	SG14	7,667		10,111	261.0	174.0	0.0294	0.1046
	SG43	7,667		9,919	261.0	174.0	0.0294	0.1046
	SG12	21,412		43,684		909.0	0.0429	0.3536
	SG15	21,729		46,952		969.0	0.0422	0.3536
Hughes Phenolic-Nylon H-5	PLH44	4,328		4,125	87.2	58.2	0.0197	0.0716
	PLH45	4,328		4,125	87.2	58.2	0.0197	0.0716
	PLH46	8,133		9,919	264.0	172.0	0.0298	0.1046
	PLH48	8,133			264.0	172.0	0.0298	0.1046
	PLH16	21,442		46,678		960.0	0.0419	0.3524
	PLH17	21,168		46,808		974.0	0.0429	0.3536
Calibration Runs	C1	4,947	4,500	5,711	83.2	80.1	0.0195	0.0659
	C2	4,279	4,500	6,085	85.4	84.5	0.0191	0.0693
	C3	8,016	9,600	10,326	230.0	178.0	0.0294	0.1023
	C4	7,133	9,600	10,791	236.0	185.0	0.0291	0.1023
	C5	21,255	32,800	41,197	1,033.0	837.0	0.0409	0.3490
	C6	21,394	29,500	43,383	1,094.0	876.0	0.0404	0.3331
	C7	4,518			86.2	72.3	0.0196	
	C8	4,500				70.1	0.0196	
					(7)	(7)		
	C9	4,624			62.8	51.0	0.0189	
	C10	4,796			59.1	52.8	0.0196	

(1) Enthalpy measured by energy balance method.

(2) Enthalpy calculated by Aerotherm Corporation using sonic flow technique

(3) Enthalpy calculated by Aerotherm Corporation using heat flux method: $h = 24 \dot{q}_{\underset{SRI}{CW}} (P_{t_2}/R_{eff})^{0.5}$.

(4) Aerotherm calorimeter "Gardon" type, steady state, Hy-Cal Engineering; sensing area 0.20-in. Constantan, shroud diameter, 1.5-in. flat face. Values corrected to 1.25-in. diameter flat face: $\dot{q}_{1.25\ in.} = 1.095\ \dot{q}_{1.5\ in.}$

NOZZLE EXIT PRESSURE P_e (atm)	GAS FLOW RATE (lb/sec)	MAXIMUM FRONT SURFACE TEMPERATURE T_{FS} $\epsilon = 1$ ($^\circ$F)		RUN TIME (sec)	CORE WEIGHT LOSS (g)	CORE CHAR WEIGHT (g)	CORE RECESSION (in.)	CHAR THICKNESS (in.)	CHAR DENSITY (lb/ft^3)
		Facility (5)	SRI (6)						
0.0016	0.0042	3,050	2,450	25.4	0.254	0.101	0.033	0.090	13.9
0.0014	0.0042	3,010	2,380	60.5	0.542	0.147	0.096	0.126	14.5
0.0016	0.0042	3,210	2,520	100.8	0.778	0.178	0.189	0.156	14.2
0.0021	0.0048		3,100	12.4	0.240	0.095	0.021	0.083	14.2
0.0021	0.0048	3,840	3,100	45.3	0.607	0.195	0.105	0.154	15.7
0.0027	0.0084	4,460	4,160	5.2	0.164	0.111	0.008	0.082	16.8
0.0027	0.0084	5,090	4,620	13.3	0.290	0.212	0.021	0.152	17.3
0.0014	0.0042	2,930	2,380	25.3	0.235	0.144	0.027	0.111	16.1
0.0014	0.0042	2,950	2,510	59.7	0.467	0.203	0.103	0.146	17.3
0.0014	0.0042	3,190	2,490	99.8	0.852	0.239	0.251	0.171	17.3
0.0021	0.0048	3,720	3,090	11.9	0.210	0.105	0.038	0.080	16.3
0.0021	0.0048	3,800	2,900	45.1	0.695	0.164	0.210	0.116	17.5
0.0027	0.0084	4,820	4,340	5.0	0.147	0.080	0.017	0.076	13.1
0.0027	0.0084	5,240	4,540	13.4	0.325	0.143	0.058	0.127	14.0
0.0014	0.0042		2,350	24.6	0.155	0.123	+0.044	0.120	12.3
0.0014	0.0042	2,600	2,280	60.4	0.280	0.225	+0.051	0.194	14.3
0.0014	0.0042		2,280	100.0	0.404	0.276	+0.025	0.217	15.8
0.0021	0.0048	3,200	2,840	12.4	0.199	0.128	0.002	0.092	17.2
0.0021	0.0048	3,470	2,840	45.3	0.578	0.177	0.120	0.111	19.7
0.0027	0.0084	4,140	3,720	5.3	0.197	0.039	0.015	0.044	11.0
0.0027	0.0084	4,310	3,720	13.0	0.451	0.078	0.086	0.065	14.9
0.0014	0.0042	2,570	2,320	25.0	0.112	0.278	+0.010	0.116	29.7
0.0014	0.0042	2,610	2,300	99.7	0.315	0.616	+0.036	0.286	26.7
0.0021	0.0048	3,220	2,740	12.5	0.262	0.130	0.051	0.058	27.8
0.0021	0.0048	3,200	2,640	45.4	0.921	0.170	0.259	0.066	31.9
0.0027	0.0084	3,590	3,170	5.2	0.339	0.057	0.066	0.043	16.4
0.0027	0.0084		3,140	13.1	0.831	0.065	0.226	0.026	31.0
0.0014	0.0042	2,950	2,460	24.8	0.260	0.093	0.026	0.084	13.7
0.0014	0.0042	3,250	2,470	99.7	0.893	0.187	0.185	0.157	14.8
0.0021	0.0048	3,640	3,090	12.4	0.238	0.087	0.018	0.078	13.8
0.0021	0.0048	3,800	2,710	45.0	0.623	0.207	0.103	0.163	15.8
0.0027	0.0084	3,840	4,040	5.2	0.159	0.114	0.009	0.083	17.0
0.0027	0.0084	4,920	4,570	13.5	0.330	0.231	0.025	0.155	18.5
0.0014	0.0042								
0.0014	0.0042								
0.0021	0.0048								
0.0021	0.0048								
0.0027	0.0084								
0.0027	0.0084								

(5) Infrared Industries "Thermodot" Mo TD9CH; viewed model through front quartz port, approximately 45° to model surface plane, 0.80 ± 0.015 microns.

(6) SRI radiometer located inside test chamber; viewed model with front surface mirror. Data has been corrected: $1.12\ T_{meas} = T_{COR}$.

(7) The Aerotherm and SRI calorimeters were sprayed with a thin coat of Teflon to determine the effect of reduced surface catalyticity.

Table B-8

TUNNEL CALIBRATION AND TEST DATA REPORTED BY AVCO CORPORATION

Ref: AVCO Report R720-HEH-66-105, August 2, 1966

	MODEL NO.	TOTAL ENTHALPY h_t (Btu/lb) (1)	HEAT TRANSFER RATE $\dot{q}_{CW}$ (Btu/ft^{2}sec) Calorimeter		MODEL STAGNATION PRESSURE P_{t_2} (atm) (4)	PLENUM PRESSURE P_{t_1} (atm)	NOZZLE THROAT DIAMETER (in.)
			Facility (2)	SRI (3)			
Teflon	T110	2,430		1,640	5.62	10.91	0.765
	T111	6,820		3,340	4.92	10.40	0.765
	T113	7,260		1,850	1.93	2.06	1.25
	T114	7,260		1,850	1.93	2.06	1.25
Phenolic-Nylon (75 lb/ft^3)	P12A2	2,430		1,640	5.62	10.91	0.765
	P12A3	6,690		3,340	4.92	10.37	0.765
	P12A4	7,260		1,850	1.93	2.05	1.25
	P12A5	7,260		1,850	1.93	2.05	1.25
Langley Phenolic-Nylon Scout R/4B	PLL47	7,000		1,850	1.93	2.03	1.25
Avcoat 5026-39	A73	7,000		1,850	1.93	2.03	1.25
Tunnel Calibration Runs	C1	2,470			5.62	10.91	0.765
	C2	2,430			5.62	10.94	0.765
	C3	2,500	1,640			10.91	0.765
	C4	2,400		1,640		10.87	0.765
	C5	6,700			4.91	10.34	0.765
	C6	7,000			4.93	10.40	0.765
	C7	7,000	3,400			10.40	0.765
	C8	7,000		3,340		10.40	0.765
	C9	7,260			1.93	2.06	
	C10	7,260	1,960			2.06	
	C11	7,260		1,850		2.06	

(1) Enthalpy determined by sonic flow method.

(2) AVCO null point transient calorimeter, 0.375-in. (sensing diameter) copper slug by 1.5-in. long, mounted in a 1.25-in. flat face shroud.

(3) SRI calorimeter values taken from tunnel calibration runs.

(4) AVCO uncooled copper pitot probe, 0.375-in diameter. Test data taken from tunnel calibration runs.

NOZZLE EXIT DIAMETER (in.)	AIR MASS FLOW (lb/sec)	MAXIMUM FRONT SURFACE TEMPERATURE T_{FS} $\epsilon = 1$ (°F) (5)	RUN TIME (sec)	CORE WEIGHT LOSS (g)	CORE CHAR WEIGHT (g)	CORE RECESSION (in.)	CHAR THICKNESS (in.)	CHAR DENSITY (lb/ft^3)
1.178	0.440		4.02	2.376		0.208		
1.178	0.273		4.03	2.679		0.228		
1.25	0.141		2.97	1.176		0.104		
1.25	0.141		10.05	3.999		0.358		
1.178	0.440	4,220	4.06	0.657	0.033	0.085	0.024	17.0
1.178	0.274	4,540 - 4,840	4.00	1.217	0.016	0.183	0.010(6)	19.8
1.25	0.140	5,280	2.97	0.396	0.101	0.016	0.057	22.0
1.25	0.141	5,440	10.01	1.053	0.174	0.114	0.076	28.4
1.25	0.141	5,550	6.02	0.440	0.069	0.144	0.055	
1.25	0.141	4,900	6.01	1.040	0.015	0.416	0.014(7)	
1.178	0.437		0.88					
1.178	0.442		0.93					
1.178	0.442		0.46					
1.178	0.441		0.52					
1.178	0.273		0.71					
1.178	0.270		0.84					
1.178	0.270		0.45					
1.178	0.270		0.41					
	0.141		1.13					
	0.141		0.36					
	0.141		0.37					

(5) Instrument Development Lab recording pyrometer (0.653 microns); viewed model directly.

(6) Model P12A3 spalled sporadically, as indicated in motion pictures and varying front surface temperatures.

(7) Model A73 lost considerable side shroud material because of incomplete honeycomb cells; $\dot{q}$ may have increased during run.

Table B-9

TUNNEL CALIBRATION AND TEST DATA REPORTED BY GIANNINI SCIENTIFIC CORPORATION

Ref: G.S.C. Test Report No. FR076-332, July 1966

	MODEL NO.	TOTAL ENTHALPY h_t (Btu/lb)	HEAT TRANSFER RATE $\dot{q}_{CW}$ (Btu/ft^{2}sec) Calorimeter		MODEL STAGNATION PRESSURE P_{t_2} (atm)	PLENUM PRESSURE P_{t_1} (atm)	NOZZLE STATIC PRESSURE P_e (atm)
			Facility	SRI			
		(1)	(2)		(4)		
Langley Phenolic-Nylon Scout R/4B	PLL1	10,200	145		0.0197	0.084	0.00155
	PLL2	10,200	146		0.0197	0.084	0.00158
	PLL90	10,200	145		0.0199	0.086	0.00156
	PLL3	10,090	65		0.0041	0.0194	0 00035
	PLL4	10,080	64		0.0041	0.0195	0.00035
	PLL5	15,390	457		0.094	0.625	0.0107
	PLL6	15,400	456		0.095	0.630	0.0106
	PLL7	15,400	457		0.095	0.624	0.0106
Avcoat 5026-39	A1	10,200	145		0.0199	0.086	0.00156
	A2	10,200	146		0.0197	0.085	0.00157
	A94	10,200	144		0.0199	0.086	0.00157
	A3	10,100	66		0.0041	0.0197	0.00036
	A4	10,090	65		0.0041	0.0195	0.00035
	A5	15,380	455		0.093	0.626	0.0104
	A6	15,400	456		0.095	0.625	0.0105
Modified Purple Blend Silicone E4A1	SP1	10,180	145		0.0197	0.085	0.00156
	SP2	10,200	146		0.0199	0.086	0.00156
	SP90	10,200	145		0.0199	0.086	0.00155
	SP3	10,100	66		0.0041	0.0194	0.00035
	SP4	10,100	64		0.0041	0.0196	0.00036
	SP5	15,360	455		0.093	0.620	0.0105
	SP6	15,400	457		0.095	0.626	0.0106
G. E. Silicone ESM 1004AP	SG1	10,200	145		0.0197	0.084	0.00155
	SG45	10,190	144		0.0199	0.085	0.00155
	SG2	10,080	65		0.0041	0.0195	0.00036
	SG3	10,100	66		0.0041	0.0197	0.00036
	SG4	15,380	456		0.093	0.624	0.0105
	SG5	15,400	457		0.095	0.626	0.0106
Hughes Phenolic-Nylon H-5	PLH1	10,200	146		0.0199	0.085	0.00156
	PLH90	10,200	144		0.0199	0.086	0.00156
	PLH2	10,100	65		0.0041	0.0196	0.00035
	PLH3	10,100	65		0.0041	0.0195	0.00035
	PLH4	15,400	457		0.095	0.625	0.0106
	PLH5	15,380	456		0.094	0.622	0.0105
			(3)				
Calibration Runs	C1	10,200	146		0.0197	0.085	0.00157
	C2	10,190		135	0.0197	0.084	0.00157
	C3	10,100	67		0.0041	0.0197	0.00036
	C4	10,100		57	0.0041	0.0193	0.00035
	C5	15,400	458		0.095		
	C6	15,400		457	0.095		

(1) Enthalpy measured by energy balance method

(2) Giannini steady state calorimeter, 0.625-in. diameter hemispherical shape, copper surface, water temperature rise type This calorimeter was calibrated with calorimeter described under (3).

(3) Giannini transient calorimeter used to calibrate (2), 0.25-in. diameter by 0.25-in. long copper slug set in graphite shroud with shape same as models.

(4) Giannini pitot probe, water-cooled, 0.625-in. diameter.

GAS FLOW RATE (lb/sec)	MAXIMUM FRONT SURFACE TEMPERATURE T_{FS} (^{o}F) $\epsilon = 1$			RUN TIME (sec)	CORE WEIGHT LOSS (g)	CORE CHAR WEIGHT (g)	CORE RECESSION (in.)	CHAR THICKNESS (in.)	CHAR DENSITY (lb/ft^3)
	Facility (5)	(6)	SRI (7)						
0.0043	3,000	2,820	2,900	9.4	0.142	0.073	0.010	0.063	14.4
0.0043	3,260	3,280	3,180	20.9	0.229	0.119	0.022	0.101	14.6
0.0043	3,680	3,800	3,620	34.7	0.384	0.214	0.073	0.159	16.7
0.00084	2,300	2,300	2,140	33.0	0.208	0.092	0.024	0.084	13.6
0.00084	2,480	2,610	2,350	79.1	0.436	0.172	0.075	0.131	16.3
0.0189	3,950			5.1	0.147	0.092	0.010	0.075	15.2
0.0189	4,230	4,350	4,180	10.8	0.249	0.156	0.030	0.114	16.9
0.0189	4,020		4,000	5.2	0.148	0.093	0.009	0.075	15.4
0.0043	3,200	3,300	3,100	11.1	0.148	0.112	0.016	0.077	18.0
0.0043	3,370	3,400	3,300	20.8	0.251	0.162	0.037	0.107	18.8
0.0043	3,300	3,500	3,290	34.7	0.361	0.212	0.072	0.144	18.3
0.00084	2,350	2,500	2,280	32.5	0.206	0.139	0.030	0.094	18.3
0.00084	2,390	2,600	2,300	78.9	0.373	0.236	0.064	0.173	17.0
0.0189	3,550	4,240	4,100	5.7	0.176	0.096	0.027	0.078	15.3
0.0189	4,150	4,360	4,250	10.7	0.286	0.127	0.062	0.099	15.9
0.0043	2,780	2.820	2,650	10.4	0.132	0.102	+0.016	0.075	16.9
0.0043	3,170		3,050	20.8	0.181	0.150	+0.030	0.125	14.9
0.0043	3,060	3,340	3,000	35.0	0.369	0.199	0.004	0.127	19.1
0.00084	2,380	2,450	2,180	32.7	0.169	0.116	+0.036	0.109	13.2
0.00084	2,400	2,485	2,250	79.0	0.286	0.197	+0.048	0.177	13.8
0.0189	3,850		3,850	5.9	0.207	0.055	0.026	0.045	15.1
0.0189	3,850	3,340	3,850	10.7	0.338	0.074	0.070	0.056	16.4
0.0043	3,020	3,240	2,950	20.9	0.255	0.181	0.043	0.077	29.2
0.0043	3,100	3,300	3,050	34.8	0.478	0.248	0.065	0.107	28.8
0.00084	2,400	2,470	2,250	32.6	0.108	0.295	+0.011	0.115	31.8
0.00084	2,380	2,455	2,230	79.2	0.193	0.488	+0.015	0.200	30.2
0.0189	3,250	3,320	3,250	5.8	0.268	0.105	0.075	0.030	43.5
0.0189	2,900	3,300		11.5	0.635	0.071	0.182	0.030	29.3
0.0043	3,300	3,360	3,250	20.8	0.229	0.108	0.014	0.094	14.2
0.0043	3,350	3,460	3,250	34.8	0.329	0.163	0.025	0.135	15.0
0.00084	2,490	2,400	2,320	32.8	0.222	0.088	0.023	0.085	12.8
0.00084	2,550	2,590	2,330	78.8	0.450	0.163	0.073	0.130	15.5
0.0189	3,850	4,010	3,800	4.9	0.125	0.084	0.004	0.068	15.3
0.0189	4,200	4,300	4,150	10.8	0.260	0.156	0.025	0.113	17.1
0.0043									
0.0043									
0.00084									
0.00084									

(5) Thermodot Mo. TD-6BT radiation thermometer (1.6-2.7 microns); viewed model through front port, approximately 40° to surface plane of model.

(6) L-N optical pyrometer (0.655 microns).

(7) SRI radiometer; viewed model through front port, approximately 40° to surface plane of model.

Table B-10(a)

TUNNEL CALIBRATION AND TEST DATA REPORTED BY MARTIN COMPANY

Ref: Martin Report ER 14356, August 26, 1966

	MODEL NO.	TOTAL ENTHALPY h_t (Btu/lb)	HEAT TRANSFER RATE $\dot{q}_{CW}$ (Btu/ft^2 sec) Calorimeter				MODEL STAGNATION PRESSURE P_{t_2} (atm)	PLENUM PRESSURE P_{t_1} (atm)
			Facility			SRI		
		(1)	(2)	(3)	(4)	(5)		
Langley Phenolic-Nylon Scout R/4B	PLL12	5,143	46.5			59.8	0.0071	0.0303
	PLL13	4,996	42.6				0.0069	0.0303
	PLL14	6,170	44.0				0.0070	
	PLL91	5,140	43.2				0.0070	0.0301
	PLL10	18,117	456.				0.0333	0.0448
	PLL11	18,117	456.				0.0333	0.0448
	PLL8	10,137	417.				0.140	0.263
	PLL9	10,947	418.				0.144	0.264
Avcoat 5026-39	A12	5,143	46.5			59.8	0.0071	0.0303
	A13	4,996	42.6				0.0069	0.0303
	A95	5,140	43.2				0.0070	0.0301
	A10	18,117	456.				0.0333	0.0448
	A11	18,445	475.				0.0340	0.0433
	A8	10,137	417.				0.140	0.263
	A9	10,947	418.				0.144	0.264
	A14	10,387	417.				0.140	0.260
Modified Purple Blend Silicone E4A1	SP13	4,933	44.4			57.5	0.0070	0.0303
	SP14	5,226	42.3				0.0070	0.0264
	SP91	5,180	44.2				0.0070	0.0316
	SP10	17,950	475.				0.0340	0.0435
	SP11	18,445	475.				0.0340	0.0433
	SP12	18,642	455.				0.0341	0.0632
	SP8	10,647	417.			547.	0.139	0.267
	SP9	10,158	408.			512.	0.144	0.263
G. E. Silicone ESM 1004AP	SG6	5,226	42.3			55.9	0.0070	0.0264
	SG46	5,180	44.2				0.0070	0.0316
	SG10	17,950	475.					0.0435
	SG7	10,387	417.				0.140	0.260
	SG8	10,038	408.				0.144	0.257
	SG9	10,158	408.			512.	0.144	0.263
Hughes Phenolic-Nylon H-5	PLH12	4,933	44.4			57.5	0.0070	0.0303
	PLH91	5,180	44.2				0.0070	0.0316
	PLH7	18,642	455.				0.0341	0.0632
	PLH10	17,950	475.				0.0340	0.0435
	PLH11	18,445	475.				0.0340	0.0433
	PLH8	10,137	417.				0.140	0.263
	PLH9	10,647	417.			547.	0.139	0.267
Calibration Runs	C1	4,824	42.8	40.7	40.0	56.8	0.0070	0.0290
	C2	18,370	485.	457.	438.	530.	0.0340	0.0435
	C3	10,820	400.	409.	387.			

(1) Enthalpy measured by energy balance method.

(2) Facility steady state calorimeter, "Gardon" asymptotic type by Thermogage Inc., 1.25-in. diameter, flat face, sensing diameter 0.10-in. constantan.

(3) Martin design slug calorimeter, 0.25-in. diameter copper slug by 0.125-in. long set in 1.25-in. diameter flat face asbestos-phenolic body.

(4) Martin design slug calorimeter, 0.625-in. copper slug by 0.125-in. long set in 1.25-in. diameter flat face asbestos-phenolic body.

(5) Facility pitot probe, 0.625-in. diameter, water-cooled.

TEST CHAMBER PRESSURE (atm)	NOZZLE EXIT PRESSURE P_e (atm)	GAS FLOW RATE (lb/sec)	MAXIMUM FRONT SURFACE TEMPERATURE T_{FS} ϵ = 1 (°F)		RUN TIME (sec)	CORE WEIGHT LOSS (g)	CORE CHAR WEIGHT (g)	CORE RECESSION (in.)	CHAR THICKNESS (in.)	CHAR DENSITY (lb/ft^3)
			Facility (6)	SRI (7)						
0.00096	0.00106	0.0030	2690	2600	70	0.401	0.160	0.054	0.126	15.7
0.00126	0.00136	0.0030	2540	2360	35	0.210	0.102	0.023	0.087	14.5
					70	0.398	0.165	0.060	0.128	16.0
0.00065	--	0.0030	2700	2440	120	0.574	0.240	0.107	0.178	16.7
0.00379	0.00459	0.0040	4310	4230	11	0.210	0.138	0.017	0.108	15.8
0.00379	0.00459	0.0040	4070	3930	5	0.128	0.075	0.004	0.063	14.8
0.00921	0.00921	0.0251	4770	4520	17	0.431	0.219	0.069	0.156	17.4
0.00854	0.00854	0.0250	4440	4300	7	0.192	0.127	0.020	0.094	16.8
0.00096	0.00106	0.0030	2780	2500	70	0.377	0.237	0.048	0.168	17.5
0.00126	0.00136	0.0030	2600	2430	35	0.197	0.128	0.024	0.096	16.5
0.00065	--	0.0030	2620	2470	120	0.537	0.338	0.060	0.236	17.8
0.00379	0.00459	0.0040	4340	4280	11	0.256	0.123	0.048	0.092	16.6
0.00369	0.00479	0.0040	4200	4150	5	0.140	0.083	0.022	0.064	16.1
0.00921	0.00921	0.0251		4350	17	0.551	0.106	0.169	0.079	16.6
0.00854	0.00854	0.0250	4460	4400	7	0.266	0.096	0.057	0.076	15.7
0.00914	0.00914	0.0249	4580	4390	17	0.601	0.095	0.188	0.076	15.5
0.00125	0.00135	0.0030	2400	2330	35	0.184	0.123	+0.033	0.107	14.3
0.00100	0.0009	0.0030	2430	2350	70	0.275	0.187	+0.049	0.153	15.2
0.00105	0.00115	0.0030	2400	2040	120	0.442	0.253	+0.048	0.200	15.7
0.00369	0.00443	0.0040	3980	3940	11	0.286	0.057	0.042	0.052	13.6
0.00369	0.00479	0.0040	3910	3830	5	0.129	0.054	0.000	0.052	12.9
0.00380	0.00482	0.0040	3920	3670	13.4	0.344	0.078	0.053	0.063	15.4
0.00909	0.00934	0.0251	4100	3840	17	0.710	0.030	0.190	0.032	11.6
0.00789	0.00789	0.0250		3860	7	0.294	0.033	0.055	0.033	12.4
0.00100	0.00090	0.0030	2430	2320	70	0.216	0.467	+0.006	0.174	33.3
0.00105	0.00115	0.0030	2380	2290	120	0.344	0.551	+0.065	0.271	25.2
0.00369	0.00443	0.0040	3500	3370	11	0.457	0.093	0.129	0.030	38.4
0.00914	0.00914	0.0249	3480	3220	17	1.350	0.077	0.415	0.011	46.8
0.00855	0.00878	0.0250		3250	17	1.276	0.065	0.373	0.016	50.4
0.00789	0.00789	0.0250	--	3220	7	0.452	0.106	0.119	0.033	39.8
0.00125	0.00135	0.0030	2660	2500	70	0.410	0.147	0.058	0.119	15.3
0.00105	0.00115	0.0030	2670	2480	120	0.639	0.196	0.078	0.171	14.7
0.00380	0.00482	0.0040	4170	3940	11	0.226	0.134	0.025	0.103	16.1
0.00369	0.00443	0.0040	4270	4220	11	0.225		0.015		
0.00369	0.00479	0.0040	4040	3850	5	0.125	0.070	0.004	0.061	14.2
0.00921	0.00921	0.0251	4720	4490	17	0.461	0.204	0.062	0.151	16.8
0.00909	0.00934	0.0251		4130	7	0.230	0.133	0.019	0.097	17.0
0.0010	0.0011									
0.00382	0.00442									

(6) Facility Pyro 650 electronic optical pyrometer; viewed model through front port, approximately 30° to model surface plane.

(7) SRI radiometer, located inside test chamber; viewed model directly, approximately 30° to model surface plane.

Table B-10(b) (Concluded)

TUNNEL CALIBRATION AND TEST DATA REPORTED BY MARTIN COMPANY FOR VARIOUS DIAMETER MODELS

Ref: Martin Report ER 14 426, November 17, 1966

	MODEL NO.	TOTAL ENTHALPY h_t (Btu/lb) (1)	MODEL STAGNATION PRESSURE P_{t_2} (atm)	PLENUM PRESSURE P_{t_1} (atm)	TEST CHAMBER PRESSURE (atm)	GAS FLOW RATE (lb/sec)	MODEL DIAMETER AND SHAPE (in.)	MODEL CORE DIAMETER (in.)
Teflon	T163	12,149	0.0205	0.241	0.00132	0.04	1.0 Hemi.	0.5
	T162	12,432	0.0203	0.240	0.00132	0.04	1.0 Hemi.	0.5
	T158	12,149	0.0205	0.241	0.00132	0.04	1.25 FF	0.625
	T159	12,145	0.0203	0.220	0.00132	0.04	1.25 FF	0.625
	T155	12,246	0.0203	0.241	0.00132	0.04	2.5 FF	1.25
	T154	12,246	0.0203	0.241	0.00132	0.04	2.5 FF	1.25
	T150	12,610	0.0203	0.250	0.00132	0.04	5.0 FF	2.5
	T151	12,406	0.0201	0.249	0.00132	0.04	5.0 FF	2.5
Hughes Phenolic-Nylon H-5	PLH163	12,145	0.0203	0.220	0.00132	0.04	1.0 Hemi.	0.5
	PLH162	12,432	0.0203	0.240	0.00132	0.04	1.0 Hemi.	0.5
	PLH159	12,145	0.0203	0.220	0.00132	0.04	1.25 FF	0.625
	PLH158	12,432	0.0203	0.240	0.00132	0.04	1.25 FF	0.625
	PLH155	12,406	0.0201	0.249	0.00132	0.04	2.5 FF	1.25
	PLH154	12,246	0.0203	0.241	0.00132	0.04	2.5 FF	1.25
	PLH151	12,610	0.0203	0.249	0.00132	0.04	5.0 FF	2.5
	PLH150	12,406	0.0201	0.250	0.00132	0.04	5.0 FF	2.5
Tunnel Calibration Runs	C1	12,196	0.0200	0.296	0.00150	0.0401		
	C2	12,725	0.0201	0.289	0.00145	0.0401		
	C3	12,071	0.0195	0.283	0.00132	0.04		
	C4	12,367	0.0204	0.265	0.00132	0.04		
	C5	11,869	0.0194	0.271	0.00126	0.04		
	C6	11,713	0.0194	0.278	0.00122	0.04		

(1) Enthalpy determined by heat balance method.

(2) Thermogage heat sink calorimeter, 1.25-in. flat face plus adapter to 2.5-in. diameter.

(3) Thermogage steady state water-cooled asymptotic calorimeters: (1) 1-in. diameter hemisphere shape, (2) 1.25-in. diameter flat face plus adapters for 2.5-in. diameter and 5-in. diameter flat face. Constantan sensing diameter 0.125 in.

(4) SRI calorimeter.

HEAT TRANSFER RATE $\dot{q}_{CW}$ (Btu/ft^{2}sec) (2)		MAXIMUM FRONT SURFACE TEMPERATURE T_{FS} $\epsilon = 1$ ($^\circ$F)		RUN TIME (sec)		CORE WEIGHT LOSS (g)	CORE CHAR WEIGHT (g)	CORE RECESSION (in.)	CHAR THICKNESS (in.)	CHAR DENSITY (lb/ft^3)
		Facility (6)	SRI (7)							
149				10		0.472		0.068		
151				35		1.607		0.228		
149				20		0.751		0,067		
155				70		3.055		0.269		
151				30		3.153		0.070		
151				100		11.088		0.248		
156				40		12.004		0.067		
156				140		43.032		0.229		
155		3,590	3,840	10		0.185	0.074	0.040	0.094	14.2
151		3,960		35		0.506	0.158	0.150	0.199	16.2
155		3,710	3,500	20		0.257	0.128	0.027	0.115	13.8
151		4,110	4,000	70		0.731	0.375	0.144	0.282	16.5
156		3,480	3,390	30		1.263	0.606	0.029	0.126	14.9
151		3,770	3,550	100		3.094	1.552	0.120	0.278	17.3
156		3,300	3,200	40		5.231	2.824	0.032	0.156	14.0
156		3,490	3,390	140		12.898	6.974	0.106	0.318	17.0

HEAT TRANSFER RATE (Btu/ft^{2}sec)

THERMOGAGE CALORIMETER (2)		THERMOGAGE CALORIMETER (3)				SRI (4)	MARTIN CALORIMETER (5)			
2.5 FF	1.25 FF	1.0 Hemi.	1.25 FF	2.5 FF	5.0 FF	1.25 FF	1.0 Hemi.	1.25 FF	2.5 FF	5.0 FF
149			246	180		254			124	
155			255		144			217		75
151	211	484					318			
171		500						240		85
155		384							132	
151		438				247	348			
156							345			

(5) Martin transient calorimeter, copper slug set in asbestos-phenolic body.

Calorimeter Shape	Overall Diameter (in.)	Slug Diameter (in.)
Hemisphere	1.0	0.125
Flat Face	1.25	0.188
Flat Face	2.50	0.250
Flat Face	5.0	0.250

(6) Facility pyrometer Pyro 650 electronic optical pyrometer, located outside test chamber; viewed model through front port approximately 38° to plane of model front surface.

(7) SRI radiometer, located inside test chamber; viewed model directly, approximately 38° to plane of model front surface.

Table B-11

TUNNEL CALIBRATION AND TEST DATA REPORTED BY SPACE GENERAL CORPORATION
Ref: SGC Report 1034-F1, July 1966

	MODEL NO.	TOTAL ENTHALPY h_t (Btu/lb)		HEAT TRANSFER RATE $\dot{q}_{CW}$ (Btu/ft^2 sec)		MODEL STAGNATION PRESSURE P_{t_2} (atm)	PLENUM PRESSURE P_{t_1} (atm)
				Calorimeter			
		(1)	(2)	Facility (3)	SRI	(4)	
Langley Phenolic-Nylon Scout R/4B	PLL22	14,925	14,990	99		0.00510	0.0266
	PLL23	14,920	14,850	97		0.00509	0.0265
	PLL94	14,855	14,990	103		0.00511	0.0266
	PLL55	24,985	24,130	346		0.01947	0.1210
	PLL56	24,765	25,340	344		0.01960	0.1234
	PLL24	5,117	5,010	158		0.092	0.514
	PLL28	5,129	5,020	150		0.092	0.514
Avcoat 5026-39	A23	15,035	14,850	101		0.00511	0.0265
	A25	15,100	14,850	95		0.00509	0.0265
	A97	14,955	15,000	101		0.00511	0.0267
	A24	24,880	25,510	345		0.01974	0.1237
	A26	24,925	26,180	346		0.01934	0.1250
	A27	5,063	5,005	157		0.093	0.512
	A28	5,134	5,020	155		0.092	0.514
Modified Purple Blend Silicone E4A1	SP22	14,855	15,110	98		0.00512	0.0268
	SP24	15,050	14,990	103		0.00511	0.0266
	SP94	14,925	14,990	105		0.00510	0.0266
	SP25	24,780	25,510	344		0.01974	0.1237
	SP26	24,800	24,840	344		0.01960	0.1224
	SP27	5,127	5,015	157		0.093	0.513
	SP28	5,093	5,020	155		0.092	0.514
G. E. Silicone ESM 1004AP	SG16	15,035	15,000	106		0.00511	0.0264
	SG48	14,920	14,990	103		0.00511	0.0266
	SG20	24,888	24,130	345		0.01947	0.1210
	SG18	5,150	5,030	155		0.093	0.510
	SG19	5,174	5,020	153		0.092	0.514
Hughes Phenolic-Nylon H-5	PLH19	14,855	14,850	102		0.00510	0.0265
	PLH94	15,035	14,990	98		0.00511	0.0266
	PLH20	24,910	24,840	345		0.01968	0.1224
	PLH21	24,875	25,510	345		0.01972	0.1237
	PLH22	5,129	5,005	157		0.092	0.512
	PLH23	5,154	5,020	153		0.092	0.514
Calibration Runs	C1	15,025	14,850	101	98.7	0.00509	0.0265
	C2	24,925	25,510	346	344.8	0.01972	0.1237
	C3	5,150	5,020	157	162.7	0.0925	0.514

(1) Enthalpy measured by energy balance method.

(2) Enthalpy calculated by SGC using sonic flow relationship: $h_t = (280 P_{t_1} A^*/\dot{m})^{2.5}$.

(3) SGC steady state calorimeter, Hy-Cal Engineering asymptotic type, 0.10-in. diameter constantan sensing area in 1.25-in. diameter flat faced shroud.

(4) SGC pitot probe, water cooled, 0.5-in. diameter.

NOZZLE EXIT PRESSURE P_e (atm)	GAS FLOW RATE (lb/sec)	MAXIMUM FRONT SURFACE TEMPERATURE T_{FS} ϵ = 1 (°F)		RUN TIME (sec)	CORE WEIGHT LOSS (g)	CORE CHAR WEIGHT (g)	CORE RECESSION (in.)	CHAR THICKNESS (in.)	CHAR DENSITY (lb/ft^3)
		Facility (5)	SRI (6)						
0.000475	0.00088	2930		15.0	0.158	0.082	0.012	0.070	14.5
0.000473	0.00088	3100	2580	30.3	0.269	0.121	0.031	0.105	14.3
0.000475	0.00088	3010	2600	50.0	0.323	0.154	0.054	0.124	15.4
0.002108	0.00329	4340	3350	15.2	0.465	0.253	0.055	0.182	17.2
0.002197	0.00329	4340	3450	6.1	0.264	0.147	0.021	0.110	16.6
0.00965	0.0259	3980	3620	14.0	0.266	0.162	0.034	0.115	17.5
0.00968	0.0259	4260		33.0	0.515	0.247	0.093	0.170	18.0
0.000476	0.00088	3125	2550	30.2	0.272	0.167	0.044	0.125	16.6
0.000476	0.00088	3050	2420	15.3	0.162	0.118	0.019	0.078	18.7
0.000477	0.00088	3080	2600	50.4	0.392	0.240	0.063	0.168	17.7
0.002237	0.00329	4100	3300	6.1	0.222	0.131	0.035	0.099	16.4
0.001974	0.00329	4385	3200	15.0	0.462	0.205	0.103	0.148	17.2
0.00971	0.0259	4060		14.0	0.310	0.139	0.070	0.098	17.6
0.00968	0.0259	4130		33.0	0.695	0.141	0.242	0.090	19.4
0.000475	0.00088	2980	2460	15.4	0.136	0.108	+0.039	0.097	13.8
0.000475	0.00088	3190	2540	30.2	0.178	0.141	+0.055	0.133	13.1
0.000477	0.00088	2975	2300	50.3	0.349	0.191	+0.033	0.167	14.2
0.002237	0.00329	3860	2950	6.1	0.238	0.101	0.005	0.089	14.1
0.002276	0.00329	3950	3000	15.0	0.537	0.121	0.101	0.091	16.5
0.00968	0.0259	3835	3540	14.0	0.333	0.104	0.052	0.077	16.8
0.00965	0.0259	3865		33.0	0.732	0.100	0.176	0.077	16.1
0.00475	0.00088	2880		30.0	0.173	0.313	0.008	0.123	31.6
0.00477	0.00088	3010	2450	50.2	0.228	0.369	0.029	0.160	28.6
0.001974	0.00329	3520	2800	15.1	0.810	0.097	0.228	0.030	40.1
0.00965	0.0259	3435	3080	14.0	0.534	0.113	0.151	0.036	38.9
0.00968	0.0259	3425	3130	33.0	1.526	0.073	0.451	0.019	47.6
0.000476	0.00088	2800		30.3	0.259	0.115	0.025	0.098	14.6
0.000477	0.00088	2980	2540	50.0	0.374	0.151	0.049	0.122	15.3
0.002276	0.00329	4060	3300	6.1	0.208	0.123	0.015	0.095	16.1
0.002237	0.00329	4180	3500	15.1	0.425	0.258	0.047	0.181	17.7
0.00970	0.0259	4035	3640	14.0	0.265	0.154	0.022	0.118	16.2
0.00966	0.0259	4190	3640	33.0	0.580	0.229	0.090	0.172	16.5
0.000477	0.00088								
0.002237	0.00329								
0.00967	0.0259								

(5) L-N optical pyrometer (0.655 microns); viewed model through front quartz port, approximately 18° to plane of model front.

(6) SRI radiometer located outside test chamber. For test condition 1 (h = 15,000, $\dot{q}$ = 100) viewed model through front port, approximately 18° to plane of model front surface. For remaining two test conditions, model was viewed through a side port 40° to jet axis, thence off front mirror 40° to plane of model front surface.

Table B-12

TUNNEL CALIBRATION AND TEST DATA REPORTED BY CORNELL AERONAUTICAL LABORATORY INC.
Ref: Letter Report Dated September 19, 1966

	MODEL NO.	SPECIFIC ENTHALPY (Btu/lb)	HEAT TRANSFER RATE $\dot{q}_{CW}$ (Btu/ft^2 sec) Calorimeter			MODEL STAGNATION PRESSURE P_{t_2} (atm)	GAS FLOW RATE (lb/sec)	RESERVOIR PRESSURE P_{t_1} (atm)	STAGNATION TEMPERATURE ($^\circ$R)
			Facility		SRI				
				(4)	(6)				
Teflon	T118	2060		618	1091	10.2	5.0	101.7	6100
	T119	2080		624	1108	10.3		102.5	6120
	T121	1940		1067	1740	29.5		98.4	5840
Phenolic-Nylon (75 lb/ft^3)	P12B1	2120		636	1115	10.0	5.0	100.40	6200
	P12B6	2080		624	1070	9.6		95.8	6120
	P12B4	1870		1028	1666	29.3		97.7	5700
Langley Phenolic-Nylon Scout R/4B	PLL44	2060		618	1075	9.9		99.0	6100
Avcoat 5026-39	A43	2040		612	1059	9.8		97.9	6050
Tunnel Calibration Run	C1	1950			1010	9.8		98.0	5860
	C2	1870	1700[1]	650[5]		19.1			
	C3	2100	2720	1040		32.4			
	C4	2050	5060[2]	1760		53.0			
	C5	1910	5450	1900		64.0			
	C6	2010	4050[3]	1990		53.0			
	C7	1810	4740	2330		63.0			

(1) Cornell transient calorimeter, 0.3-in. nose radius, hemispherical shape, 0.090-in. diameter by 0.125-in. long OFHC copper slug potted in 0.125-in. diameter bore with insulating cement, Ch-Al thermocouple spot welded to back face.

(2) Cornell calorimeter, 0.25-in. nose radius, hemispherical shape, 0.150-in. diameter by 0.506-in. long OFHC copper slug with 0.020-in. long flanges at each end for press fit into 0.160-in. diameter bore. Sheathed Ch-Al exposed junction thermocouple inserted into 0.022-in. diameter hole from rear of slug to within 0.020-in. from gage front face and gold soldered in place. Data reduction is by finite differences scheme on IBM computer.

(3) Identical to (2) except for 0.5-in. nose radius.

(4) Estimated from the relation furnished by Cornell: $\dot{q} = 0.3(H_s - H_w)$ at $P_{t_2} = 10$ atm and $\dot{q} = 0.55(H_s - H_w)$ at $P_{t_2} = 30$ atm.

(5) Heat flux adjusted to 1.25-in. flat face: (1) $0.55\ \dot{q}_1 0.6/1.25)^{0.5} = 0.382\ \dot{q}_1$, (2) $0.55\ \dot{q}_2(0.5/1.25)^{0.5} = 0.348\ \dot{q}_2$, (3) $0.55\ \dot{q}_3(1.0/1.25)^{0.5} = 0.492\ \dot{q}_3$.

(6) Estimated from Run C1 and the relation: $\dot{q} = 0.0744\ (P_{t_2}/R_{eff})^{0.5}\Delta h$.

STAGNATION DENSITY ρ_s (slugs/ft^3)	MACH NO. M_∞	FREE STREAM PRESSURE P_∞ (atm)	FREE STREAM TEMPERATURE T_∞ ($^\circ$R)	FREE STREAM DENSITY ρ_∞ (slugs/ft^3)	DISTANCE ROTOR TO MODEL (in.)	MAXIMUM FRONT SURFACE TEMPERATURE T_{FS} $\epsilon = 1$ ($^\circ$F) (7)	RUN TIME (sec)	CORE WEIGHT LOSS (g)	CORE CHAR WEIGHT (g)	CORE RECESSION (in.)	CHAR THICKNESS (in.)
0.00200	3.67	0.549	2370	0.00285	4	1080	2.0	1.139		0.103	
0.00201	3.67	0.554	2380	0.00286	4	1290	4.7	2.674		0.241	
0.0061	2.72	3.00	2360	0.00156	2.25		4.0	(8)			
0.00193	3.67	0.542	2420	0.00276	4	4030	2.1	0.611	0.000	0.099	0.000
0.00188	3.67	0.517	2380	0.00267	4	4400	6.0	1.727	0.000	0.280	0.000
0.0062	2.72	2.98	2300	0.00159	2.25	4400	3.1	2.903	0.000	0.470	0.000
0.00194	3.67	0.535	2370	0.00278	4	4200	4.1	(8)			
0.00195	3.67	0.528	2360	0.00275	4	4050	4.0	(8)			
0.00202	3.67	0.530	2280	0.00286	4		2.2				

(7) Facility Thermodot optical pyrometer; views model front surface through rotor tubes, 1.6 to 2.7 microns.

(8) Model disintegrated during test.

APPENDIX C

MODEL TEMPERATURE DATA

This appendix contains internal and external temperature data reported by the participating facilities for the models instrumented with thermocouples. The data were taken from the temperature plots reported by the facilities, and sufficient data have been included to allow reproduction of the original curves. The tunnel operating data for each model may be obtained by consulting the appropriate facility data table and model number in Appendix B. The various materials are designated by the model prefix letters described earlier.

Appendix C

MODEL EXTERNAL AND INTERNAL TEMPERATURE DATA

FACILITY	MODEL NO.	INITIAL THERMO-COUPLE DISTANCE FROM MODEL FRONT FACE (in.) (1)	THERMO-COUPLE TEMPERA-TURE RISE (°F) (2)	TIME (sec)	FRONT SURFACE TEMPERA-TURE $\epsilon = 1$ (°F) (3)	CHAR, VIRGIN MATERIAL INTERFACE TEMPERA-TURE (°F) (4)	TIME CHAR INTERFACE PASSED THERMO-COUPLE (sec)
GDB-Ames	A93	0.113	80	5	2660	1190	20
			370	10	2760		
			790	15	2790		
			1280	20	2830		
			1680	25	2850		
			1930	30	2880		
			2410	40	2900		
		0.226	50	30		800	60
			90	40			
			170	50	2930		
			300	60	2900		
			450	70	2930		
			550	75			
		0.330	60	50			
			80	60			
			120	70			
MPDB-Ames	A84	0.104	30	5		1380	22
			170	10			
			540	15			
			1130	20			
			1590	25			
		0.222	20	10		1280	50
			75	20			
			280	30			
			630	40			
			1110	50			
		0.305	10	10			
			20	20			
			50	30			
			120	40			
			240	50			
		0.410	5	10			
			20	30			
			35	50			
MPDB-Ames	A85	0.103	20	4	2700	1460	16
			230	8	3010		
			690	12	3150		
			1590	16	3220		
			2070	20	3280		
		0.211	10	5			
			15	10			
			50	15			
			140	20			
		0.321	10	5			
			15	10			
			20	15			
			120	20			
			130	25			
		0.424	5	5			
			10	10			
			20	15			
			20	15			
			20	20			
			25	25			
AMPD-Langley	A90	0.107	30	4			
			70	6			
			150	8			
			320	10			
			790	12			
			1420	14	3920		

Appendix C (Continued)

FACILITY	MODEL NO.	INITIAL THERMO-COUPLE DISTANCE FROM MODEL FRONT FACE (in.) (1)	THERMO-COUPLE TEMPERA-TURE RISE (°F) (2)	TIME (sec)	FRONT SURFACE TEMPERA-TURE $\epsilon = 1$ (°F) (3)	CHAR, VIRGIN MATERIAL INTERFACE TEMPERA-TURE (°F) (4)	TIME CHAR INTERFACE PASSED THERMO-COUPLE (sec)
AMPD-Langley	A90	0.209	40	6		1900	16.8
			70	8			
			140	10			
			270	12			
			580	14			
		0.311	5	5			
			40	10			
			70	15			
		0.420	200	20			
			5	10			
			50	20			
Aerotherm	A98	0.113	100	5	2700	1490	20
			480	10	2810		
			960	15			
			1430	20	2860		
			1820	25			
		0.215	40	10		1140	46
			130	20			
			360	30	2910		
			810	40	2950		
			1400	50	3000		
		0.313	20	20		990	72
			130	40			
			530	60	3170		
			1310	80	3170		
		0.424	10	20		990	104
			30	40			
			110	60			
			300	80			
			820	100			
Giannini	A94	0.101	5	2	2450	1160	14.4
			30	5	2800		
			190	8	2950		
			360	10	3100		
			810	13			
			1210	15	3160		
			1660	18			
		0.213	10	10		1070	34
			120	20	3210		
			290	25			
			600	30	3360		
			1090	35			
Martin	A95	0.103	30	5		1190	29
			200	10	2370		
			410	15			
			660	20	2500		
			910	25			
			1200	30			
		0.216	60	20		1060	72
			170	30			
			330	40	2600		
			520	50			
			730	60	2620		
		0.314	10	20			
			60	40			
			200	60			
			390	80	2600		
			630	100	2620		
		0.415	10	40			
			90	80			
			370	120			

Appendix C (Continued)

FACILITY	MODEL NO.	INITIAL THERMO-COUPLE DISTANCE FROM MODEL FRONT FACE (in.) (1)	THERMO-COUPLE TEMPERA-TURE RISE (°F) (2)	TIME (sec)	FRONT SURFACE TEMPERA-TURE $\epsilon = 1$ (°F) (3)	CHAR, VIRGIN MATERIAL INTERFACE TEMPERA-TURE (°F) (4)	TIME CHAR INTERFACE PASSED THERMO-COUPLE (sec)
Space General	A97	0.110	70	5		1000	17.5
			290	10	2950		
			690	15			
			1250	20	3000		
			1700	25			
		0.203	70	15		1050	41.5
			140	20			
			260	25			
			450	30	3050		
			670	35			
			940	40	3070		
			1200	45	3100		
			50	30			
			100	40			
			250	50			
GDB-Ames	PLL96	0.094	80	5	2400	1200	20
			250	10	2590		
			640	15	2690		
			1170	20	2770		
			1580	25	2840		
		0.226	50	20		1140	70.5
			200	40	2990		
			400	50	3040		
			620	60	3020		
			1140	70	3020		
		0.328	60	30			
			100	50			
			110	60			
			170	70			
		0.426	10	30			
			50	50			
			90	90			
MPDB-Ames	PLL87	0.095	10	5		800	25.5
			50	10			
			170	15			
			370	20			
			630	25			
		0.220	10	10			
			50	20			
			80	30			
			130	40			
			250	50			
		0.310	5	10			
			10	20			
			40	30			
			80	40			
			90	50			
MPDB-Ames	PLL89	0.149	20	4		1320	25
			40	8			
			90	12			
			220	16			
			480	20			
			880	24			
		0.234	5	5			
			15	10			
			30	15			
			50	20			
		0.332	5	5			
			10	10			
			15	15			
			20	20			
		0.438	5	5			
			10	10			
			15	15			
			20	20			

Appendix C (Continued)

FACILITY	MODEL NO.	INITIAL THERMO-COUPLE DISTANCE FROM MODEL FRONT FACE (in.) (1)	THERMO-COUPLE TEMPERA-TURE RISE (°F) (2)	TIME (sec)	FRONT SURFACE TEMPERA-TURE $\epsilon = 1$ (°F) (3)	CHAR, VIRGIN MATERIAL INTERFACE TEMPERA-TURE (°F) (4)	TIME CHAR INTERFACE PASSED THERMO-COUPLE (sec)
AMPD-Langley	PLL93	0.114	70	4		1400	11.6
			110	6			
			280	8			
			720	10			
			1430	12	3940		
		0.198	70	10		1420	24.2
			100	15			
			310	20			
			640	22			
			1280	24			
		0.314	30	15			
			70	20			
			80	25			
Aerotherm	PLL97	0.095	50	5		1060	19
			250	10	2750		
			650	15			
			1180	20	2880		
			1600	25			
		0.220	20	10		980	58
			70	20			
			120	30	2900		
			250	40	2960		
			510	50	3050		
		0.310	40	20		940	89
			70	40			
			150	60	3130		
			500	80			
			1600	100			
		0.399	40	20			
			70	40			
			110	60			
			170	80			
			820	100			
Giannini	PLL90	0.119	10	5	3100	1200	16.2
			180	10	3450		
			950	15	3420		
			1450	20	3580		
		0.220	15	10		800	33.4
			70	20			
			130	25	3610		
			360	30	3670		
			960	35	3660		
Martin	PLL91	0.111	20	5		980	35
			70	10	2200		
			130	15			
			180	20	2320		
			290	30			
			1150	40	2460		
		0.221	40	20		840	91
			140	40			
			300	60	2560		
			560	80	2640		
			1010	100	2700		
		0.314	20	20			
			50	40			
			90	60			
			160	80			
			380	100			
		0.415	30	40			
			80	80			
			170	120			

Appendix C (Continued)

FACILITY	MODEL NO.	INITIAL THERMO-COUPLE DISTANCE FROM MODEL FRONT FACE (in.) (1)	THERMO-COUPLE TEMPERA-TURE RISE (°F) (2)	TIME (sec)	FRONT SURFACE TEMPERA-TURE $\epsilon = 1$ (°F) (3)	CHAR, VIRGIN MATERIAL INTERFACE TEMPERA-TURE (°F) (4)	TIME CHAR INTERFACE PASSED THERMO-COUPLE (sec)
Space General	PLL94	0.104	50	5		960	21
			170	10	2800		
			460	15	2860		
			800	20	2900		
			1170	25	2920		
		0.211	20	20		1000	68
			70	30	2940		
			210	40	2960		
			450	50	3010		
		0.284	30	30			
			50	40			
			80	50			
GDB-Ames	PLH98	0.115	30	5	2440	1170	28
			120	10	2650		
			290	15	2740		
			530	20	2800		
			880	25	2840		
			1360	30	2880		
			2070	40	2940		
		0.212	110	30		1100	62
			240	40			
			460	50	2980		
			850	60	3040		
			1540	70	3060		
			1740	75			
		0.314	40	40			
			70	50			
			110	60			
			200	70			
		0.431	10	30			
			30	50			
			50	70			
MPDB-Ames	PLH97	0.115	20	5		840	30
			50	10			
			130	15			
			270	20			
			510	25			
			840	30			
			1260	35			
		0.212	10	10			
			25	20			
			50	30			
			125	40			
			200	50			
		0.314	5	10			
			15	30			
			40	50			
		0.431	2	10			
			10	30			
			25	50			
AMPD-Langley	PLH93	0.114	20	4		1540	12.6
			80	6			
			210	8			
			580	10			
			1260	12	3940		
		0.216	5	10		1440	27.6
			40	15			
			150	20			
			660	25			
		0.309	10	20			
			25	25			
			100	30			

Appendix C (Continued)

FACILITY	MODEL NO.	INITIAL THERMO COUPLE DISTANCE FROM MODEL FRONT FACE (in.) (1)	THERMO-COUPLE TEMPERA-TURE RISE (°F) (2)	TIME (sec)	FRONT SURFACE TEMPERA-TURE $\epsilon = 1$ (°F) (3)	CHAR, VIRGIN MATERIAL INTERFACE TEMPERA-TURE (°F) (4)	TIME CHAR INTERFACE PASSED THERMO-COUPLE (sec)
Giannini	PLH90	0.111	10	5	2300	960	19.6
			110	10	2750		
			360	15	2950		
			870	20	3130		
			1400	25	3200		
		0.205	10	10			
			40	20			
			90	25			
			160	30	3300		
			260	35	3370		
Martin	PLH91	0.115	90	10	2160	1130	45
			150	15			
			250	20	2250		
			380	25			
			510	30			
			890	40	2380		
			1280	50			
		0.211	30	20		1160	101
			140	40			
			300	60	2480		
			590	80			
		0.313	10	20			
			20	40			
			70	60			
			130	80	2560		
			240	100	2640		
		0.405	10	40			
			40	80			
			130	120			
Space General	PLH94	0.111	110	10	2750	1060	27
			270	15	2840		
			520	20	2900		
			850	25	2940		
			1280	30	2940		
		0.211	40	20			
			130	30			
			240	40	2960		
			440	50	2970		
GDB-Ames	SP96	0.095	50	5	2540	1190	41.5
			170	10	2540		
			310	15	2540		
			490	20	2510		
			840	30	2470		
			1120	40	2430		
			1280	50	2400		
		0.220	100	30			
			150	40			
			200	50			
			280	60	2360		
			350	70	2340		
			400	75			
		0.337	20	30			
			60	50			
			100	70			
		0.405	10	30			
			20	50			
			50	70			
MPDB-Ames	SP89	0.120	60	5	2610	1280	20.5
			210	10	2850		
			520	15	2880		
			1160	20	2890		
			1680	25	2890		

Appendix C (Continued)

FACILITY	MODEL NO.	INITIAL THERMO-COUPLE DISTANCE FROM MODEL FRONT FACE (in.) (1)	THERMO-COUPLE TEMPERA-TURE RISE (°F) (2)	TIME (sec)	FRONT SURFACE TEMPERA-TURE $\epsilon = 1$ (°F) (3)	CHAR, VIRGIN MATERIAL INTERFACE TEMPERA-TURE (4)	TIME CHAR INTERFACE PASSED THERMO-COUPLE (sec)
MPDB-Ames	SP89	0.241	5	5			
			10	10			
			25	15			
			50	20			
			75	25			
		0.311	2	5			
			4	15			
			6	25			
		0.421	2	5			
			4	15			
			6	25			
MPDB-Ames	SP85	0.099	60	5		1020	24
			210	10			
			410	15			
			680	20			
			1020	35			
			1300	30			
		0.207	40	10			
			110	20			
			240	30			
			460	40			
			740	50			
		0.325	10	10			
			30	30			
			70	50			
		0.416	5	10			
			10	30			
			20	50			
AMPD-Langley	SP93	0.085	20	2		1580	12.6
			110	4			
			280	6			
			580	8			
			1000	10			
			1510	12	3600		
		0.189	20	10		1440	30.6
			70	15			
			170	20			
			410	25			
Aerotherm	SP97	0.101	100	5	2140		
			350	10	2280		
			600	15			
		0.208	20	10		1190	38
			50	20	2290		
			100	30	2270		
			200	40	2260		
			310	50	2250		
			420	60	2240		
		0.303	20	20			
			60	40			
			140	60			
			250	80			
			330	100			
		0.409	20	20			
			50	40			
			100	60			
			140	80			
			210	100			
Martin	SP91	0.097	70	10	2230	740	62
			220	20	2290		
			340	30			
			470	40	2320		
			550	50			
			610	60	2380		

Appendix C (Continued

FACILITY	MODEL NO.	INITIAL THERMO-COUPLE DISTANCE FROM MODEL FRONT FACE (in.) (1)	THERMO-COUPLE TEMPERA-TURE RISE (°F) (2)	TIME (sec)	FRONT SURFACE TEMPERA-TURE $\epsilon = 1$ (°F) (3)	CHAR, VIRGIN MATERIAL INTERFACE TEMPERA-TURE (°F) (4)	TIME CHAR INTERFACE PASSED THERMO-COUPLE (sec)
Martin	SP91	0.198	40	20			
			160	40			
			320	60			
			480	80	2390		
		0.314	20	40			
			120	80			
			260	120	2400		
		0.411	10	40			
			50	80			
			120	120			
Giannini	SP90	0.099	20	5	2600	1340	22.7
			200	10	2800		
			500	15	2850		
			1000	20	3000		
			1400	25			
		0.216	30	20			
			100	30	3000		
Space General	SP94	0.097	80	5	2720	1460	33.5
			210	10	2800		
			450	15	2840		
			770	20	2870		
			1070	25	2900		
			1300	30	2920		
			1460	35	2940		
		0.189	50	20			
			140	30			
			250	40	2950		
			370	50	2960		
GDB-Ames	SG39	0.091	250	5	2540	1540	26.5
			610	10	2590		
			1020	15	2600		
			1410	20	2600		
			1670	25			
		0.220	130	20			
			270	30	2610		
			430	40	2630		
			590	50	2640		
			790	60	2650		
			980	70	2650		
			1040	75			
		0.318	90	30			
			150	40			
			210	50			
			300	60			
			390	70			
		0.407	40	30			
			100	50			
			160	70			
MPDB-Ames	SG53	0.099	190	5	2680	1240	14
			560	10	2780		
			1080	15	2840		
			1620	20	2870		
			1960	25	2870		
		0.211	10	5			
			35	10			
			90	15			
			190	20			
			310	25			
		0.308	5	5			
			30	15			
			60	25			
		0.411	2	5			
			10	15			
			25	25			

Appendix C (Continued)

FACILITY	MODEL NO.	INITIAL THERMO-COUPLE DISTANCE FROM MODEL FRONT FACE (in.) (1)	THERMO-COUPLE TEMPERA-TURE RISE (°F) (2)	TIME (sec)	FRONT SURFACE TEMPERA-TURE $\epsilon = 1$ (°F) (3)	CHAR, VIRGIN MATERIAL INTERFACE TEMPERA-TURE (°F) (4)	TIME CHAR INTERFACE PASSED THERMO-COUPLE (sec)
MPDB-Ames	SG51	0.089	100	5		1520	19.2
			590	10			
			1100	15			
			1440	20			
			1650	25			
		0.215	40	10			
			130	20			
			300	30			
			530	40			
			800	50			
		0.313	10	10			
			20	20			
			60	30			
			110	40			
			170	50			
		0.405	5	10			
			10	20			
			20	30			
			40	40			
			60	50			
AMPD-Langley	SG49	0.110	30	2		1840	12.4
			190	4			
			430	6			
			770	8			
			1220	10	2570		
		0.205	5	5		1440	23.4
			65	10			
			220	15			
			550	20			
		0.288	5	10			
			25	15			
			80	20			
			190	25			
Martin	SG46	0.114	80	2		1410	47
			160	4			
			250	6			
			700	8			
			1220	10	2240		
			1610	15			
		0.218	100	5			
			210	10			
			340	15			
			490	20	2300		
			830	30			
			1160	40	2320		
		0.399	130	20			
			310	40			
			550	60	2340		
			900	80	2360		
			40	40			
			180	80			
			450	120			
Space General	SG48	0.168	80	10	2700	1300	45
			330	20	2780		
			690	30	2850		
			1100	40	2920		
			1450	50	2980		
		0.191	50	10		1250	60
			200	20			
			440	30			
			710	40			
			960	50			

Appendix C (Concluded)

FACILITY	MODEL NO.	INITIAL THERMO-COUPLE DISTANCE FROM MODEL FRONT FACE (in.) (1)	THERMO-COUPLE TEMPERA-TURE RISE (°F) (2)	TIME (sec)	FRONT SURFACE TEMPERA-TURE $\epsilon = 1$ (°F) (3)	CHAR, VIRGIN MATERIAL INTERFACE TEMPERA-TURE (°F) (4)	TIME CHAR INTERFACE PASSED THERMO-COUPLE (sec)
Space General	SG48	0.310	50	30			
			130	40			
			230	50			
Giannini	SG45	0.101	120	5	2800	1300	17.4
			500	10	2850		
			940	15	2900		
			1500	20	2900		
			1900	25	3000		
		0.215	20	10			
			150	20			
			410	30			

(1) Thermocouple distance from original model face determined from X-ray photographs.

(2) Thermocouple temperature minus original starting model temperature at the time indicated in adjacent column.

(3) Front surface temperature measured with facility optical pyrometer at the time indicated in the preceding column.

(4) Char back face and virgin material interface temperature determined by method described in Section IV-C.

APPENDIX D

SUMMARY OF PHASE II CORRELATION DATA

This appendix tabulates, by material, information calculated from the data in Appendices B and C. This information was used in preparing the various graphs and correlations appearing in this report. Where multiple runs are shown, by listing more than one model number on the same line, the values represent averages of the available data.

SUMMARY OF CORRELATION DATA

MATERIAL	FACILITY	MODEL NO.	MASS LOSS RATES (lb/ft^2 sec)		HEAT TRANSFER RATE (Btu/ft^2 sec)		MODEL STAGNATION PRESSURE (atm)	ENTHALPY (Btu/lb)		EFFECTIVE MODEL RADIUS (ft)	FRONT SURFACE TEMPERATURE (^oR) $\epsilon = 1$	$\dot{q}_{SRI}/\dot{m}_t$
			$\dot{m}_t$	$\dot{m}_p$	$\dot{q}_{SRI}$ CW	$\dot{q}_{FAC}$ CW	P_{t_2}	Δh_{meas} CW (1)	Δh_{calc} SRI CW (2)	R_{eff} (3)	T_{FS}	CW Btu/lb
Langley Phenolic-Nylon Scout R/4B (PLL)	GBD-Ames	PLL54,57,96	0.00716	0.00629	81	68	0.0109	10,270	7,721	0.172	3,490	11,313
		PLL58,59	0.0104	0.0114	118	113.5	0.0106	22,680	11,406	0.172	3,720	11,346
		PLL60 61	0.0111	0.0140	178	141.9	0.0182	16,440	13,130	0.172	4,120	16,036
	MPDB-Ames	PLL70,69,87	0.00686	0.0094	117.1	96.3	0.00572	12,664	15,408	0.172		17,070
		PLL72,71,89	0.0111	0.0129	212.2	169.1	0.00812	19,638	23,435	0.172		19,117
	AMPD-Langley	PLL30,32,93,33	0.0240	0.0238	263		0.284	4,750	4,911	0.172	4,560	10,958
		PLL29,30	0.0303	0.0300	526		0.293	9,550	9,670	0.172	5,270	17,350
		PLL34,35	0.0556	0.0505	1,115		0.735	9,550	12,940	0.172	5,690	20,100
	ESB-Langley	PLL54,52	0.0257		203	177	0.281	3,100	3,811	0.172		7,898
	MSC-Houston (supersonic)	PLL65	0.0143		410	436	0.0117	11,350	37,722	0.172	4,350	28,671
		PLL66	0.0190		810	800	0.0170	24,350	61,820	0.172	4,410	42,632
		PLL67	0.0186		1,020	988	0.0192	33,850	73,258	0.172	4,270	54,839
	MSC-Houston (subsonic)	PLL38,39	0.0211	0.0273		403	1.0	8,251		0.172	4,840	
		PLL40,41	0.0245	0.0263		595	1.0	9,452		0.172	4,680	
		PLL36,37,95	0.0131	0.0140		100	1.0	4,336		0.172	3,510	
		PLL42	0.0151			205	1.0	5,475		0.172	3,565	
	Aerotherm	PLL43,46,97	0.00721	0.00905	80.1	88	0.0204	4,598	5,581	0.172	3,670	11,110
		PLL45,48	0.0116	0.0139	188	270	0.0301	7,462	10,784	0.172	4,300	16,207
		PLL15,18	0.0161	0.0303	947	1,160	0.0427	21,260	45,608	0.172	5,550	58,820
	AVCO	PLL47	0.0756		1,850	1,960	1.93	6,850	13,252	0.172	6,010	24,471
	Giannini	PLL1,2,90	0.0100	0.0234	138	145	0.0198	10,050	9,760	0.172	4,140	13,800
		PLL3,4	0.0051	0.0063	54	64.5	0.0041	9,935	8,392	0.172	2,940	10,588
		PLL5,6,7	0.0187	0.0316	457	457	0.0945	15,345	14,794	0.172	4,690	24,439
	Martin	PLL13,12,91	0.00435	0.00576	60	44.1	0.0070	4,793	7,136	0.172	3,160	13,793
		PLL11,10	0.0142	0.0286	500	456	0.0333	17,817	27,268	0.172	4,770	35,211
		PLL9,8	0.0248	0.0329	500	417.5	0.142	10,242	13,204	0.172	5,230	20,161
	Space General	PLL22,23,94	0.0051	0.00632	98	99	0.0051	14,750	13,656	0.172	3,560	19,216
		PLL55,56	0.0228	0.0345	344	345	0.0195	24,720	24,497	0.172	4,800	15,088
		PLL24,28	0.0136	0.0178	156	154	0.092	4,973	5,118	0.172	4,720	11,471
Hughes Phenolic-Nylon H-5 (PLH)	GDB-Ames	PLH6,98	0.00940	0.00849	81	67.5	0.0108	10,300		0.172	3,550	8,617
		PLH42,43	0.00973	0.0113	125	129	0.0102	22,600		0.172	3,960	12,847
		PLH24,50	0.0170	0.0197	166	163.1	0.0185	16,470		0.172	3,930	9,764
	MPDB-Ames	PLH62,61,97	0.00838		92.2	85.7	0.00582	12,111		0.172		11,000
		PLH65,63,64	0.0108		223.9	176.1	0.00787	19,094		0.172		20,731

MATERIAL	FACILITY	MODEL NO.	MASS LOSS RATES ($lb/ft^2 sec$)		HEAT TRANSFER RATE ($Btu/ft^2 sec$)		MODEL STAGNATION PRESSURE (atm) P_{t_2}	ENTHALPY (Btu/lb)		EFFECTIVE MODEL RADIUS (ft) R_{eff}	FRONT SURFACE TEMPERATURE (^oR) $\epsilon = 1$ T_{FS}	$\dot{q}_{SRI\ CW} / \dot{m}_t$ Btu/lb
			$\dot{m}_t$	$\dot{m}_p$	$\dot{q}_{SRI\ CW}$	$\dot{q}_{FAC\ CW}$		$\Delta h_{meas\ CW}$ (1)	$\Delta h_{calc\ SRI\ CW}$ (2)	(3)		
Hughes Phenolic-Nylon H-5 (PLH) (continued)	AMPD-Langley	PLH26,93,28	0.0228	0.0219	267		0.284	4,750		0.172	4,500	11,711
		PLH25,27	0.0280	0.0280	549		0.293	9,550		0.172	5,190	19,607
		PLH29,30	0.0491	0.0437	1,139		0.735	9,550		0.172	5,780	23,198
	ESB-Langley	PLH41,40	0.0196		203	177	0.281	2,955		0.172		
	MSC-Houston (supersonic)	PLH54	0.0154		400	431	0.0117	11,350		0.172	4,330	25,947
		PLH55	0.0200		808	797	0.0170	24,450		0.172	4,265	40,400
		PLH56	0.0211		1,040	1,000	0.0192	34,000		0.172	4,300	49,298
	MSC-Houston (subsonic)	PLH32,33	0.0220	0.0280		408	1.0	8,085		0.172	4,880	
		PLH34,35	0.0245	0.0304		600	1.0	9,275		0.172	4,595	
		PLH31	0.0136			101	1.0	4,493		0.172	3,440	
		PLH36	0.0174			205	1.0	4,980		0.172	3,660	
	Aerotherm	PLH44,45	0.00877	0.00916	58.2	87.2	0.0197	4,178		0.172	2,930	6,636
		PLH46,48	0.0122	0.0154	172	264	0.0298	7,983		0.172	3,550	14,098
		PLH16,17	0.0203	0.0313	967	1,180	0.0419	21,155		0.172	5,030	47,635
	Giannini	PLH1,90	0.00750	0.0109	139	146	0.0199	10,050		0.172	3,810	18,533
		PLH2,3	0.00512	0.0078	55	65	0.0041	9,950		0.172	3,010	10,742
		PLH4,5	0.0237	0.0330	456	456	0.0945	15,240		0.172	4,660	19,241
	Martin	PLH12,91	0.00474	0.00425	57.5	44.3	0.0070	4,757		0.172	3,130	12,131
		PLH10,11,7	0.0172	0.0310	510	468.3	0.0340	18,046		0.172	4,730	29,651
		PLH9,8	0.0240	0.0280	547	417	0.1395	10,102		0.172	5,180	22,792
	Space General	PLH19,94	0.00606	0.00720	99	100	0.00511	14,795		0.172	3,440	16,337
		PLH20,21	0.0249	0.0387	344	345	0.0197	24,740		0.172	4,640	13,815
		PLH22,23	0.0173	0.0189	157	155	0.092	4,990		0.172	4,550	9,075
	AMPD-Langley	PLH153,154	0.0050		78.5		0.0192	9,500		0.550		15,700
		PLH156,157	0.00605		89.5		0.0192	8,900		0.344		14,800
		PLH160,161	0.0091		126.5		0.0192	8,900		0.172		13,900
		PLH164,165	0.0158		271		0.0192	9,400		0.0416		17,200
	Martin	PLH162,163	0.00496			144	0.0203	12,300		0.688	3,950	
		PLH158,159	0.00674			180	0.0203	12,300		0.344	4,230	
		PLH154,155	0.00980		250	250	0.0202	12,330		0.172	4,570	25,500
		PLH150,151	0.0193			451	0.0202	12,500		0.0416	4,420	
Avcoat 5026-39, HC/G (A)	GDB-Ames	A53,54,61,93	0.0066	0.0122	121	122.5	0.0102	21,970	11,923	0.172	4,010	18,333
		A55,56	0.0117	0.0153	177	165	0.0185	16,520	12,950	0.172	4,120	15,128
		A57,60	0.00462	0.00658	84	66	0.0108	10,380	8,044	0.172	3,380	18,182
	MPDB-Ames	A72,71,84	0.00654	0.00998	105.3	97.6	0.00582	13,109	13,736	0.172		16,101
		A76,75,85	0.0113	0.0180	215.2	188.2	0.00947	19,342	22,000	0.172	3,790	19,044

Appendix D (Continued)

MATERIAL	FACILITY	MODEL NO.	MASS LOSS RATES ($lb/ft^2 sec$)		HEAT TRANSFER RATE ($Btu/ft^2 sec$)		MODEL STAGNATION PRESSURE (atm) P_{t_2}	ENTHALPY (Btu/lb)		EFFECTIVE MODEL RADIUS (ft) R_{eff}	FRONT SURFACE TEMPERATURE (^oR) $\epsilon = 1$ T_{FS}	$\dot{q}_{SRI\ CW}/\dot{m}_t$ Btu/lb
			$\dot{m}_t$	$\dot{m}$	$\dot{q}_{SRI\ CW}$	$\dot{q}_{FAC\ CW}$		$\Delta h_{meas\ CW}$ (1)	$\Delta h_{calc\ SRI\ CW}$ (2)	(3)		
Avcoat 5026-39, HC/G (A) (continued)	AMPD-Langley	A30,90,34	0.0302	0.0258	270		0.284	4,750	5,042	0.172	4,380	8,940
		A29,33,31,32	0.0452	0.0302	523		0.293	9,550	9,615	0.172	5,060	11,550
		A35,45	0.117		1,102		0.735	9,550	12,792	0.172	5,140	9,410
	ESB-Langley	A7,48	0.0241	0.0228	203	177	0.279	2,925	3,824	0.172		
	MSC-Houston (supersonic)	A62	0.0166		400	431	0.0117	11,350	36,800	0.172	4,340	8,423
		A63	0.0194		790	780	0.0170	25,316	60,299	0.172		24,096
		A64	0.0222		980	954	0.0192	33,850	70,385	0.172	4,340	44,144
	MSC-Houston (subsonic)	A38,39	0.0266	0.0245		403	1.0	8,251		0.172	4,770	
		A40,41	0.0283	0.0264		595	1.0	9,452		0.172	4,560	
		A36,37,91	0.0175	0.0129		104	1.0	4,491		0.172	3,860	
		A42,92	0.0222	0.0207		208	1.0	4,901		0.172	3,700	
	Aerotherm	A74,44,98	0.0151	0.0162	196	267	0.0298	7,077	11,299	0.172	4,260	12,980
		A58,59	0.0220	0.0283	941	1,155	0.0431	21,800	45,108	0.172	5,700	42,773
		A15,17	0.00861	0.0111	76.5	84	0.0182	4,633	5,643	0.172	3,650	8,885
	AVCO	A73	0.179		1,850	1,960	1.93	6,850	13,252	0.172	5,360	10,335
	Giannini	A1,2,94	0.00938	0.0134	138	145	0.0198	10,050	9,760	0.172	3,760	14,712
		A3,4	0.00373	0.0063	55	65.5	0.0041	9,950	8,548	0.172	2,850	14,745
		A5,6	0.0226	0.0289	455	455	0.094	15,240	14,769	0.172	4,610	20,133
	Martin	A13,12,95	0.00413	0.00413	59.8	44.1	0.0070	4,793	7,113	0.172	3,240	14,479
		A11,10	0.0200	0.0232	505	465.5	0.0337	17,981	27,377	0.172	4,800	15,250
		A9,8,14	0.0321	0.0297	500	417.3	0.141	10,190	13,251	0.172	5,040	15,576
	Space General	A23,25,97	0.0069	0.00986	98	99	0.00510	14,880	13,656	0.172	3,585	14,203
		A24,26	0.0280	0.0336	345	346	0.0195	24,750	24,562	0.172	4,845	12,321
		A27,28	0.0210	0.0223	158	156	0.0925	4,948	5,170	0.172	4,590	7,523
Modified Purple Blend Silicone, E4A1 (SP)	GDB-Ames	SP48,49,96	0.00394	0.00505	80	66.5	0.0107	10,270		0.172	3,140	20,305
		SP51,52	0.0048	0.00776	114	120.5	0.0097	21,700		0.172	3,540	23,750
		SP50	0.0106		172	159.8	0.0185	16,330		0.172	3,790	16,226
	MPDB-Ames	SP66,65,85	0.00555	0.00822	103.5	90.5	0.00582	12,128		0.172		
		SP68,67,89	0.0090	0.0136	221	172.3	0.00847	19,721		0.172	3,440	18,649
	AMPD-Langley	SP30,90,32	0.0181	0.0155	269		0.284	4,750		0.172	4,060	14,862
		SP29,31	0.0524	0.0456	510		0.293	9,550		0.172	4,600	9,732
		SP34,35,33	0.104	0.103	1,065		0.735	9,550		0.172	4,630	10,240
	ESB-Langley	SP45,46	0.00821	0.0141	203	177	0.281	2,945		0.172		24,726

Appendix D (Continued)

MATERIAL	FACILITY	MODEL NO.	MASS LOSS RATES ($lb/ft^2 sec$)		HEAT TRANSFER RATE ($Btu/ft^2 sec$)		MODEL STAGNATION PRESSURE (atm)	ENTHALPY (Btu/lb)		EFFECTIVE MODEL RADIUS (ft)	FRONT SURFACE TEMPERATURE	$\dot{q}_{SRI\ CW}/\dot{m}_t$ Btu/lb
			$\dot{m}_t$	$\dot{m}_p$	$\dot{q}_{SRI\ CW}$	$\dot{q}_{FAC\ CW}$	P_{t_2}	$\Delta h_{meas\ CW}$ (1)	$\Delta h_{calc\ SRI\ CW}$ (2)	R_{eff} (3)		
Modified Purple Blend Silicone, E4A1 (SP) (continued)	MSC-Houston (supersonic)	SP59	0.0156		400	426	0.0117	11,350		0.172	3,985	25,641
		SP60	0.0248		800	794	0.0170	24,350		0.172	4,360	32,258
		SP61	0.0277		990	958	0.0192	33,850		0.172	4,350	35,740
	MSC-Houston (subsonic)	SP42,39	0.0249			400	1.0	8,329		0.172	4,660	
		SP40,41	0.0354			595	1.0	9,693		0.172	4,400	
		SP36,27,95	0.0186			104	1.0	4,317		0.172	3,860	
		SP38	0.0196			205	1.0	4,850		0.172	3,680	
	Aerotherm	SP56,53,97	0.00352	0.00457	77.7	83.2	0.020	4,416		0.172	3,060	22,074
		SP55,57	0.0120	0.0135	200	263	0.0298	7,008		0.172	3,930	16,667
		SP15,18	0.0339	0.0394	955	1,160	0.0428	21,610		0.172	4,770	28,171
	Giannini	SP1,2,90	0.00952	0.0173	138	145	0.0198	10,050		0.172	3,630	14,496
		SP3,4	0.00263	0.00443	55	65	0.0041	9,950		0.172	2,860	20,913
		SP5,6	0.0283	0.0323	456	456	0.094	15,230		0.172	4,310	16,113
	Space General	SP13,14,91	0.00678	0.0114	101	102	0.00512	14,790		0.172	3,570	14,897
		SP11,10,12	0.0348	0.0370	343	344	0.0196	24,640		0.172	4,410	9,856
		SP9,8	0.0218	0.0215	158	156	0.0925	4,935		0.172	4,325	7,247
G.E. Silicone, ESM1004AP (SG)	GDB-Ames	SG51,52	0.00665	0.00987	88	70.4	0.0106	10,220		0.172	3,100	13,233
		SG50	0.0106	0.0129	120	122.5	0.0098	21,970		0.172	3,670	11,321
		SG35,39	0.0143	0.0169	170	169.3	0.0183	16,440		0.172	3,750	11,888
	MPDB-Ames	SG56,55,51	0.00284	0.00965	90.5	90.5	0.00582	12,978		0.172		36,761
		SG58,57,53	0.0155	0.0178	168.5	168.5	0.00827	19,232		0.172	3,330	13,600
	AMPD-Langley	SG22,49,24	0.0382	0.0355	257		0.284	4,750		0.172	4,290	6,727
		SG21,23	0.099	0.0976	514		0.293	9,550		0.172	4,180	5,191
		SG25	0.157		1,110		0.735	9,550		0.172	4,240	7,070
	ESB-Langley	SG34,33	0.0110	0.0127	203	177	0.281	2,940		0.172		18,455
	MSC-Houston (supersonic)	SG59,60	0.0280		400	435	0.0117	11,350		0.172	3,620	14,286
		SG61	0.0433		790	780	0.0170	23,350		0.172	3,840	18,245
		SG62	0.0538		980	954	0.0192	34,000		0.172	4,035	18,216
	MSC-Houston (subsonic)	SG28	0.0612			400	1.0	8,050		0.172	3,780	
		SG29,30	0.0859	0.0891		607	1.0	9,175		0.172	3,850	
		SG26,27,50	0.0264	0.0317		105	1.0	4,627		0.172	3,565	
	Aerotherm	SG41,42	0.00282	0.00750	69.1	80.3	0.0202	4,003		0.172	3,070	24,504
		SG14,43	0.0208	0.022	174	261	0.0294	7,517		0.172	3,680	8,365
		SG12,15	0.0644	0.0655	939	1,150	0.0425	21,420		0.172	4,050	14,581
	Giannini	SG1,45	0.0165	0.0216	138	145	0.0197	10,050		0.172	3,560	8,363
		SG2,3	0.00186	0.00617	55	65.5	0.0041	9,950		0.172	2,360	29,570
		SG4,5	0.0635	0.0605	456	456	0.095	15,240		0.172	3,710	6,656

Appendix D (Continued)

MATERIAL	FACILITY	MODEL NO.	MASS LOSS RATES ($lb/ft^2 sec$)		HEAT TRANSFER RATE (Btu/ft^2 sec)		MODEL STAGNATION PRESSURE (atm)	ENTHALPY (Btu/lb)		EFFECTIVE MODEL RADIUS (ft)	FRONT SURFACE TEMPERATURE (^oR) $\epsilon = 1$	$\dot{q}_{SRI\ CW} / \dot{m}_t$
			$\dot{m}_t$	$\dot{m}_p$	$\dot{q}_{SRI\ CW}$	$\dot{q}_{FAC\ CW}$	P_{t_2}	$\Delta h_{meas\ CW}$ (1)	$\Delta h_{calc\ SRI\ CW}$ (2)	R_{eff} (3)	T_{FS}	Btu/lb
G.E. Silicone ESM1004AP (SG) (Continued)	Martin	SG6,46	0.00264	0.00439	55.9	43.3	0.0070	4,903		0.172	2,890	21,174
		SG10	0.0430		520	475	0.0170	17,650		0.172	3,960	12,093
		SG9,8,7	0.0890	0.0810	512	411	0.142	9,894		0.172	3,940	5,752
	Space General	SG16,48	0.00282	0.00568	103	104	0.00511	14,820		0.172	3,470	36,525
		SG20	0.0556		344	345	0.0195	24,738		0.172	3,980	6,187
		SG18,19	0.0540	0.0518	156	154	0.0925	5,012		0.172	3,885	2,888
Teflon, TFE (T)	MPDB-Ames	T117,116	0.0214		100	88.8	0.00597	11,613		0.172		4,672
		T115,112	0.0306		221	176.5	0.00847	18,922		0.172		7,222
	AMPD-Langley	T124	0.121		516		0.293	9,550		0.172		4,264
		T126	0.225		1,055		0.735	9,550		0.172		4,688
	MSC-Houston (supersonic)	T129,130	0.0543		410	435	0.0117	11,350		0.172		7,550
		T131	0.0656		790	780	0.0170	24,350		0.172		12,042
		T133	0.0790		960	928	0.0192	34,350		0.172		12,151
	Cornell	T118	0.590		1,091	618	10.3	1,910		0.172		1,849
		T119	0.590		1,108	624	10.3	1,930		0.172		1,877
	AVCO	T110	0.612		1,640	1,640	5.62	2,280		0.172		2,679
		T111	0.690		3,340	3,400	4.92	6,670		0.172		4,840
		T113,114	0.412		1,850	1,960	1.93	7,110		0.172		4,490
	AMPD-Langley	T153,154	0.0220		74		0.0192	9,250		0.550		3,363
		T156,157	0.0203		92.4		0.0192	9,450		0.344		4,551
		T160,161	0.0299		133.5		0.0192	9,400		0.172		4,464
		T164,165	0.0458		250		0.0192	8,650		0.0416		5,458
	Martin	T163,162	0.0200			144	0.0204	12,500		0.688		
		T158,159	0.0292			180	0.0204	12,246		0.344		
		T155,154	0.0476		250	250	0.0203	12,145		0.172		5,252
		T150,151	0.0683			451	0.0202	12,300		0.0416		
High-Density Phenolic-Nylon (P)	MPDB-Ames	P11A6, P11A5	0.0117		116.1	102.5	0.00597	13,207		0.172		9,923
		P12B3, P12A7	0.0171		223.7	173.9	0.00812	18,725		0.172		13,081
	AMPD-Langley	P11A2	0.0369		524		0.293	9,550		0.172		14,200
		P11A3, P11A4	0.0672		996		0.735	9,550		0.172		14,821

Appendix D (Concluded)

MATERIAL	FACILITY	MODEL NO.	MASS LOSS RATES ($lb/ft^2 sec$)		HEAT TRANSFER RATE ($Btu/ft^2 sec$)		MODEL STAGNATION PRESSURE (atm) P_{t_2}	ENTHALPY (Btu/lb)		EFFECTIVE MODEL RADIUS (ft) R_{eff} (3)	FRONT SURFACE TEMPERATURE ($^\circ R$) $\epsilon = 1$ T_{FS}	$\dot{q}_{SRI_{CW}} / \dot{m}_t$ Btu/lb
			$\dot{m}_t$	$\dot{m}_p$	$\dot{q}_{SRI_{CW}}$	$\dot{q}_{FAC_{CW}}$		$\Delta h_{meas_{CW}}$ (1)	$\Delta h_{calc_{SRI_{CW}}}$ (2)			
High-Density Phenolic-Nylon (P)	MSC-Houston (supersonic)	P11B1, P11B2	0.0219		400	432	0.0117	11,350		0.172		18,264
		P11B3	0.0281		840	818	0.0170	26,350		0.172		29,893
		P11B5	0.0267		980	954	0.0192	34,150		0.172		36,704
	AVCO	P12A2	0.168		1,640	1,640	5.62	2,280		0.172		9,761
		P12A3	0.315		3,340	3,400	4.92	6,540		0.172		10,603
		P12A4	0.138		1,850	1,960	1.93	7,110		0.172		13,405
		P12A5	0.109		1,850	1,960	1.93	7,110		0.172		16,972
	Cornell	P12B1, P12B6	0.300		1,093	630	9.8	1,950		0.172		3,643
		P12B4	0.970		1,666	1,028	29.3	1,720		0.172		1,717

(1) $\Delta h_{meas_{CW}} = h_{t_{FAC}} - h_{CW}$ h_{CW} was assumed to equal 150 for all runs.

(2) $\Delta h_{calc_{SRI_{CW}}} = 24 (\dot{q}_{SRI_{CW}}) (R_{eff})^{0.5} / (P_{t_2})^{0.5}$

(3) $R_{eff} = R_{Hemisphere} = 3.3 R_{Flat\ Face}$

APPENDIX E

DIMENSIONLESS CORRELATION OF PREVIOUS DATA

This appendix provides a dimensional analysis of ablation variables and suggests several approaches to correlating mass loss data. These approaches are used to interpret data from the Phase I round robin and to compare them with data from the ablation literature.

A. Dimensional Analysis of Mass Loss Data

The correlation data given in Table I of the Phase I report[1] showed some interesting similarities between the power functions for Teflon and high-density phenolic-nylon. For each correlation used, except where the exponents were adjusted (see Ref. 1, Table I, Note 4), the exponents on the heating rate measured by the SRI calorimeter were identical or varied by less than 5 percent. The exponents on the stagnation pressure had greater spread but were less critical. It was therefore considered that a correlation might be the same for both Teflon and high-density phenolic-nylon and that only the proportionality constant would differ because of differences in material parameters.

A dimensional analysis of the type described by Buckingham[18] was therefore undertaken. The analysis considered two types of variables: those pertaining to the model and those pertaining to the environment to which they are exposed. The model variables include:

$\dot{m}_t$ = total mass loss rate—lb/ft^2 sec

R_{eff} = effective radius of curvature—ft

ΔH_D = overall heat of decomposition required to convert the original abalation material to gaseous end products—Btu/lb*

* The abbreviation lb will always be used to designate pound mass but pound force when combined with the word "force."

The environmental variables are:

$\dot{q}_{CW}$ = cold wall heat transfer rate—Btu/ft^2 sec

P_{t_2} = model stagnation pressure—atm

Δh = enthalpy potential; stream enthalpy minus cold wall enthalpy—Btu/lb

S_R = proportionality constant in Fay-Riddell relation, see equation (5)—ft$^{1.5}$ sec atm$^{0.5}$/lb

This last variable is shown by Fay-Riddell[7] to be given by the fluid properties of the gas stream, as follows:

$$S_R = \frac{\left(\frac{p}{\rho\mu}\right)_c^{0.1}\left(\frac{p}{\rho\mu}\right)_s^{0.4}\left(\frac{\rho}{2p}\right)_s^{0.25}\left[\frac{1}{1-(p_\infty/p_s)}\right]^{0.25}}{0.763\left[\frac{\psi(N_{Le})}{N_{Pr}^{0.6}}\right]} \qquad \text{(E-1)}$$

where p, ρ, and μ are pressure, density, and viscosity, respectively; the subscripts c, s, and ∞ denote front edge of char layer, front edge of boundary layer, and free stream, respectively; and

$$\psi(N_{Le}) = [1 + (N_{Le}^{0.52} - 1)(H_D/h_s)] \qquad \text{(E-2)}$$

Here N_{Le} and N_{Pr} are the Lewis and Prandtl numbers for the gas, H_D is the heat of dissociation (and ionization), and h_s is the stagnation enthalpy of the gas. For the fluid properties of air under the usual range of reentry conditions, the numerical value of S_R = 24(=1/0.0417).

The term ΔH_D is actually an average expression of all the thermal and chemical parameters describing the pyrolysis of each specific ablating material. As such it includes, in a complex manner, such variables as char and virgin polymer density, thermal conductivity, specific heat, heats of pyrolysis, thermal properties of the gas products, etc.

The above model and environmental variables must next be expressed in terms of as few dimensions as possible, e.g., mass, length, and time. This can be done by using the appropriate conversion factors, as follows:

VARIABLE	UNITS	CONVERTED VARIABLE	CONVERTED UNITS
$\dot{m}_t$	lb/ft^2 sec	$\dot{m}_t$	lb/ft^2 sec
R_{eff}	ft	R_{eff}	ft
ΔH_D	Btu/lb	$\Delta H_D J_m g_c$	ft^2/sec^2
$\dot{q}_{CW}$	Btu/ft^2 sec	$\dot{q}_{CW} J_m g_c$	lb/sec^3
P_{t_2}	atm	$P_{t_2} F_p g_c$	$lb/ft\ sec^2$
Δh	Btu/lb	$\Delta h J_m g_c$	ft^2/sec^2
S_R	$ft^{1.5}$ sec $atm^{0.5}/lb$	$S_R^2 F_p g_c$	ft^2/lb

where

$$g_c = 32.17 \text{ lb ft/lb force sec}^2$$
$$J_m = 778 \text{ lb force ft/Btu}$$
$$F_p = 2116 \text{ lb force/ft}^2 \text{ atm} \qquad \text{(E-3A)}$$

For convenience these conversion factors can be combined as

$$K = (J_m g_c)^{0.5}/F_p g_c = 2.325 \times 10^{-3} \text{ ft}^2 \text{ atm sec/lb}^{0.5} \text{ Btu}^{0.5} \qquad \text{(E-3B)}$$

According to the Rayleigh rule,[19] these seven dimensional variables (the conversion constants do not count) can be combined into four dimensionless groups (number of variables, 7, minus number of dimensions, 3). The most convenient forms of these were found to be

$$\pi_m = \dot{m}_t (S_R)^2 R_{eff}/(\Delta H_D)^{0.5} K \qquad \text{(E-4)}$$

$$\pi_q = \dot{q}_{CW} (S_R)^2 R_{eff}/(\Delta H_D)^{1.5} K \qquad \text{(E-5)}$$

$$\pi_p = P_{t_2} (S_R)^2 R_{eff}/\Delta H_D (K)^2 \qquad \text{(E-6)}$$

$$\pi_f = \dot{q}_{CW} S_R (R_{eff})^{0.5}/\Delta h (P_{t_2})^{0.5} \qquad \text{(E-7)}$$

The last dimensionless group is actually the Fay-Riddell relation when π_f is unity. Thus, this group is equal to unity under supersonic flow conditions.

Using the same type of power function as that used in the correlations in the Phase I report[1], a simple relation between these groups is

$$\pi_m = a_0 \pi_q^n \pi_p^m \pi_f^s \qquad \text{(E-8)}$$

Under supersonic conditions this reduces to

$$\pi_m = a_0 \pi_q^n \pi_p^m \qquad \text{(E-9)}$$

Expansion of (E-9) in dimensional terms leads to

$$\dot{m}_t = a_0 (S_R^2 R_{eff})^{n+m-1} (\Delta H_D)^{(1-3n-2m)/2} (K)^{1-n-2m} (\dot{q}_{CW})^n (P_{t_2})^m \qquad \text{(E-10)}$$

For constant effective radius* and material, this reduces to

$$\dot{m}_t = a (\dot{q}_{CW})^n (P_{t_2})^m \qquad \text{(E-11)}$$

with

$$a = a_0 (S_R^2 R_{eff})^{n+m-1} (\Delta H_D)^{(1-3n-2m)/2} (K)^{1-n-2m} \qquad \text{(E-12)}$$

Equation (E-11) is identical to the correlation given in Equation (22) of the Phase I Report.[1] Therefore, the data from that report can be used in the dimensional correlation.

B. Interpretation of Results for High-Density Ablation Materials

1. Combined Correlation for Teflon and Phenolic-Nylon

The similarity between the values of n for the Teflon and phenolic-nylon correlations in the Phase I report led to an attempt to combine these data into a single correlation. This required a two-step process which was iteratively performed on a computer. First, values of n and m were assumed. The calculated values for the SRI calorimeter (cold wall heating rate), and including Giannini and Martin data, were from the Phase I correlation

* The value of R_{eff} for the Phase I round robin was 0.172 ft.

	TEFLON	PHENOLIC NYLON	AVERAGE
n	0.57	0.55	0.56
m	0.25	0.13	0.19
a	0.0060	0.0018	

In the first step, the average values of n and m were used in the regression program to calculate the value of "a" in Equation (E-11) for the form showing the highest multiple correlation coefficient for the Teflon data; similarly the best value of "a" for the phenolic-nylon data was calculated. For models of the same effective radius, Equation (E-12) shows that

$$(a)_P/(a)_T = [(\Delta H_D)_P/(\Delta H_D)_T]^{(1-3n-2m)/2} \qquad \text{(E-13)}$$

Based on Chapman's work[20], the heat of decomposition, ΔH_D, for Teflon was taken to be 940 Btu/lb. Equation (E-13) then permitted calculation of $(\Delta H_D)_P$ from the two values of "a".

In the second step, the values of π_m, π_q, and π_p were calculated for both Teflon and phenolic-nylon, using the appropriate values of ΔH_D, and the regression program was used to calculate new values of n and m, and also a_0 for the combined data. If these values of n and m were those initially assumed, the iteration was stopped; otherwise these were used as the new input to the first step of the program.

The results of the completed iteration were

$$n = 0.54, \quad m = 0.19, \quad a_0 = 1.01$$

$$\Delta H_D = 940 \text{ Btu/lb for Teflon (assumed)}$$

$$\Delta H_D = 6470 \text{ Btu/lb for phenolic-nylon}$$

The last value is intermediate to the range of theoretical values (4300 to 7300 Btu/lb) quoted by Wick[21].

Thus, for the Phase I round-robin data, the correlation obtained by the regression program, namely,

$$\pi_m = 1.01\, \pi_q^{0.54} \pi_p^{0.19} \qquad \text{(E-14)}$$

showed a standard deviation of 10.7 percent. The data include that from Giannini and Martin* but exclude runs in which the heating load (heating rate multiplied by the run duration) was less than 2000 Btu/ft^2 for Teflon and 4000 Btu/ft^2 for high-density phenolic-nylon. These exclusions were made to minimize the use of data from the presteady-state period of the runs. A plot of the correlation, with the standard deviation indicated, is shown in Fig. E-1. The range of variables covered was as follows:

$$\dot{m}_t = \begin{cases} 0.0129\text{-}0.218 \text{ lb/ft}^2 \text{ sec for Teflon} \\ 0.00699\text{-}0.0547 \text{ lb/ft}^2 \text{ sec for phenolic-nylon} \end{cases}$$

$$\dot{q}_{\substack{SRI \\ CW}} = 36\text{-}726 \text{ Btu/ft}^2 \text{ sec}$$

$$P_{t_2} = 0.0066\text{-}1.18 \text{ atm}$$

$$\Delta h_{meas} = 1215\text{-}14{,}960 \text{ Btu/lb}$$

The range of dimensional variables was

$$\pi_m = 3.70\text{-}303, \qquad \pi_q = 3.03\text{-}1070, \qquad \pi_p = 15.3\text{-}23{,}000$$

Thus, the correlation, which compares $(\pi_m)_{obs}$ with $(\pi_m)_{calc}$, covers nearly a hundredfold range.

The Phase I round robin had only one set of subsonic data, that from Manned Spacecraft Center—NASA, and the Fay-Riddell group, π_f, which was calculated using the measured enthalpy, had values ranging from only 0.45 to 0.73. For this reason no attempt was made to determine the value of s in Equation (E-8). In fact there is no evidence that this is the form in which π_f should be used in the correlation. Any form involving π_f which reduces to Equation (E-9) when π_f equals unity is possible.

2. Separate Correlation for Teflon and Phenolic-Nylon

An alternative approach is to use the average values of n and m and the resultant values of $(\Delta H_D)_P$ and a_0 from the first step of the iteration.

In this case the results are

$$n = 0.56 \text{ (assumed)}, \quad m = 0.19 \text{ (assumed, } \quad a_0 = 0.93$$

$$\Delta H_D = 940 \text{ Btu/lb for Teflon (assumed)}$$

$$\Delta H_D = 6040 \text{ Btu/lb for phenolic-nylon}$$

* The value of $\dot{q}_{\substack{SRI \\ CW}}$ was not reported by these two facilities but was estimated from their calibration runs.

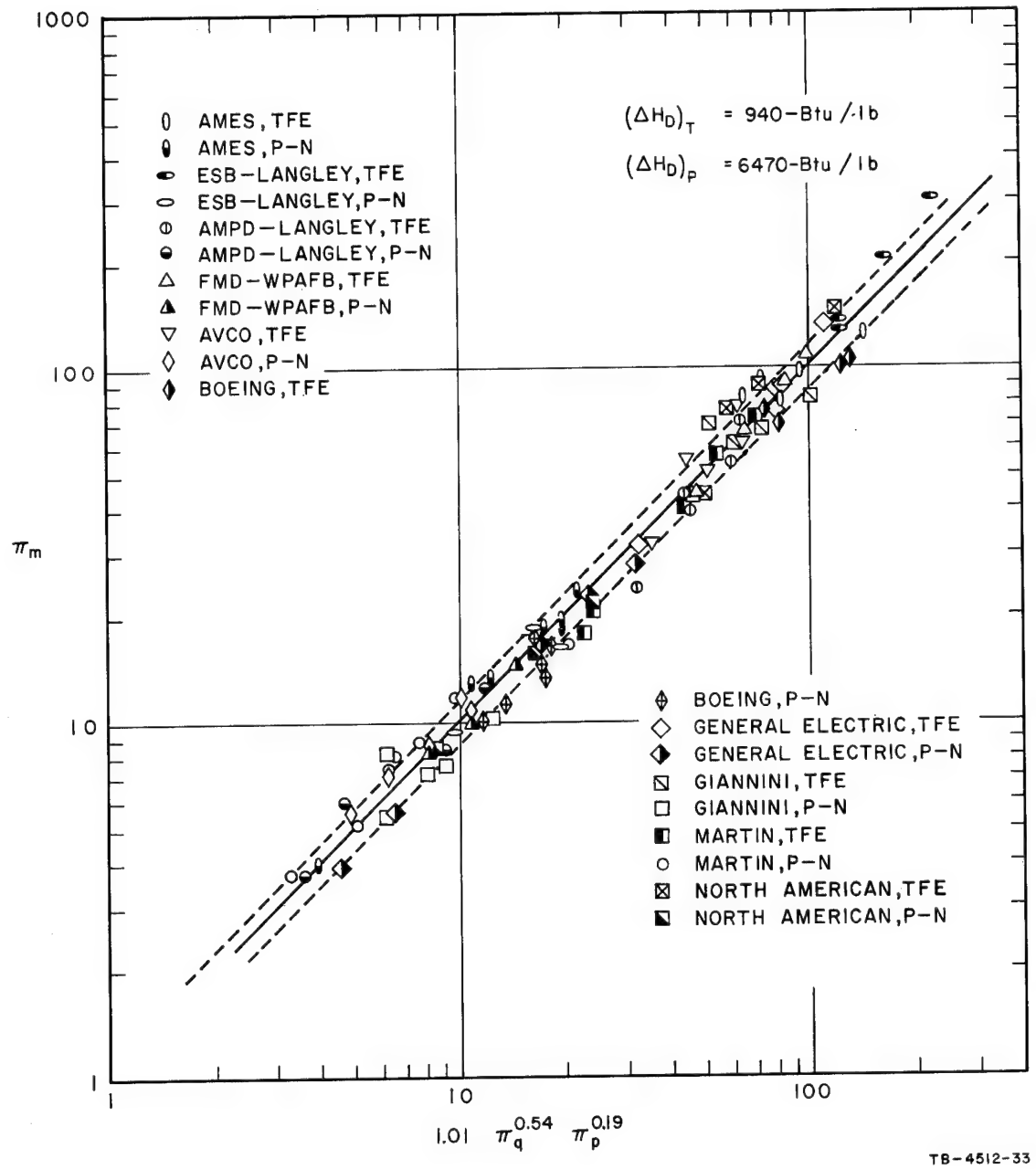

FIG. E-1 DIMENSIONLESS CORRELATION OF PHASE I ROUND-ROBIN DATA

Using the same data as for Equation (E-14) the correlation

$$\pi_m = 0.93\ \pi_q^{0.56}\ \pi_p^{0.19} \qquad \text{(E-15)}$$

has a standard deviation of 10.9 percent.

This implies that there may be a number of sets of n, m, $(\Delta H_D)_P$, and a_0 values having only slightly higher percent standard deviations than those shown for the correlation in Equation (E-14). Calculations in which n and m were varied by ±0.05 and $(\Delta H_D)_P$ by ±1500 Btu/lb showed that the standard deviation increased only a few percent. Typical results are given below for calculations based on simple values of n and m.

	SET 1	SET 2	SET 3	SET 4
n (assumed)	0.5	0.54	0.56	0.6
m (assumed)	0.25	0.19	0.19	0.15
a_0 (obtained by iteration)	0.87	1.01	0.93	0.88
$(\Delta H_D)_P$ (obtained by iteration)	8390	6470	6040	6900
Percent standard deviation (calculated)	13.1	10.7	10.9	12.1

It is apparent therefore that an independent source for the value of the overall heat of decomposition, ΔH_D, would eliminate the iterative process and would permit more accurate values for a_0 and percent standard deviation to be obtained. In addition, it is not certain that the Teflon and high-density phenolic-nylon data should be forced into the same correlation. If they should not be combined, then it is not so important that the value of ΔH_D be known since Equation (E-10), which is based on the same dimensional analysis, can be written as

$$\dot{m}_t = b(R_{eff})^{n+m-1}\ \dot{q}_{CW}^{n} P_{t_2}^{m} \qquad \text{(E-16A)}$$

or alternatively,

$$\dot{m}_t(R_{eff}) = b(\dot{q}_{CW}R_{eff})^{n}(P_{t_2}R_{eff})^{m} \qquad \text{(E-16B)}$$

where

$$b = a(R_{eff})_{RR}^{1-n-m} \qquad \text{with} \qquad (R_{eff})_{RR} = 0.172 \text{ ft} \qquad \text{(E-17)}$$

and with "a" defined as in Equation (E-12). Thus, the constant b will be specific for each material, although its numerical value will depend on the units used for $\dot{m}$, R_{eff}, $\dot{q}_{CW}$, and P_{t_2} and on the values of n and m found for that material.. Therefore, from the Phase I round robin the values of "a", n, and m are those already tabulated preceding Equation (E-13). For $\dot{m}_t$ in lb/ft^2 sec, $\dot{q}_{CW}$ in Btu/ft^2 sec, and P_{t_2} in atm, the numerical values of b are

$$(b)_T = 0.0044 \text{ lb ft}^{-0.68} \text{ sec}^{-0.43} \text{ Btu}^{-0.57} \text{ atm}^{-0.25}$$

$$(b)_P = 0.0010 \text{ lb ft}^{-0.58} \text{ sec}^{-0.45} \text{ Btu}^{-0.55} \text{ atm}^{-0.13}$$

Thus, the mass loss rates for Teflon and high-density phenolic-nylon become

$$(\dot{m}_t)_T = 0.0044 \, (R_{eff})^{-0.18} (\dot{q}_{\substack{CW \\ SRI}})^{0.57} (P_{t_2})^{0.25} \qquad \text{(E-18A)}$$

$$(\dot{m}_t)_P = 0.0010 \, (R_{eff})^{-0.32} (\dot{q}_{\substack{CW \\ SRI}})^{0.55} (P_{t_2})^{0.13} \qquad \text{(E-18B)}$$

Another form of these relations is

$$(\dot{m}_t R_{eff})_T = 0.0044 (\dot{q}_{\substack{CW \\ SRI}} R_{eff})^{0.57} (P_{t_2} R_{eff})^{0.25} \qquad \text{(E-19A)}$$

$$(\dot{m}_t R_{eff})_P = 0.0010 \, (\dot{q}_{\substack{CW \\ SRI}} R_{eff})^{0.55} (P_{t_2} R_{eff})^{0.13} \qquad \text{(E-19B)}$$

These dimensionally valid equations, as well as the dimensionless correlation combining the data for the two materials, can be checked with the results from Phase II; this is done in Sec. IV-B.

C. Inclusion of Literature Data

The open literature on supersonic arc-jet testing was reviewed to locate ablation data on Teflon and high-density phenolic-nylon. A major requirement was that mass loss rate, cold wall heating rate,* stagnation pressure, and effective radius either be directly tabulated or capable of being calculated from other tabulated data. In addition, the composition of the materials had to be nearly identical to those used in the round robin.

The applicable data and their sources are given in Table E-1. These data were converted into the dimensionless form of Equation (E-14). A plot of this correlation is given in Fig. E-2 which can be compared directly with Fig. E-1. As can be seen, only the Walberg data on phenolic-nylon models do not fit the correlation, this will be considered in more detail in Sec. IV-B. Excluding the Walberg data, the standard deviation for the literature data is 9.6 percent. Combined with the round-robin data the overall standard deviation is 10.3 percent. The range of variables covered was

$$\dot{m}_t = \begin{cases} 0.0132\text{-}1.22 \text{ lb/ft}^2 \text{ sec for Teflon} \\ 0.0233\text{-}0.596 \text{ lb/ft}^2 \text{ sec for phenolic-nylon} \end{cases}$$

$$\dot{q}_{CW} = 21.6\text{-}3000 \text{ Btu/ft}^2 \text{ sec}$$

$$P_{t_2} = 0.0030\text{-}33.0 \text{ atm}$$

$$\Delta h_{meas} = 420\text{-}7470 \text{ Btu/lb}$$

$$R_{eff} = 0.0156\text{-}0.55 \text{ ft}$$

The dimensionless variables had a range of

$$\pi_m = 2.24 - 1130, \qquad \pi_q = 1.47 - 2510, \qquad \pi_p = 37.1 - 1,260,000$$

For the literature data the correlation, which compares $(\pi_m)_{obs}$ with $(\pi_m)_{calc}$, has nearly a five hundredfold range. In combining the round-robin and literature data, the range of variables was

$$\dot{m}_t = \begin{cases} 94.5\text{-fold for Telfon} \\ 85.2\text{-fold for phenolic-nylon} \end{cases} \qquad P_{t_2} = 11{,}000\text{-fold}$$

$$\Delta h_{meas} = 35.7\text{-fold}$$

$$\dot{q}_{CW} = 139\text{-fold} \qquad R_{eff} = 35.3\text{-fold}$$

* The heating rate must be that measured, or calculated, for a calorimeter having the same shape and dimensions as the model used.

Table E-I

LITERATURE DATA FOR THE ABLATION OF TEFLON AND HIGH DENSITY PHENOLIC-NYLON

LITERATURE SOURCE	MATERIAL	MODEL OR RUN NUMBER	MASS LOSS RATE $\dot{m}_t$ (lb/ft^2 sec)	HEAT TRANSFER RATE $\dot{q}_{FAC\ CW}$ (Btu/ft^2 sec)	MODEL STAGNATION P_{t_2} (atm)	ENTHALPY h_t (Btu/lb)	MODEL RADIUS R_{eff} (ft) (1)
Compton, D. L., Winovich, W , Wakefield, R M. NASA TN D 1332, August 1962	Teflon		0.0132	21.6	0.031	2190	0.206
			0.0315	44.7	0.031	2490	0.103
			0.0364	61.2	0.031	2700	0.0686
			0.057	87.0	0.031	2990	0.0343
Chapman, A. J. NASA TN D 1520, April 1963	Teflon	1	1.00	2500	8.1	2700	0.0208
		2	0.89	2160	5.45	2950	0.0208
		3	0.918	2640	4.95	3950	0.0208
		4	0.718	2440	4.86	6600	0.0689
		5	1.10	2200	11.80	2700	0.0345
		6	1.10	2500	5.88	4300	0.0345
		7	1.10	2540	6.75	4200	0.0345
		8	1.07	2970	6.94	4450	0.0345
		9	1.04	3000	7.22	4750	0.0345
Farmer, R. W. WADD Tech Report 60-648, November 1960	Teflon	4	0.61	620	4.	1170	0.0156
		5	0.64	1040	4.	1840	0.0156
		6	0.92	1540	4.	2600	0.0156
Graves, K. W. C.A.L. BM-1526-G-8 AD 469965	Teflon	2	1.22	2000	33.0	1900	0.025
		10	0.95	1740	21.5	1870	0.025
		11	0.67	1480	14.4	1850	0.025
		46	0.96	1540	8.0	1670	0.025
Winters, C. W. NASA TN D 1500	Teflon	90 (2)	0.182	340	5.1	2410	0.55
		91	0.229	530	7.5	3130	0.55
Winters, C. W. NASA TN D 2383	Teflon	28 (3)	0.154	200	13.0	940	0.55
		29	0.254	410	20.2	1550	0.55
		30	0.174	250	8.7	1450	0.55
		35	0.050	72	1.46	1010	0.55
Vojvodich, N. S. NASA, Ames Research Center	Teflon	1	0.0538	148	0.039	6380	0.1155
		2	0.0558	198	0.044	7616	0.1155
		3	0.0552	176	0.041	6888	0.1155
		4	0.0510	132	0.037	5992	0.1155
		5	0.032	108	0.016	5460	0.1155
		6	0.045	126	0.019	6720	0.1155
		7	0.048	158	0.021	7644	0.1155
		8	0.055	172	0.022	8176	0.1155

Table E-I (Continued)

LITERATURE SURVEY	MATERIAL	MODEL OR RUN NUMBER	MASS LOSS RATE $\dot{m}_t$ (lb/ft^2 sec)	HEAT TRANSFER RATE $\dot{q}_{FAC\ CW}$ (Btu/ft^2 sec)	MODEL STAGNATION P_{t_2} (atm)	ENTHALPY h_t (Btu/lb)	MODEL RADIUS R_{eff} (ft) (4)
Vojvodich, N. S. (Concluded)		9	0.0226	59	0.0044	5796	0.1155
		10	0.0246	76	0.005	6860	0.1155
		11	0.0275	77	0.005	7056	0.1155
		12	0.0295	95	0.0057	8400	0.1155
		13	0.0241	62	0.0035	7168	0.1155
		14	0.0218	65	0.0035	7560	0.1155
		15	0.0187	50	0.0030	5936	0.1155
		16	0.0808	214	0.100	4619	0.077
		17	0.0564	147	0.050	4508	0.077
		18	0.0744	203	0.050	6011	0.077
		19	0.0341	59	0.030	4047	0.1155
		20	0.0122	26	0.003	4924	0.1155
Paul, N. J., Falk, F., Kauffman, L. O. Johns Hopkins Report TG881, December 1966	Teflon	145 (4)	0.385	700	1.28	2840	0.033
		146	0.395	743	1.29	3000	0.033
		147	0.403	785	1.32	3030	0.033
		148	0.459	1075	1.48	4000	0.033
		111	0.0547	861	3.7	2100	0.033
		122	0.553	850	3.5	2130	0.033
		112	0.626	1051	3.9	2470	0.033
		205	0.640	1040	3.6	2640	0.033
		119	0.620	789	6.13	1540	0.033
		114	0.632	819	6.24	1580	0.033
		241	0.771	1187	6.9	2120	0.033
		127	0.809	1275	7.1	2250	0.033
		127	0.811	1305	7.2	2270	0.033
Lundell, J. H. AIAA J. 3,2087-95 (1965)	High-Density Phenolic-Nylon 75 lb/ft^3	1	0.0394	101	0.16	2420	0.0312
		5	0.0233	99	0.045	3080	0.0312
		9	0.0384	176	0.16	3310	0.0312
		13	0.0368	193	0.072	3040	0.0312
		17	0.0387	145	0.16	3210	0.0312
Walberg, G. D., Crouch, R. K. NASA TN D 3465, August 1966	High-Density Phenolic-Nylon 75 lb/ft^3	1	0.150	306	7.28	< 571	0.0156
		2	0.181	455	7.28	744	0.0156
		3	0.230	614	7.28	1038	0.0156
		5	0.176	308	7.28	< 571	0.0156
		6	0.248	445	7.28	744	0.0156
		7	0.338	609	7.28	1118	0.0156

Table E-I (Concluded)

LITERATURE SOURCE	MATERIAL	MODEL OR RUN NUMBER	MASS LOSS RATE $\dot{m}_t$ (lb/ft^2 sec)	HEAT TRANSFER RATE $\dot{q}_{FAC\ CW}$ (Btu/ft^2 sec)	MODEL STAGNATION PRESSURE P_{t_w} (atm)	ENTHALPY h_t (Btu/lb)	MODEL RADIUS R_{eff} (ft) (4)
Walberg, G. D. NASA Langley Research Center	High-Density Phenolic-Nylon 75 lb/ft^3	I 1	0.181	769	7.20	1495	0.0208
		2	0.239	794	7.31	1530	0.0208
		3	0.208	874	7.49	1663	0.0208
		4	0.218	1087	7.65	1980	0.0208
		II 1	0.179	648	5.17	1000	0.0688
		2	0 290	875	10.69	934	0.0688
		3	0.596	1064	14.30	980	0.0688

(1) $R_{eff} = R_{Hemisphere} = 3.3\ R_{Flat\ Face}$.

(2) Free flight data. Instantaneous rates at 90 and 91 sec after launch; the period of maximum velocity during flight. Enthalpy and stagnation calculated from velocity and air density.

(3) Free flight data. Instantaneous rates at 28, 29, 30, and 35 sec after launch. Enthalpy, stagnation pressure calculated from velocity and air density.

(4) Model stagnation pressure from relation: $P_{t_2} = 0.75\ P_{t_1}$. Heat Flux calculated from relation: $\dot{q} = 0.0417\ (P_{t_2}/R_{eff})^{0.5}(h_{ARC} - 150)$.

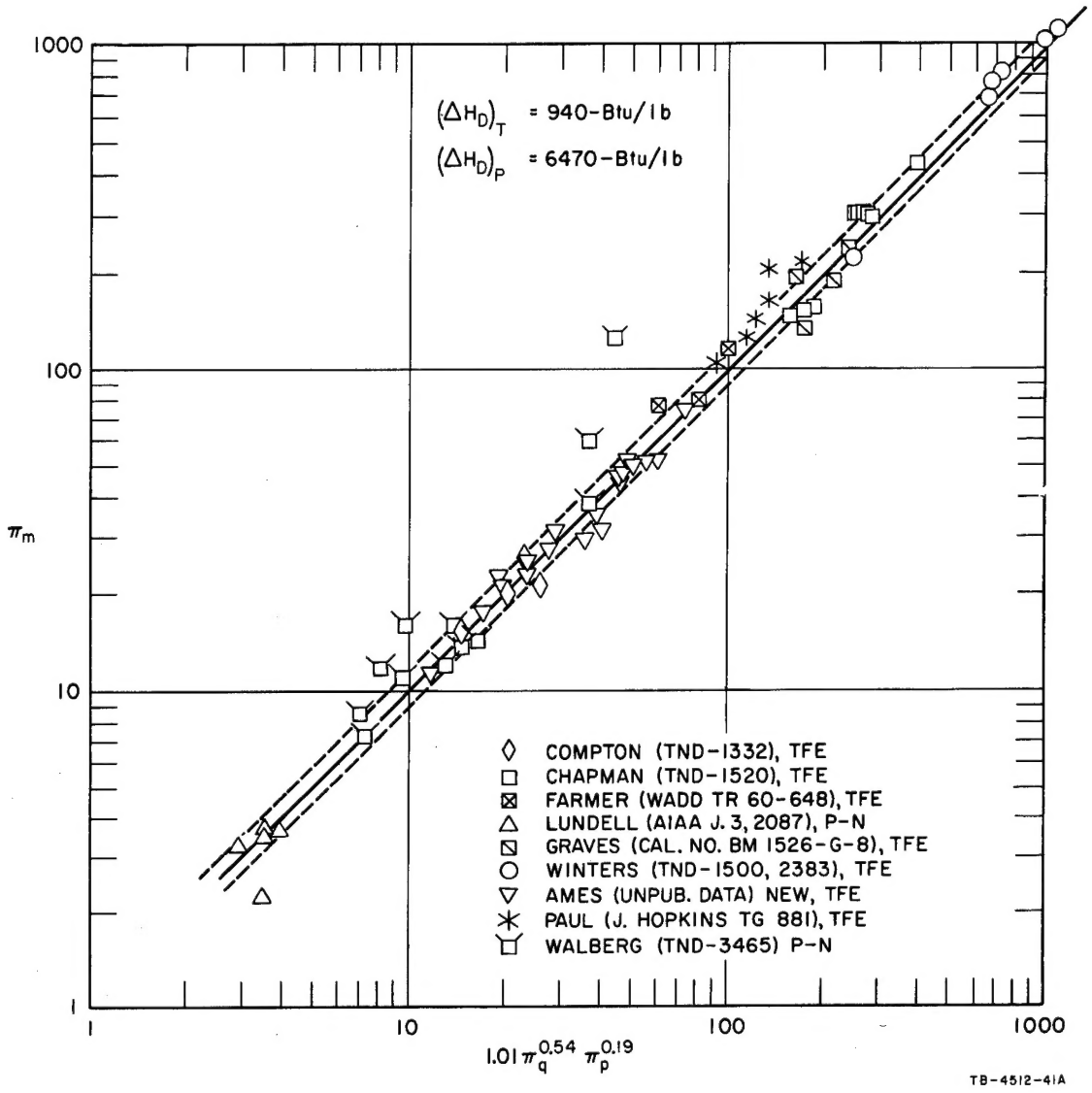

FIG. E-2 DIMENSIONLESS CORRELATION OF LITERATURE DATA

REFERENCES

1. Hiester, N. K., and Clark, C. F., NASA Contractor Report, NASA CR-379, "Feasibility of Standard Evaluation Procedures for Ablating Materials," February 1966

2. Winovich, W., NASA TN D2132, "On the Equilibrium Sonic-Flow Method for Evaluating Electric-Arc Air-Heater Performance," March 1964

3. Pope, R. B., "Measurement of Enthalpy in Low-Density Air Flows," AIAA J. 6, 103 (1968).

4. Jorgensen, L. H., NASA TN D-2233, "Total Enthalpy of a One-Dimensional Nozzle Flow with Various Gases," September 1964

5. JANAF Interim Thermochemical Tables, Dow Chemical Company, Midland, Michigan, December 31, 1960

6. Hansen, C. F., NASA TN R-50, "Approximation for the Thermodynamic and Transport Properties of High Temperature Air," March 1958

7. Fay, J. A., and Riddell, F. R., "Theory of Stagnation Point Heat Transfer in Disassociated Air," J. Aero. Sci., 25, 73-85 (1958)

8. Lees, L., "Laminar Heat Transfer over Blunt Nosed Bodies at Hypersonic Flight Speeds," Jet Propulsion, 26, 259-69 (1956)

9. Marvin, J. G., and Sinclair, R. A., "Convective Heating in Regions of Large Favorable Pressure Gradient," AIAA 5th Aerospace Sciences Meeting, New York, January 23-26, 1967

10. Stoney, W. E., and Markly, J. T., NACA TN4300, "Heat Transfer and Pressure Measurements on Flat-Faced Cylinders at a Mach No. of 2," July 1958

11. Goulard, R., " On Catalytic Recombination Rates in Hypersonic Stagnation Heat Transfer," Jet Propulsion, 28, 737-45 (1958)

12. Lundell, J. H., Wakefield, R. M., and Jones, J. W., "Experimental Investigation of a Charring Ablative Material Exposed to Combined Convective and Radiative Heating," AIAA J., 3, 2087-95 (1965)

13. Scala, S. M., "The Ablation of Graphite in Dissociated Air, I. Theory," General Electric Space Sciences Laboratory Report R62SD72, September 1962

14. Chapman, A. J., NASA TN D2196, " Effect of Weight, Density and Heat Load on Thermal Shielding Performance of Phenolic Nylon," June 1964

15. NASA, Manned Spacecraft Center Report, MSC-A-R-66-4, "Postlaunch Report for Mission AS 201 (Apollo Spacecraft 009)," May 6, 1966

16. NASA, Manned Spacecraft Center Report, MSC-A-R-66-5, "Postlaunch Report for Mission AS 202 (Apollo Spacecraft 011)," October 12, 1966

17. Rosensweig, R. E., and Beecher, N., "Theory for the Ablation of Fiberglass-Reinforced Phenolic Resin," AIAA J., 1, 1802-9 (1963)

18. Buckingham, E., "On Physically Similar Systems: Illustrations of the Use of Dimensional Analysis," Phys. Rev., 4, 345 (1914)

19. Rayleigh, L., "The Principle of Similitude," Nature, 95, 66 (1915)

20. Chapman, A., NASA TND 1520, "An Experimental Investigation of Several Ablation Materials in an Electric Arc-Heated Air Jet," April 1963

21. Wick, B. H., "Ablation Characteristics and Their Evaluation by Means of Arc Jets and Arc Radiation Sources," paper presented at 7th International Aeronautical Congress, Paris, June 11-20, 1965